NEUTRINO PRODUCTION AND TRANSPORT DURING GRAVITATIONAL COLLAPSE

Thesis by

John Richard Bond

In Partial Fulfillment of the Requirements

For the Degree of

Doctor of Philosophy

California Institute of Technology

Pasadena, California

1979

(Submitted July 18, 1978)

And when I beheld my devil, I found him serious, thorough, profound, solemn: it was the Spirit of Gravity — through him all things are ruined.

One does not kill by anger but by laughter. Come, let us kill the Spirit of Gravity!

— Friedrich Nietzsche, 1885
Thus Spake Zarathustra

ACKNOWLEDGMENTS

Finally, the most pleasant part of the thesis process arrives: to sit back, quaff a few, and bring to mind the experience of these past five years, and raise my stein to all of those individuals who have passed through my life in this period, either quickly or slowly, enriching it, and creating the Experience.

To the Mansion, that great old white house on Magnolia Avenue, the center of my Caltech social life; to those of the many Mansion eras, to the dwellers, and to those who just came over to play; to Arvind and Barry and Bill and Heather and Carol; to Chris and Flash and Ted and Lee; to Henry and Jenny and MJ; to Rich and Sandy; to Tricia.

The other pole of my Caltech experience was Kellogg: the faculty, the staff, and the students have all become friends over these years, and in discussions with them, many of the ideas expressed in this thesis took shape. To George Fuller, Dave Tubbs, and Richard Ward who listened and critically responded to many of the results of this work. To Syd Falk, who was instrumental in the early stages of this work, and from whom I learned the way of the big code; his techniques are firmly imprinted upon the spatial code. To Charlie Barnes, who kept me thinking about other implications of neutral currents.

To Steve Koonin, with whom I went to the Neils Bohr Institute and returned a seasoned researcher; his patient teaching by example of his approach to physics work is gratefully acknowledged.

And above all, to Willy Fowler, my advisor, who played a crucial role in the development of this thesis, who can infect even me with his

fantastic Enthusiasm, and who radiates a shining example of where physics can lead the individual.

I dedicate this work to my mother and in memory of my father, who was passionately interested in the possibilities of the mind.

This research has been financially supported throughout the years by the National Science Foundation [PHY76-83685].

ABSTRACT

The P-N method is developed to describe the transport of neutrinos in collapsing stellar cores, and the multigroup flux limited diffusion and equilibrium diffusion approximations are obtained from it. An effective Lagrangian for weak neutral and charged current neutrino interactions which is applicable to low energy neutrino processes is derived. The neutrino source functions which enter into the P-N equations are given a many body theory formulation in terms of weak current-current correlation functions. Within this framework, we deal, in turn, with the scattering reactions $\nu A \rightarrow \nu A$, $\nu A \rightarrow \nu A^*$, $\nu N \rightarrow \nu N$ (both for non-degenerate and degenerate nucleons), $\nu e \rightarrow \nu e$, and $\nu\nu \rightarrow \nu\nu$, and the production and absorption reactions $e^- p \rightleftarrows n \nu_e$, $e^+ n \rightleftarrows p \bar{\nu}_e$, $e^- {}^A_Z \rightleftarrows {}^A_{(Z-1)} \nu_e$, $e^+ e^- \rightleftarrows \nu\bar{\nu}$, and $\gamma_{p\ell} \rightleftarrows \nu\bar{\nu}$. These equations are then applied to the various phases of neutrino flow during iron core collapse: the transparent stage to the onset of trapping; the approach of electron neutrinos to beta-equilibrium; the evolution of the muon neutrino and antineutrino distribution functions towards the Fermi-Dirac form; the conditions under which ν_μ $\bar{\nu}_\mu$ radiative energy loss exceeds the ν_e loss; comparison of the P-1 and flux limited diffusion methods of spatial transport in a static pre-bounce core.

TABLE OF CONTENTS

1. SUPERNOVAE AND NEUTRINOS: INTRODUCTION

1.1 INTRODUCTION

The transformation of a white dwarf to a neutron star liberates about one hundred million electron volts of its gravitational potential energy per baryon and most of its electron lepton number. Electron neutrinos transport the lepton number. Neutrinos and antineutrinos of all types carry the bulk of the energy away.

If the energy released in the collapse of the hot iron/nickel white dwarf core of a massive star at the endpoint of its evolution can couple with an efficiency of one percent or so to the overlying mantle, the mantle and envelope of the star may be ejected, with the result a Type II supernova explosion. Neutrinos deposit energy and momentum in the mantle. Does this deposition cause or contribute to ejection? The theoretical answer depends upon the input physics.

The idea of a supernova representing the catastrophic transition of the interior stellar state has been around since Baade and Zwicky's (1934) connection of supernovae to neutron star formation. Yet, no believable and workable supernova model has been constructed to date.

This is due in large part to the complex interweaving of the hydrodynamics of implosion and explosion with neutrino radiative transfer in regimes of matter at the limit of theoretical knowledge. The equation of state governs the collapse rate, strength of generated shock waves, and elemental abundances. The abundances

determine the rate of neutrino loss and matter heating; this, in turn, governs the thermodynamic conditions upon which the equation of state depends. Historically workers have used the simplest approximations to treat neutrino transport and the equation of state; when these were found inadequate, the next simplest were tried. The hope was for a definitive answer: yes, supernovae occur via the implosion/explosion mechanism, or, no, they do not. Instead, the results are quite sensitive to changes in the input physics; the answer remains maybe. In recent years, an all out effort has been launched by many groups to unravel the physics of collapse.

This effort was spurred on in part by the dramatic expansion in our knowledge of the interactions of neutrinos with matter that has occurred in the last few years: a new weak force mediated by the exchange of a neutral massive spin one boson was discovered; the existence of a new flavor of neutrino was inferred. A qualitative change in the theoretical picture of core collapse results from the inclusion of these new effects.

Neutrino transport, with special attention paid to the neutral current processes which neutrinos participate in, is the subject of this thesis.

1.2 SUPERNOVA OBSERVATIONS

Supernova (SN) stars suddenly flare to a photon luminosity a billion times that of the sun, and are ten thousand times brighter than novae. At least six SN were observed in historical times, those in

the years 385 A.D., 1006, 1054 (the Crab), 1181, 1572 (Tycho's SN), and 1604 (Kepler's SN)(Clark and Stephenson 1977); in addition, Cas A apparently exploded in the seventeenth century, but was not observed. The debris from these explosions are seen as extended radio sources; approximately one hundred such SN remnants are known in our Galaxy. In 1885, the first extragalactic SN was observed, in Andromeda; it was not until the twenties of this century when Andromeda was recognized as an island universe distinct from our own that the tremendous optical energy released in supernovae became known. By now, $\sim$ 400 extragalactic SN have been seen.

Observers have obtained the optical spectra and light curve (luminosity as a function of time) of many of these events (see, for example, Kirshner *et al.* 1973), on the basis of which SN have been classed into two types, I and II. The light curves of both types rise steeply to maximum brightness, then quickly fall, with the peak lasting about twenty days; the subsequent decline in Type I is almost exponential, that in Type II has a slowly falling plateau, then a precipitous drop, although not all Type II's look the same. From the spectrum, information on the expansion velocity, temperature, and radius of the photosphere, as well as on elemental abundances can be obtained. Type II have hydrogen, and heavier elements have been identified; Kirshner and Kwan (1975) have estimated the mass of the expanding envelope to be from two to five solar masses with an abundance distribution compatible with solar system values for three particular SN which occurred in 1969, 1970, and 1973. The expansion

kinetic energy is $\sim$ 0.1 to 0.5 MeV per baryon, so with the Kirshner-Kwan estimate, a kinetic energy between $\sim 5\times10^{50}$ to 5×10^{51} ergs is obtained; the time integrated optical energy output is less, $\lesssim 3\times10^{49}$ ergs.

Type I's have little or no hydrogen, larger expansion kinetic energies per baryon and light energy output than Type II's; the spectrum is difficult to analyze, and the composition is only poorly known.

The type of galaxy in which the SN types are predominantly found (I in elliptical, II in spiral), the spatial distribution within galaxies (II in spiral arms), and the SN birth rates (estimated by Tammann (1974) to be one every 20 ± 10 years in our Galaxy) all contribute to our knowledge of supernovae. A fairly clear picture of Type II SN emerges: they involve young massive stars of Population I. For Type I supernovae, the picture is fuzzier.

The first pulsar was observed in 1967. A few years later, the Crab pulsar was identified (Comella et al. 1969). It has been estimated that there are perhaps half a million pulsars in our Galaxy (see Green 1977). With Gold's (1968) identification of pulsars with rotating, magnetized neutron stars, and this figure, it is clear that gravitational collapse is a relatively common phenomenon; we know of no other way a neutron star can form.

The Crab Nebula has been called the Rosetta Stone for the field of supernova physics. It was a supernova, by the testimony of ancient Chinese records, and it is an expanding number of filaments and cloud of gas, lit up by the energy supplied by a central neutron

star; it radiates in all wavelength bands. If the expansion is extrapolated back in time it agrees with the Chinese date; the pulsar slowdown lifetime is also consistent with this date. This object, and the Vela pulsar with its associated ten thousand year old supernova remnant, provide the most compelling observational evidence for the core implosion/mantle or envelope explosion hypothesis.

1.3 BEFORE AND AFTER COLLAPSE

Stars with masses between about eight and fifty solar masses evolve an onion skin configuration: an iron/nickel white dwarf core supported by relativistic electron degeneracy pressure forms in the center with a mass near the Chandrasekhar limit of 1.4 $M_\odot$; it is surrounded in succession by layers of (primarily) silicon, oxygen, neon, carbon, helium, and hydrogen. Near the boundary between one layer and the next, a shell burns the thermonuclear fuel of the outer layer into its ashes, the composition of the inner layer; in particular, the core slowly grows in mass as the silicon burning shell accretes matter onto it. The stellar envelope has a red giant structure of radius between 10^{13} and 10^{14} cm, although this, and the amount of hydrogen left in the outer layers, are sensitive to the rate of mass loss from the star in its earlier evolutionary phases. Stars of fifteen and twenty-five solar masses have, for the first time, been numerically evolved from the main sequence to this presupernova configuration (Weaver et al. 1977).

The core collapses; most of the mantle (the silicon to carbon layers) and all of the envelope cannot respond dynamically to the

rapid collapse and remain essentially stationary, in hydrostatic equilibrium. Let there be a strong shock wave: while passing through the mantle, this shock can trigger the explosive ignition of some unburned fuel, for example, burning silicon to iron peak elements. The mantle and envelope are dispersed into interstellar space, enriching it in heavy elements, causing chemical evolution of the galaxy. The modern theory of nucleosynthesis rests upon supernovae as the primary site. To explain the observed elemental abundances, it seems necessary to lock up most of the core matter in a collapsed remnant; otherwise, too many neutron rich nuclei would be predicted to exist (Weaver et al. 1977). This is further evidence for the implode/explode scenario.

When the shock emerges at the surface of the envelope, a fraction of a day after the core collapse, the light curve begins its rapid rise; the observed features of Type II light curves can be explained by this mechanism alone, provided the shock energy is in the neighborhood of 10^{51} ergs (Falk and Arnett 1977, Chevalier 1976); Type I's may need, in addition, another energy source, such as the decay of radioactive nuclei (Colgate and McKee 1969), to obtain the exponential decay (Lasher 1975).

Supernovae are thought to be the source of cosmic rays and perhaps their accelerators. The shock plays an important role in the energy balance of the interstellar medium. Star formation can apparently be triggered by the incidence of the shock on a molecular cloud. A supernova that exploded near the birth date of the solar

system, perhaps even triggering the collapse of the protosolar nebula, has been suggested to explain some of the isotopic anomalies found in meteorites.

And, of course, neutron stars and maybe black holes are the collapsed remnants of these explosions.

There is one missing ingredient in this grand design which places the supernova phenomenon at the apex of much of astrophysical theory: the cause.

1.4 INSTABILITY INITIATORS AND EXPLOSION MECHANISMS

Burbidge et al. (1957), B^2FH, were the first to suggest a mechanism by which the core would become unstable after all its thermonuclear energy was spent: at high temperature, iron peak elements photodisintegrate into alpha particles and neutrons; at an even higher temperature, alpha particles break down into nucleons. Fowler and Hoyle (1964), FH, amplified and extended the B^2FH ideas by proposing a specific presupernova model, emphasizing the importance of neutrino emission for the collapse of massive cores, suggesting another instability mechanism for very massive stars (with carbon/oxygen cores more massive than $\sim 30\ M_\odot$), that resulting from the neutrino-antineutrino energy loss due to the annihilation of electrons and positrons, and specifying a mechanism for mantle ejection, namely, the thermonuclear burning of unburned oxygen in the mantle as it falls in and heats up.

Cameron (1958) proposed another mechanism for the onset of instability: degenerate electrons are captured by nuclei, thereby

robbing the core of its pressure support against its self gravity; the core becomes progressively more neutron rich, it neutronizes.

For massive iron cores ($\gtrsim 2\ M_\odot$), photodecomposition initiates the phase of rapid collapse; for less massive cores, such as the ones with mass near the Chandrasekhar limit which arise from evolutionary calculations (Arnett 1977a, Weaver et al. 1977), collapse is initiated by electron capture which lowers the Chandrasekhar mass below the core mass.

Colgate and White (1966), CW, constructed the first numerical hydrodynamical model of the implosion/explosion phenomenon. Three important ingredients were added to SN theory: a core opaque to neutrinos in the late stages of collapse, a shock wave formed as a result of matter accreting onto a small inner core, and the deposition of energy by neutrinos in the mantle and its subsequent rapid expansion which generates another shock wave. Their neutrino transport was no transport at all: energy was deposited in the last mean free path.

Arnett (1966, 1967) improved on the neutrino physics, using the equilibrium diffusion approximation (EDA) with neutrinos flowing down the temperature gradient, and emphasized the importance of muon neutrinos as carriers of the bulk of the energy from the collapsing core.

Ivanova et al. (1967) suggested energy deposition can trigger the thermonuclear burning of mantle oxygen and thus tied together the FH and CW mechanisms. The shock formed when the core halted, the bounce shock wave, propagated through their mantle and envelope;

this suggested another possible explosion mechanism, but was found to be not of sufficient intensity to produce a supernova.

Wilson (1971) used general relativistic equations of motion to describe the hydrodynamics and the Boltzmann transport equation to treat the flow of both electron and muon neutrinos. One model exploded; the neutrinos acted only as a slight damper to the now predominant bounce shock wave. This third explosion mechanism seems now to be the most important (Wilson 1977, Bruenn 1975, van Riper 1977).

When low energy neutrinos are elastically scattered by nuclei, they transfer momentum but very little energy; this suggests a fourth mechanism for mantle blowoff, by neutrino momentum deposition (as opposed to the CW energy deposition mechanism). This process requires neutral current interactions, and with their discovery, a new era of work on iron core collapse was initiated, led off by Wilson (1974), who used his 1971 code with the inclusion of neutrino-nucleus scattering to find explosions were sensitive to the value of the neutral current coupling chosen.

1.5 PHASES OF THE NEUTRINO FLOW

It has subsequently been found that explosions are also sensitive to variations in other inputs to the collapse codes, such as in the equation of state, in the neutrino processes and in the method used for their transport. Two methods of transport are now used in coupled radiation-hydrodynamic codes: flux limited diffusion (Wilson et al. 1975, Wilson 1976, 1977, Bruenn 1975, Arnett 1977) and the equilibrium diffusion approximation where flows down

neutrino chemical potential gradients as well as down temperature gradients are now allowed (Mazurek 1975, 1976, Sato 1975). Not all neutrino processes are included in these works, and those that are are often not treated correctly.

We approach neutrino transport using the underlying structure imposed by the P-N equations of transfer (derived in Chapter 3) and show how the two approximations mentioned above follow from it. The Pauli exclusion principle, which limits the states into which the neutrinos can be produced or scattered, causes considerable complications: nonlinearities appear in the neutrino source functions.

In Chapter 2, we review the present experimental and theoretical status of the weak interactions and obtain an effective Lagrangian suitable for the description of the low energy processes in which neutrinos participate during gravitational collapse.

We formulate a many body treatment of neutrino interactions in matter using dynamical correlation functions of the currents which enter into this Lagrangian, then proceed to deal with the many neutrino scattering, production, and absorption mechanisms of importance in supernovae within this framework (Chapters 4 and 5).

The P-N equations with all the source functions included are thus set up. It is applicable to any white dwarf to neutron star or black hole transformation, not just those associated with iron core collapse. For example, other arenas include mass transfer onto a white dwarf in a binary system which sends its mass over the Chandrasekhar limit, the Finzi and Wolf (1967) mechanism of slow

electron capture on white dwarfs decreasing the Chandrasekhar mass below the star's mass, and the collapse of degenerate carbon cores once (and if) these pass through the flashing phase (Chechetkin et al. 1976). Only the thermodynamic history differs from that of iron core collapse, not the neutrino physics.

In Chapter 6, the nature of the neutrino flow at each phase in iron core collapse is discussed in the light of numerical simulations. Initially, the core is transparent to neutrinos. The uncertainty in electron capture rates on heavy nuclei and in elemental abundances, especially of free protons, reflects itself in the evolution of the central regions of the core in thermodynamic phase space. We find, however, that the trajectory in the density-temperature plane converges to a common one almost independently of compression rate, equation of state uncertainties, and initial conditions. The density at which neutrinos are trapped (i.e., neutrino occupation numbers are no longer small compared with unity) is obtained. At a higher density, which we determine, these trapped electron neutrinos attain an equilibrium distribution.

The core at this stage consists of three fairly well determined zones: a core-mantle composed of iron peak elements which is adjacent to the silicon burning shell; interior to this, a neutronization shell consisting of alphas, heavy nuclei, free neutrons and some free protons, which is suffering photodecomposition and copious electron capture; an inner core composed primarily of free neutrons with some heavy nuclei, alphas and free protons. Whether

the protons are locked into heavy nuclei or are free is the crux of the equation of state uncertainty. Definitive statements about neutrino distributions must await the resolution of this problem. The neutrino luminosity is dominated by neutrinos emitted in the neutronization shell; whether or not momentum deposition can push off the mantle depends on the flow from this region.

The equation of state uncertainty makes it difficult to determine the density at which the inner core, which collapses homologously (Arnett 1977), halts, accretes matter onto it, and generates a bounce shock wave: it may be at subnuclear densities (Wilson 1977, Arnett 1977) or at supranuclear densities, as in the pre-neutral current collapses.

When the core temperature is sufficiently high, the hot neutron star can lose more energy in muon neutrinos than in electron neutrinos. Conditions under which this can happen are obtained in Chapter 6, and approximations are proposed to treat their flow.

The neutrino transport method used must bridge the regime of diffusive flow of a degenerate Fermi gas in the inner core to the regime of free streaming in the core-mantle. We explore this transition by comparing numerical solutions of the P-1 and flux limited diffusion equations in an idealized test case, a core frozen in structure just prior to bounce. The resulting electron neutrino luminosity is not sufficiently great to cause a supernova explosion: the fourth blowoff mechanism, neutrino momentum deposition, cannot work in the configuration chosen.

As the central density rises, first the electron neutrinos, then the muon neutrinos and antineutrinos, and finally the electron antineutrinos attain equilibrium with the matter in the inner core and collapse with it, escaping on diffusion timescales which are long compared with the dynamical time.

2. THE WEAK INTERACTION TAILORED FOR ASTROPHYSICAL NEUTRINO PROCESSES

The field of neutrino astrophysics has undergone a small revolution within the last few years, an offshoot of the more momentous revolution in high energy physics. There, experiments probing distances much smaller than the nucleon size have displayed the reality of quarks inside the proton and have uncovered new quarks, leptons, and interactions. It was the discovery of the weak neutral current interaction which precipitated the recent flurry of activity in neutrino astrophysics.

2.1 EXPERIMENTS WITH NEUTRINO BEAMS

Experimentalists have presently at their disposal neutrino beams in four different energy regimes. Electron antineutrinos from nuclear reactors have the lowest energy, $\sim$ 1 to 5 MeV, with a flux $\sim 2 \times 10^{13}$ $\bar{\nu}_e$ - $cm^{-2}s^{-1}$ (Avignone 1970). It was with such a reactor, at Savannah River in 1955, that Reines and Cowan first observed a neutrino-induced reaction, $\bar{\nu}_e + p \rightarrow e^+ + n$. Recently, Gurr, Reines, and Sobel (1976) have reported the observation of $\sim$ 6 events attributed to the reaction $\bar{\nu}_e + e^- \rightarrow \bar{\nu}_e + e^-$. This scattering reaction implies a direct coupling occurs between electron neutrinos and electrons; this is written symbolically as $(\bar{\nu}_e \nu_e)(\bar{e}e)$, or $(\bar{\nu}_e e)(\bar{e}\nu_e)$, in the current-current notation with the spacetime properties suppressed (Clayton 1968).

The Cern neutrino beam consists of ν_μ's and $\bar{\nu}_\mu$'s arising from the decay of mesons produced from protons accelerated in the

Cern proton synchrotron; the mean energy is $\sim$ 1.5 GeV (Blietschau et al. 1977). It is with this beam that the first reported neutral current inclusive reaction, $\nu_\mu + A \rightarrow \nu_\mu + X$, occurred (Hasert et al. 1973). Here, A is a heavy nucleus and X is anything. This inclusive reaction implies a coupling $(\bar{\nu}_\mu \nu_\mu)(\bar{u}u)$ and/or $(\bar{\nu}_\mu \nu_\mu)(\bar{d}d)$, where u and d are the up and down quarks, respectively. There are no strangeness changing neutral current interactions $(\bar{\nu}_\mu \nu_\mu)(\bar{s}d)$, as is evidenced, for example, by the fact that the decay rate for the reaction $K_s \rightarrow \mu^+\mu^-$ is at least 4×10^{-9} below the rate for the charged current strangeness changing reaction $K^+ \rightarrow \mu^+\nu_\mu$ (Trippe et al. 1976). There is no evidence for the coupling $(\bar{\nu}_\mu \nu_\mu)(\bar{s}s)$, although it is predicted by theory.

Shortly after the Cern discovery, two groups, HPWF (Benvenuti et al. 1974) and CITF (Barish et al. 1975), confirmed the existence of neutrino-induced inclusive reactions in which no meson is seen in the final state. At FNAL, there are a number of neutrino beams the experimentalist can choose from. The most intense one ($\sim 10^5$ ν_μ cm^{-2} s^{-1}, time averaged) has a mean energy of $\sim$ 15 GeV, and its distribution extends to $\sim$ 300 GeV. Unfortunately ν_μ and $\bar{\nu}_\mu$ are unseparated in this beam, and only $\sim 1.5 \times 10^3$ ν_μ cm^{-2} s^{-1} have energy > 70 GeV. Another type, the dichromatic beam, allows selection of ν_μ or $\bar{\nu}_\mu$, and has the lower energy neutrinos cut out, at the expense of a decreased intensity. There are two energy peaks: the first, centered $\sim$ 50 GeV, with average intensity $\sim 10^3$ ν_μ cm^{-2} s^{-1}, arises from π decay; the second, centered $\sim$ 150 GeV,

with average intensity $\sim 100\ \nu_\mu\ cm^{-2}\ s^{-1}$, arises from K decay (Barish 1978). There are now similar high energy neutrino beams at Cern. Inclusive experiments continue to provide the best neutral current data.

Another neutrino beam, at Brookhaven (BNL), with mean energy $\sim$ 1 GeV, has been used to see elastic neutrino-nucleon scattering: $\nu_\mu + p \to \nu_\mu + p$ (Lee *et al.* 1976, Cline *et al.* 1976 a,b), $\bar{\nu}_\mu + p \to \bar{\nu}_\mu + p$ (Cline *et al.* 1976 a,b). Exclusive single pion production by neutrino scattering, $\nu + p \to \nu + p + \pi^\circ$, $\nu + n + \pi^+$ has been observed (S.J. Barish *et al.* 1974). Reactions with more pions in the final state, as well as the inclusive reaction $\nu + A \to \nu + \pi + X$ have also been observed (Hasert *et al.* 1975).

The leptonic reactions $\bar{\nu}_\mu + e \to \bar{\nu}_\mu + e$ (Hasert *et al.* 1973, Blietschau *et al.* 1976, Faissner *et al.* 1976) and $\nu_\mu + e \to \nu_\mu + e$ (Faissner *et al.* 1976) have been seen at Cern. Although only a few events have been recorded, the demonstration of existence is important: not only is there a $(\bar{\nu}_e \nu_e)(\bar{e}e)$ coupling, but there is also a $(\bar{\nu}_\mu \nu_\mu)(\bar{e}e)$ coupling, a pure neutral current effect.

No low energy neutral current neutrino-hadron experiments that have been successful have been reported, although, for example, an upper limit has been obtained for the reaction $\bar{\nu}_e + d \to \bar{\nu}_e + n + p$ using reactor neutrinos (Gurr *et al.* 1974). Neutrino beams of intermediate energy can be created using the LAMPF meson factory. In particular, ν_e's from μ^+ decay, with mean energy $\sim$ 30 MeV and intensity $\sim 10^8\ \nu_e\ cm^{-2}\ s^{-1}$, are being produced (Donnelly *et al.* 1974,

1975); this beam is being used to study $\nu_e + e \rightarrow \nu_e + e$, the only purely leptonic scattering reaction involving electrons and neutrinos not yet observed. Some nuclear experiments have been suggested: the inelastic scattering reaction $\nu + A \rightarrow \nu + A^*$, where A^* is an excited state of nucleus A, can, perhaps, be seen in these beams (Donnelly et al. 1974, 1975).

This exhausts the energy ranges of neutrino beams under man's control: 2 MeV $\bar{\nu}_e$'s in nuclear reactors, 20 MeV ν_e's, $\bar{\nu}_\mu$'s at meson factories, 2 GeV ν_μ, $\bar{\nu}_\mu$ at Cern, BNL, Serpukhov, and 20-200 GeV ν_μ, $\bar{\nu}_\mu$ at the highest energy accelerators, FNAL and now Cern.

Natural sources of neutrinos exist in the cosmos. The most familiar source is (presumably) the sun; ν_e's are produced by the $p + p \rightarrow d + e^+ + \nu_e$ reaction with mean energy $\sim$ 0.2 MeV, and flux at earth $\sim 6 \times 10^{10}$ ν cm^{-2} s^{-1} (Bahcall and Ulrich 1976). As is well known, the higher energy ($\sim$ 7 MeV) solar neutrinos arising primarily from ^{8}B decay (predicted flux $\sim 5 \times 10^6$ cm^{-2} s^{-1}) do not give the theoretically expected counting rate for the reaction $\nu_e + {}^{37}Cl \rightarrow e^- + {}^{37}Ar$ which occurs in Davis's solar neutrino detector, 100,000 gallons of the cleaning fluid tetrachlorethylene (C_2Cl_4) (Bahcall and Davis 1976). Gravitational collapse of the cores of massive stars is heralded by a burst of electron neutrinos from neutronization with a mean energy 10-20 MeV, and an intensity at earth $\sim 10^{13}$ d^{-2} (cm^{-2} s^{-1}), where d is the distance from the earth to the imploding star in kiloparsecs; the burst lasts for $\sim$ 1 second. Davis's ν_e detector can observe such an event if it is within

$\sim$ 5 kpc (Bahcall 1977). In fact, in 1972, Davis had a high run; perhaps his detector registered a supernova; or perhaps it was just a statistical fluctuation. A large number of $\bar{\nu}_e$, ν_μ, $\bar{\nu}_\mu$ are also emitted, arising from thermal processes. Landé and collaborators (Landé et al. 1974, Frati et al. 1975) have Cerenkov counters located in the Homestake gold mine, where Davis's detector is, and in two other places, with which they can register cosmic $\bar{\nu}_e$ by the reaction $\bar{\nu}_e + p \rightarrow n + e^+$ occurring in water; the minimum detectable neutrino energy, 15 MeV, is rather too high to see many thermally produced $\bar{\nu}_e$'s from collapse. Much attention has been given recently to very high energy neutrinos which arise from cosmic ray collisions in space and in our atmosphere (Margolis et al. 1977). Perhaps $\sim$ 150 high energy atmospheric ν_μ events have been recorded to date (Reines 1977); for example, an experiment run from 1964-1967 utilized scintillation counters in a gold mine in South Africa to record 39 ν-produced mesons (Reines et al. 1971). Detectors with large volumes of ocean as the target have been proposed to further study these neutrinos (Dumand 1976). At the other extreme, the background neutrino radiation, a relic of the big bang, has mean energy $\sim$ 1/2 millivolt, and intensity $\sim 1.3 \times 10^{11}$ ν cm^{-2} s^{-1} ster^{-1} for each kind in the standard big bang model. If neutrinos are massive, or form a degenerate Fermi sea (Weinberg 1962), these numbers no longer hold. The upper limit on the mass of ν_e is $\sim$ 30 ev (Efremenko 1976), and on the mass of ν_μ is $\sim$ .65 MeV. Cosmological arguments can be used to further restrict the neutrino masses to be at most $\sim$ 50 ev, or

at least 2 GeV (Cowsik and McLelland 1972, Lee and Weinberg 1977).

2.2 GAUGE THEORIES

The history of physics may be understood, ideally, as the attempt to integrate more and more natural phenomena into a unified viewpoint. The recent attempts to unify weak and electromagnetic phenomena led to two theoretical predictions, the existence of neutral current interactions and of a new flavor of quark; both have been confirmed by experiments performed after the predictions were made.

The Weinberg-Salam model (Weinberg 1967, Salam 1968) is a Yang-Mills theory (Yang and Mills 1954, Gell-Mann and Glashow 1961) based on the internal symmetry group $SU(2)^{weak} \otimes U(1)$: the Lagrangian density is invariant under the unitary transformations of this group at each point in space, i.e., under gauge transformations of the second kind. If the ground state (vacuum) is not invariant under this group, the gauge symmetry is termed spontaneously broken. The gauge group has four generators, three components of weak (as opposed to strong) isospin arising from $SU(2)^{weak}$, and one weak hypercharge operator arising from U(1). To each generator, there is associated a massless spin one meson, a gauge vector boson. The electric charge, a linear combination of the third component of weak isospin and weak hypercharge, generates a one-dimensional subgroup of the gauge group, under which the vacuum is invariant. The gauge vector boson of this group is the photon, which is massless. There is a three-dimensional subgroup of the gauge group under which the

vacuum is not invariant; the vector mesons associated with the three generators of this group can obtain a mass, by a mechanism first expounded by Higgs (1964). One assumes the existence of a doublet (under SU(2) rotations) of complex scalar particles (four real fields) with a specific form of self-coupling. This self-interaction ensures that in the state of lowest energy, the scalar field has a nonvanishing expectation value. Each massless vector boson which is to become massive absorbs (eats) one of the four real fields to make its longitudinal component. After the magic of the Higgs mechanism has been performed by the model-building theorist, three real scalar fields have disappeared, uniting with three massless vectors to form three massive vectors: the W^+, W^- bosons, carriers of the charged current force, and the Z_o boson, carrier of the neutral current force. In addition, one real scalar field is left, a Higgson, which couples to fermions, to the massive gauge bosons, and to itself. The fermions originally included in the theory were leptons; the extension to hadrons was undertaken by Weinberg (1972). It is the weak fermion-fermion interaction which is of primary concern to us, as the other particles are too heavy to be produced in astrophysical environments. Indeed, the mass of the W, m_w, is $\gtrsim$ 30 GeV according to experiment (Barish 1978), and according to the Weinberg-Salam (W.S.) theory is $\sim$ 70 GeV; the mass of the Z_o, m_z, is theoretically even heavier than the W. The Higgson mass is estimated to be greater than a few GeV (Weinberg 1976). If there is more than one Higgs doublet in the theory, this lower bound on the

Higgson mass may no longer hold. It is remarkable that this theory may predict a nonzero cosmological constant; the cosmological constant can be viewed as a measure of the stress-energy of the vacuum (Zel'dovich 1967), and this stress-energy enters into Einstein's equations. A number of other gauge models have been proposed, based upon the Yang-Mills Lagrangian, and utilizing the Higgs mechanism to generate the large mass difference between the photon and the weak vector mesons.

The fermion-vector boson interaction is described by the Lagrangian

$$L = g\, J_\mu^{CC}\, W^{\mu\dagger} + g\, J_\mu^{CC\dagger} W^\mu + \tilde{g}\, J_\mu^{NC}\, Z^\mu + e\, J_\mu^{em}\, A^\mu \quad . \quad (2.1)$$

Here, the electromagnetic current is the conventional one

$$J_\mu^{em} = -\bar{e}\gamma_\mu e - \bar{\mu}\gamma_\mu \mu + 2/3\ \bar{u}\gamma_\mu u - 1/3\ \bar{d}\gamma_\mu d - 1/3\ \bar{s}\gamma_\mu s + 2/3\ \bar{c}\gamma_\mu c \quad (2.2)$$

as is the charged current

$$J_\mu^{CC} = \bar{\nu}_e \gamma_\mu (1-\gamma_5) e + \bar{\nu}_\mu \gamma_\mu (1-\gamma_5)\mu + \bar{u}\gamma_\mu (1-\gamma_5)(\cos\theta_c\ d + \sin\theta_c\ s) + \bar{c}\gamma_\mu (1-\gamma_5)(-d\ \sin\theta_c + s\ \cos\theta_c) \quad (2.3)$$

The gamma matrix notation is that of Bjorken and Drell (1964) and Abers and Lee (1973). In this notation, $1/2(1-\gamma_5)$ projects out left-handed helicity. The lepton fields are e, μ, ν_e, ν_μ and the quark fields are u, d, s, c. There is an implicit sum over quark color indices in these currents. The Cabibbo angle, θ_c, is $\sim 13°$ (Roos 1974). The coupling constants g and $\tilde{g}$ are related to the Fermi

coupling constant, $G_F = 1.01 \times 10^{-5}\ m_p^{-2}$, by

$$\frac{G_F}{\sqrt{2}} = \frac{g^2}{m_W^2} = \frac{2\tilde{g}^2}{m_Z^2} \tag{2.4}$$

The coupling constant e is the usual electric charge, and A_μ is the photon field.

In the limit in which only u and d quarks are important, the hadronic pieces of these currents involve only

the isoscalar vector current:

$$J_\mu^S = 1/3\ \bar{q}\gamma_\mu q \tag{2.5}$$

the isovector vector current:

$$J_\mu^{Vi} = \bar{q}\gamma_\mu t^i q \quad , i = 1,2,3 \tag{2.6}$$

the isoscalar axial vector current:

$$J_{5\mu}^S = 1/3\ \bar{q}\gamma_\mu\gamma_5 q \tag{2.7}$$

the isovector axial vector current:

$$J_{5\mu}^{Vi} = \bar{q}\gamma_\mu\gamma_5 t^i q \ , \ i = 1,2,3 \tag{2.8}$$

Here, q is a column vector consisting of 2 Dirac spinor fields:

$$q = \begin{pmatrix} u \\ d \end{pmatrix}$$

Under the symmetry group of isotopic spin, q transforms as a doublet. The matrices t^i are given by $\tau^i/2$, with τ^i the Pauli spin matrices. We further define

$$J_\mu^{V\pm} = J_\mu^{V1} \pm i\ J_\mu^{V2} \tag{2.9}$$

$$J_{5\mu}^{V\pm} = J_{5\mu}^{V1} \pm i\ J_{5\mu}^{V2} \tag{2.10}$$

In this notation, neglecting the strange and charm degrees of freedom,

$$J^{em}_{\mu,\ hadron} = \frac{1}{2} J^{S}_{\mu} + J^{V3}_{\mu} \tag{2.11}$$

$$J^{CC}_{\mu,\ hadron} = \cos\theta_c \ (J^{V+}_{\mu} - J^{V+}_{5\mu}) \tag{2.12}$$

The neutral current can be parametrized by

$$\begin{aligned} J^{NC}_{\mu} = {} & \alpha_e \bar{\nu}_e \gamma_\mu (1 - \gamma_5)\nu_e + \alpha_\mu \bar{\nu}_\mu \gamma_\mu (1 - \gamma_5)\nu_\mu \\ & + \bar{e}\gamma_\mu (c_{Ve} - c_{Ae}\gamma_5)\, e + \bar{\mu}\gamma_\mu (c_{V\mu} - c_{A\mu}\gamma_5)\mu \\ & + \bar{u}\gamma_\mu (c_{Vu} - c_{Au}\gamma_5)u + \bar{d}\gamma_\mu (c_{Vd} - c_{Ad}\gamma_5)d \\ & + \bar{s}\gamma_\mu (c_{Vs} - c_{As}\gamma_5)s + \bar{c}\gamma_\mu (c_{Vc} - c_{Ac}\gamma_5)c \end{aligned} \tag{2.13}$$

This neutral current is not general: assumptions have already been made. It is assumed that the current is a linear combination of vector and axial vector pieces, which is true of all gauge models, and the neutrino couples in a purely left-handed manner. The hadronic piece of this current may be written in terms of $SU(2)^{strong}$ currents (when s and c are not involved) as

$$J^{NC}_{\mu,\ hadron} = c_{Vo}\, J^{S}_{\mu} + c_{V1}\, J^{V3}_{\mu} - c_{Ao}\, J^{S}_{5\mu} - c_{A1}\, J^{V3}_{5\mu} \tag{2.14}$$

The values for the various coefficients in the W.S. theory, which depend only upon one parameter, the Weinberg angle θ_W, are listed in Table 1, together with a figure showing the range of $\sin^2\theta_W$ allowed by the experiments (Figure 1).

2.3 THE CURRENT-CURRENT LIMIT

In astrophysical applications and in experiments performed

to date, the momenta transferred in the reactions are much less than the masses of the intermediate bosons. The W and Z propagators are proportional to delta functions of position and time in this limit, and the fermion-fermion interaction, which is mediated by W and Z exchange, reduces to the current-current form. An appropriate weak interaction effective Lagrangian is, for charged currents

$$L_{CC} = - \frac{G}{\sqrt{2}} J_{\mu}^{CC} J_{CC}^{\mu\dagger} \tag{2.15}$$

and for neutral currents

$$L_{NC} = - \frac{G}{2\sqrt{2}} J_{\mu}^{NC} J_{NC}^{\mu} \tag{2.16}$$

There may be many neutral intermediate bosons, hence many neutral currents; the effective Lagrangian is then the sum over many terms of the form 2.16.

We now decompose the effective neutral current Lagrangian into its component parts, such as $(\bar{\nu}_{\mu} \nu_{\mu})(\bar{e}e)$, then we blind ourselves to the path we have taken from gauge theories, and unravel the properties of the effective interaction from experiments alone. Notable in this effort are the experimentalists themselves and Sakurai and collaborators (Hung and Sakurai 1977 a,b, Sakurai 1976).

Consider first the spacetime structure of the neutral current: does it involve scalar (S), pseudoscalar (P), and tensor (T), or the more familiar vector (V) and axial vector (A)? Pure S and P have been ruled out (Barish 1978); a linear combination of S, P, and T is still possible.

Before dealing with each of the current-current terms which can affect astrophysics, we first treat some of the possibilities that have been suggested which modify the neutral current Lagrangian.

A new heavy charged lepton, the tau, has apparently been discovered (Perl et al. 1977). It is too massive to play a role in astrophysics. Presumably, however, it has its own neutrino, ν_τ. The limit on the mass of the tau neutrino is at the moment rather poor, 600 MeV. If the ν_τ is massless, or of small mass, and couples as $(\bar{\nu}_\tau \nu_\tau)(\bar{q}q)$, and $(\bar{\nu}_\tau \nu_\tau)(\bar{e}e)$ in a fashion similar to ν_μ, then it plays essentially the same astrophysical role as ν_μ's do, as we shall see. The more light neutrinos there are, the greater the astrophysical implications. If there is an interaction by which left-handed neutrinos are channeled into right-handed ones, then the evolution of right-handed neutrinos in a collapsing stellar core would have to be followed in time. Do electron neutrinos develop an amplitude to be ν_μ as they propagate? Such neutrino oscillations have been proposed by Pontecorvo (1967) to explain the low solar neutrino counting rate. Reactor $\bar{\nu}_e$'s have been used to search for oscillations; no evidence has yet been found (Sobel 1976).

2.4 $(\bar{e}e)(\bar{q}q)$, $(\bar{q}q)(\bar{q}q)$, $(\bar{e}e)(\bar{\mu}\mu)$, $(\bar{e}e)(\bar{e}e)$

Recent experiments on atomic systems (Lewis et al. 1977, Baird et al. 1977) and in nuclei (Barnes et al. 1978) give results below those predicted on the basis of W.S. theory. The theoretical calculations upon which those predictions were based have recently become clouded in uncertainty. Some theorists have seen the apparent smallness of

parity violation as evidence for another neutral weak boson, Z_o'. The sum of the two current-current Lagrangians, one from Z_o exchange and one from Z_o' exchange, can be arranged to give no parity violation in atoms and nuclei, and yet agree with W.S.-like models as far as the neutrino interaction with matter is concerned. If there are two or more neutral currents, then the parity violation measurements will shed no light on the neutrino-nucleon and neutrino-electron couplings; with one neutral current only, such information is obtained.

2.5 $(\bar{\nu}_e\nu_e)(\bar{e}e)$, $(\bar{\nu}_\mu\nu_\mu)(\bar{e}e)$

The electron-type neutrinos interact with electrons via the exchange of both charged and neutral intermediate vector bosons. The charged current Lagrangian

$$L_{cc} = -\frac{G}{\sqrt{2}}\ \bar{\nu}_e(x)\gamma_\mu(1-\gamma_5)e(x)\ \bar{e}(x)\gamma_\mu(1-\gamma_5)\nu_e(x)$$

is amenable to a Fierz transformation which brings the interaction to the form of the neutral piece. The $(\bar{\nu}_e\nu_e)(\bar{e}e)$ effective interaction Lagrangian is then

$$L = -\frac{G}{\sqrt{2}}\ \bar{\nu}_e\gamma_\mu(1-\gamma_5)\nu_e\ :\ \bar{e}\gamma^\mu(C_{Ve} - C_{Ae}\gamma_5)e \qquad (2.17)$$

The coefficients C_{Ve}, C_{Ae} are related to the neutral coefficients c_{Ve}, c_{Ae} (see equation 2.13) by

$$C_{Ve} = \alpha_e c_{Ve} + 1 \qquad (2.18)$$

$$C_{Ae} = \alpha_e c_{Ae} + 1 \qquad (2.19)$$

Muon neutrinos, and perhaps tau neutrinos, exchange only the neutral intermediate vector boson with the electron. No fierzing is necessary. The interaction is again given by 2.17, with the replacements $\nu_e \to \nu_\mu$, $C_{Ve} \to C_{V\mu}$, $C_{Ae} \to C_{A\mu}$, with

$$C_{V\mu} = \alpha_\mu \, c_{Ve} = C_{Ve} - 1 \tag{2.20}$$

$$C_{A\mu} = \alpha_\mu \, c_{Ae} = C_{Ae} - 1 \tag{2.21}$$

The second equality holds if muon-electron universality is assumed.

Eventually C_{Ve}, C_{Ae}, $C_{V\mu}$, and $C_{A\mu}$ may be determined entirely by experiment; at the moment, the uncertainties are so great that we must resort to a model to evaluate these coefficients, which are given in Table 1 for the W.S. model. The data from the $\bar{\nu}_e + e^- \to \bar{\nu}_e + e^-$, $\bar{\nu}_\mu + e^- \to \bar{\nu}_\mu + e^-$, $\nu_\mu + e^- \to \nu_\mu + e^-$ experiments are analyzed in Figure 1 in terms of the allowed range of the one paramenter upon which these theories depend. Cross sections for these and other reactions going by the $(\bar{\nu}\nu)(\bar{e}e)$ coupling are given in Table 2.

In the late stages of stellar evolution, when the stellar core is burning carbon or heavier nuclei, the heat energy generated by nuclear reactions and gravitational contraction is radiated away primarily in the form of neutrino antineutrino pairs. The dominant energy loss mechanisms are due to the $(\bar{\nu}\nu)(\bar{e}e)$ coupling: the pair annihilation neutrino process $(e^+e^- \to \nu\bar{\nu})$, the plasmon-neutrino process $(\gamma_{p\ell} \to \nu\bar{\nu})$ and the photoneutrino process $(\gamma_{p\ell} + e \to e + \nu + \bar{\nu})$. Knowledge of the energy loss rates per unit volume is sufficient to calculate the effects of neutrino emission on stellar evolution; these

were given in the charged current only case ($C_{Ve} = C_{Ae} = 1$, $C_{A\mu} = C_{A\mu} = 0$) by Beaudet, Petrosian, and Salpeter (1967). The addition of neutral currents changes the emission rates by less than a factor of two in the W.S. model, for $\sin^2\theta_w \sim .3$ (Dicus 1972).

When the core of the star collapses, it becomes opaque to neutrinos. An equilibrium distribution of neutrinos can build up. In that case, differential production rates are required. These are calculated in Chapter 5 for the processes $e^+e^- \to \nu\bar{\nu}$ and $\gamma_{pl} \to \nu\bar{\nu}$. Differential scattering rates are also needed for the scattering of neutrinos of all types by electrons; this is dealt with in Chapter 4.

2.6 $(\bar{\nu}_e\nu_e)(\bar{\nu}_e\nu_e)$, $(\bar{\nu}_\mu\nu_\mu)(\bar{\nu}_e\nu_e)$

The scattering of neutrinos by neutrinos can become important in supernova cores once the density of neutrinos can build up to near equilibrium values. The Lagrangian for $\nu_e + \nu_e \to \nu_e + \nu_e$ and $\nu_e + \bar{\nu}_e \to \nu_e + \bar{\nu}_e$ is

$$L = -\frac{G}{2\sqrt{2}}\,\alpha_e^2\;\bar{\nu}_e\gamma_\mu(1-\gamma_5)\nu_e\cdot\bar{\nu}_e\gamma^\mu(1-\gamma_5)\nu_e \quad , \qquad (2.22)$$

and for $\nu_\mu + \nu_e \to \nu_\mu + \nu_e$, $\bar{\nu}_\mu + \nu_e \to \bar{\nu}_\mu + \nu_e$, $\nu_e + \bar{\nu}_e \to \nu_\mu + \bar{\nu}_\mu$ etc. is

$$L = -\frac{G}{\sqrt{2}}\,\alpha_e\alpha_\mu\;\bar{\nu}_e\gamma_\mu(1-\gamma_5)\nu_e\;\bar{\nu}_\mu\gamma^\mu(1-\gamma_5)\nu_\mu \qquad (2.23)$$

In the W.S. model, $\alpha_e = \alpha_\mu = 1$. Cross sections for the astrophysically important reactions dependent on the $(\bar{\nu}\nu)(\bar{\nu}\nu)$ coupling are given in Table 2.

2.7 $(\bar{\nu}\nu)(\bar{n}n)$, $(\bar{\nu}\nu)(\bar{p}p)$

The hadronic parts of the three currents 2.2, 2.3, and 2.13 are expressed in terms of quark fields. In astrophysical processes under consideration here, we excite no nucleon resonances; the hadronic currents can be written in terms of nucleon fields. The matrix elements of the chiral currents 2.5 - 2.8 between nucleon states are given in terms of form factors

$$\langle p'\sigma'\tau'|J_\mu^S(0)|p\sigma\tau\rangle = \frac{\langle\tau'|\tau\rangle}{\sqrt{2E2E'}}\bar{u}'(g_{V0}\gamma_\mu - i\sigma_{\mu\lambda}\frac{q^\lambda}{2m_n}f_{V0})u \tag{2.24}$$

$$\langle p'\sigma'\tau'|J_\mu^{Vi}(0)|p\sigma\tau\rangle = \frac{\langle\tau'|t^i|\tau\rangle}{\sqrt{2E2E'}}\bar{u}'(g_{V1}\gamma_\mu - i\sigma_{\mu\lambda}\frac{q^\lambda}{2m_n}f_{V1})u \tag{2.25}$$

$$\langle p'\sigma'\tau'|J_{5\mu}^S(0)|p\sigma\tau\rangle = \frac{\langle\tau'|\tau\rangle}{\sqrt{2E2E'}}\bar{u}'(g_{A0}\gamma_\mu - \frac{f_{A0}}{2m_n}q_\mu)\gamma_5 u \tag{2.26}$$

$$\langle p'\sigma'\tau'|J_{5\mu}^{Vi}(0)|p\sigma\tau\rangle = \frac{\langle\tau'|t^i|\tau\rangle}{\sqrt{2E2E'}}\bar{u}'(g_{A1}\gamma_\mu - \frac{f_{A1}}{2m_n}q_\mu)\gamma_5 u \tag{2.27}$$

The use of these currents, which involve only u and d quarks, ignores the $\bar{s}s$ virtual pair content of the proton sea. The initial nucleon state is $|p\sigma\tau_3\rangle$, with p the momentum (E is the energy), σ the spin projection on the z-axis, and τ the third component of isospin; $|p'\sigma'\tau'\rangle$ is the final nucleon state. The nucleon states are normalized to unity. The initial and final nucleon Dirac spinors, u, u', are normalized by

$$\bar{u}(p\sigma)\gamma^\mu u(p\sigma) = 2p^\mu \tag{2.28}$$

Momentum wave functions are box-normalized to a volume Ω , which is not explicitly written. The nucleon mass is m_n, $q = p - p'$ is the four-momentum transfer, and the form factors are all functions of q^2. Isoinvariance is assumed and possible second-class current effects have been ignored. Linear combinations of the vector form factors give the usual electromagnetic form factors.

When the four-momentum transfers are much less than the nucleon mass, the $q^2 = 0$ limit can be taken in the form factors. Then, only the g_{V0}, g_{V1}, g_{A0}, g_{A1} terms survive. By the conserved vector current hypothesis, we have

$$g_{V0}\ (q^2 = 0) = g_{V1}\ (q^2 = 0) = 1 \tag{2.29}$$

The axial terms, g_{A1} and g_{A0}, are obtained experimentally and estimated theoretically respectively. The isovector axial vector form factor, which we hereafter call g_A, is

$$g_A = g_{A1}\ (q^2 = 0) \simeq 1.25 \tag{2.30}$$

The isoscalar axial vector form factor is estimated by Adler (1975) to be

$$g_{A0}\ (0) \simeq \frac{3}{5}\, g_A \simeq 0.75 \tag{2.31}$$

In most neutral current theories, c_{A0} vanishes, so the value of $g_{A0}(0)$ is not required.

In this limit, the effective neutral current Lagrangian for the $(\bar{\nu}\nu)(\bar{q}q)$ interaction can be expressed in terms of an effective

hadronic current

$$L = -\frac{G}{\sqrt{2}} \bar{\nu}_e \gamma_\mu(1-\gamma_5)\nu_e \quad J^\mu_{had,\ NC} \tag{2.32}$$

which is, in turn, expressible in terms of the composite proton and neutron fields, p(x) and n(x):

$$\begin{aligned} J^\mu_{had,\ NC} &= \bar{p}\gamma^\mu(C_{Vp}-C_{Ap}\gamma_5)p + \bar{n}\ \gamma^\mu(C_{Vn}-C_{An}\gamma_5)\ n \\ &= \bar{N}\left[\gamma^\mu(C_{V0}+C_{V1}t_3) - \gamma^\mu\gamma_5\ (C_{A0}+C_{A1}t_3)\right] N \end{aligned} \tag{2.33}$$

Here, the nucleon field, an isodoublet, is

$$N = \begin{pmatrix} p \\ n \end{pmatrix}$$

The proton has its third component of isospin, t_3, positive which is the particle physics convention. The coefficients have the $q^2 = 0$ form factors absorbed into them. How close are we to determining them from experiment alone? Hung and Sakurai (1977b), using the available semileptonic neutral current data, determine two possible solutions for the set of four parameters C_{V0}, C_{V1}, C_{A0}, C_{A1} ; within each solution set, the range allowed for each of the parameters is still rather large. One solution gives values close to those predicted by the W.S. model, with $\sin^2\theta \sim 0.3$; the W.S. coefficients are given in Table 1.

If universality is assumed, the $(\bar{\nu}_\mu \nu_\mu)(\bar{N}N)$ and $(\bar{\nu}_\tau \nu_\tau)(\bar{N}N)$ couplings are exactly the same as the $(\bar{\nu}_e \nu_e)(\bar{N}N)$ coupling.

The charged current Lagrangian is the usual

$$L = -\frac{G}{\sqrt{2}} \cos\theta_c \, \bar{e} \, \gamma_\mu (1 - \gamma_5) \, \nu_e \, J^\mu_{had,\ cc} + \text{h.c.} \qquad (2.34)$$

with h.c. denoting the Hermitian conjugate, and

$$J^\mu_{had,\ cc} = \bar{p} \, \gamma^\mu (1 - g_A \gamma_5) n = \bar{N} \, \gamma^\mu (1 - g_A \gamma_5) t_+ \, N \qquad (2.35)$$

2.8 ALLOWED NUCLEAR TRANSITIONS

There is a formula for the squared transition amplitude which we will apply again and again in calculating charged and neutral current (CC and NC respectively) rates. It is often adequate for our purposes to consider the nucleons as moving nonrelativistically (even for nucleons in the interior of a nucleus); terms of order v/c are neglected; the nucleon currents reduce to

$$J^0_{had,\ NC} = N^\dagger(x) \, (C_{V0} + C_{V1} t_3) \, N(x) \qquad (2.36a)$$

$$J^i_{had,\ NC} = - N^\dagger(x) \, (C_{A0} + C_{A1} t_3) \, \sigma^i \, N(x) \quad , i=1,2,3 \qquad (2.36b)$$

$$J^0_{had,\ CC} = N^\dagger(x) \, t_+ \, N(x) \qquad (2.37a)$$

$$J^i_{had,\ CC} = -g_A N^\dagger(x) \, t_+ \, \sigma^i \, N(x) \quad , \ i=1,2,3 \qquad (2.37b)$$

where $t_+ = t_x + i t_y$, σ^i are the Pauli spin matrices, and N(x) now denotes the isodoublet of 2-component Pauli spinor fields $\begin{pmatrix} p \\ n \end{pmatrix}$.

The amplitude for a nuclear state $|\, i J_i M_i \,\rangle$ of angular momentum J_i , and z-component of angular momentum, M_i , consisting of A_i nucleons to emit a neutrino-antineutrino pair of momenta q and q'

respectively and go into a final nuclear state $|fJ_fM_f\rangle$ is given by

$$T_{fi} = \langle fJ_fM_f \; ; \; \nu(q) \; \bar{\nu}(q') \; |T| iJ_iM_i \rangle$$

where T is the T-matrix, defined in terms of the S-matrix by

$$\langle b|S|a\rangle = \delta_{b,a} - 2\pi i \; \delta(E_b - E_a) \; \langle b|T|a\rangle \tag{2.38}$$

where a is the initial state with energy E_a, and b is the final state with energy E_b. The amplitude for the transition to lowest order in the weak coupling constant is

$$T_{fi} = \frac{G}{\sqrt{2}} \; \frac{\bar{u}(q)\gamma_\mu(1-\gamma_5)v(q')}{\sqrt{2\nu 2\nu'}} \int \langle fJ_fM_f|J^\mu_{NC}(x)|iJ_iM_i\rangle \, d^3x e^{-i(q+q')\cdot x}$$

$$= (2\pi)^3\delta^{(3)}(p_i - p_f - q - q') \; \frac{G}{\sqrt{2}} \; \frac{\bar{u}(q)\gamma_\mu(1-\gamma_5)v(q')}{\sqrt{2\nu 2\nu'}} \langle f|J^\mu_{NC}(0)|i\rangle \tag{2.39}$$

Here, ν is the neutrino energy, u(q) is its spinor, ν' is the antineutrino's energy and v(q') is its spinor.

We next take the modulus squared of T_{fi} and sum over both the nuclear and neutrino spins; since the neutrinos are left-handed, they have only one helicity, and the sum over spins is implied. The sum over neutrino and antineutrino spinors is easily performed, using

$$\sum u(q)\bar{u}(q) = \not{q} \quad , \quad \sum v(q)\bar{v}(q) = \not{q} \tag{2.40}$$

with the result

$$\sum_{\substack{\text{neutrino} \\ \text{spins}}} |T_{fi}|^2 = (2\pi)^3\delta(p_i - p_i - q - q') \; \frac{G^2}{8\nu\nu'} \; \text{Tr} \; \not{q}\gamma_\mu(1-\gamma_5)\not{q}'\gamma_\nu(1-\gamma_5)$$

$$\cdot \langle f|J^\mu(0)|i\rangle \; \langle i|J^{\nu\dagger}(0)|f\rangle \tag{2.41}$$

The trace over gamma matrices is readily performed; we use this result often:

$$\mathrm{Tr}\ \not{q}\gamma_\mu(1-\gamma_5)\not{q}'\gamma_\nu(1-\gamma_5) = 8(q_\mu q'_\nu + q_\nu q'_\mu - q\cdot q' g_{\mu\nu} + i\,\varepsilon_{\nu\mu}(q',q)) \qquad (2.42a)$$

Here,

$$\varepsilon_{\nu\mu}(q',q) \equiv \varepsilon_{\nu\mu\alpha\beta}\, q^{\alpha'} q^{\beta} \qquad (2.42b)$$

where $\varepsilon_{\nu\mu\alpha\beta}$ is the completely antisymmetric 4-tensor, with $\varepsilon_{0123} = 1$. The (+---) metric is used.

Now, we turn to the evaluation of the hadronic current matrix elements in the nonrelativistic limit:

$$\langle f|J^0(0)|i\rangle = \langle f|\sum_{a=1}^{A}(C_{V0}+C_{V1}\ t_3^{(a)})\ e^{i\,\underset{\sim}{k}\cdot\underset{\sim}{r}_a}|i\rangle \qquad (2.43a)$$

$$\langle f|\underset{\sim}{J}(0)|i\rangle = -\langle f|\sum_{a=1}^{A}(C_{A0}+C_{A1}\ t_3^{(a)})\,\underset{\sim}{\sigma}^{(a)} e^{i\,\underset{\sim}{k}\cdot\underset{\sim}{r}_a}|i\rangle \qquad (2.43b)$$

The sum is over the A nucleons in the nucleus, with $\underset{\sim}{r}_a$ the position of each nucleon taken relative to the nuclear center of mass, and $\underset{\sim}{k} = \underset{\sim}{p}_i - \underset{\sim}{p}_f = -(\underset{\sim}{q} + \underset{\sim}{q}')$. These matrix elements are sometimes called the form factors for the operators $(C_{V0} + C_{V1}\ t_3)$ and $-(C_{A0} + C_{A1}\ t_3)\,\underset{\sim}{\sigma}$ respectively. The positions $\underset{\sim}{r}_a$ are effectively restricted to lie within the nuclear radius, R, a distance of $\sim$ 6.5 fm for ^{209}Bi, the heaviest stable nucleus. For momentum transfers $|\underset{\sim}{k}| \lesssim R^{-1}$ $\sim$ (30 MeV for Bi), we may expect that a multipole expansion of the phase $e^{i\,\underset{\sim}{k}\cdot\underset{\sim}{r}_a}$ will be useful. The first term in this expansion gives the allowed transitions. Higher order terms in k are forbidden

transitions; at the same time as these are treated, the relativistic terms which were neglected in the current must also be included.

For allowed transitions, the spin-summed-matrix-element-squared reduces to

$$\text{NC:} \quad \sum_{\text{spin}} |T_{fi}|^2 = (2\pi)^3 \, \delta^{(3)} (\underset{\sim}{p}_i - \underset{\sim}{p}_f - \underset{\sim}{q} - \underset{\sim}{q}') \, G^2 \left\{ |M_F|^2 (1 + \hat{q}\cdot\hat{q}') + |M_{GT}|^2 \left(1 - \tfrac{1}{3} \hat{q}\cdot\hat{q}'\right) \right\} \tag{2.44}$$

where $\hat{q}$ denotes the unit vector in the direction of the neutrinos momentum. The allowed Fermi matrix element is

$$\text{Fermi:} \quad |M_F|^2 \equiv (2J_i + 1) \left\langle (C_{V0} + C_{V1} \, t_3) \right\rangle_{fi}^2 = \sum_{M_i M_f} \left| \left\langle f J_f M_f \right| \sum_{a=1}^{A} (C_{V0} + C_{V1} \, t_3^{(a)}) \left| i J_i M_i \right\rangle \right|^2 \tag{2.45a}$$

and the allowed Gamow-Teller matrix element is

$$\text{Gamow-Teller:} \quad |M_{GT}|^2 \equiv (2J_i + 1) \left\langle (C_{A0} + C_{A1} \, t_3) \underset{\sim}{\sigma} \right\rangle_{fi}^2 = \sum_{M_i M_f} \left| \left\langle f \right| \sum_{a=1}^{A} (C_{A0} + C_{A1} \, t_3^{(a)}) \underset{\sim}{\sigma}^{(a)} \left| i \right\rangle \right|^2 \tag{2.45b}$$

The formula 2.44 is the one we wished to derive. It holds for ν_μ as well as ν_e, and, if we replace $\underset{\sim}{q}$ by $-\underset{\sim}{q}$ in the momentum conserving delta function, it holds for neutrino-nucleus and antineutrino-nucleus scattering. Low energy cross sections for neutrino scattering by nucleons, bound and free, are given in Table 2.

For charged current processes, a formula very similar to 2.44 can be derived for β-decay:

$$\text{CC:} \quad \sum_{\text{spins}} |T_{fi}|^2 = (2\pi)^3 \, \delta^{(3)}(\underset{\sim}{p}_i - \underset{\sim}{p}_f - \underset{\sim}{p}_e - \underset{\sim}{q}) \; G^2 \; F(Z_i, E_e)$$
$$\cdot \left\{ |M'_F|^2 (1 + V_e \, \hat{p}_e \cdot \hat{q}) + |M'_{GT}|^2 (1 - \tfrac{1}{3} V_e \hat{p}_e \cdot \hat{q}) \right\} \qquad (2.46)$$

where the momentum, energy, and speed of the electron are $\underset{\sim}{p}_e$, E_e, and V_e respectively, and $\underset{\sim}{q}$ is the antineutrino's momentum. The matrix elements are

$$\text{Fermi:} \quad |M'_F|^2 = (2J_i + 1) \langle t_+ \rangle^2_{fi} = \sum_{M_i M_f} |\langle f| \sum_{a=1}^{A} t_+^{(a)} |i\rangle|^2 \qquad (2.47a)$$

$$\text{Gamow-Teller:} \quad |M'_{GT}|^2 = (2J_i + 1) \; g_A^2 \langle \underset{\sim}{\sigma} t_+ \rangle^2_{fi}$$
$$= \sum_{M_i M_f} |\langle f| \sum_{a=1}^{A} \underset{\sim}{\sigma}^{(a)} \; t_+^{(a)} |i\rangle|^2 \; g_A^2 \qquad (2.47b)$$

The function $F(Z_i, E_e)$ is the usual Coulomb factor which describes the distortion of the outgoing electron wave due to Coulomb interactions with the nucleus (Konopinski 1966). The derivation of 2.46 does not follow that of 2.44: a Coulomb wave of the electron replaces the free wave of the neutrino. The same formula may be applied to free electron capture, except, of course, the momentum conserving delta function must be modified to treat the new kinematics, and $t_+ \to t_-$; for β^+ -decay, $Z \to -Z$ in F, $t_+ \to t_-$.

The notation $\langle t_+ \rangle^2_{fi}$ is a minor variant of the usual $\langle 1 \rangle^2_{fi}$, which is often used in β-decay literature (Konopinski 1966); neutral current matrix elements are then expressible in this notation.

The selection rules for CC and NC allowed nuclear reactions are identical:

Fermi: $\Delta J = 0$, $\Delta\pi$ = no, $\Delta T = 0$ (2.48a)

Gamow-Teller: $\Delta J = 0, \pm 1$, no $0 \to 0$, $\Delta\pi$ = no, $\Delta T = 0, \pm 1$ (2.48b)

Here, π is parity and T is total isospin.

The CC formula, 2.46, is used in the calculation of $e^- + p \rightleftarrows n + \nu_e$, and of the capture of electrons by heavy nuclei, $e^- + {}^A_Z \to \nu_e + {}^A(Z-1)$, and its inverse, neutrino absorption $\nu_e + {}^A_Z \to e^- + {}^A(Z+1)$ (Chapter 5).

It can be seen immediately that the operator in the NC Fermi matrix element is $C_{V0}B + C_{V1}\,T_3$, where B is the baryon number operator, and T_3 is the third component of total isospin; the state $|i\rangle$, with Z_i protons, and N_i neutrons, is an eigenstate of both, and therefore

$$\left\langle (C_{V0} + C_{V1}\,t_3) \right\rangle^2_{fi} = \left(C_{V0} A_i + C_{V1} \frac{Z_i - N_i}{2} \right)^2 \delta_{fi} \qquad (2.49)$$

which is zero if f and i are not equal. If C_{V0} is not zero, the cross-section for elastic neutrino-nucleus scattering, $\nu + A \to \nu + A$, is proportional to A^2, a result first noted by Freedman (1974). We treat this reaction in detail in Chapter 4, along with inelastic neutrino-nucleus scattering, $\nu + A \to \nu + A^*$, and neutrino-nucleon scattering $\nu + N \to \nu + N$.

Here, we illustrate the use of 2.44 in calculating the emission rate for neutrino de-excitation of a nuclear state, $A_i \to A_f + \nu + \bar{\nu}$.

The rate of transition is given by Fermi's Golden Rule:

$$\Gamma_{fi} = \frac{1}{2J_i+1} \int \frac{d^3p_f}{(2\pi)^3} \frac{d^3q}{(2\pi)^3} \frac{d^3q'}{(2\pi)^3} 2\pi\ \delta(E_i-E_f-\nu-\nu') \sum_{\text{spins}} |T_{fi}|^2$$

$$= \int \frac{d^3p_f}{(2\pi)^3} \frac{d^3q}{(2\pi)^3} \frac{d^3q'}{(2\pi)^3} 2\pi\ \delta(E_i-\nu-\nu'-E_f)(2\pi)^3\ \delta^{(3)}(\underset{\sim}{p}_i-\underset{\sim}{q}-\underset{\sim}{q}'-\underset{\sim}{p}_f)$$

$$\cdot\ G^2 \left\langle (C_{A0}+C_{A1}\ t_3)\sigma \right\rangle^2 (1 - \tfrac{1}{3}\ \hat{q}\cdot\hat{q}')$$

Only the Gamow-Teller matrix element contributes, since the Fermi matrix element vanishes. We integrate over $\underset{\sim}{p}_f$, getting rid of the momentum conserving delta function, which leaves us with an energy conserving delta function. We neglect the recoil energy imparted to the daughter nucleus by the decay; in so doing, we make an error $\sim Q_{fi}/M_f$ (where $Q_{fi} = M_i-M_f$ is the Q-value of the reaction) which is negligible for heavy nuclei. The remaining integrations are straightforward, yielding

$$\Gamma_{fi} = \frac{G^2}{60\pi^3} Q_{fi}^5 \left\langle (C_{A0}+C_{A1}\ t_3)\sigma \right\rangle_{fi}^2 \qquad (2.50)$$

By multiplying by Q_{fi}, summing over all possible final states for a given initial state, and then summing over all thermally populated initial states weighted by their number densities, we arrive at an energy loss rate per unit volume due to nuclear de-excitation by $\nu\bar{\nu}$ pairs. This process can play a role, but apparently never a dominant one, in the cooling of stars. It has an interesting history. Shortly after Feynman and Gell-Mann proposed their weak interaction theory, Bludman (1958) suggested an alternate theory with

neutral currents included. On the basis of this, Pontecorvo (1963) suggested the possible astrophysical importance of the nuclear de-excitation process, and a number of authors did some calculations to show it had little effect (Baier and Khriplovich 1964, Sakashita and Nishida 1964). In 1974, Bahcall, Trieman, and Zee rediscovered this process, derived equation 2.50, and applied it to solar and white dwarf cooling. A higher temperature and density study of this process again concluded it never dominates stellar energy loss (Crawford et al. 1976).

Another pre-Weinberg-Salam mention of neutral current effects in astrophysics is more interesting. Bahcall and Frautschi (1964) footnote a remark made by Fowler and Hoyle at a 1963 Caltech seminar in which the importance of neutrino-nucleon scattering for supernovae was pointed out. We amplify this remark in the following chapters.

3. TRANSPORT THEORY: THE P-N METHOD FOR NEUTRINOS

Neutrinos produced in the collapsing cores of supernova stars display a rich variety of transport phenomena, reflecting the interplay of the many timescales associated with the event. A snapshot of the core prior to the first hydrodynamical bounce shows three distinct regions: in the center, which is comprised of hot quasi-free nucleons, the neutrinos form a degenerate Fermi gas collapsing with the matter; in the mantle and envelope, the neutrinos are almost freely streaming; in between, there is a transition regime, which encompasses the neutronizing shell, where the neutrino flow is neither in the diffusion nor in the streaming limit. This latter region is crucial for the determination of the effect of neutrinos on the dynamics of a supernova explosion. What scheme can be used to bridge these various regimes?

3.1 THE BOLTZMANN TRANSPORT EQUATION

The Boltzmann transport equation (BTE) provides an adequate starting point. The neutrino distribution function (which we hereafter denote by the symbol df), $n(\underset{\sim}{q},x)$, is the mean occupation number of the state of momentum $\underset{\sim}{q}$ in the neighborhood of the spacetime point $x = (x^{\alpha})$; the BTE describes the temporal and spatial evolution of the df, as well as its momentum space evolution. Since one cannot simultaneously specify position and momentum, how can the df be defined? One strategy is to coarse grain phase space ($(\underset{\sim}{x},\underset{\sim}{q})$ - space) into cells of volume h^3 (h = Planck's constant); the df is then the

cell occupation number, a well-defined quantum mechanical quantity (Osborn and Yip 1966). One can go a long way towards deriving the BTE in this formulation. In any case, if the spatial inhomogeneities of n are of long wavelength compared with the typical de Broglie wavelength, the BTE approach to transport seems to be valid (Osborn and Yip 1966, de Boer and van Weert 1976). This is certainly true for neutrinos in stellar situations.

The neutrinos are produced in accelerating and gravitating matter, and undergo Doppler shifts and ray bending. The neutrinos, when free, follow null geodesics in spacetime, and are restricted to lie on the massless hypersurface $q^2 = 0$, which defines the neutrino energy ν as a function of the 3-momentum $\underset{\sim}{q}$, and the metric tensor $g_{\alpha\beta}$. The BTE takes the form (Ehlers 1971, Lindquist 1966)

$$q^\alpha \frac{\partial n}{\partial x^\alpha} - \Gamma^i_{\alpha\beta}\, q^\alpha q^\beta \frac{\partial n}{\partial q^i} = \nu \mathcal{S}[n] \tag{3.1}$$

where Greek indices run from 0 to 3, Latin indices from 1 to 3, the $\Gamma^\alpha_{\beta\gamma}$ are the Christoffel symbols of the second kind derived from the metric, and the (x) and $\underset{\sim}{q}$ dependences of n and $\mathcal{S}$ are implicit. The combination $\nu\mathcal{S}$, where $\mathcal{S}$ is the source function, a nonlinear operator on the space of df's, is a scalar under arbitrary coordinate transformations, as is n itself. The BTE transforms covariantly, even though it doesn't look manifestly covariant. Any three momentum space variables could have been chosen to parametrize the massless hypersurface; we choose the energy and two angles to specify the neutrino direction, rather than the three momentum space components, below.

3.2 THE SOURCE FUNCTION

The form of $\mathcal{S}$ may often be specified in terms of the transition operator T. Hereafter, we take the further factor of $(2\pi)^3\delta^{(3)}(\underset{\sim}{p}_b-\underset{\sim}{p}_a)$ out of the T-matrix in the defining equation (2.38); the T-matrix is then a Lorentz invariant. If we consider the scattering of neutrinos by fermions of type j, as in νn, νp, and νe scattering, and the scattering is solely 2-body with the particles of type j uncorrelated, then, by Fermi's Golden Rule

$$\mathcal{S}_{\nu j\to\nu j}[n] = -\int\frac{d^3q'}{(2\pi)^3}\int\frac{d^3p}{(2\pi)^3}\sum_\sigma\int\frac{d^3p'}{(2\pi)^3}\sum_{\sigma'}(2\pi)^4\delta^{(4)}(p+q-p'-q')$$

$$\cdot\Big\{\big|\langle\nu(q');j(p'\sigma')|T|\nu(q);j(p\sigma)\rangle\big|^2 f_j(p\sigma)(1-f_j(p'\sigma'))$$

$$\cdot(1-n(q'))n(q) - \big|\langle\nu(q);j(p\sigma)|T|\nu(q');j(p'\sigma')\rangle\big|^2$$

$$\cdot f_j(p'\sigma')(1-f_j(p\sigma))n(q')(1-n(q))\Big\} \qquad (3.2)$$

Here, $f_j(p\sigma)$ is the invariant single particle df for particles of type j, with momentum $\underset{\sim}{p}$ and z-component of spin $\sigma/2$. The relativistic invariance of the combination $\nu\mathcal{S}$ can be made manifest. We first absorb a factor $\sqrt{\nu\nu'EE'}$ into the T-matrix elements, which results in Lorentz invariant quantities by making the momentum space wave functions Lorentz invariant; we then make the compensating change in the momentum space volume elements $d^3p \to d^3p/E$, $d^3p' \to d^3p'/E'$, $d^3q' \to d^3q'/\nu'$ which are all invariant. By d^3q/ν we understand that volume element we obtain by transformation from a local Lorentz frame; it then includes a Jacobian term $\sqrt{-g}\ dq^1dq^2dq^3/\nu$, where $\sqrt{-g}$ is the

square root of the negative of the determinant of the metric tensor.

The first term on the right hand side of 3.2, proportional to n(q), gives scattering "out of the beam," and the second term, proportional to (1-n(q)) gives scattering "into the beam." All distribution functions are evaluated at the same spacetime point: the collision occurs at a single point.

The smallness of the weak coupling constant, G_F, allows us to consider only the lowest order term of the transition operator, which is just the phenomenological current-current Hamiltonian for the scattering of neutrinos described in Chapter 2. There are certain situations when it is inadequate to consider the nucleons and electrons as independent particles due to their interactions with the medium in which they reside. The source function then involves the auto-correlation of the matter currents in the ensemble representing the local stellar state, a formalism which is developed in Appendix 3, and used extensively in Chapters 4 and 5. Matter here and hereafter is meant to refer to everything but neutrinos; it includes electrons, positrons, nucleons, nuclei and photons. As long as neutrinos are themselves uncorrelated with matter, the scattering source function can be written

$$\mathcal{S}_{sc}[n] = -\int \frac{d^3q'}{(2\pi)^3} R(\underset{\sim}{q}\to\underset{\sim}{q}')n(q)(1-n(q')) + \int \frac{d^3q'}{(2\pi)^3} R(q'\to q)n(q')(1-n(q)) \qquad (3.3)$$

where $R(\underset{\sim}{q}\to\underset{\sim}{q}')$ is the scattering kernel, the sum over all of the

individual scattering kernels $R_j(q \to q')$ for each process; $\nu\nu' R(q \to q')$ is an invariant. For matter moving with the flow 4-velocity U, the scattering kernels depend upon the variables $(q \cdot U)$, $(q' \cdot U)$, and $(q \cdot q')$, as well as on the local thermodynamic parameters of the medium, the temperature, density, and chemical potentials for each of the species. In the local rest frame of matter, this dependence reduces to the energies ν, ν', and the angular variable $\hat{q} \cdot \hat{q}'$, where $\hat{q}$ is a unit vector in the direction of the incoming neutrino's momentum.

The emission and absorption of neutrinos, going by the couplings $(\bar{\nu}_e e)(\bar{n}p)$ and $(\bar{e}\nu_e)(\bar{p}n)$, contribute to the source function the term

$$\delta_\beta[n] = - \Gamma_a(q) n(q) + \Gamma_p(q)(1-n(q)) \qquad (3.4)$$

where Γ_p is the production rate for a neutrino of momentum q and Γ_a is the absorption rate. In the local rest frame, these rates depend upon the neutrino's energy ν only, and upon the thermodynamic variables defining the state of matter. Processes which give terms of this form are, for example, $e^- + p \rightleftarrows n + \nu_e$, $e^- + {}^A_Z \rightleftarrows {}^A_{(Z-1)} + \nu_e$, and $n + e^- + p \to n + n + \nu_e$.

Neutrinos can also be produced by thermal processes in $\nu\bar{\nu}$ pairs, through the interactions $(\bar{\nu}\nu)(\bar{e}e)$, $(\bar{\nu}\nu)(\bar{n}n)$, and $(\bar{\nu}\nu)(\bar{p}p)$. Until muons are produced, which happens rather late in the collapse, these mechanisms are the only sources of $\nu_\mu, \bar{\nu}_\mu$ and $\nu_\tau, \bar{\nu}_\tau$; there is no δ_β term for these types of neutrinos. The source function is

$$\mathcal{S}_{th}[n,\bar{n}] = +\int \frac{d^3q'}{(2\pi)^3} R_p(q,q')(1-n(q))(1-\bar{n}(q')) - \int \frac{d^3q'}{(2\pi)^3} R_a(q,q')n(q)\bar{n}(q') \quad (3.5)$$

where $\bar{n}$ is the df for the antiparticle to the particle the evolution of whose df, n, we are following. The production kernel, $R_p(q,q')$, is the rate at which a neutrino of momentum q and an antineutrino of momentum q' are produced; the absorption kernel, $R_a(q,q')$, is the rate for the inverse process, $\nu\bar{\nu}$ annihilation into matter.

The scattering of neutrinos by neutrinos must be treated in a manner different from the scattering of neutrinos by matter. The source function for this process, $\mathcal{S}_{\nu\nu}$, is given in Appendix 1 (equation A1.1); it is a quartic polynomial in the df.

3.3 DETAILED BALANCE AND EQUILIBRIUM

Certain very general relations hold between the kernels in $\mathcal{S}_{sc}$ and $\mathcal{S}_{th}$ which can be determined explicitly from the definitions or through the principle of detailed balance. Thus

$$R(q'\to q) = e^{-\beta((q\cdot U)-(q'\cdot U))}R(q\to q') \quad (3.6)$$

and therefore $\mathcal{S}_{sc}$ vanishes for a Fermi-Dirac (FD) distribution at the matter temperature $k_BT = \beta^{-1}$ with an arbitrary chemical potential μ_ν:

$$n = (e^{\beta((q\cdot U) - \mu_\nu)} + 1)^{-1} \quad (3.7)$$

The function $\mathcal{S}_{th}$ vanishes when both neutrinos and antineutrinos have a FD df with chemical potentials of opposite sign:

$$\mu_\nu = -\mu_{\bar{\nu}} \tag{3.8}$$

when equilibrium is attained; thus the thermal production and absorption kernels satisfy

$$R_a(\underset{\sim}{q},\underset{\sim}{q}') = e^{-\beta((q\cdot U) + (q'\cdot U))} R_p(\underset{\sim}{q},\underset{\sim}{q}') \tag{3.9}$$

If the beta source, δ_β, attains equilibrium (i.e., 3.4 vanishes), the resulting df is

$$n_{EQ} = \left(\frac{\Gamma_a}{\Gamma_p} + 1\right)^{-1} \tag{3.10}$$

If the matter is in nuclear statistical equilibrium, so that the chemical potentials of all the heavy nuclei are related to the proton and neutron chemical potentials, then even though Γ_p includes electron captures on heavies as well as on free nucleons, the relation

$$\Gamma_a(q) = e^{\beta((q\cdot U) - (\mu_p + \mu_e - \mu_n))} \Gamma_p(q) \tag{3.11}$$

holds; then 3.10 is a FD df (3.7) with

$$\mu_{\nu_e} = \mu_p + \mu_e - \mu_n \tag{3.12}$$

the condition for neutrino beta-equilibrium. We append the adjective neutrino to beta-equilibrium to distinguish it from the beta-equilibrium in neutron stars in which the neutrino concentration is zero. If $\bar{\nu}_e$'s were in beta-equilibrium, their chemical potential would satisfy the relation

$$\mu_{\bar{\nu}_e} = \mu_n + \mu_{e+} - \mu_p = \mu_n - \mu_e - \mu_p \tag{3.13}$$

Certainly 3.12 may be satisfied and 3.13 may not be in which case 3.8 is also not satisfied: there can be partial equilibrium. The chemical potentials include the rest mass energy here.

The source function $\delta_{\nu\nu}$ vanishes for an arbitrary FD df.

The matter is always in local thermodynamic equilibrium (LTE): the collapse timescale, the neutrino production, absorption, and scattering timescales are all very long compared with the time it takes matter to relax to equilibrium if it is in a nonequilibrium state. The relaxation is due to Coulombic particle-particle and electromagnetic particle-photon interactions. Strong and electromagnetic nuclear reactions occur on such short timescales that nuclear statistical equilibrium holds; all nuclear concentrations are functions of three thermodynamic variables: the number density of baryons, ρ_B, the temperature, T, and Y_e, the number of protons, bound and free, in the medium per baryon. The matter equation of state is specified by the internal energy of matter per baryon (including rest mass energy), ε, and the pressure of matter, p ; both are functions only of ρ_B, T, and Y_e .

3.4 SPHERICAL COLLAPSE

The evolution of matter in the core is given by the transport equations for four conserved quantities: the baryon number (for ρ_B), the lepton number (for Y_e), the energy (for ε, and indirectly, T), and the momentum (for the mean baryon velocity $\underline{v}$). These equations are coupled to the BTE for each type of neutrino and antineutrino.

The natural reference frame within which to work is the one

in which matter is locally at rest; the use of these comoving coordinates leads to simplifications in the form of $\mathcal{S}$.

We assume the collapse is spherically symmetric. In real supernovae, rotation and magnetic fields may play an important role (Fowler and Hoyle 1964, Le Blanc and Wilson 1970, Meier et al. 1976). The df is then $n = n(\nu,\mu,b,t)$, a function only of the neutrino energy ν, the time t, the cosine of the angle that the neutrino's momentum makes with the radial direction, $\mu = \hat{q}\cdot\hat{e}_r$, and the radial coordinate b which is the baryon number enclosed within a radius r at time t. In this baryon number variable, material derivatives reduce to partial derivatives:

$$\frac{d}{dt} = \left(\frac{\partial}{\partial t}\right)_r + v\left(\frac{\partial}{\partial r}\right)_t = \left(\frac{\partial}{\partial t}\right)_b \tag{3.14}$$

where the subscript b means at constant b, and the velocity is related to the radius

$$r = r(b,t) \tag{3.15}$$

by

$$v(b,t) = \left.\frac{\partial r(b,t)}{\partial t}\right)_b \tag{3.16}$$

The transport equations for the conserved quantities are:

$$\text{baryon number:} \quad 4\pi r^2 \rho_B \left.\frac{\partial r}{\partial b}\right)_t = 1 \tag{3.17a}$$

$$\text{lepton number:} \quad \rho_B \left.\frac{\partial Y_e}{\partial t}\right)_b = -\int \frac{d^3q}{(2\pi)^3} \left(\mathcal{S}_{\nu_e} - \mathcal{S}_{\bar{\nu}_e}\right) \tag{3.17b}$$

$$\text{energy:} \quad \rho_B \left[\left(\frac{\partial \varepsilon}{\partial t} \right)_b + p \left(\frac{\partial}{\partial t} \frac{1}{\rho_B} \right)_b \right]$$

$$= -\int \frac{d^3q}{(2\pi)^3} \nu \left(\delta_{\nu_e}[n] + \delta_{\bar{\nu}_e}[n] + \delta_{\nu_\mu}[n] + \delta_{\bar{\nu}_\mu}[n] \right) \tag{3.17c}$$

$$\text{momentum:} \quad \rho_m \left(\frac{\partial v}{\partial t} \right)_b + 4\pi r^2 \rho_B \left(\frac{\partial p}{\partial b} \right)_t + \frac{G m_b}{r^2} \rho_m$$

$$= -\int \frac{d^3q}{(2\pi)^3} \underset{\sim}{q} \cdot \hat{e}_r [\delta_{\nu_e} + \delta_{\bar{\nu}_e} + \delta_{\nu_\mu} + \delta_{\bar{\nu}_\mu}] \tag{3.17d}$$

where ρ_m is the mass density and $m_b = m(b,t)$ is the mass enclosed within the "radius" b. If composition were not changing in time, and rest mass energy were not transformed to thermal energy, then m_b would be time independent, and m_b would serve as an adequate radial coordinate; it is not an adequate radial coordinate. General relativistic effects have not been included in these equations; they are apparently unimportant until the latest stage of collapse, the post bounce stages (Arnett 1977).

The df's obey the BTE, valid to first order in v/c, given by Castor (1972)

$$\mathcal{D}_s[n] + \mathcal{D}_v[n] = \delta[n] \tag{3.18a}$$

We have separated out two terms on the right hand side, $\mathcal{D}_s$ which takes the same form if the matter is static or moving and $\mathcal{D}_v$ which occurs only if matter is in motion:

$$\mathcal{D}_s[n] = \frac{\partial n}{\partial t} + c\mu \, 4\pi r^2 \rho_B \frac{\partial n}{\partial b} + c \frac{(1-\mu^2)}{r} \frac{\partial n}{\partial \mu} \tag{3.18b}$$

$$\mathcal{D}_v[n] = (1-\mu^2)(\mu(\frac{3v}{r} + \frac{1}{\rho}\frac{\partial\rho}{\partial t})\frac{\partial n}{\partial \mu} + \left[(\frac{3v}{r} + \frac{1}{\rho}\frac{\partial\rho}{\partial t})\mu^2 - \frac{v}{r}\right]\nu\frac{\partial n}{\partial \nu} \qquad (3.18c)$$

As Castor points out, this equation can be derived using the simple metric

$$ds^2 = dt^2 - \left(\frac{db}{4\pi r^2 \rho_B}\right)^2 - r^2(d\theta^2 + \sin^2\theta\, d\phi^2) \qquad (3.19)$$

and equation 3.1. If we begin with the transport equation in the inertial frame where coordinates are (t_I, r, θ, ϕ)

$$\frac{\partial n}{\partial t_I} + c\mu_I \frac{\partial n}{\partial r} + c\frac{(1-(\mu_I)^2)}{r}\frac{\partial n}{\partial \mu_I} = \frac{\nu}{\nu_I}\delta \qquad (3.20)$$

where δ is the source function in the local rest frame and ν_I and $\nu_I\mu$ are the neutrino energy and radial momentum in the inertial frame, the frame of the fixed stars, then transform to comoving coordinates using

$$dt = \gamma\,(dt_I - vdr) \qquad (3.21a)$$

$$\frac{db}{4\pi r^2 \rho_B} = \gamma\,(dr - vdt_I) \qquad (3.21b)$$

$$\nu = \gamma\nu_I\,(1 - v\mu_I) \qquad (3.21c)$$

$$\mu = \frac{\mu_I - v}{1 - v\mu_I} \qquad (3.21d)$$

$$\gamma = (1 - v^2)^{-1/2} \qquad (3.21e)$$

then we obtain 3.18 when terms of order $(v/c)^2$ and $(\frac{\partial v}{\partial t})_b$ are neglected. When the gravitational effects on radiation become

important, there is no global inertial frame from which we can derive these equations by transformation; we must use 3.1 directly. Lindquist (1966) gives the necessary modification of 3.18.

What is the meaning of the $\mathcal{D}_\nu$ term? Consider the case in which the radius scales as $r(b,t) = r(b,0)a(t)$; $\mathcal{D}_\nu$ reduces to $-(\dot{a}/a)\nu\ \partial/\partial\nu$; if n is μ and b independent, the transfer equation reduces to

$$\frac{\partial n}{\partial t} = \frac{\dot{a}}{a}\nu\ \frac{\partial}{\partial \nu}\ n + \delta \quad , \tag{3.22}$$

appropriate to an homogeneous medium which is expanding or contracting; this is also the transfer equation for a Friedmann cosmology. In the absence of sources and sinks, or when sources balance sinks, $\delta = 0$ and $n(\nu,t) = n(\nu a(t)/a(0),\ t = 0)$ solves the equation. As the spatial volume contracts, the momentum space volume expands in such a way that the product, the phase space volume, remains constant. If the neutrinos are completely coupled to matter, then as the core contracts, the neutrino energies scale upward, and the neutrino Fermi energy rises: this is the behaviour of the neutrino gas when the diffusion time from the core becomes long compared with the collapse time ($|a/\dot{a}|$) of the core, i.e., after trapping has occurred.

What methods exist to solve the BTE as it stands? Neutron transport, in nuclear reactors and in our atmosphere, and photon transport, in stellar atmospheres for example, have both had many techniques applied to them, many of which have also been applied to neutrino transfer. Tubbs (1978) has used the Monte Carlo method to

consider the approach of ν_e's to equilibrium in an infinite homogeneous medium consisting of free nucleons and electrons; Y_e is allowed to evolve, but the values of T and ρ are frozen. No transport has yet been included. Yueh and Buchler (1977a,b) have attacked the problem using the discrete ordinate (or S-N) method: one finite differences the BTE in the angular variable μ as well as in the variables ν, b, and t; there are (N+1) - angles in the S-N method, often chosen to be zeros of the Legendre polynomial P_{N+1} ; angular integrals appearing in δ are performed using a Gauss-Legendre quadrature scheme. For plane geometries and simple sources, the S-N method is closely related to the P-(N-1) method; in spherical geometry and for complicated sources, this is not so. Yueh and Buchler (1977b), who have no ρ, T or Y_e evolution, give results when the ν_e df has built up to steady state for N = 2, 4. Lichtenstadt et al. (1977) have tried an S-8 scheme, but have not included time derivatives in the BTE. Wilson (1971, 1974) has modelled the BTE and the hydrodynamic equations with all of the general relativistic effects included. His 1971 work demonstrated that with charged currents only it was difficult to generate a supernova from spherically symmetric collapses; the neutrino physics and equation of state included most of the charged current processes, but not always correctly, and the equation of state was somewhat crude. The numerical modelling was undoubtedly the most sophisticated yet, even if the input physics was not as refined. His 1974 work was the first attempt to include neutral current effects. Along with changes in the input physics,

Wilson has changed his numerical method of solving the BTE; he now uses flux limited diffusion (see below). The P-N or spherical harmonic method can also be applied to treat the flow of neutrinos. The diffusion approximation, both multigroup (energy-dependent) and gray (energy-independent), follow from it.

3.5 THE P-N EQUATIONS

The df is expanded in Legendre polynominals in the angular variable $\mu = \hat{q} \cdot \underset{\sim}{e}_r$, where $\underset{\sim}{e}_r$ is the unit vector in the radial direction:

$$n(\nu,\mu,b,t) = \sum_{\ell=0}^{\infty} n_\ell(b,\nu,t)\ P_\ell(\mu)(2\ell + 1) \tag{3.23a}$$

$$n_\ell(b,\nu,t) = \frac{1}{2}\int_{-1}^{1} P_\ell(\mu)\ n(\nu,\mu,b,t)\ d\mu \tag{3.23b}$$

We further expand the source functions, the scattering, production, and absorption kernels in Legendre polynominals:

$$\mathcal{S}[n] = \sum_{\ell=0}^{\infty} (2\ell+1)\ P_\ell(\mu)\ \mathcal{S}^{(\ell)}[n] \tag{3.24a}$$

$$R(q \to q') = \sum (2\ell+1)\ P_\ell(\hat{q}\cdot\hat{q}')\ R_\ell(\nu \to \nu') \tag{3.24b}$$

$$R_p(q,q') = \sum (2\ell+1)\ P_\ell(\hat{q}\cdot\hat{q}')\ R_{p\ell}(\nu,\nu') \tag{3.24c}$$

$$R_a(q,q') = \sum (2\ell+1)\ P_\ell(\hat{q}\cdot\hat{q}')\ R_{a\ell}(\nu,\nu') \tag{3.24d}$$

Each of the kernels' moments satisfies the same detailed balance relations as do the kernels themselves, 3.6 and 3.9. The equation describing the evolution of the moment n_ℓ has coupled to it a countable infinity of other moments through the nonlinear terms in the scattering and thermal production terms. These equations, derived in Appendix 1, are:

$$\ell=0: \left[\frac{\partial n_0}{\partial t} + c4\pi\rho_B \frac{\partial}{\partial b} r^2 n_1\right]_s + \left[\frac{\dot{\rho}}{3\rho}\nu\frac{\partial}{\partial\nu} n_0 + \left(\frac{3v}{r} + \frac{\dot{\rho}}{\rho}\right)\left(2n_2 + \nu\frac{\partial}{\partial\nu} n_2\right)\right]_v = \mathcal{S}^{(0)} \tag{3.25a}$$

$$\mathcal{S}_\beta^{(0)} = -\Gamma_a(\nu)\, n_0(\nu) + \Gamma_p(\nu)(1-n_0(\nu)) \tag{3.25b}$$

$$\mathcal{S}_{sc}^{(0)} = -\Gamma_s(\nu)\, n_0(\nu) + \int_{\nu'} n_0(\nu')\, R_0(\nu'\to\nu) + \sum_{\ell=0}^{\infty}(2\ell+1)\, n_\ell(\nu)\int_{\nu'} n_\ell(\nu')(R_\ell(\nu\to\nu')-R_\ell(\nu'\to\nu)) \tag{3.25c}$$

$$\mathcal{S}_{th}^{(0)} = \Gamma_{th}(\nu)(1-n_0(\nu)) - \int_{\nu'} R_{p0}(\nu,\nu')\,\bar{n}_0(\nu') + \sum_{\ell=0}^{\infty}(2\ell+1)\int_{\nu'} n_\ell(\nu)\bar{n}_\ell(\nu')(R_{p\ell}(\nu,\nu')-R_{a\ell}(\nu,\nu')) \tag{3.25d}$$

$$\mathcal{S}_{\nu\nu}^{(0)} = \text{(see Appendix 1, equation A1.25 for } \nu_e+\nu_e \to \nu_e+\nu_e) \tag{3.25e}$$

$$\ell=1: \quad \left[\frac{\partial n_1}{\partial t} + \frac{1}{3}\, c4\pi r^2 \rho_B \frac{\partial}{\partial b}\, n_0 + \frac{2}{3}\, c4\pi r^2 \rho_B \frac{\partial}{\partial b}\, n_2 + \frac{2c}{r}\, n_2\right]_s$$

$$+ \left[\frac{1}{5}\left(\frac{4v}{r} + \frac{3\dot{\rho}}{\rho}\right) \nu \frac{\partial}{\partial \nu}\, n_1 + \frac{2}{5}\left(\frac{3v}{r} + \frac{\dot{\rho}}{\rho}\right) n_1\right.$$

$$\left. + \left(\frac{3v}{r} + \frac{\dot{\rho}}{\rho}\right)\left(\frac{2}{5}\, \nu \frac{\partial}{\partial \nu}\, n_3 + \frac{8}{5}\, n_3\right)\right]_v = \mathcal{S}^{(1)} \tag{3.26a}$$

$$\mathcal{S}_\beta^{(1)} = -(\Gamma_a(\nu) + \Gamma_p(\nu)) n_1(\nu) \tag{3.26b}$$

$$\mathcal{S}_{sc}^{(1)} = -\Gamma_s(\nu) n_1(\nu) + \int_{\nu'} R_1(\nu' \to \nu) n_1(\nu')$$

$$+ \sum_{\ell=0}^{\infty} (\ell+1)\left\{n_\ell(\nu) \int_{\nu'} n_{\ell+1}(\nu')(R_{\ell+1}(\nu \to \nu') - R_{\ell+1}(\nu' \to \nu))\right.$$

$$\left. + n_{\ell+1}(\nu) \int_{\nu'} n_\ell(\nu')(R_\ell(\nu \to \nu') - R_\ell(\nu' \to \nu))\right\} \tag{3.26c}$$

$$\mathcal{S}_{th}^{(1)} = -\Gamma_{th}(\nu) n_1(\nu) - \int_{\nu'} R_{p1}(\nu, \nu') \bar{n}_1(\nu')$$

$$+ \sum_{\ell=0}^{\infty} (\ell+1)\left\{n_\ell(\nu) \int_{\nu'} \bar{n}_{\ell+1}(\nu')(R_{p,\ell+1}(\nu, \nu')\right.$$

$$- R_{a,\ell+1}(\nu, \nu')) + n_{\ell+1}(\nu) \int_{\nu'} \bar{n}_\ell(\nu')(R_{p\ell}(\nu, \nu')$$

$$\left. - R_{a\ell}(\nu, \nu'))\right\} \tag{3.26d}$$

$$\mathcal{S}_{\nu\nu}^{(1)} \approx 0 \tag{3.26e}$$

$$\ell \geq 2: \left[\frac{\partial n_\ell}{\partial t} + \frac{(\ell+1)}{(2\ell+1)} \left(c4\pi r^2 \rho_B \frac{\partial}{\partial b} n_{\ell+1} - (\ell+2) \frac{c}{r} n_{\ell+1}\right)\right.$$

$$+ \frac{\ell}{2\ell+1} \left(c4\pi r^2 \rho_B \frac{\partial}{\partial b} n_{\ell-1} - (\ell-1) \frac{c}{r} n_{\ell-1}\right) \Big]_s$$

$$+ \left[\left\{\frac{\ell(\ell-1)}{(2\ell-1)(2\ell+1)} \left(\nu \frac{\partial}{\partial \nu} n_{\ell-2} - (\ell-2) n_{\ell-2}\right)\right.\right.$$

$$+ \frac{1}{(2\ell-1)(2\ell+3)} \left((2\ell(\ell+1)-1)\nu \frac{\partial}{\partial \nu} n_\ell + \ell(\ell+1) n_\ell\right)$$

$$\left.\left. + \frac{(\ell+1)(\ell+2)}{(2\ell+1)(2\ell+3)} \left(\nu \frac{\partial}{\partial \nu} n_{\ell+2} + (\ell+3) n_{\ell+2}\right)\right\} \left(\frac{3v}{r} + \frac{\dot{\rho}}{\rho}\right)\right.$$

$$\left. - \frac{v}{r} \nu \frac{\partial}{\partial \nu} n_\ell \right]_v = s^{(\ell)} \tag{3.27a}$$

$$s_\beta^{(\ell)} = -(\Gamma_a(\nu) + \Gamma_p(\nu)) n_\ell(\nu) \tag{3.27b}$$

$$s_{sc}^{(\ell)} = \text{(see Appendix 1, equation A1.14)} \tag{3.27c}$$

$$s_{th}^{(\ell)} = \text{(see Appendix 1, equation A1.16)} \tag{3.27d}$$

$$s_{\nu\nu}^{(\ell)} \approx 0 \tag{3.27e}$$

We have let

$$\Gamma_s(\nu) = \int_{\nu'} R_0(\nu \to \nu') = \tau_s^{-1} \tag{3.28}$$

$$\Gamma_{th}(\nu) = \int_{\nu'} R_{p0}(\nu, \nu') = \tau_{th}^{-1} \tag{3.29}$$

denote the scattering and thermal production rates respectively. The notation

$$\int_{\nu'} f(\nu') \equiv \int_0^\infty \frac{(\nu')^2 d\nu'}{2\pi^2(\hbar c)^3} \; f(\nu') \tag{3.30}$$

is the neutrino phase space integral of an arbitrary function $f(\nu)$. The speed of light, c, has been included in the left-hand side of equations 3.25a, 3.26a, and 3.27a, and the dimension is inverse time; if $\hbar$ and c are left out of the right hand side, we can always reinsert enough powers of them to obtain this dimension; we usually leave them out.

The P-N approximation generally refers to the truncation of this infinite heirarchy of equations at ℓ=N, with the specification of n_ℓ, $\ell \geq$ N+1, being obtained by ansatz. The usual prescription is to assume $n_\ell = 0$ for $\ell \geq$ N+1. Whereas the invariance properties of the BTE allow simple transformation from one frame to another, this invariance does not survive the truncation process; the P-1 approximation in the local rest frame of matter is not the P-1 approximation in the inertial frame, but rather the df contains all of the higher moments.

The notation $[\quad]_s$ in equations 3.25a, 3.26a, and 3.27a means that the term in the square brackets arises from $\mathcal{D}_s$; it couples n_ℓ to the immediately higher and lower moments $n_{\ell+1}$, $n_{\ell-1}$. The $\mathcal{D}_v$ term, $[\quad]_v$, couples n_ℓ to $n_{\ell+2}$ and $n_{\ell-2}$. If the timescale $n_0/\dot{n}_0$ is of the order of a diffusion timescale which is slower or comparable to the hydrodynamical timescale given by $(\dot{\rho}/\rho)^{-1}$, then the times in $[\quad]_v$ become as important as those in $[\quad]_s$, and

must be included.

The absorption rate which appears in the $\ell \geq 1$ equation is modified by the addition of the production term. This modified absorption coefficient,

$$\Gamma_a' = \Gamma_a + \Gamma_p \quad , \tag{3.31}$$

which appears when FD statistics are operating, is analogous to the modified absorption coefficient, $\Gamma_a' = \Gamma_a - \Gamma_p$, which appears in photon transport, when Bose-Einstein statistics are operative. The latter modification is due to stimulated emission; the former has been termed forced absorption by Imshenik and Nadezhin (1971, 1973). An occupied neutrino state inhibits emission into that state; if the forward (outgoing) directions are more occupied than the backward (incoming) ones, the net emission will be backward peaked. This inhibited emission tends to relax anisotropies in the df towards zero on a timescale Γ_p^{-1} by only allowing emission in directions complementary to the anisotropies.

In the absence of neutrino degeneracy, when the df $n<<1$, only the terms linear in n survive in $\delta_{sc}^{(\ell)}$; the quadratic terms are an expression of the blocking of phase space due to the buildup of neutrino occupation number. In the thermal source function moments, if we again assume neutrino nondegeneracy, only $\delta_{th}^{(0)}$ survives, and it is given by $\Gamma_{th}(\nu)$; with the inclusion of neutrino degeneracy terms, there appear linear terms in n_ℓ and $\bar{n}_\ell$ in $\delta_{th}^{(\ell)}$, which compete at the same level with neutrino-antineutrino annihilation into matter.

The scattering is termed conservative if the energy of the outgoing neutrino is exactly the energy of the incoming neutrino:

$$R_\ell(\nu\to\nu') = 2\pi\delta(\nu-\nu')\, A_\ell(\nu) \tag{3.32}$$

If the scattering is conservative, which is a good approximation in the reactions $\nu+A \to \nu+A$ and $\nu+N \to \nu+N$, where A is a heavy nucleus and N is a free nucleon, then the quadratic terms in $s_{sc}^{(\ell)}$ all cancel. Further, if we note that

$$A_0(\nu) = \frac{\pi\Gamma_s(\nu)}{\nu^2} \quad , \tag{3.33}$$

we see immediately that

$$s_{sc,\ cons}^{(0)} = 0 \quad ; \tag{3.34}$$

i.e., there is no energy redistribution in conservative scattering. The higher source function moments are

$$s_{sc,\ cons}^{(\ell)} = -\Gamma_s(\nu)\left(1 - \frac{A_\ell(\nu)}{A_0(\nu)}\right) n_\ell(\nu) \tag{3.35}$$

In the ℓ=1 case, we define the transport rate and lifetime due to conservative scattering by

$$\Gamma_{tr,\ cons} = -\Gamma_s\left(1 - \frac{A_1}{A_0}\right) \quad , \tag{3.36}$$

so

$$s_{sc,\ cons}^{(1)} = -\Gamma_{tr,cons}(\nu)\, n_1(\nu) \tag{3.37}$$

The calculation of A_ℓ, and hence $\Gamma_{tr,cons}$, depends on the detailed

angular distribution of the conservative scattering reaction. The quadratic terms also cancel in $\mathcal{S}_{sc,cons}$ itself and thus do not appear in the BTE.

When the scattering is nonconservative, 3.32 is not true, generally $\nu' \neq \nu$, and the nonlinear terms must be included in $\mathcal{S}_{sc}^{(\ell)}$; this is the complication which arises in νe scattering.

There are two approximations we propose to deal with neutrino-neutrino scattering. The first is that given by 3.25e, 3.26e, and 3.27e. This approximation can follow the effect of $\nu_e + \nu_e \rightarrow \nu_e + \nu_e$ in the early stages of neutronization, before the df is near equilibrium. It is exact in a homogeneous medium, when the df is angle independent. When nearer to equilibrium, we may take the formulae derived for $\nu_e + e \rightarrow \nu_e + e$, replace the electron df by the ν_e df, and make other modifications to be detailed in the next chapter to obtain a more tractable source function for this reaction. The second technique can be applied to $\nu_\mu + \nu_e \rightarrow \nu_\mu + \nu_e$ and other neutrino-neutrino reactions.

3.6 INITIAL AND BOUNDARY CONDITIONS

Initial conditions (IC) and boundary conditions (BC) must be specified in the BTE and P-N equations. The former are straightforward: we usually assume there are no neutrinos to begin with

$$n(\nu,\mu,b,t) = 0 \qquad \text{IC BTE} \tag{3.38}$$

$$n_\ell(\nu,b,t) = 0 \qquad \text{IC P-N} \tag{3.39}$$

There are two types of volumes in which the transport equations

are solved. The first is a spherical shell which has an outer radius R_0 and an inner radius R_i; the second is a sphere ($R_i = 0$). Actually, the inner and outer radii may move; it is the baryon number enclosed within radius R_i, B_i, and the baryon number enclosed within radius R_0, B_0, which define the shell. The incoming neutrino df must be specified at the outer radius

$$n(\nu,\mu,B_0,t) = F_{OUT}(\nu,\mu,t) \qquad \mu < 0 \tag{3.40}$$

and the outgoing neutrino df must be specified at the inner radius

$$n(\nu,\mu,B_i,t) = F_{IN}(\nu,\mu,t) \qquad \mu > 0 \tag{3.41}$$

unless $R_i = B_i = 0$, in which case n must be finite which implies n is isotropic at the center.

If we solve the BTE for a shell configuration, we will find that there is a stream of neutrinos flowing in the backward (inward) direction through the inner radius, some of which will be scattered forward, reentering the shell: the specification of the BC at $b = B_i$ is impossible to decouple from the transport problem for the region $b < B_i$. If the inner radius is sufficiently interior, so that there are many optical depths above it, it may be a good approximation to assume that the diffusion approximation holds for $b < B_i$; a plausible F_{IN} can then be given, a FD df with temperature and neutrino chemical potential fixed; if the radiation acts to significantly change the state of matter in the shell, by heating and/or neutronization, then F_{IN} would change in response, resulting in a boundary value problem which is probably not well posed. If F_{IN} is isotropic, and given by

3.7, we term this a luminous surface BC.

At the outer boundary, one also has to worry about backscatter into the shell. In practice, we choose the outer radius so that the optical depth of the overhead matter, $r > R_0$, is small compared with unity and take

$$F_{OUT} = 0 \ . \tag{3.42}$$

Given F_{IN} and F_{OUT}, these BC can be immediately applied to the S-N method: the df on the boundaries is specified at each of the appropriate discrete angles.

It is generally impossible to satisfy 3.40 and 3.41 at each angle in the P-N method. Rather, certain integrals of these BC are required to hold. If we deal with odd order P-N, then (N+1)/2 BC are needed, which are usually taken to be the Marshak BC

$$\int_{-1}^{0} d\mu \ P_\ell(\mu) \ [n(\nu,\mu,B_0,t) - F_{OUT}] \ = 0 \qquad \ell = 1,3,..,N \tag{3.43a}$$

$$\int_{0}^{1} d\mu \ P_\ell(\mu) \ [n(\nu,\mu,B_i,t) - F_{IN}] \ = 0 \qquad \ell = 1,3,..,N \tag{3.43b}$$

The P-N method for N even is less accurate than for N odd, and we do not discuss its BC here. See Pomraning (1973) for a more complete discussion of boundary conditions.

3.7 FROM DIFFUSION TO STREAMING: SAMPLE DISTRIBUTIONS

The P-N equations are capable of describing diffusion on the one hand ($n_\ell << n_0$ for all $\ell \neq 0$) and free streaming on the other ($n_\ell = n_0$ for all ℓ). As an illustration of this transition, suppose

the df were elliptical:

$$n(\nu,\mu,b,t) = \frac{n(\nu,\mu=0,\ b,t)}{1-\ \alpha(\nu,b,t)\mu} \tag{3.44a}$$

$$\alpha = 1 - \frac{n(\mu=0)}{n(\mu=1)} \tag{3.44b}$$

We can then express all higher moments in terms of the first two by solving the difference equation

$$n_{\ell+1} = \frac{1}{\alpha(n_1/n_0)} \cdot \frac{2\ell+1}{\ell+1} \cdot n_\ell - \frac{\ell}{\ell+1}\ n_{\ell-1} \quad , \ell \geq 1 \tag{3.45a}$$

and the transcendental equation which expresses α as a function of n_1/n_0

$$\frac{1}{2\alpha}\ (1 - \alpha \frac{n_1}{n_0})\ \ell n \left(\frac{1+\alpha}{1-\alpha}\right) = 1 \tag{3.45b}$$

A plot of α, which runs from 0 to 1, along with a plot of n_2/n_0 and n_3/n_0, against n_1/n_0 is given in Figure 2.

Another angular distribution, one in which the neutrinos are confined to a forward cone and are isotropic within that cone

$$n(\nu,\mu,b,t) = \frac{2\ n_0(b,\nu,t)}{1-\mu_c}\ \chi_{(\mu_c,1)}\ (\mu) \tag{3.46}$$

can be used to illustrate the forward peaking of the df as one moves away from an emitting surface. If each element of a spherical surface of radius R_c radiates isotropically, and all inward radiation is completely absorbed, then the radiant df at $r = R_c$ will be 3.46 with $\mu_c = 0$. If the emission is time independent and there is no further emission, absorption, or scattering in the region $r > R_c$ then the df

at radius r is given by 3.46 with

$$\mu_c(r) = \sqrt{1 - \left(\frac{R_c}{r}\right)^2} \quad ; \tag{3.47a}$$

the cone angle, arccos (μ_c), which is 90° at R_c has shrunk to 30° at $2R_c$ and $\sim 6°$ at $10R_c$. The moments obey

$$n_0(r,\nu) = \left(\frac{R_c}{r}\right)^2 \frac{n_0(R_c,\nu)}{1+\mu_c(r)} \tag{3.47b}$$

$$n_1(r,\nu) = \frac{1+\mu_c(r)}{2} \; n_0(r,\nu) \tag{3.48a}$$

$$n_2(r,\nu) = \frac{\mu_c(1+\mu_c)}{2} \; n_0(r,\nu) \tag{3.48b}$$

$$n_3(r,\nu) = \frac{5\mu_c^2-1}{4} \frac{(1+\mu_c)}{2} \; n_0(r,\nu) \tag{3.48c}$$

All higher moments rapidly build up to the streaming limit as r becomes large relative to R_c. One can use 3.48 to express all higher moments in terms of n_0 and n_1 as in the elliptical case.

The two angular distributions show us that whenever n_1 becomes comparable to n_0, then the higher moments are not negligible.

3.8 THE P-1 EQUATIONS

To adequately treat the streaming limit, must we use the P-N equations for N large? The matter evolution equations 3.17 involve integrals of $\delta^{(0)}$ and $\delta^{(1)}$ only, and thus integrals of the first two moment equations only. It is primarily the effects of neutrinos on the hydrodynamics and thermodynamics of matter which are of concern in the supernova problem; this suggests we use the P-1 method. Since the $\ell = 0$ and $\ell = 1$ equations, 3.25 and 3.26, include n_2 and n_3 on the

transport side and all higher moments in $s^{(0)}$ and $s^{(1)}$, some truncation scheme must be adopted to decouple them from the higher moment equations. We introduce the Eddington factors, f for the second moment and f_3 for the third moment, which are functions of n_0, n_1, b, t and ν :

$$n_2 = \frac{3}{2}\left(f - \frac{1}{3}\right) n_0 \qquad (3.49a)$$

$$n_3 = \frac{5}{2}\left(f_3 - \frac{3}{5}\right) n_0 \qquad (3.49b)$$

The most obvious choice is to set

$$n_2 = 0, \quad f = \frac{1}{3} \qquad (3.50a)$$

$$n_3 = 0, \quad f_3 = \frac{3}{5} \qquad ; \qquad (3.50b)$$

the resulting equations 3.25, 3.26, 3.50 form an approximation which, following Falk and Arnett (1977), we call the time dependent Eddington approximation (TDEA). The TDEA will not reproduce the streaming limit: in the absence of sources, the BTE is a hyperbolic equation with group speed c; in the absence of sources, the TDEA is a hyperbolic equation with speed $c/\sqrt{3}$. The Eddington factors, f and f_3, both go to one as the streaming limit is approached. Some scheme for f and f_3 which interpolates between 1/3 and 1, and 3/5 and 1 respectively, such as that given by the elliptic distribution 3.45, is necessary to reproduce both the diffusion and streaming limits.

Higher moments than n_0 and n_1 enter into the source functions $s^{(0)}$ and $s^{(1)}$ through the nonconservative scattering and thermal

production processes. In the diffusion limit, the terms involving n_0 and perhaps n_1 completely swamp the terms involving n_2, n_3, ... In the streaming limit, all moments are equal, but then n_0 is small compared with unity (the neutrinos are not degenerate), and none of the quadratic terms in $\delta_{sc}^{(0)}$ and $\delta_{sc}^{(1)}$ is important. The same argument holds for δ_{th} . We retain moments up to and including the second in δ_{sc} and δ_{th} .

The Marshak BC 3.43, with 3.42 become simply

$$\frac{1}{2} n_0 - n_1 = 0 \qquad b = B_0 \tag{3.51}$$

$$\frac{1}{2} n_0 + n_1 = \int_0^1 F_{IN} \mu d\mu \qquad b = B_i \tag{3.52}$$

unless B_i is zero, in which case

$$n_1 \ (b = 0) = 0 \qquad \text{if } B_i = 0 \tag{3.53}$$

If a luminous surface interior BC is valid, then F_{IN} is isotropic; and 3.52 becomes

$$n_0 + 2n_1 = F_{IN} \qquad b = B_i \tag{3.54}$$

Since $n_1 << n_0$ in order for the diffusion limit to hold at the interior boundary, we may consider another interior BC

$$n_0 = F_{IN} \qquad b = B_i \tag{3.55}$$

When the optical depth of the shell is much greater than the ratio of exterior to interior radius, R_0/R_i , solutions with 3.54 and 3.55 are the same.

It is more conventional to write the moment equations in terms of the energy density of neutrinos per unit energy,

$$J(\nu) = \frac{\nu^3}{2\pi^2(\hbar c)^3} n_0 \quad , \tag{3.56a}$$

the momentum flux per unit energy,

$$H(\nu) = c\frac{\nu^3}{2\pi^2(\hbar c)^3} n_1 \quad , \tag{3.56b}$$

the radial neutrino pressure per unit energy,

$$K(\nu) = \frac{\nu^3}{2\pi^2(\hbar c)^3} (\tfrac{2}{3} n_2 + \tfrac{1}{3} n_0) \qquad (= fJ(\nu)) \tag{3.56c}$$

and the radial pressure flux per unit energy,

$$N(\nu) = c\frac{\nu^3}{2\pi^2(\hbar c)^3} (\tfrac{2}{5} n_3 + \tfrac{3}{5} n_1) \qquad (= f_3 H(\nu)) \tag{3.56d}$$

If we multiply 3.25a and 3.26a by $\nu^3/2\pi^2(\hbar c)^3$, then we obtain Castor's (1972) equations 31 and 32, except that our sources are more complicated; Arnett (1977) sets $f_3 = 0$ rather than $= 3/5$ to obtain his $\ell = 1$ equation (5), but since he then uses the diffusion approximation, it doesn't matter.

We denote the integrals of J, H, K and N by the same symbols except that we add the subscript ν and further define

$$u_\nu = \frac{J_\nu}{\rho_B} = \frac{1}{\rho_B}\int_\nu \nu n_0 \tag{3.57a}$$

$$Y_\nu = \frac{1}{\rho_B}\int_0^\infty \frac{d\nu}{\nu} J(\nu) = \frac{1}{\rho_B}\int_\nu n_0 \tag{3.57b}$$

$$F_\nu = \int \frac{d\nu}{\nu} H(\nu) = \int_\nu n_1 c \tag{3.57c}$$

where u_ν is the neutrino energy per baryon, Y_ν is the neutrino number per baryon, and F_ν is the number flux. These energy integrated quantities satisfy the gray equations

$$\rho_B \left[\frac{\partial Y_\nu}{\partial t} + 4\pi \frac{\partial}{\partial b}(r^2 F_\nu)\right] = \int_\nu \mathcal{S}^{(0)} \tag{3.58a}$$

$$\rho_B \left[\frac{\partial u_\nu}{\partial t} + K_\nu \frac{\partial}{\partial t}\left(\frac{1}{\rho_B}\right) + 4\pi \frac{\partial}{\partial b}(r^2 H_\nu)\right] - (3K_\nu - J_\nu)\frac{v}{r} = \int_\nu \nu \mathcal{S}^{(0)} \tag{3.58b}$$

$$\frac{1}{c}\frac{\partial H_\nu}{\partial t} + 4\pi r^2 \rho_B \frac{\partial K_\nu}{\partial b} + \frac{3K_\nu - J_\nu}{r} - \frac{2}{3}\left(\frac{3v}{cr} + \frac{\dot{\rho}}{\rho}\right) H_\nu = \int_\nu \nu \mathcal{S}^{(1)} \tag{3.58c}$$

which are inputs into the equations of motion 3.17. Thus, the (electron) lepton number per baryon

$$Y_{L_e} = Y_e + Y_{\nu_e} - Y_{\bar{\nu}_e} \tag{3.59a}$$

and the lepton number flux

$$F_{L_e} = F_{\nu_e} - F_{\bar{\nu}_e} \tag{3.59b}$$

satisfy the conservation law equation

$$\frac{\partial Y_{L_e}}{\partial t} + 4\pi \frac{\partial}{\partial b} r^2 F_{L_e} = 0 \tag{3.59c}$$

which is just 3.17b. Notice that Y_e is related to the electron and positron concentrations per baryon, Y_{e-} and Y_{e+} , by

$$Y_e = Y_{e-} - Y_{e+} \tag{3.60}$$

It is unfortunate that this confusing notation has arisen.

The P-1 equations are finite differenced in Appendix 4 and the results are given in Chapter 6. We solve 3.25 a,b,c, 3.26 a,b,c with 3.17b,c but not 3.17d (no dynamics) for ν_e's.

3.9 THE P-0 APPROXIMATION

Consider the P-0 approximation: n_1 is zero, 3.25 has no spatial derivatives and there is no transport; the neutrino df just builds up toward its equilibrium value. These equations are appropriate for an infinite homogeneous medium and are solved in Chapter 6.

3.10 DIFFUSION (MGDA, FLD, CA AND EDA)

From the P-1 equation, we obtain the multigroup or energy dependent diffusion approximation (MGDA) by (a) setting f = 1/3, f_3 = 3/5, (b) neglecting $\partial n_1 / \partial t$ and all terms in square bracket $[\quad]_v$ in 3.26a, and (c) assuming all scatterings are conservative and there are no thermal sources in $\mathcal{S}^{(1)}$. With all this, 3.26a reduces to Fick's law of diffusion

$$n_1 = -\frac{1}{3} c \tau_{tr} 4\pi r^2 \rho_B \frac{\partial}{\partial b} n_0 \tag{3.61a}$$

$$H(\nu) = - D(\nu) \left(4\pi r^2 \rho_B \frac{\partial}{\partial b}\right) J(\nu) \qquad (3.61b)$$

where the full transport lifetime τ_{tr}, the transport mean free path λ_{tr}, and the diffusion coefficient D, which all depend on energy, and position and time through the thermodynamic parameters, are

$$\tau_{tr}^{-1} = (c\lambda_{tr})^{-1} = \Gamma_{tr} = \Gamma_{tr,cons} + \Gamma_a + \Gamma_p \qquad (3.62)$$

$$D = \frac{1}{3} c^2 \tau_{tr} \qquad (3.63)$$

The imposition of 3.32 upon neutrino electron scattering is clearly incorrect; however, neutrino scattering by nuclei and nucleons or neutrino absorption always dominates the opacity, at least with Weinberg-Salam model parameters, which suggests such an approximation may not be too bad. The further approximation of taking A_1 in 3.36 zero is often made (Arnett 1977).

The MGDA consists of Fick's law substituted into 3.25a. In practice, approximate descriptions are used for $\delta^{(0)}_{sc,\nu e \to \nu e}$ (Arnett 1977, Wilson et al. 1975), and also for $\delta^{(0)}_{th}$ when it is included (Wilson et al. 1975).

The MGDA is a parabolic equation for constant D. The streaming limit cannot be obtained from it. To alleviate this, the diffusion coefficient is modified

$$\tilde{D} = D\phi \qquad (3.64a)$$

where ϕ is called a flux limiter. Arnett (1977) and Wilson et al. (1975) use

$$\phi = \frac{1}{1-D(1/n_0)(4\pi r^2 \rho_B \frac{\partial}{\partial b}) n_0} \qquad (3.64b)$$

When ϕ is unity ($\lambda_{tr} << h_\nu$), the usual diffusion approximation is obtained. Here, h_ν is the neutrino scale height, $h_\nu = \left|\frac{1}{n_0}\frac{\partial n_0}{\partial r}\right|^{-1}$. At low optical depth ($\lambda_{tr} >> h_\nu$), Fick's law becomes $n_1 = n_0$ or $H(\nu) = cJ(\nu)$, which reproduces the streaming limit. How accurate is flux-limited diffusion (FLD) in the intermediate region ($\lambda_{tr} \sim h_\nu$) ? Wilson et al. (1975) state that it results in at most a 10% error in temperature when compared with exact transport equation solutions; Yueh and Buchler (1977b) indicate it fares well in comparison with their S-2 and S-4 results. The test configurations in both cases are somewhat idealized. FLD has become one of two standard methods to transport neutrinos in coupled radiation-hydrodynamic codes (Arnett 1977, Wilson et al. 1975, Bruenn 1975).

The other standard method of transport, the conduction approximation (CA), is cruder than the MGDA and is derived from it. The isotropic component of the df, n_0, is assumed given by a FD df, 3.7, which we call n_{FD}. Then, Fick's law becomes

$$n_1 = -D(\nu)\, n_{FD}\,(1-n_{FD})\, 4\pi r^2 \rho_B \left(\frac{\nu}{T^2}\frac{\partial T}{\partial b} + \frac{\partial \eta_\nu}{\partial b}\right) \qquad (3.65)$$

where

$$\eta_\nu = \mu_\nu \beta \qquad (3.66)$$

is the neutrino degeneracy parameter. The integral of 3.65, when

multiplied by the appropriate powers of energy, yield the constitutive equations

$$F_\nu = -\left(D_1 \frac{\partial \rho Y_\nu}{\partial T}\right) 4\pi r^2 \rho_B \frac{\partial}{\partial b} T - \left(D_0 \frac{\partial \rho Y_\nu}{\partial \eta_\nu}\right) 4\pi r^2 \rho_B \frac{\partial}{\partial b} \eta_\nu$$

$$= -\left(D_1 3\rho_B Y_\nu \frac{1}{T}\right) 4\pi r^2 \rho_B \frac{\partial}{\partial b} T - \left(D_0 \frac{\partial \rho Y_\nu}{\partial \eta_\nu}\right) 4\pi r^2 \rho_B \frac{\partial}{\partial b} \eta_\nu \qquad (3.67a)$$

$$H_\nu = -\left(D_2 \frac{\partial \rho u_\nu}{\partial T}\right) 4\pi r^2 \rho_B \frac{\partial T}{\partial b} - \left(D_1 \frac{\partial \rho u_\nu}{\partial \eta_\nu}\right) 4\pi r^2 \rho_B \frac{\partial \eta_\nu}{\partial b}$$

$$= -\left(D_2 4\rho_B u_\nu \frac{1}{T}\right) 4\pi r^2 \rho_B \frac{\partial T}{\partial b} - (D_1 3k_B T \rho_B Y_\nu)\ 4\pi r^2 \rho_B \frac{\partial \eta_\nu}{\partial b} \qquad (3.67b)$$

where

$$D_k = \frac{\int_\nu \nu^k\ n_{FD}\ (1-n_{FD})\ D(\nu)}{\int_\nu \nu^k\ n_{FD}\ (1-n_{FD})} \quad , \ k = 0,1,2 \qquad (3.67c)$$

are essentially Rosseland mean diffusion coefficients, closely related to the coefficients introduced by Imshenik and Nadezhin (1971, 1973) and elaborated upon by Bludman and van Riper (1977). Neutrinos flow down temperature and chemical potential gradients. For conservative scattering only, $D(\nu) \sim \nu^{-2}$ and D_k can be expressed in terms of Fermi functions

$$F_k(\eta) = \int_0^\infty \frac{x^k}{e^{x-\eta}+1}\, dx \qquad (3.68)$$

$$D_0 = D(\nu=T) \frac{1}{(1+e^{-\eta\nu}) 2F_1(\eta)} \tag{3.69a}$$

$$D_1 = D(\nu=T) \frac{F_0}{3F_2} \tag{3.69b}$$

$$D_2 = D(T) \frac{F_1}{2F_3} \tag{3.69c}$$

Notice that, for a FD df,

$$\rho_B Y_\nu = \frac{(kT)^3}{2\pi^2(\hbar c)^3} F_2(\eta_\nu) \tag{3.70}$$

$$u_\nu = Y_\nu kT F_3/F_2 \tag{3.71}$$

The constitutive equations 3.67 are then plugged into 3.58 to yield two diffusion equations for the two diffusing quantities, the temperature and the neutrino chemical potential. The right hand sides of 3.58a and b, the source terms, are in general nonzero. If the sources are zero, then the CA reduces to the equilibrium diffusion approximation (EDA); the chemical potentials of the neutrinos are given by their equilibrium values, 3.12 for ν_e, 3.13 for $\bar{\nu}_e$, and 0 for ν_μ, $\bar{\nu}_\mu$. It is this EDA for ν_e, $\bar{\nu}_e$ which Imshenik and Nadezhin develop. It was used extensively with $\mu_\nu = 0$ in early work on the neutrino energy deposition supernova model(Arnett (1966, 1967), Schwartz (1967), and much Russian work detailed in Zel'dovich and Novikov (1971)). Mazurek (1975, 1976) and Sato (1975) have used the EDA with $\mu_\nu \neq 0$ in their supernova codes in the post neutral current era.

In the EDA, the concept of neutrino photosphere enters, the spherical surface which is $\sim 2/3$ of a Rosseland mean free path from the stellar surface. The Rosseland optical depth is

$$\tau_{OP,R}(b,t) = \int_b^{B_s} \frac{c}{3D_2(b,t)} \frac{db}{4\pi r^2 \rho_B} \tag{3.72}$$

where B_s is the baryon number of the star. There are actually two other Rosseland means, corresponding to the choice of D_0 or D_1 rather than D_2 . The energy dependent optical depth is more illuminating:

$$\tau_{OP}(\nu,b,t) = \int_b^{B_s} \frac{\Gamma_{tr}(\nu,b,t)}{c} \frac{db}{4\pi r^2 \rho_B} \tag{3.73}$$

Assuming there are no composition changes, the b that is 1 optical depth for a 5 MeV ν is at depth 4 for a 10 MeV ν and at depth 25 for a 25 MeV ν . The position of the neutrino photosphere is energy dependent. Indeed, neutrino photosphere is a misleading concept due to the extreme energy dependence of the neutrino opacities.

In this bewildering array of approximations, at what level can we say we have adequately treated neutrino transport? To couple radiative to hydrodynamical flows is an expensive and tricky enterprise. When the EDA works, we want to use it. If the EDA and the CA fail and yet FLD works, we want to use it. The historical progression in neutrino transport was to assume the simplest

approximations worked until proven otherwise, then to adopt the next simplest. This direction proceeds from the end of this chapter back to the beginning. We need to justify the approximations. In rather idealized situations, the S-N and Monte Carlo methods have been used to answer some of these questions. The P-1 method is more general than the diffusion approximations; it is the ground from which they spring. It too can answer these questions, with a wide variety of sources, upon which we now turn our attention.

4. SCATTERING SOURCES

Neutrinos scatter from nucleons, bound and free, from electrons, from themselves, and from their antineutrinos. We deal with each in turn. In all concrete numerical results, the Weinberg-Salam model with $\sin^2 \theta_W = 0.3$ is used.

4.1 COHERENT NUCLEAR SCATTERING: $\nu+A \rightarrow \nu+A$

The elastic scattering of neutrinos by heavy nuclei dominates transport in both the neutronization and mantle regions by giving the greatest contribution to the transport mean free path. The recent regeneration of interest in the neutrino-induced supernova model was a consequence of Freedman's (1974) observation that the cross-section for this process goes as the square of the mass number of the nucleus if the hadronic neutral current has an isoscalar vector component (see Table 2). This alters in a qualitative manner the supernova model from that determined with only charged current processes included.

Fermi's Golden Rule for the scattering kernel (see 3.2, 3.3) can be combined with the spin-summed-matrix-element for allowed nuclear transitions, 2.44, to yield

$$R(\nu A \rightarrow \nu A; \underset{\sim}{q} \rightarrow \underset{\sim}{q}') = \int \frac{d^3 p_i}{(2\pi)^3} f_i(\underset{\sim}{p}_i) \int \frac{d^3 p_f}{(2\pi)^3} (1+\theta_f f_f(\underset{\sim}{p}_f)) \cdot 2\pi\delta(E_f+\nu'-E_i-\nu)$$

$$(2\pi)^3 \delta^{(3)}(\underset{\sim}{p}_f+\underset{\sim}{q}'-\underset{\sim}{p}_i-\underset{\sim}{q}) \; G_F^2 \; g_i \cdot \left\{ (1+c) \left\langle (C_{V0}+C_{V1} t_3) \right\rangle^2 \right.$$

$$\left. + \; (1-\frac{1}{3} c) \left\langle (C_{A0}+C_{A1} t_3) \underset{\sim}{\sigma} \right\rangle^2 \right\} \qquad (4.1)$$

The distribution function for the initial state of the nucleus is $f_i(p_i)$, that for the final state is $f_f(p_f)$. The parameter θ_f is 1 if the final state particle is a boson, -1 if it is a fermion. For complex nuclei, in the density-temperature regimes of interest, the df's are Maxwell-Boltzmann; $\theta_f f_f$ can be neglected in comparison with unity. The temperature, density, and composition dependences, and through them, the spacetime dependences, of $R(\nu A \to \nu A)$ are not explicitly indicated in 4.1. The incoming neutrino energy is ν , the outgoing energy is ν' , and $c=\hat{q}\cdot\hat{q}'$ is the cosine of the angle between the initial and final neutrino momenta. Since the matrix elements depend upon the structure of the nuclear state, we treat the set of resonant excited states of the nucleus with spin angular momentum J_i and mass M_i as an independent particle with partition function $g_i = 2J_i+1$.

Nuclear recoil energies are of order ν^2/Am_N , where m_N is the nucleon mass and A is the baryon number of the nucleus: a 20 MeV neutrino imparts $\sim$ 8 keV to an ^{56}Fe nucleus, $\sim$ 110 keV to a ^{4}He nucleus. The final energy of the neutrino is then almost equal to its initial energy, thus allowing the conservative approximation (3.32) to be used, so (4.1) reduces to

$$R(\nu A \to \nu A;\ \underset{\sim}{q} \to \underset{\sim}{q}') = 2\pi\delta(\nu-\nu')\ G^2 n_i\ [(1+c)\ Q_W^2 + (1-\tfrac{1}{3}\ c) f_{GT} Q_W^2] \qquad (4.2)$$

where we have inserted (2.49) into this expression, defining the weak charge of the nucleus to be

$$Q_W = C_{Vn}N + C_{Vp}\ Z = C_{V0}A + C_{V1}\left(\frac{Z-N}{2}\right) \tag{4.3}$$

and have defined the ratio of Gamow-Teller to Fermi matrix elements

$$f_{GT} = \frac{\left\langle (C_{A0}+C_{A1}t_3)\ \underset{\sim}{\sigma}\right\rangle^2}{Q_W^2} \tag{4.4}$$

The concentration of nuclei of type i is n_i , which is related to Y_i , the number per baryon by

$$n_i = \rho_B Y_i \tag{4.5}$$

The source (3.3) is then

$$\delta_{s\epsilon,\nu A}[n] = -\Gamma_S(\nu)\ n(\nu,\mu) + \Gamma_S(\nu)(n_0(\nu) + \frac{1-f_{GT}/3}{1+f_{GT}}\mu n_1(\nu)) \tag{4.6}$$

where n_0 and n_1 are the first two moments of the df $n(\nu,\mu)$, and the scattering rate (3.28) is

$$\begin{aligned}\Gamma_S(\nu) &= n_i \frac{G^2}{\pi} Q_W^2\ (1+f_{GT})\nu^2 \\ &= 2.65\quad \rho_{11} Y_i A_i^2 \left(\frac{\nu}{1\ \text{MeV}}\right)^2 \cdot \left(\frac{Q_W}{0.3A_i}\right)^2 (1+f_{GT}) \qquad s^{-1}\end{aligned} \tag{4.7}$$

The numerical evaluation is trivial if we remember $G^2/\pi = 1.63 \times 10^{-44}$ MeV^{-2} cm^2 ; in this way, we do not have to reinsert any $\hbar$'s, only the occasional c. Notice that $\Gamma_S(\nu) = n_i \sigma c$ where σ is the lab frame cross section for the process given in Table 2. By the density ρ ($\rho_{11} = \rho/10^{11}$) we mean the baryon density multiplied by the atomic mass unit m_u

$$\rho \equiv m_u \rho_B = (\rho_B \cdot 1\ \text{cm}^3)/N_A \qquad (\text{g/cm}^3)$$

where N_A is Avogadro's number; this is not the mass density. It is the transport inverse lifetime

$$\Gamma_{tr,\nu A}(\nu) = \Gamma_S(\nu A) \frac{2/3+10/9\ f_{GT}}{(1+f_{GT})}$$

$$= 1.77\ \rho_{11} Y_i A_i^2 \left(\frac{\nu}{\text{MeV}}\right)^2 \cdot \left(\frac{Q_W}{0.3A_i}\right)^2 \cdot \left(1+\frac{5f_{GT}}{3}\right) \quad s^{-1} \qquad (4.8)$$

which is of more interest than the scattering inverse lifetime in conservative reactions. Since the neutrinos transfer no energy to the medium in each scatter, $\delta^{(0)} = 0$; since the scattering kernel (4.2) is linear in c, $\delta^{(\ell)} = 0$ for all $\ell \geq 2$.

Usually, Q_W is taken to be $C_{V0}A$ and f_{GT} is taken to be zero. How large are the errors in such an approximation? For ^{56}Ni , ^{4}He and all other N=Z nuclei, Q_W is indeed $C_{V0}A$; for ^{56}Fe and ^{54}Fe , a rather abundant species (Weaver et al. 1977) in slightly neutron rich media, $(Q_W/0.3A)^2$ is 1.1 and 1.05 respectively : the approximation can lead to a 5 to 10% error.

What of f_{GT} ? The Gamow-Teller matrix element vanishes for any spin zero state. Even-even nuclei are the most abundant in nuclear statistical equilibrium (NSE) and their ground states have zero spin. The first few excited states of such nuclei are vibrational or rotational, with spins 2, 4, 6 . . . . A spin two state with excitation energy E_X above the ground state has a population 5 exp $(-E_X\beta)$ relative to the ground state's population. Consider ^{56}Fe and ^{56}Ni with first excited states at .89 and 2.7 MeV respectively. At

temperatures characteristic of the neutronizing shell, 1.5 MeV, the populations relative to the ground state are 2.8 and 0.83 respectively : the excited states cannot be neglected. The relationship between β-decay matrix elements and ft-values

$$\langle t_+ \rangle^2 + g_A^2 \langle \sigma t_+ \rangle^2 = 10^{(3.8 - \log_{10} ft)} \qquad (4.9)$$

together with the relation between $\langle \sigma t_3 \rangle^2$ and $\langle \sigma t_+ \rangle^2$ obtained from the Wigner-Eckhart theorem by assuming isoinvariance (equation 4.14b below) allows us to estimate f_{GT} ; immediately we can see f_{GT} is zero for self conjugate nuclei such as the abundant ^{56}Ni and ^{28}Si for all excited states, whether of zero isospin or not, for models with $C_{A0} = 0$, such as W.S. Even for superallowed ft values, $\sim 10^{3.5}$, f_{GT} is less than 1% for heavy iron peak nuclei. After the iron-helium phase transition, for a neutron rich medium, light nuclei that are unstable in the laboratory, such as ^5He, appear in NSE mixtures (Epstein and Arnett 1975). A simple shell model picture of ^5He as a ^4He core and a neutron in a $p_{3/2}$ orbital yields $\langle (C_{A0}+C_{A1}t_3)\sigma \rangle^2 = 20/3\ C_{An}^2$, and $f_{GT} = 0.9$ with $(Q_W/0.3A)^2 = (1.28)$. Similarly, for ^3H , the matrix element is $3\ C_{An}^2$, so $f_{GT} \simeq 1$, and $(Q_W/0.3A)^2 \simeq 1.49$. Bernabeu (1975) first analyzed corrections of this nature and came to the same conclusion. The corrections for the light elements are not negligible. However, models show that the helium-like zone in the neutronizing region is rather narrow, and for this reason such a correction can be ignored.

The total transport rate is the sum over all levels in a nucleus,

and then over all nuclei, labelled by (Z,N). If we neglect f_{GT}, the sum over all levels can be performed : the result is (4.8) with Y_i now interpreted as the number of nuclei with proton and neutron numbers (Z_i,N_i) per baryon.

4.2 INELASTIC NEUTRINO-NUCLEUS SCATTERING $\nu+A \to \nu+A^*$

There is another opacity source associated with neutrino-nucleus collisions, namely that due to inelastic scattering $\nu+A_i \to \nu+A_f$, where the final nuclear state f of mass M_f is not the same as the initial nuclear state i of mass M_i . We apply 4.1, again neglect nuclear recoil, and obtain the analogue of 4.2:

$$R(\nu A_i \to \nu A_f; \underset{\sim}{q} \to \underset{\sim}{q}') = 2\pi\delta(\nu-Q-\nu')\, n_i G^2 \left(1-\tfrac{1}{3}c\right) \left\langle (C_{A0}+C_{A1}t_3)\underset{\sim}{\sigma}\right\rangle_{fi}^2 \qquad (4.10)$$

with one important difference: the scattering is nonconservative; the incident neutrino loses an amount of energy $Q = M_f - M_i$. The source functions look formidable

$$\begin{aligned} \mathcal{S}_{sc}^{(0)}(\nu A_i \to \nu A_f) = {} & -\Gamma_S(\nu)n_0(\nu) + \Gamma_S(\nu+2Q)n_0(\nu+Q) + \Gamma_S(\nu)n_0(\nu)n_0(\nu-Q) \\ & -\Gamma_S(\nu+2Q)n_0(\nu)n_0(\nu+Q) - \tfrac{1}{3}\Gamma_S(\nu)n_1(\nu)n_1(\nu-Q) \\ & + \tfrac{1}{3}\Gamma_S(\nu+2Q)n_1(\nu)n_1(\nu+Q) \end{aligned} \qquad (4.11)$$

$$\begin{aligned} \mathcal{S}_{sc}^{(1)}(\nu A_i \to \nu A_f) = {} & -\Gamma_S(\nu)n_1(\nu) - \tfrac{1}{9}\Gamma_S(\nu+2Q)n_1(\nu+Q) - \frac{\Gamma_S(\nu)}{9} n_0(\nu)n_1(\nu-Q) \\ & + \tfrac{1}{9}\Gamma_S(\nu+2Q)n_0(\nu)n_1(\nu+Q) + \Gamma_S(\nu)n_1(\nu)n_0(\nu-Q) \\ & - \Gamma_S(\nu+2Q)n_1(\nu)n_0(\nu+Q) - \tfrac{2}{9}\Gamma_S(\nu)n_2(\nu)n_1(\nu-Q) \\ & + \tfrac{2}{9}\Gamma_S(\nu+2Q)n_2(\nu)n_1(\nu+Q) \end{aligned} \qquad (4.12)$$

but are the simplest of those for nonconservative scattering; by comparing with 3.25c and 3.26c the origin of each of the terms is apparent. Neutrinos of energy $\nu+Q$ can be downscattered by energy Q "into the beam" of energy ν , and those of energy ν may be downscattered by Q "out of the beam." The scattering rate is

$$\Gamma_S(\nu) = n_i \frac{G^2}{\pi} \left\langle (C_{A0}+C_{A1}t_3)\underset{\sim}{g} \right\rangle_{fi}^2 (\nu-Q)^2 \, \theta(\nu-Q) \qquad (4.13)$$

where θ is the Heaviside unit function; ν must exceed threshold in order for the reaction to proceed. Again this is $n_i c\sigma$ where σ is the lab cross section given in Table 2. The total scattering rate is obtained by summing over all possible final states in the nucleus that are connected to the initial state by the selection rules (2.48b) appropriate to Gamow-Teller transitions, then summing over all possible initial states, which includes thermally populated excited states.

The matrix element which enters is the same as that for nuclear de-excitation $A^* \rightarrow A+\nu+\bar{\nu}$, although the Q dependence is quite different. Now, however, 20 MeV neutrinos can excite the nucleus to very high energies, much higher than are thermally populated, and the subsequent decay of the resonant state A^* can be by particle emission as well as by photo-de-excitation. At higher energies still, neutrinos can induce spallation of the nucleus.

It is rather difficult to calculate the matrix elements to such highly excited states since their nuclear structure is usually not known. We are helped in this by a number of effects. The initial state is thermally populated, thus low lying. The energy dependence

of Γ_S tends to weight low lying final levels most heavily. The matrix elements of the one body operators, $S_{\sim p}$ and $S_{\sim n}$, the total intrinsic spins of the protons and neutrons respectively, which enters into 4.13, are small between a low lying initial state and a highly excited final state whose structure is quite different. Within the shell model, we can see that these transitions will be dominated by those final states in which a nucleon flips its spin, but maintains the same orbital angular momentum as the initial state ($j=\ell+1/2 \rightarrow j=\ell-1/2$). The superallowed transitions between isospin analogue states that often dominate β-decay do not occur in inelastic neutrino nucleus scattering, since the analogue of the initial state is itself, for the parent and the daughter are the same; thus, it is f_{GT} which is affected. Even-even nuclei are the most abundant, and their first few excited states are of even spin. The threshold for the excitation of the first M1 resonance can be rather high, the first level with isospin 1 is perhaps at 8.14 MeV above the ground state in ^{56}Ni. The log ft for the electron capture between the ^{56}Ni ground state and the ^{56}Co 1^+ state at 1.72 MeV is 4.4. If we assume the state at 8.14 MeV is 1^+ and the analogue of the ^{56}Co state (following Fowler and Fuller 1978), and use the relations

$$\frac{\langle \sigma t_3 \rangle_{fi}^2}{\langle \sigma t_+ \rangle_{fi}^2} = \frac{T_i+1-T_{3i}}{T_i+T_{3i}+2} \quad , \quad T_f = T_i+1 \tag{4.14a}$$

$$= \frac{T_{3i}^2}{(T_i-T_{3i})(T_i-T_{3i}+1)} \quad , \quad T_f = T_i \tag{4.14b}$$

$$= \frac{T_i+T_{3i}}{T_i-T_{3i}-1} \quad , \quad T_f = T_i - 1 \qquad (4.14c)$$

which hold among members of an isomultiplet, and (4.9), we obtain $\langle \sigma t_3 \rangle^2 = .08$ for the transition. The ratio of the cross section for exciting this level to the elastic scattering cross section is 2.4×10^{-5} for 10 MeV neutrinos, 3.2×10^{-4} for 25 MeV neutrinos. The range of normal allowed ft's, $\sim 10^4 - 10^{5.7}$, and hence of $\langle \sigma t_3 \rangle^2$ shows us that this is the typical result. Inelastic scattering is tiny as an opacity source when compared with elastic scattering. This is true for individual transitions; but there are so many 1^+ levels in the nucleus, there is even a giant magnetic dipole resonance, that perhaps when we sum over all these levels we get a large result. The strengths are limited by a sum rule for the Gamow-Teller matrix elements:

$$\sum_f \langle (C_{A0}+C_{A1}t_3)\sigma \rangle_{fi}^2 = \frac{1}{2J_i+1} \langle i | \sum_{a=1}^{A} (C_{A0}+C_{A1}t_3^a)\sigma^a \cdot \sum_{b=1}^{A} (C_{A0}+C_{A1}t_3^b)\underset{\sim}{\sigma}^b | i \rangle$$

$$= \frac{4}{2J_i+1} \sum_M \langle iM | (C_{Ap}\underset{\sim}{S}_p + C_{An}\underset{\sim}{S}_n)^2 | iM \rangle \qquad (4.15)$$

We may obtain an upper limit to the magnitude of inelastic scattering by having the sum rule saturated at zero excitation energy:

$$\Gamma_S(\nu) \leq n_i \frac{G^2}{\pi} \nu^2 \left(4. \sum_M \langle iM | (C_{Ap}\underset{\sim}{S}_p + C_{An}\underset{\sim}{S}_n)^2 | iM \rangle - \langle (C_{A0}+C_{A1}t_3)\sigma \rangle_{ii}^2 \right) \qquad (4.16)$$

If we are dealing with very high excitation energy, say 30 MeV, and all of the sum rule strength is below 10 MeV, this may not be such a bad approximation. In ^{56}Ni, the giant M1 resonance is estimated to be at $\sim$ 12.4 MeV by Fowler (1978) based on a comparison with ^{56}Co states; the ground state GT sum rule strength, estimated at 48/7 in section 5.3, is all put at 12.4 MeV. For 10 MeV neutrinos, the

giant M1 would not be excited; for 25 MeV neutrinos, the ratio of inelastic to elastic scattering for the ground state changes from 3.2×10^{-4} to 1.4×10^{-2}, and the sum rule expression (4.16) predicts 5×10^{-2} is an upper limit, a factor of 3.6 too high; by 40 MeV, it is only two too high. Some authors (Wilson 1977, Mazurek 1977) have neutronizing regions extending to electron chemical potentials of 40 MeV, and neutrinos are produced with $\sim$ 5/6 of this energy on the average, suggesting this approximation will work there. At high enough neutrino energy, forbidden transitions begin to be less suppressed, which would cause some modification of this prescription if heavies survived till very late in the collapse when the neutrino chemical potential can rise to $\sim$ 100 MeV. Then, however, the neutrinos are in equilibrium and only the total transport lifetime is important. Again using the shell model this sum rule gives zero for a doubly closed magic nucleus such as ^{40}Ca. There is no coherent addition of amplitudes in this matrix element; the result is of order unity, giving a value for the scattering rate which still pales in comparison with the elastic scattering value.

The inelastic scattering of neutrinos by nuclei can heat up the mantle region, something that the elastic scattering process cannot do; however, neutrino-electron scattering dominates over $\nu A \rightarrow \nu A^*$ as an energy deposition mechanism; the latter is $\lesssim$ 50% of the former for 20 MeV electron neutrinos passing through matter characterized by a 10 MeV electron chemical potential ($\rho \sim 1.4 \times 10^{10}$ g/cc, characteristic of the mantle); for muon neutrinos, the ratio may rise

to greater than unity due to the smaller ν_μ-e scattering opacity.

4.3 FINITE NUCLEAR SIZE EFFECTS

When the wavelength of the neutrino approaches the radius of the nucleus upon which it is incident, the neutrino no longer "sees" a point nucleus of some total weak charge Q_W . The phase contribution from each of the nucleons to the scattering amplitude cease to be approximately the same; coherence breaks down. For iron, the radius is about $1.1A^{1/3}$ fm $\sim$ $(47\ \text{MeV})^{-1}$; for helium, it is even smaller, $\sim$ $(113\ \text{MeV})^{-1}$. The correction is small for the neutrino energies typical of the neutronization and mantle regions. If heavy neutron rich nuclei can survive in the inner core, then its effect must be included, for there the neutrino energies rise to $\sim$ 100 MeV and higher. This elastic scattering, when present, determines the diffusion coefficient, and if the cross section is lowered, the diffusion time decreases.

The Fermi and Gamow-Teller matrix elements, 2.45, become $\left\langle (C_{V0}+C_{V1}t_3)\exp\ (i\underset{\sim}{k}\cdot\underset{\sim}{r})\right\rangle_{fi}^2$ and $\left\langle (C_{A0}+C_{A1}t_3)\underset{\sim}{\sigma}\ \exp(i\underset{\sim}{k}\cdot\underset{\sim}{r})\right\rangle_{fi}^2$ respectively, where $\underset{\sim}{k} = \underset{\sim}{q}-\underset{\sim}{q}'$ is the momentum transfer to the nucleus. For the ν+A$\rightarrow\nu$+A process in particular,

$$\left\langle (C_{V0}+C_{V1}t_3)\exp(ik\cdot r)\right\rangle_{ii}^2 = \left|C_{Vn}\ F_{ni}(\underset{\sim}{k}) + C_{Vp}\ F_{pi}\ (\underset{\sim}{k})\right|^2 \qquad (4.17)$$

where the neutron form factor of the state i is defined by

$$F_{ni}(k) = \left\langle i\left|\rho_n(\underset{\sim}{k})\right|i\right\rangle \qquad (4.18)$$

where $\rho_n(k)$ is the Fourier transform of the neutron density operator.

At zero momentum transfer, $\rho_n(\underset{\sim}{k}=0)$ is the neutron number operator, $F_{ni}(0) = N_i$, and 2.49 is recovered. The proton form factor is similarly defined; it has been measured by elastic electron scattering, and is given in a reasonable approximation (Freedman 1974) by

$$F_{pi}(k^2) = Z_i e^{-b_i k^2} \tag{4.19}$$

where $b_i = r_i^2/6$ and r_i is the root mean square nuclear radius. If we assume the neutrons have the same density distribution in the nucleus as the protons, and we know this is not always true, then $F_{ni} \simeq F_{pi}$, and (4.17) can be evaluated. If recoil is still neglected, and for heavy nuclei even at high neutrino energy this is a good approximation, and f_{GT} is also neglected, then the modification of the scattering and transport rates is

$$\Gamma_S(\text{finite nuclear size}) = \Gamma_S(\text{point nucleus},4.7)[e^{-\gamma}-(1-\gamma)]2/\gamma^2 \tag{4.20a}$$

$$\Gamma_{tr}(\text{finite nuclear size}) = \Gamma_{tr}(\text{point nucleus},4.8)[\gamma-2+(\gamma+2)e^{-\gamma}]6/\gamma^3 \tag{4.20b}$$

where

$$\gamma = 8b_i\nu^2 = 4.1\text{x}10^{-5}\ A^{2/3}\left(\frac{\nu}{1\ \text{MeV}}\right)^2 \quad , \text{ for } r_i = r_0\ A^{2/3}\ , \ r_0 = 1.1$$

This agrees with the result given by Yueh and Buchler (1977b) apart from a factor of γ (their y) in their $A_1^{(\nu A)}$. That the finite nuclear size effect plays an important role at high energy can be seen in Figure 5 which plots the ratio of the transport lifetimes calculated using 4.20b and 4.8 with $f_{GT}=0$. Because $k^2 = 2\nu^2(1-c)$ favors forward

directions, the transport rate is decreased more than the scattering rate by this effect.

4.4 ION-ION CORRELATION EFFECTS

If the neutrino wavelength is greater than the internucleus spacing, we may expect phase interference to manifest itself in the scattering amplitude. At high temperatures, the phases coming from different nuclei are random: the total scattering rate depends upon the number of scattering centers, not on the square of the number. At low temperature, nuclear motions become correlated due to electrostatic repulsion: in the extreme, as in the mantle of a cold neutron star, a Coulomb lattice forms.

Just as the scattering of neutrons from a medium, whether it be a gas, a liquid, or a solid, probes the density-density correlation function, so the scattering of neutrinos probes the weak current-current correlation function. We develop this formalism in Appendix 3. For nonrelativistic nucleons, when electron-nucleon correlations can be ignored, and nuclear polarization is unimportant, and both conditions are valid in the supernova core, the scattering kernel for neutrinos by nucleons, bound and free, is

$$R(\underset{\sim}{q}\rightarrow\underset{\sim}{q}') = G^2(1+c)\ S_{J^\circ J^\circ}(\underset{\sim}{k},\omega) + G^2(1-\tfrac{1}{3}\,c)S_{\underset{\sim}{J}\cdot\underset{\sim}{J}}(\underset{\sim}{k},\omega) \qquad (4.21)$$

where the current-current correlation functions for nucleons are given by

$$S_{J^\circ J^\circ}(k) = \int d^4x\ e^{i(k\cdot x)}\ \left\langle J^\circ_{had,NC}(x)\ J^\circ_{had,NC}(0)\right\rangle \qquad (4.22)$$

$$S_{\underset{\sim}{J}\cdot\underset{\sim}{J}}(k) = \int d^4x\, e^{i(k\cdot x)} \left\langle J^{\circ}_{had,NC}(x) \cdot \underset{\sim}{J}_{had,NC}(0) \right\rangle \qquad (4.23)$$

where the hadronic current components $J^{\circ}_{had,NC}$, $\underset{\sim}{J}_{had,NC}$ are given by 2.36a and 2.36b respectively. The expectation, $\langle \quad \rangle$, denotes an average over the local thermodynamic ensemble of the medium. The currents are evolved in time by the full matter Hamiltonian (with strong and electromagnetic, but no weak, forces). The 4-momentum transfer to the medium is $k = (\omega, \underset{\sim}{k}) = q - q'$.

When we take the ensemble to be $|i\rangle\langle i|$, where $|i\rangle$ is a nuclear state, the current-current correlation functions reduce to strength functions for the neutral current operators, which are similar to the well-known beta strength functions (see equations A3.28 - A3.30 and the discussion therein). The sum rule (4.15) is then just the zeroth moment of $S_{\underset{\sim}{J}\cdot\underset{\sim}{J}}$,

$$\text{SUM RULE: } \Omega \int S_{\underset{\sim}{J}\cdot\underset{\sim}{J}}(\underset{\sim}{k},\omega)\, \frac{d\omega}{2\pi} = \text{(equation 4.15)} \quad \text{for small } |k| \qquad (4.24)$$

where Ω is an arbitrary box normalization volume kept in for dimensional purposes. For small k, the sum rule for $S_{J^{\circ}J^{\circ}}$ is trivial; for larger $\underset{\sim}{k}$, not only are finite nuclear size effects included, since (4.17) is this correlation function evaluated at $\omega=0$ (apart from an Ω), but also forbidden transitions to excited states are included for $\omega \neq 0$. These latter effects are tiny.

At finite temperature in an infinite medium, these correlation functions contain information not only on the matrix elements between the resonant states of individual nuclei, but also on the correlations

among nuclei. If the nuclei are close together, how can we isolate the nucleons bound in one nucleus from those in another? Of course we cannot: the medium acts on the nucleus altering its properties, for example, its surface energy; fermion exchange terms may become important. If the nuclei are sufficiently far apart, we may hope to make a fairly clean separation between internal nucleus properties and external nucleus-nucleus properties; it is as if point nuclei are interacting only electromagnetically with each other (except that nuclear reactions must be included). The correlation functions are often separated into two parts, the self part which contains the internal excitation information, and the distinct part which contains nucleus-nucleus information as van Hove first did in 1954. If large correlated clusters of nucleons (heavy neutron-rich nuclei) can survive till rather late in the collapse, at high densities, then this separation may break down. We assume the separation works, so for small kR, where R is the nuclear radius,

$$S_{J^\circ J^\circ}(\underset{\sim}{k},\omega) \simeq \sum_{ij} (C_{Vn}N_i + C_{Vp}Z_i)(C_{Vn}N_j + C_{Vp}Z_j) \left\langle \rho_i(k\omega)\rho_j(x=0) \right\rangle \qquad (4.25)$$

where the sum is over all nuclear species i whose density operator is $\rho_i(x)$, with Fourier transform in space and time, $\rho_i(k\omega)$; the free neutron and proton are included in this sum. Partial dynamic liquid structure factors in multicomponent plasmas are defined by

$$S^D_{ij}(k\omega) = \frac{1}{\sqrt{n_i n_j}} \left\langle \Delta\rho_i(k\omega)\ \Delta\rho_j(x=0) \right\rangle \qquad (4.26)$$

where $\Delta\rho_i = \rho_i - \left\langle \rho_i \right\rangle$, and $n_i = \left\langle \rho_i \right\rangle$.

From the earlier discussion, it is apparent that the Gamow-Teller terms, which enter into $S_{\underset{\sim}{J}\cdot\underset{\sim}{J}}$, are negligible compared with the Fermi terms for heavy nuclei, and can be neglected for light nuclei. They cannot be neglected for neutrons and protons as we shall see.

Nuclei interact through their electric charges. In the mantle region, where, to a good approximation, only iron peak elements are present, the charges differ by small amounts, and each species behaves approximately the same; $S^D_{ij} = S^D$ is independent of species i and j. The scattering kernel is then

$$R(q\to q') \simeq G^2(1+c) \quad S^D(k\omega)\rho_B \sum_i (Q^2_{Wi}\ Y_i) \tag{4.27}$$

For small k, the neglect of recoil is a valid approximation, and

$$S^D(k\omega) \approx 2\pi\delta(\omega)S^S(\underset{\sim}{k}) \tag{4.28}$$

where the static liquid structure factor is related to its dynamic counterpart by

$$S^S(\underset{\sim}{k}) = \int S^D(\underset{\sim}{k}\omega)\ \frac{d\omega}{2\pi} \tag{4.29}$$

In other words, we saturate the "sum rule" (4.29) at zero energy transfer; the scattering is conservative, and (4.28) in (4.27) reduces to (4.2) if S^S is unity, the case if the nuclei are uncorrelated.

Flowers and Itoh (1974) pointed out that the supernova core is thermodynamically similar to a liquid metal; the nuclei are like ions. Itoh (1975) then showed that the Coulomb correlation among the ions drastically modifies the elastic scattering of low energy ($\sim$3 MeV)

neutrinos. To support this contention, he took the Debye-Huckel formula for the structure factor

$$S^S(k) \simeq \frac{k^2a^2}{k^2a^2+3\Gamma} \tag{4.30}$$

and calculated an effective neutrino scattering cross section, that is, a Γ_S , and found a large difference between it and the uncorrelated version. The Coulomb liquid is characterized by the dimensionless parameter

$$\Gamma = \frac{Z^2e^2}{akT} \approx 0.1 \frac{Z^2}{A^{1/3}} \frac{\rho_{11}^{1/3}}{T_{10}} \tag{4.31}$$

introduced by Brush et al. (1966) and the ion sphere radius,

$$a = \left(\frac{4}{3}\pi n_i\right)^{-1/3} \sim 16 \frac{A^{1/3}}{\rho_{11}^{1/3}} \quad \text{fm} \tag{4.32}$$

where the charge and mass number of the nuclei are Z and A , ρ_{11} and T_{10} are the density and temperature in units of 10^{11} g/cm^3 and 10^{10} K. If the plasma is multicomponent rather than one component, more parameters are necessary to characterize the medium (Hansen et al. 1977). The electrons play a negligible role in static Coulomb interactions due to their extreme degeneracy (Hansen 1973).

The Debye-Huckel law breaks down as a good approximation for large momentum transfers. In the iron-nickel mantle, at $\rho_{11} = 2$ and $T_{10} = 2.4$, $\Gamma \simeq 10$ and $a \simeq 50$ fm, and Itoh's results cannot be used above a neutrino energy of 3 MeV. J. P. Hansen (1973) presents Monte Carlo results for the liquid structure factor of the classical one

component plasma at $\Gamma = 10$; Figure 4 is constructed from his table and the Debye-Huckel law (4.30) is compared with it. The Fourier transform of the static liquid structure factor is directly related to the pair distribution function, $g(\underset{\sim}{r})$, which gives the probability that there is a particle at position $\underset{\sim}{r}$ given that there is one at position $\underset{\sim}{0}$. Coulomb repulsion results in g(r) being almost zero for distances less than the ion sphere radius, overshooting slightly at the ion sphere radius, and then settling down to unity. At higher Γ , the oscillations become greater. This is reflected in $S^S(k)$: the peak at $ka \sim 5$ sharpens and shoots up to a higher maximum and the oscillations continue out to $ka \sim 15$ before the function settles down to one. At $\Gamma \sim 155$, the Coulomb liquid becomes a Coulomb lattice (Pollack and Hansen 1973), and S^S is nonzero only in the neighborhood of reciprocal lattice vectors.

To obtain the transport lifetime at energy ν , we must integrate (4.27) from $k = 0$ to $k = 2\nu$, which we do numerically. The comparison of the uncorrelated transport lifetime with this correlated lifetime is given as a function of energy in Figure 5, along with the form factor deviation at high energy. At 10 MeV, with wavelength 20 fm, the difference is 25%, dropping to $\sim$ 2% at 15 MeV.

Notice the local maximum at 7 MeV; if the differential cross section were isotropic, instead of proportional to 1+c , no such maximum would exist; the local maximum in the Γ_S curve is in a slightly different position. At the same density and temperature, for a helium plasma, $\Gamma \sim 0.13$, a $\sim$ 20 fm and the Debye-Huckel approximation

is not too bad (Hansen et al. 1977); at 10 MeV, the wavelength is equal to the ion sphere radius, and the uncorrelated transport rate is 20% too high; at 15 MeV, it is 10% too high.

4.5 $\nu N \rightarrow \nu N$

In the inner core, the matter is hot and dense and consists primarily of quasifree neutrons and protons. In the neutronization region, where the alpha concentration is high, there are many quasifree neutrons, but rather few protons. In the mantle there are almost no free nucleons; they are almost all locked up in heavy nuclei. The scattering of neutrinos by nucleons is a dominant opacity source in the interior.

In a sense, we have already discussed this process for nondegenerate nucleons; if we reread the neutrino-nucleus elastic scattering section, starting with equation (4.2), passing through to equation (4.8), with the values

$$Q_W = C_{VN} \tag{4.33}$$

$$f_{GT} = 3C_{AN}^2/C_{VN}^2 \tag{4.34}$$

substituted, we are then reading about neutrino-nucleon (N=n) and neutrino-proton (N=p) scattering.

Most authors (Tubbs and Schramm 1975, Lamb and Pethick 1976, Yueh and Buchler 1976, 1977b, Bludman and van Riper 1977) have taken C_{An} to be 1/2 in the W.S. model rather than $g_A/2$, thereby coming to the erroneous conclusion that $\nu n \rightarrow \nu n$ is isotropic (i.e., c-independent

in equation (4.2)). By doing so, they make a 42% error in the scattering rate (4.7) and a 47% error in the transport rate (4.8).

More generally, νN scattering is described in terms of the density-density and spin-spin correlation functions by the kernel 4.21. A complete many body calculation of these correlation functions would include, for example, the processes ν+N+N→ν+N+N and ν+zero sound → ν+zero sound as well as νN→νN. However, the latter process dominates in the absence of nucleon clustering into nuclei. It may be calculated within the framework of the independent quasiparticle approximation (see section A2.2 in Appendix 2). When recoil is neglected, so the scattering is conservative, we obtain the scattering and transport rates

$$\Gamma_S = n_N \frac{G^2}{\pi} \nu^2 (C_{VN}^2 + 3C_{AN}^2)\, S_{NN}^S(0) = \begin{cases} 41.9\ \rho_{11}\ S_{nn}^S(0) Y_n \nu^2 & s^{-1} \\ 34.8\ \rho_{11}\ S_{pp}^S(0) Y_p \nu^2 & s^{-1} \end{cases} \tag{4.35}$$

$$\Gamma_{tr} = \frac{2}{3} n_N \frac{G^2}{\pi} \nu^2 (C_{VN}^2 + 5C_{AN}^2)\, S_{NN}^S(0) = \begin{cases} 43.3\ \rho_{11}\ S_{nn}^S(0) Y_n \nu^2 & s^{-1} \\ 38.5\ \rho_{11}\ S_{pp}^S(0) Y_p \nu^2 & s^{-1} \end{cases} \tag{4.36}$$

in terms of the static liquid structure factor at zero momentum transfer

$$S_{NN}^S(0) = \frac{1}{n_N} \int \frac{2d^3p}{(2\pi)^3} f_N(E_p)(1-f_N(E_p)) = \frac{\partial \ell n\ n_N}{\partial \eta_N} \tag{4.37}$$

Here, n_N is the neutron (N=n) or proton (N=p) concentration, and η_N is the nucleon degeneracy parameter, the chemical potential divided by the temperature. The nucleon is assumed not to change its energy in the collision; it must be scattered from an occupied state to an

unoccupied state at the same energy; therefore, the rates for a nondegenerate gas of nucleons (4.7 and 4.8) are modified by the factor $S^S_{NN}(0)$ which is the probability for finding a particle-hole pair at the same energy.

In order to obtain 4.35 and 4.36, we have assumed that the dynamic liquid structure factor is proportional to a delta function at $\omega=0$; i.e., the scattering is conservative. In Appendix 2, section A2.2, we show that, for nondegenerate nonrelativistic particles, it is, in fact, a Gaussian in ω with mean value $k^2/2m$ and standard deviation $\sqrt{k_B T/m}\ k$, where k is the momentum transfer to the medium (equation A2.12b). Both factors must be small compared with the incident neutrino energy in order for the conservative approximation to work. Otherwise, νN scattering would have to be dealt with as a nonconservative process. In zero temperature nuclear matter, neutrinos must deposit energy in order to raise nucleons above the Fermi sea; the structure factor (Figure 6) does not look like a delta function, and the scattering kernels (Figure 8) have outgoing neutrino energies spread over a relatively broad range below the incident neutrino energy.

Sawyer (1975) has used the fluctuation equation of state (Goodstein 1975) appropriate to classical systems

$$S^S_{NN}(0) = \rho(k_B T)\ K_T \tag{4.38}$$

where the isothermal compressibility is

$$K_T = \frac{\partial \ell n\ n_N}{\partial p} \tag{4.39}$$

and p is the pressure, to treat the modification of the scattering due to strong nucleon-nucleon interactions, using cold nuclear matter equations of state. He only deals with the modification of the Fermi term, neglecting the Gamow-Teller, which dominates the Fermi part by a factor of ~ 4.7. In regions where the equation of state is softer than that of a free nucleon gas, νN scattering is relatively enhanced; in regimes where the equation of state hardens due to the short-range repulsive forces, νN scattering is decreased relative to the free Fermi gas value.

When the neutrino wavelength is small compared with the internucleon spacing, the independent quasiparticle approximation will become the appropriate mode of description; 4.38 is then just 4.37. At normal nuclear matter density, this corresponds to neutrino energies in excess of 55 MeV, which is small compared with typical neutrino Fermi energies at that density. In the high energy, high temperature regime, 4.35, 4.36 can be used.

Suppose we adopt a simple effective mass formula for the energy E_p within the independent quasiparticle framework (A2.11, A2.14); we then obtain at low temperature

$$S^S_{NN}(0) \simeq \frac{m^*_N (kT)}{p^2_F(N)} \tag{4.40}$$

where $p_F(N)$ is the Fermi momentum of the nucleon, related to the density by

$$p_F(N) = (3\pi^2 n_N)^{1/3} = 111(\rho_{13} Y_N)^{1/3} \text{ MeV} \tag{4.41}$$

and m_N^* is the effective mass at the Fermi surface

$$\frac{1}{m_N^*} = \left(\frac{dE_p}{pdp}\right)_{p=p_F(N)} \tag{4.42}$$

As the temperature goes to zero, $S_{NN}^S(0)$ goes to zero, and the conservative approximation breaks down. We must resort to the zero temperature nonconservative scattering results: the ℓ=0 moment of the scattering kernel is given by equation A2.13 and is plotted in Figure 8 for νn scattering at the density 5×10^{13} g/cc and the neutron number per baryon Y_n = 0.9 for a few incident neutrino energies. A more complete discussion is given in Appendix 2.

We would like to use the conservative scattering approximation whenever possible. When the scattering rate 4.35 (or 4.36) with 4.40 is smaller than the zero temperature scattering rate A2.13c, we may expect that it fails; it breaks down when

$$\nu \gtrsim \frac{k_B T}{v_F} \tag{4.43}$$

where v_F is the velocity at the Fermi surface. The neutrino chemical potential typically exceeds this bound at high densities; recoil effects cannot be neglected, and the zero temperature formula A2.13c is more suitable.

If we compare either of these formulae for νN scattering in degenerate Fermi liquids with the nondegenerate scattering rate, it is evident that degeneracy inhibits scattering. Brown (1977) has suggested that neutrinos may flash out of the core when nucleons go degenerate,

due to this relative decrease of the scattering rate, and therefore, in the diffusion time. However, just as the nondegenerate scattering rate 4.35 increases with increasing density, so does the degenerate rate A2.13c. In fact, when the neutrinos are quite degenerate, the diffusion coefficients D_k of equation 3.67c all become equal to $D(\mu_\nu)$, independent of k, where μ_ν is the neutrino chemical potential. The diffusion constant does not then depend upon the particular power law dependence of the scattering rate, whether it be 2 as in 4.35 or 3 as in A2.13c, except in its relation to the transport lifetime evaluated at the neutrino chemical potential. The diffusion constant in both cases falls as $\rho^{-5/3}$. It does not suddenly decrease as the neutron degeneracy line is crossed, although it may fall by a factor of ~ 2 due to the different Y_ν/Y_n dependence of the nondegenerate and degenerate diffusion constants (the former is $\sim (Y_n/Y_\nu)^{1/3}$ times the latter). At these high neutrino energies, the neutrino absorption process can dominate the opacity; this process too is relatively suppressed when nucleons become degenerate; it is very small when the number of neutrons greatly exceeds the number of protons.

Suppose neutrinos are also extremely degenerate. The nonlinear terms in 3.26c lower the effective transport rate below Γ_s, due to final state blocking. This effect supports Brown's conjecture.

We define the baryon degeneracy parameter, η_B, by

$$\rho_B = \frac{(2m\ k_B T)^{3/2}}{2\pi^2}\ F_{1/2}\ (\eta_B) \qquad (4.44)$$

If Y_n were one, η_B and η_n would be identical. The line $\eta_B = 0$

corresponds to a transition line from nondegeneracy to degeneracy: nucleons are semi-degenerate. Beyond $\eta_B = 10$ the nucleons are quite degenerate. The relevant curves are displayed in Figure 9, where we have also included Arnett's (1977) central zone trajectory to show a typical thermodynamic history of the core.

4.6 $\nu e \rightarrow \nu e$

Neutrino-electron scattering is a decidedly nonconservative process: when the neutrinos are nondegenerate, and their energy is high compared with the electron Fermi energy, they lose an average of one half of their energy in each collision with a degenerate electron gas (Tubbs and Schramm 1975); when their energy is much lower than the electron Fermi energy, we can show that the mean energy transferred to the plasma by the neutrino is exactly one-third of its incident energy. Neither the conservative approximation nor the Fokker-Planck approximation (as Wilson 1974 once used) will adequately reproduce its effects. Not only are integrations over the outgoing neutrino energy introduced in the moment equations which are linear in the neutrino distribution function, but the onset of neutrino degeneracy introduces a further complication: the moment equations have a quadratic nonlinearity in the source terms (as in equations 3.25c, 3.26c, and 3.27c).

In Appendix 2, in section A2.1, we evaluate the current-current correlation function of an electron plasma in the independent quasiparticle approximation, and use it in section A2.3 to obtain the first three moments of the neutrino-electron scattering kernels; for

the reaction $\nu_e+e \rightarrow \nu_e+e$, for extremely relativistic electrons,

$$R_\ell(\nu\rightarrow\nu') = (C_{Ve}+C_{Ae})^2\ \gamma_\ell(\nu\rightarrow\nu') + (C_{Ve}-C_{Ae})^2\ \bar{\gamma}_\ell(\nu\rightarrow\nu') \qquad (4.45)$$

where

$$\gamma_\ell(\nu\rightarrow\nu') = \frac{2G^2}{3\pi}\frac{\nu^3}{\beta(\nu')^2}\int_{max(0,-\beta\omega)}^{\infty}\frac{d\xi}{(e^{\xi-\eta}+1)(1+e^{\eta-\xi-\beta\omega})}\phi_\ell(\frac{\xi}{\beta\nu}\ ;\ \frac{\nu'}{\nu}) \qquad (4.46)$$

and the dimensionless functions ϕ_ℓ are polynomials in $\xi/\beta\nu$ and rational functions of ν'/ν , and are given by equations A2.22 and A2.23 for ℓ=0, 1, 2. The kernel $\bar{\gamma}_\ell$ is given by the same expression 4.46 except ϕ_ℓ is replaced by $\bar{\phi}_\ell$ which are defined by equation A2.25. The neutrino energy transfer to the plasma is $\omega=\nu-\nu'$, and β is the inverse temperature in energy units. The two exponential terms in the denominator arise from the electron df for the initial electron and the hole df (= $1-f_e$) for the final electron. The Fermi energy of the electron is η/β . Generally, the evaluation of 4.46 requires a numerical integration over ξ .

Examples of the ℓ=0 spectra for three different incident neutrino energies are given in Figure 10 for conditions characteristic of the neutronizing shell; there, we see the neutrinos dominantly downscatter in energy when they collide with an electron gas; the width of the spectrum near the peak is fairly broad. However, even at η=14 , the value of the electron degeneracy parameter chosen for this figure, there is a significant amount of upscattering (i.e., the final neutrino energy exceeds the incident neutrino energy). Upscattering is related to downscattering by equation 3.6. As the

temperature is lowered to zero, the upscattering decreases to zero; as the temperature is raised, the amount of upscattering increases as we show in Figure 11.

The higher ℓ moments have a more complicated form than the ℓ=0 one; they can be negative as well as positive. A typical example of the relation between the first three moments is given in Figure 12 for an incident neutrino energy of 25 MeV. The scattering is never strongly anisotropic; the ℓ=0 moment is usually significantly greater than the higher ones. When the energy transfer to the plasma is small, the neutrinos are somewhat forward peaked; when it is large, the scattering is backward peaked. We expect this behavior in neutrino scattering off individual electrons and, regardless of incident neutrino energy, this is the general trend.

These scattering kernels are applicable to a wide variety of processes, necessitating change in the neutral current constants only:

$$\bar{\nu}_e + e^- \rightarrow \bar{\nu}_e + e^- \quad : \quad C_{Ae} \rightarrow -C_{Ae} \quad \text{in} \quad 4.45 \qquad (4.47a)$$

$$\nu_\mu + e \rightarrow \nu_\mu + e \quad : \quad C_{Ve} \rightarrow C_{V\mu} \ , \ C_{Ae} \rightarrow C_{A\mu} \ \text{in 4.45} \qquad (4.47b)$$

$$\bar{\nu}_\mu + e \rightarrow \bar{\nu}_\mu + e \quad : \quad C_{Ve} \rightarrow C_{V\mu} \ , \ C_{Ae} \rightarrow -C_{A\mu} \ \text{in 4.45} \qquad (4.47c)$$

The changes in 4.47a, with the further change $\eta \rightarrow -\eta$ in 4.46, give the kernels for $\nu_e + e^+ \rightarrow \nu_e + e^+$, but due to the relative paucity of positrons in these supernova cores, this process can be ignored.

The inverse scattering lifetime, Γ_S , defined by equation 3.28, is useful as an indicator of the relative importance of νe scattering. To obtain it requires a further numerical integration, this time over

the final neutrino energy. In certain limiting cases, for very low or very high energy neutrinos (relative to the electron Fermi energy) analytic formulae can be obtained (equations A2.27a, b). With charged current constants ($C_{Ve} = C_{Ae} = 1$) , these formulae were first derived by Bahcall (1964) and elaborated upon by Hansen (1966). Tubbs and Schramm (1975) extended them to include neutral currents, and also gave some numerical values of Γ_S for two neutrino energies.

Apart from our work, a number of other authors have investigated the effects of $\nu_e e$ scattering and have independently obtained some of these scattering moments; Yueh and Buchler (1977b) obtained the $\ell=0$ and $\ell=1$ moments (our $\bar{\phi}_o$, equation A2.25a,b does not agree with theirs; one of their (ν')'s should be a ν); Tubbs (1978) has obtained the $\ell=0$ moments for his Monte Carlo code.

Within the inner core, where the nucleons are free, the neutrino distribution function is essentially isotropic and Fermi-Dirac. There is a small outward flowing neutrino current proportional to the gradient of the isotropic part of the df ; the proportionality constant is the diffusion constant; the diffusion constant at high neutrino energies is dominated by the absorption $\nu_e + n \rightarrow e^- + p$, and at low neutrino energies by either emission $e^- + p \rightarrow \nu_e + n$ or conservative scattering $\nu + n \rightarrow \nu + n$ depending upon the relative magnitudes of Y_p and Y_n. In the mantle and envelope, the elastic scattering of neutrinos by nuclei dominates the opacity. Neutrino-electron scattering never dominates (although it competes with $\nu n \rightarrow \nu n$ when neutrons are degenerate, as can be seen by comparing A2.27a with A2.13c). Graphs

of the rates for the various processes interior to the neutronizing shell (Figure 13) and in the mantle (Figure 14) emphasize this point.

What, then, is the role of νe scattering? It can redistribute the neutrino energy spectrum, in particular downscattering high energy neutrinos to low energy, accelerating the rate of approach to a Fermi-Dirac distribution; conservative processes serve to confine neutrinos in the core, but do not redistribute energy. This downscattering of neutrinos dumps energy into the plasma, thereby heating it; this is the second role which νe scattering plays, as an energy deposition mechanism. It also results in momentum deposition, but in small amounts compared with conservative scattering (Figure 14).

We discuss these roles in more detail in Chapter 6, both for electron and muon neutrinos. There we find, for example, the reaction $\nu_\mu\ e \rightarrow \nu_\mu\ e$ is the thermalizer of the ν_μ production spectrum. In Figures 13 and 14, the shapes of the scattering rates for the other types of neutrinos are similar to those for $\nu_e e$, but are lower: $\bar{\nu}_e e$ is lower by a factor varying between 1 at low energy and 0.46 at high energy; $\nu_\mu\ e$ varies between 0.18 and 0.11 of the $\nu_e\ e$ curve; $\bar{\nu}_\mu\ e$ is within 0.18 and 0.16. These ranges are independent of the particular density and temperature. This is in contrast to the rates for the scattering of the other types of neutrinos by nuclei and nucleons: at energies low compared with the nucleon mass the scattering rates for $\bar{\nu}_e N$, $\nu_\mu N$, $\bar{\nu}_\mu N$ are the same as for $\nu_e N$.

With the discovery of neutral currents, νe scattering was

unseated by coherent neutrino-nucleus scattering as the dominant opacity source in the mantle and envelope. The picture of a supernova model changed from neutrino energy deposition (Colgate and White 1966) to neutrino momentum deposition. In the energy deposition model, νe scattering was to be the mechanism by which the gravitational energy from core collapse could be dumped in the mantle, heating it, causing a rapid expansion, shock wave generation and outward propagation, perhaps triggering the thermonuclear detonation of unburned nuclear fuel such as oxygen (Fowler and Hoyle 1964), and ultimately leading to matter expulsion, a supernova. Wilson (1971), and, more recently, Chechetkin et al. (1976) have shown that within the charged current framework, the opacity due to νe scattering alone is not sufficient to generate a supernova by the above mechanisms. Both of these works overestimated the heating effects by not including the scattering "into the beam" terms in 3.25c. Neutrino-electron scattering dominates as a mantle heating mechanism over absorption on nuclei $\nu+A \rightarrow e^- +A$ (Bahcall and Frautschi 1964), and, as we have seen, over $\nu+A \rightarrow \nu+A^*$.

4.7 $\nu\nu \rightarrow \nu\nu$

It is remarkable that such an exotic process can ever become an important mechanism. The neutrino concentration in the core builds up to a level similar to the electron concentration when neutrino-beta equilibrium is reached. Further, the cross section for the scattering of neutrinos by neutrinos is similar to that for νe scattering, as is shown in Table 2 and in Flowers and Sutherland (1976). The rate of

$\nu\nu$ scattering is then of the same magnitude as the rate of νe scattering; $\nu\nu$ scattering accelerates even more the approach of the neutrino distribution to Fermi-Dirac.

The source function for this process has a quartic nonlinearity which is difficult to deal with generally. In section A1.2 of Appendix 1, we derive the zeroth moment of the $\nu_e\nu_e \rightarrow \nu_e\nu_e$ source in the limit that the neutrino distribution function is isotropic ($n_1 << n_0$). This expression, A1.25, is exact in an infinite homogeneous medium. The numerical implementation is complicated when an energy bin averaging technique such as that described in Appendix 4 is used; this can be alleviated by adopting the usual technique of finite differencing in energy space.

There is another easier approximation which we can use to deal with neutrino-neutrino scattering, one in which we exploit the similarity to νe scattering. We assume, as far as quantities integrated over neutrino energy are concerned, that the nonequilibrium ν df is approximately a FD df, 3.7, with the value of η_ν adjusted to agree with the nonequilibrium neutrino number per baryon (3.57b): detailed differences between the true df and its FD approximation, $\tilde{n}$, such as a low energy deficiency in the nonequilibrium df, will be washed out by the energy integration. This approximation is undoubtedly poor in the mantle where the neutrinos are approaching free streaming, but there the neutrino concentration is so low that this reaction is unimportant.

In the νe scattering kernels, we make the following changes:

f_e is replaced by $\tilde{n}$, and

$$\nu_e\nu_e \to \nu_e\nu_e \quad : \quad C_{Ve} \to \alpha_e^2 \quad , \quad C_{Ae} \to \alpha_e^2 \text{ ; multiply by 1/4 in 4.45} \tag{4.48a}$$

$$\bar{\nu}_e\nu_e \to \bar{\nu}_e\nu_e \quad : \quad C_{Ve} \to \alpha_e^2 \quad , \quad C_{Ae} \to -\alpha_e^2 \quad \text{in 4.45} \tag{4.48b}$$

$$\nu_\mu\nu_e \to \nu_\mu\nu_e \quad : \quad C_{Ve} \to \alpha_e\alpha_\mu \quad , \quad C_{Ae} \to \alpha_e\alpha_\mu \quad \text{in 4.45} \tag{4.48c}$$

$$\bar{\nu}_\mu\nu_e \to \bar{\nu}_\mu\nu_e \quad : \quad C_{Ve} \to \alpha_e\alpha_\mu \quad , \quad C_{Ae} \to -\alpha_e\alpha_\mu \quad \text{in 4.45} \tag{4.48d}$$

and similarly, we can give prescriptions for the other possible reactions; however, those in 4.48 will dominate. By the time we have to worry about $\nu_\mu, \bar{\nu}_\mu$ which are produced in neutrino-antineutrino pair processes, the electron neutrinos will already be in equilibrium; in that case, 4.48c and 4.48d will be excellent approximations to describe the thermalization of the ν_μ and $\bar{\nu}_\mu$ production spectra due to these neutrino-neutrino processes, as we shall see in Chapter 6.

In order to be consistent, in 4.48a, we should include only n_0 terms in the source (which implies $\delta^{(1)} \simeq 0$) since we have assumed approximate isotropy by substituting $\tilde{n}$ for n_0 ; in practice, this is no obstacle, for it is these terms which dominate thermalization of the spectrum.

Using this prescription to relate $\nu\nu$ scattering to νe scattering, any approximation scheme used to treat the relaxation of neutrinos to equilibrium due to $\nu_e e$ scattering, such as that used by Arnett (1977), can be immediately adapted to treat relaxation due to neutrino self-scattering.

5. PRODUCTION AND ABSORPTION

The capture of electrons by protons and heavier nuclei dominates neutrino production in the early stages of collapse. It is this reaction, together with the photodisintegration of nuclei, which initiates the dynamical instability. The electron neutrinos produced in neutronization carry away most of the lepton number of the core and much of the gravitational energy released in the collapse. The production lifetime for this process, along with lifetimes for related processes, is calculated in the first four sections. Later in the core's collapse, $\nu\bar{\nu}$ pairs created in leptonic and semileptonic processes become important transporters of energy and momentum; we deal with a variety of such processes in subsequent sections.

5.1 $e^- + p \rightleftarrows n + \nu_e$

This electron capture process in stellar interiors has received extensive treatment in the literature (see Freedman et al., 1977 for references). Here, we derive the production rate using the correlation function formalism appropriate to charged current reactions as given in section A3.5 of Appendix 3. The incoming electron's energy is so high, and the charge on the proton so low that the electron's Coulomb wave function is essentially a plane wave: the Coulomb factor is unity. Electrons are effectively uncorrelated with nucleons. The production rate for a neutrino of energy ν is A3.34,

$$\Gamma_p(\nu) = \int \frac{d^3p_e}{(2\pi)^3} f_e(p_e)\, G^2[(1+v_e c)S_{J^0 J^0\dagger}(k\omega)+(1-\tfrac{1}{3}v_e c)S_{\underset{\sim}{J}\cdot\underset{\sim}{J}\dagger}(k\omega)], \quad (5.1)$$

where $\underset{\sim}{k} = \underset{\sim}{p}_e - \underset{\sim}{q}$, $\omega = E_e - \nu$, $c = \hat{p}_e \cdot \hat{q}$, v_e is the electron's speed, and f_e is its distribution function. The correlation functions are defined in a manner similar to A3.10b.

This expression is quite general: it describes electron capture on heavy nuclei and the modified URCA process as well as $e^- + p \rightarrow n + \nu_e$. Within the independent quasiparticle approximation of section A2.2 in Appendix 2, the correlation functions for nucleons reduce to

$$S_{J^0 J^0 \dagger} = g_v^2 \, n_p \, S_{np}^D \, (k\omega) \tag{5.2a}$$

$$S_{\underset{\sim}{J} \cdot \underset{\sim}{J}\dagger} = 3 g_A^2 \, n_p \, S_{np}^D \, (k\omega) \tag{5.2b}$$

where

$$n_p S_{np}^D \, (k\omega) = \int \frac{2 d^3 p_p}{(2\pi)^3} \, f_p(p_p) \int \frac{d^3 p_n}{(2\pi)^3}$$

$$\cdot \, (1 - f_n(p_n)) \, 2\pi \delta(E_p + m_p - E_n - m_n + \omega) \, (2\pi)^3 \delta^{(3)}(\underset{\sim}{p}_p + \underset{\sim}{k} - \underset{\sim}{p}_n) \tag{5.2c}$$

is a dynamic liquid structure factor for this proton to neutron transition; it is related to $\langle (p^\dagger n)(k\omega)(n^\dagger p)(0) \rangle$, rather than being given by equation 4.26 which is zero for uncorrelated nucleons. The integral over ω of $S_{np}^D(k\omega)$ is $S_{np}^S(k)$, a static structure factor.

We assume here that the nucleon energies are just the kinetic energies, and nucleon recoil can be neglected. The production rate is then

$$\Gamma_p(\nu) = \frac{G^2}{\pi}(g_v^2 + 3g_A^2)n_p\, S_{np}^S(0)\,(\nu+Q)^2\, f_e(\nu+Q)v_e$$

$$= 167.2\,\rho_{11}Y_p\, S_{np}^S(0)\,\left(\frac{\nu+Q}{1\ \text{MeV}}\right)^2 f_e(\nu+Q)v_e \qquad s^{-1}\ . \quad (5.3a)$$

where $Q = m_n - m_p \simeq 1.3$ MeV , and

$$v_e = \left(1 - \frac{m_e^2}{(\nu+Q)^2}\right)^{1/2} \quad (5.3b)$$

This expression is valid at lower densities, when the electrons are nonrelativistic, as well as at the high densities of interest here. This reaction has a threshold; only those electrons with energy greater than Q can react to produce neutrinos, as is evident from the argument of f_e in 5.3a . The static np structure factor at zero momentum transfer is a thermodynamic quantity, just as the nn and pp static structure factors were:

$$S_{np}^S(0) = \frac{1}{n_p}\int 2\,\frac{d^3p}{(2\pi)^3}\, f_p(E_p)(1-f_n(E_n)) = \frac{n_n - n_p}{n_p(e^{\beta(\mu_n-\mu_p)}-1)} \quad (5.3c)$$

In the nondegenerate regime, this structure factor is one, and our result agrees with that given by Tubbs and Schramm (1975) and Yueh and Buchler (1976).

Yueh and Buchler (1976) calculated the production rate at a variety of neutrino energies, temperatures, and densities without neglecting recoil and compared it with 5.3. The production lifetime is reduced to a two-fold integration which they evaluate numerically.

In the density-temperature regime of importance in the early stages of collapse, when nucleons are nondegenerate, 5.3 with $S^S_{np}(0) = 1$ is valid to within $\sim$ 10%. We also get equation 5.3 by applying the formula 2.46 in Chapter 2 to Fermi's Golden Rule.

If we had only free nucleons, the lifetime to produce 30 MeV neutrinos at $\sim 10^{11}$ g/cm^3 is measured in microseconds; the reabsorption lifetime is similarly short. Neutrino beta-equilibrium would be rapidly attained, in times much shorter than the dynamical time, which is many milliseconds. However, not until the late stages of collapse is the free proton abundance per baryon, Y_p, large (of order 10^{-1}); at 10^{12} g/cc it is perhaps 10^{-3}. The neutronization rate is clearly quite sensitive to the value of the function $Y_p(Y_e,\rho,T)$, which is determined from nuclear statistical equilibrium calculations. At present, Y_p is not very well determined in supernova core material.

The absorption lifetime is similarly derived using either the current-current correlation function formulation or Fermi's Golden Rule and equation 2.46. With the neglect of recoil, the result is

$$\Gamma_a(\nu) = n_n \frac{G^2}{\pi} (g_V^2 + 3g_A^2)(\nu+Q)^2(1-f_e(\nu+Q))v_e \; S^S_{pn}(0)$$

$$= 167.2 \; \rho_{11} Y_n \; S^S_{pn}(0) \left(\frac{\nu+Q}{1 \text{ MeV}}\right)^2 (1-f_e(\nu+Q))v_e \quad \text{s}^{-1} \qquad (5.4a)$$

where

$$S^S_{pn}(0) = \frac{n_n - n_p}{n_n(1-e^{-\beta(\mu_n-\mu_p)})} = e^{\beta(\mu_n-\mu_p)} S^S_{np}(0) \qquad (5.4b)$$

which is related to Γ_p by the detailed balance condition 3.11.

In order to calculate the neutronization rate, 3.17b, and the rate of heat loss from the medium to the neutrinos, 3.17c, we must evaluate certain integrals over the neutrino energy involving the production and absorption rates and the neutrino df. Generally, these must be evaluated numerically, since the neutrino df is neither zero nor Fermi-Dirac.

If the neutrino df is FD, or approximately so, and we can neglect the mass difference of the neutron and proton and the electron mass (a good approximation due to the high electron chemical potential), the neutronization rate can be given in terms of Fermi functions, 3.68:

$$-(\dot{Y}_e)_{e^-p} = \left[\frac{G^2}{2\pi}\,(g_V^2 + 3g_A^2)\right] \frac{e^{\eta_p}(Y_n - Y_p)(1-\exp(\eta_n+\eta_\nu-\eta_p-\eta_e))}{(1-e^{-(\eta_e-\eta_\nu)})(e^{\eta_n}-e^{\eta_p})}$$

$$\cdot \frac{T^5}{\pi^2}\,(F_4(\eta_e)-F_4(\eta_\nu)) \qquad (5.5a)$$

$$\xrightarrow[\eta_\nu \to -\infty]{} \left\{\rho_B \frac{G^2}{\pi}\,(g_V^2 + 3g_A^2)\right\} \frac{T^2}{2}\, Y_p Y_e \frac{F_4}{F_2}(\eta_e) \qquad (5.5b)$$

Here, T is the temperature in energy units; when T is measured in MeV, the numerical factor in square brackets is .181 s^{-1} per baryon. The energy loss rate per baryon is related to 5.5a by

$$\dot{q}_{e^-p} = (\dot{Y}_e)_{e^-p}\; T\, \frac{F_5(\eta_e) - F_5(\eta_\nu)}{F_4(\eta_e) - F_4(\eta_\nu)} \qquad (5.5c)$$

The $\eta_\nu \to -\infty$ limit gives the case when neutrino phase space is unfilled. The ratio of $\dot{q}$ to $\dot{Y}_e$ is the mean energy at which the neutrinos are produced, which, for an extremely degenerate Fermi gas of electrons is $5\mu_e/6$: since the cross section rises as the square of the energy, it favors capture from high energy electrons, and the average energy of the neutrinos is $\sim$ 11% higher than the average internal energy of the electrons.

When equilibrium is attained, the chemical potentials of the reactants and products balance, and the neutronization and energy loss rates given by 5.5 vanish.

Production and absorption rates are compared with other processes in Figure 13. For the conditions chosen, the value of Y_p is probably too high; more protons may be locked into heavy nuclei, although this is still quite uncertain. This figure, however, emphasizes an important point. At high energy, neutrino absorption by neutrons dominates neutrino scattering by neutrons; at low energy, the degeneracy cuts down the absorption rate, and $\nu n \to \nu n$ dominates over absorption. However, it is not Γ_a which enters into the transport rate, but rather $\Gamma'_a = \Gamma_a + \Gamma_p$, and at low energies, the electron capture rate, Γ_p , can dominate over νn scattering. Whether it does or not depends upon the number of free protons compared with the number of free neutrons; under the conditions given in Figure 13, it does. At very small energy, it always will since the rate of production of zero energy neutrinos is nonzero due to the Q of the reaction.

Therefore, with just charged currents, there was still neutrino trapping in the inner core; the addition of neutral current reactions served to extend the trapping region to beyond the neutronizing shell, as well as changing the interplay of neutrinos and the mantle.

When nucleons go degenerate, and the number of neutrons differs significantly from the number of protons, the static np structure factor (5.3c), which goes as $\exp(-\beta(\mu_n-\mu_p))$, becomes very small and the reaction rate for $e^- + p \rightarrow n + \nu_e$ becomes negligible. Corrections to the independent particle approximation calculation of this rate must be included. The independent pair approximation (de Shalit and Feshbach 1974) adds in dynamical (as opposed to statistical) two body correlations in nuclear matter, which give rise to the modified URCA reactions: $n+e^- + p \rightarrow n+n+\nu_e$, $n+n \rightarrow n+e^- + p+\bar{\nu}_e$ (Bahcall and Wolf 1965). These reactions will serve to maintain neutrino beta-equilibrium in the early stages of cooling of the neutron star which may result from core collapse. Dynamical two body correlations in nuclear matter also give rise to the bremsstrahlung process $N+N \rightarrow N+N+\nu+\bar{\nu}$ (Flowers, Sutherland, and Bond 1975) which takes over as the main $\nu\bar{\nu}$ pair creation mechanism from the plasmon neutrino process (section 5.7) once the hot neutron star has cooled sufficiently.

At even higher densities, perhaps twice that of normal nuclear matter, the (charged) pion field may have a nonzero expectation value in the ground state of nuclear matter: a pion condensate may form (Migdal 1978, and references therein). The mediation of the

reaction $e^- p \to n\nu_e$ by the pion condensate, which we loosely write in the form $e^- + n \to n + \nu_e + \langle \pi^- \rangle$, greatly enhances its rate (Maxwell et al., 1977; Kiguchi, 1977). If the condensate exists, this reaction dominates the cooling of neutron stars (at least after the initial electron neutrinos from neutronization have been lost). Otherwise, the modified URCA and nucleon bremsstrahlung processes dominate (until nuclear matter goes superfluid).

5.2 $e^+ + n \gtrless \bar{\nu}_e + p$

The calculation of the production and absorption rates for this reaction is similar to that for $e^- p \gtrless n\nu_e$, with the results

$$\Gamma_p = \left\{ \rho_B \frac{G^2}{\pi} (g_v^2 + 3g_A^2) \right\} Y_n (\nu - Q)^2 \, \bar{f}_e(\nu - Q) S_{pn}^S(0) \, \theta(\nu - Q) \tag{5.6a}$$

$$\Gamma_a = \left\{ \rho_B \frac{G^2}{\pi} (g_v^2 + 3g_A^2) \right\} Y_p (\nu - Q)^2 \, (1 - \bar{f}_e(\nu - Q)) S_{np}^S(0) \, \theta(\nu - Q) \tag{5.6b}$$

where the positron's df is $\bar{f}_e$, which is approximately a Maxwell-Boltzmann in supernova cores, for there, $\eta_e \gtrsim 10$, and $\eta_{e^+} = -\eta_e$.

Using this approximation, the protonization rate due to positron capture is

$$(\dot{Y}_e)_{e^+ n} = \left[\rho_B \frac{G^2}{\pi} (g_v^2 + 3g_A^2) \right] T^2 \, (6 + 3t + t^2/2) [Y_{\bar{e}} Y_n - 2 Y_{\bar{\nu}} Y_p] \tag{5.7a}$$

and the energy loss rate is

$$(\dot{q})_{e^+ n} = (\dot{Y}_e)_{e^+ n} \, 5T \, \frac{(1 + 3t/5 + 3t^2/20 + t^3/60)}{(1 + t/2 + t^2/12)} \tag{5.7b}$$

where $t = Q/T$, $Y_{\bar{e}}$ is the abundance of positrons per baryon. When energies are measured in MeV, the term in curly brackets is numerically $167.2\ \rho_{11}\ \ s^{-1}$. Since the mean $\bar{\nu}_e$ energy is only about 5T, and therefore of thermal rather than Fermi energy magnitude, terms of order t cannot be neglected as they were in electron capture.

This reaction competes with the $\nu_e\bar{\nu}_e$ production processes as a $\bar{\nu}_e$ producer. It has the advantage of being unaffected by ν_e degeneracy which occurs well before $\bar{\nu}_e$ equilibrium.

5.3 $e^- + (N,Z) \rightarrow \nu_e + (N+1,\ Z-1)$

The capture of electrons by heavy nuclei, part of the URCA process, is difficult to deal with in these supernova cores, as one constantly presses up against the boundaries of known nuclear physics, and is forced to pass beyond, making educated guesses for ft-values, for spins and parities of levels, and even for level energies.

The inverse production lifetime, calculated either using the correlation function formalism appropriate to charged current processes (section A3.5 of Appendix 3) or, more simply, equation 2.46 is quite similar in form to that obtained for $e^-p \rightarrow n\nu_e$ (equation 5.3, with $S_{np}(0) = 1$)

$$\Gamma_p(e^-+A_i \rightarrow \nu_e+A_f\ ;\ \nu) = n_i \frac{G^2}{\pi} (\nu+Q_{fi})^2\ f_e(\nu+Q_{fi})(g_V^2\langle t_-\rangle_{fi}^2+g_A^2\langle \sigma t_-\rangle_{fi}^2)$$

$$\cdot\ v_e\ F(Z_i,\nu+Q_{fi})\ \theta(\nu+Q_{fi}) \qquad (5.8)$$

where $Q_{fi} = M_f - M_i$ is the mass difference between the final (f) and initial (i) nuclear states whose spins have already been summed over, F is the Coulomb factor, and the Fermi and Gamow-Teller matrix elements for allowed transitions are defined by equation 2.47. To evaluate 5.8 for given f and i necessitates knowledge of the matrix elements, which are related to the ft-values by 4.9; usually, experimental knowledge is unavailable and theoretical knowledge is sketchy for the same reasons that plagued us in the evaluation of inelastic $\nu A \rightarrow \nu A^*$ matrix elements. Indeed, the problems are quite similar, and this discussion follows that of section 4.2.

Assuming we know the ft-values, we must sum over all possible final states accessible by an allowed transition to the initial state. The high electron Fermi energy implies that the capture may occur into very highly excited states of the daughter nucleus; thus, we must know the masses and number of these allowed states in regions where the nuclear level density is extremely high, as well as at low excitation energy where the level density is low and the nuclear structure is at least partially known.

We must sum over all of the thermally populated levels of each nuclear species, weighted by the Boltzmann factor, then sum over all nuclear species, weighted, of course, by their abundances, which are determined by nuclear statistical equilibrium calculations as functions of ρ, T and Y_e .

This is a formidable task indeed. Nonetheless, a number of workers have attempted to calculate integrated rates. Fowler and

and Hoyle (1964) discussed the capture rates on a number of iron group nuclei. Hansen (1966) and later Mazurek et al. (1974) calculated rates for a broad range of nuclei near the valley of beta stability, using simple choices of ft-values and energy level spacings. Taking these rates, Epstein and Arnett (1975) calculated the neutronization rate ($\dot{Y}_e$) and the mean energy loss to neutrinos for matter in NSE and fit the result to a four species model, consisting of one typical heavy (dubbed iron), one typical light (dubbed alpha), and the free neutron and proton. These results, and extrapolations of them, have often been used in collapse calculations (Arnett 1977, Wilson 1977, Epstein, Norgaard and Bond 1978). Unfortunately, only ground state partition functions were used in the calculation of NSE, which grossly underestimates the number of heavy nuclei present at high temperature, since excited states are then plentifully populated. In the very early stages of collapse, just after core silicon burning, Y_e falls less than 0.44, the lower boundary of the Epstein and Arnett calculations (Weaver, Zimmerman and Woosley 1977, Arnett 1977). Collapse occurs entirely in the extrapolated regime in a neutron rich medium. Further, these rates break down when the neutrino phase space builds enough to suppress production into already occupied states. NSE calculations valid over a wider region of thermodynamic phase space (ρ, T, Y_e space) are clearly necessary, both to obtain neutronization rates on heavies and to give the equation of state (EOS) whose knowledge is crucial for the dynamics. This problem is now receiving much attention (Engelbrecht, Fowler, and Woosley 1978,

Lattimer and Ravenhall 1977).

Recently, Fowler, Fuller, and Newman (1977) have recalculated the rates for important iron group nuclei, giving also differential production rates, i.e., Γ_p's, using detailed nuclear level structures. Others have attacked the problem using the gross theory of beta decay (Takahashi and Yamada 1969, Takahashi 1971), which is a prescription for obtaining the beta strength functions (see section A3.5 of Appendix 3) in a Fermi gas independent particle model of the nucleus, a method which its practitioners hope will be a reasonable approximation for very neutron rich nuclei for which detailed nuclear information is lacking.

When does electron capture on free protons dominate electron capture on heavies, so knowledge of $Y_p(Y_e,\rho,T)$ is sufficient to obtain the neutronization rates? As in the section on inelastic neutrino-nucleus scattering, we take ^{56}Ni as our concrete example. For the single level transition $e^- + {}^{56}\text{Ni}$ (g.s., 0+) $\rightarrow \nu_e + {}^{56}\text{Co}$ (1.72 MeV, 1^+), the ft value is measured (log ft = 4.4). If we neglect the mass difference (Q_{fi} = 0.4 MeV) and set the Coulomb factor equal to one which should be true at high energy, then

$$\frac{\Gamma_p(e^- + {}^{56}\text{Ni} \rightarrow \nu_e + {}^{56}\text{Co}(1.72\text{MeV},1^+))}{\Gamma_p(e^- p \rightarrow n\nu_e)} = \frac{Y({}^{56}\text{Ni(g.s.)})}{Y_p}\frac{(ft)_n}{(ft)}$$

$$= 7.8\text{x}10^{-4}\left(\frac{Y({}^{56}\text{Ni(g.s.)})56}{Y_p}\right)$$

where $(ft)_n$ is the ft-value of the neutron, $10^{3.04}$. In order for

this single level electron capture on ^{56}Ni to win out over e^-p , the mass fraction of ^{56}Ni in its ground state must be greater than the free proton mass fraction by $\sim$ 1300.

When does Y_p exceed 10^{-3}? Early in the collapse, it is lower than this value, and e^-A exceeds e^-p ; late in the collapse, Y_p is greater than 10^{-3} , and e^-p dominates. With the present EOS uncertainty, the transition point cannot be pinned down.

At high electron Fermi energy, we may saturate the sum rule at zero energy as we did in the inelastic scattering case, producing an upper bound on the electron capture rate of a nucleus in state i:

$$\Gamma_{p,i}(\nu) \lesssim n_i \frac{G^2}{\pi} f_e(\nu)\nu^2 \left\{ g_V^2 \left(T_i(T_i+1)-T_{3i}(T_{3i}-1)\right) + g_A^2 \left\langle i \middle| \sum_{a,b} \tilde{\sigma}^a t_+^a \cdot \tilde{\sigma}^b t_-^b \middle| i \right\rangle \right\} \tag{5.9}$$

where we have explicitly evaluated the Fermi sum in terms of the total isospin T_i and the third component of isospin T_{3i} of the state i. We have assumed the energy is sufficiently high that the Coulomb factor is one; otherwise, $F(Z_i,\nu)$ can be inserted into this equation.

When we evaluate the sum rules for ^{56}Ni, we obtain zero for the Fermi sum rule for all T = 0 states, and these are all the low lying ones which will be thermally populated. The ground state of ^{56}Ni is approximated by its shell model configuration of eight $f_{7/2}$ protons and eight $f_{7/2}$ neutrons; only the transitions of $f_{7/2}$ neutrons are then included, yielding a Gamow-Teller sum rule of 8(12/7), a

result which assumes perfect overlap between the neutron and proton shell model states, leading to overestimation, but neglects collective effects, which acts to balance this overestimation. The GT sum rule for $\nu+A \rightarrow \nu+A^*$ is just one-half of this (if $C_{A0} = 0$), and has already been used. The Gamow-Teller sum rule evaluation is more difficult for the excited states of ^{56}Ni; we make the crude approximation that all states have 8(12/7) for this value, in order to make numerical estimates. Then, adapting 5.5b, we obtain an integrated capture rate per ^{56}Ni per electron of $\sim 1.06 \times 10^5$ s^{-1} at $\rho Y_e = 10^{11}$ g/cc. When we use the techniques of Fowler, Fuller, and Newman (1977) for ft-value assignment to obtain our sum rule, we find the approximation 5.9 gives values within $\sim$ 40% of theirs at $\mu_e = 24$ MeV ($\rho Y_e \simeq 10^{11}$ g/cc).

If we use the above upper bound on ^{56}Ni capture, the ^{56}Ni mass fraction must only be greater than the proton mass fraction by $\sim$ 15 in order for electron capture on ^{56}Ni to dominate over the capture on protons. This compares with the previous value of $\sim$ 1300 obtained using only one low-lying state, emphasizing the importance of the inclusion of all the sum rule strength.

At high density and temperature, for nuclei far off the valley of beta stability, the prescription 5.9 requires only sum rule estimation, surely an easier task than beta strength estimation.

At even higher density, when the momentum transfer to the nucleus approaches the inverse of the nuclear radius, forbidden transitions can no longer be neglected, and the electron capture rate finally approaches the number of protons in the nucleus times the

free proton capture rate. In the latest phases of collapse, when the electron Fermi energy is $\sim$ 100 MeV, we are either in, or nearing, this region; the transition between use of 5.9 and use of 5.3 (with Y_p the total proton abundance, both bound and free) has yet to be worked out. It is not even known whether such neutron rich nuclei will be present at this stage of collapse.

We may apply 5.5c, with obvious modifications, to obtain the energy loss rate to neutrinos. When Q values can be neglected, the mean energy at which the neutrinos are produced is again $5\mu_e/6$.

5.4 $\nu_e + (N,Z) \rightarrow e^- + (N-1,Z+1)$

Neutrino absorption by heavy nuclei, the inverse of the electron capture reaction, has a differential rate

$$\Gamma_a(\nu_e+A_f \rightarrow e^-+A_i;\nu) = n_i \frac{G^2}{\pi} (\nu+Q_{fi})^2 f_e(\nu+Q_{fi})(g_V^2\langle t_+\rangle_{if}^2+g_A^2\langle \sigma t_+ \rangle_{if}^2)$$

$$\cdot v_e F(Z_i,\nu+Q_{fi})\ \theta(\nu+Q_{fi}) \qquad (5.10)$$

which satisfies the detailed balance relation 3.11. However, the highly excited states of the daughter nucleus for electron capture are rarely thermally populated, and serve as parent nuclear states for neutrino absorption only enough to ensure that the neutrino beta-equilibrium condition, 3.12, is indeed the appropriate equilibrium even when heavy nuclei are present; this would not be so if the matter were not in NSE.

To obtain absorption rates on those nuclear states which are

abundantly present, the same procedures in matrix element evaluations as were used in the inverse process must be followed. Bahcall and Frautschi (1964) used a Fermi gas model of the nucleus to evaluate absorption rates, yielding results they estimate to be valid at high neutrino energies (> 15 MeV). The sum rule saturation at zero energy can also be used as an approximation. In any case, this absorption process on heavies is small compared with νe scattering and so plays little role in energy deposition; it plays an even smaller role in momentum deposition.

5.5 $\nu\bar{\nu}$ PRODUCTION AND STELLAR EVOLUTION

The loss of energy from matter by the emission of $\nu\bar{\nu}$ pairs is naturally and generally expressed in the language of the weak current-current correlation functions which depend upon the 4-momentum transfer to the medium, $(\omega,\underset{\sim}{k})$. The scattering of neutrinos by matter probes the spacelike domain of these functions, $\omega \lesssim k$, as we saw in Chapter 4. The production of $\nu\bar{\nu}$ pairs probes the timelike domain, $\omega \gtrsim k$; in addition, ω is negative, for the medium loses the energy required to create the $\nu\bar{\nu}$ pair. The timelike region with ω positive, so the medium gains energy, describes the inverse reaction, $\nu\bar{\nu}$ annihilation. The various domains in ωk space are displayed in Figure 3.

Once a star has developed a carbon/oxygen core, the energy loss in $\nu\bar{\nu}$ pairs exceeds the energy loss in photons; from this stage onward, the neutrino losses exert a controlling influence on the

evolution of the stellar core. The core can only be temporarily supported against gravitational contraction by means of temperature, and therefore pressure, gradients set up by the heat energy released in thermonuclear reactions.

The way in which this occurs for stars more massive than perhaps 8 $M_\odot$ (this number is quite uncertain) illustrates how neutrino losses determine the structure of presupernova stars. Arnett (1972a,b, 1974a,b, 1977a) numerically evolves helium cores through the various advanced burning states, and finds over a wide mass range that the iron/nickel cores converge to approximately the Chandrasekhar limit of $\sim 1.4\ M_\odot$, with the basic onionskin structure of the ashes from earlier burning stages layered on top of it. Both results, core convergence and the onionskin model itself, depend in an essential way not only on the existence of neutrino losses, but also on their detailed density and temperature dependence.

Energy can be produced in the core of the star by either nuclear burning or gravitational contraction. If the star is burning fuel at its center, the energy generated can be transported by either neutrinos, in which case it moves at the speed of light, almost completely decoupled from the stellar matter through which it passes, or by convection: once the central temperature is beyond $\sim$ 40 KeV, photon diffusion and electron conduction become inefficient energy transporters (Arnett 1974). Convection, by itself, cannot release energy from the star: it only mixes it over the convective region. Neutrinos take the energy away.

If the nuclear energy generation at the center exceeds the neutrino energy losses, the energy imbalance causes the central temperature to rise. Once the temperature gradient becomes superadiabatic in a region, convection sets in over that region. The convective core will grow until the nuclear source balances the neutrino sink when averaged over the core. The composition is uniform throughout the convective core and the core is smaller for more advanced burning stages; the result is the onionskin model of massive stellar cores: iron and nickel, the ashes of silicon burning are surrounded by a layer of silicon, then a shell of oxygen and neon, a shell of carbon and oxygen, a layer of helium and finally of hydrogen.

With no neutrino losses, our presupernova models would have quite different interior structures (Ikeuchi et al. 1971).

Stars with carbon/oxygen cores more massive than $\sim 2\ M_\odot$ cool by $e^+e^- \rightarrow \nu\bar{\nu}$; stars with C/O cores less massive than $\sim 1.44\ M_\odot$ cool by $\gamma_{p\ell} \rightarrow \nu\bar{\nu}$; cores with masses in between these two limits cool sometimes by the pair annihilation process, sometimes by the plasmon neutrino process, with the latter tending to dominate at higher densities. If the C/O core mass exceeds $\sim 30\ M_\odot$, the $e^+e^- \rightarrow \nu\bar{\nu}$ losses result in a dynamical instability, the core collapses, undergoes a hydrodynamic bounce, ignites remaining nuclear fuel, and seems most often to lead to no remnant, although lower mass cores undergoing this instability can leave black hole remnants. The result is the pair instability supernova, first proposed by Fowler and

Hoyle (1964), numerically modelled by Rakavy and Shaviv (1967) and Fraley (1968) and summarized in Barkat's (1975) review of neutrino processes in stellar evolution.

In all these cases, the neutrinos are freely streaming from the star and enter into the stellar evolution equations only as a local energy sink. The energy loss rate in $\nu\bar{\nu}$ pairs (emissivity in erg g^{-1} s^{-1}), Q, is the required quantity, and this can be expressed in terms of the current-current correlation functions (using the formalism of section A3.3 of Appendix 3):

$$\dot{Q} = \frac{1}{\rho}\int \frac{d^4k}{(2\pi)^4} S_{J^\alpha J^\beta}(+\underset{\sim}{k},+\omega)(k^\alpha k^\beta - k^2 g^{\alpha\beta})(-\omega)\theta(k^2)\theta(-\omega) \qquad (5.11a)$$

$$= \frac{1}{\rho}\int_0^\infty \frac{\omega d\omega}{2\pi}\int_0^\omega \frac{k^2 dk}{2\pi^2}\,(r_1(k,-\omega)k^2 + r_2(k,-\omega)(3\omega^2-2k^2)) \qquad (5.11b)$$

Here, θ is the Heaviside unit function, the k^2 in 5.11a is the square of the four-momentum, and ρ is the density. The k^2 in equation 5.11b is the square of the three-momentum. The scalars r_1 and r_2 introduced in Appendix 3, equation A3.23, completely characterize the energy loss rates; the differential $\nu\bar{\nu}$ production spectra probe, in addition, a third scalar, a term which arises from VA interference; two more scalars are generally needed to describe the full current-current correlation function, which are not probed by either neutrino scattering or $\nu\bar{\nu}$ production and absorption.

This simple expression (the hard part is the full evaluation of r_1 and r_2) includes <u>all</u> $\nu\bar{\nu}$ production processes. Those which have been treated in the literature and found to be of importance are the

three BPS processes, $e^+e^- \to \nu\bar{\nu}$, $\gamma_{p\ell}\, e \to e\, \nu\bar{\nu}$ (the photoneutrino process), $\gamma_{p\ell} \to \nu\bar{\nu}$ (Beaudet, Petrosian, and Salpeter 1967), electron-nucleus bremsstrahlung, $e^- + {}^A_Z \to e^- + {}^A_Z + \nu\bar{\nu}$ (Gandelman and Pinaev 1960, Festa and Ruderman 1969, Cazzola et al. 1971), and the related $e^-p \to e^-p\nu\bar{\nu}$ and $e^-n \to e^-n\nu\bar{\nu}$ in neutron star interiors (Flowers 1973). Further, the purely neutral current reactions $n+n \to n+n+\nu\bar{\nu}$, $n+p \to n+p+\nu\bar{\nu}$ (Flowers, Sutherland, and Bond 1975) have been found to be of importance in neutron star cooling; ${}^A_Z{}^* \to {}^A_Z + \nu\bar{\nu}$ has already been discussed in Chapter 2. The other $\nu\bar{\nu}$ processes mentioned also have neutral current corrections: the corrections to the BPS processes in certain regimes have been given by Dicus (1972), and the first of the bremsstrahlung processes has been treated with neutral currents by Dicus et al. (1976).

Over the years, many other $\nu\bar{\nu}$ production processes have been considered and found to be unimportant relative to the above ones: $\gamma + {}^A_Z \to {}^A_Z + \nu\bar{\nu}$, $e^- + e^- \to e^- + e^- + \nu\bar{\nu}$, $\gamma\gamma \to \nu\bar{\nu}$, $\gamma\gamma \to \gamma\nu\bar{\nu}$, $\gamma e \to \gamma e\, \nu\bar{\nu}$, and synchrotion radiation, $e^- \to e^- + \nu\bar{\nu}$ in the presence of a magnetic field (see Kuchowicz 1972 for references).

5.6 $e^+e^- \to \nu\bar{\nu}$

The important new complication which arises in dense collapsing stellar cores is the high neutrino opacity which causes the neutrinos to be trapped and the neutrino phase space to fill up to equilibrium levels, which results in a reduction in the neutrino emissivity. Finally, at high density, it is the equilibrium diffusion

approximation which describes the flow of these neutrinos, with the emissivity serving only to maintain the Fermi-Dirac form of the zeroth moment of the distribution function. The physics required to treat the $\nu\bar{\nu}$ production processes in the regime intermediate between free streaming and equilibrium diffusion is given here, first for the pair annihilation mechanism, then for the plasmon neutrino mechanism (section 5.7).

The pair annihilation process is the only $\nu\bar{\nu}$ production mechanism which can be described in the independent particle approximation of Appendix 2. The derivation of the moments of the production kernels for $e^+e^- \rightarrow \nu\bar{\nu}$ follows closely the derivation of the moments of the $\nu e \rightarrow \nu e$ scattering kernels, a result to be expected since the former is a crossed reaction of the latter. When the temperature is sufficiently high that the positrons, as well as the electrons, are extremely relativistic, as in iron core collapse, the ℓ^{th} moment of the production kernel, obtained in section A2.4 of Appendix 2, is

$$R_{p\ell}(\nu,\nu') = (C_{Ve}+C_{Ae})^2\, \gamma_{p\ell}(\nu,\nu') + (C_{Ve}-C_{Ae})^2\, \bar{\gamma}_{p\ell}(\nu,\nu') \qquad (5.12)$$

where

$$\gamma_{p\ell}(\nu,\nu') = \frac{2G^2}{3\pi}\frac{\nu^3}{(\nu')^2}\, kT \int_0^{\beta|\omega|} \frac{\phi_{p\ell}(\xi,\nu,\nu')\, d\xi}{(e^{\xi-\eta}+1)(\exp(\beta|\omega|-\xi-\eta)+1)} \qquad (5.13)$$

with η the electron's degeneracy parameter, ν the neutrino's energy, ν' the antineutrino's energy, and $\phi_{p\ell}$ is given in detail by equations

A2.35, A2.36, A2.37, and A2.38 for ℓ = 0, 1, 2. An equation similar to 5.13 holds for $\bar{\gamma}_{p\ell}$, with another function, $\bar{\phi}_{p\ell}$, replacing $\phi_{p\ell}$. The integration, which must in general be performed numerically, is over ξ , the electron energy divided by kT; the range of integration is finite here, in contrast to the semi-infinite range encountered in νe scattering. Except for this difference, the form of equations 5.12 and 5.13 is the same as that of 4.45 and 4.46. We use Gauss-Legendre instead of Gauss-Laguerre integration to evaluate these integrals. The ℓ = 0 moment of the production kernel is displayed for various neutrino energies as a function of the antineutrino energy in Figure 15 for a particular choice of ρY_e (4×10^{12} g/cc) and temperature (1.2×10^{11} K). This figure is for $\nu_\mu \bar{\nu}_\mu$ production rather than $\nu_e \bar{\nu}_e$ production: $C_{V\mu}$ and $C_{A\mu}$ should replace C_{Ve} and C_{Ae} in 5.12.

The $\nu\bar{\nu}$ absorption process, $\nu\bar{\nu} \rightarrow e^+e^-$, also requires the evaluation of a kernel, which is related to the production kernel 5.12 by the detailed balance condition 3.9, i.e.,

$$R_{a\ell}(\nu,\nu') = e^{-\beta(\nu+\nu')} R_{p\ell}(\nu,\nu') \tag{5.14}$$

To obtain the ν absorption opacity from this requires knowledge of the $\bar{\nu}$ distribution function, which is, in general, a nonequilibrium one.

The production rate for a neutrino of energy ν when the antineutrinos are nondegenerate is related to the ℓ = 0 moment of the kernel by an integral over the antineutrino phase space (equation 3.29):

$$\Gamma^{\nu}_{th}(\nu) = \int R_{p0}(\nu,\nu') \frac{(\nu')^2 d\nu'}{2\pi^2} \tag{5.15a}$$

The production rate for an antineutrino of energy ν' (when the neutrinos are nondegenerate) is

$$\Gamma_{th}^{\bar{\nu}}(\nu') = \int R_{p0}(\nu,\nu') \frac{\nu^2 d\nu}{2\pi^2} \qquad (5.15b)$$

These two spectra are unequal as we can see from Figure 16: the difference is a result of VA interference and arises in a similar manner to the inequality of νe and $\bar{\nu} e$ scattering rates.

The total energy loss rate to $\nu_e\bar{\nu}_e$ pairs is related to these Γ's by

$$\dot{Q} = \frac{1}{\rho} \int \nu\, \Gamma_{th}^{\nu}(\nu) \frac{\nu^2 d\nu}{2\pi^2} + \frac{1}{\rho} \int \nu'\, \Gamma_{th}^{\bar{\nu}}(\nu') \frac{(\nu')^2 d\nu'}{2\pi^2} \qquad (5.16)$$

which is another way to write equation 5.11. In the e.r. limit, $\dot{Q}$ and the $\nu\bar{\nu}$ production rate (i.e., $\dot{Y}_{\nu_\mu}$, or equivalently $\dot{Y}_{\bar{\nu}_\mu}$) are given by very simple formulae, A2.43 and A2.41 respectively. In the limit in which the electrons are quite degenerate, as they are in the iron core collapses, and thus the positrons are nondegenerate, analytic expressions can be given. We find the mean energy which the $\nu\bar{\nu}$ pair is created with (for nondegenerate neutrinos) is $4\mu_e/5 + 4\sqrt{}kT$: the neutrinos and antineutrinos are created with energies similar to the magnitude of the electron Fermi energy rather than with the thermal energy. This is simply because the electrons which annihilate are from near the top of the Fermi sea.

The emissivity per unit neutrino energy is obtained from Γ_{th}^{ν}

by multiplying it by $\nu^3/2\pi^2$ which shifts the peak from that indicated in Figure 16 toward higher energies, nearer the Fermi energy of the electron. When these ν and $\bar{\nu}$ spectra are multiplied instead by $\nu^2/2\pi^2$, which gives the number of ν's and $\bar{\nu}$'s created per unit energy, the area under each resulting curve is the same: the number of neutrinos produced must, of course, equal the number of antineutrinos produced.

When the core collapse is hot, $e^+e^- \rightarrow \nu\bar{\nu}$ dominates over $\gamma_{p\ell} \rightarrow \nu\bar{\nu}$. The line of demarcation between the region of pair dominance and the region of plasmon dominance (defined as the set of points at which the energy loss rates are approximately equal) is different for $\nu_e\bar{\nu}_e$ production and $\nu_\mu\bar{\nu}_\mu$ production: both are shown in the temperature-electron density (ρY_e) plane, the former in Figure 17, the latter in Figure 18. The plasmon neutrino rate for $\nu_\mu\bar{\nu}_\mu$ creation is very sensitive to the value of the Weinberg angle ($\sin^2\theta_W = 0.3$ is used here as elsewhere), and as the Weinberg angle drops towards $\sin^2\theta_W \simeq 0.25$, this line moves to the (reader's) right.

Also plotted in Figure 18 is Arnett's (1977) central trajectory in this phase plane. In his model, the plasmon rate dominates $\nu_e\bar{\nu}_e$ production in the early stages of collapse, but both processes, e^+e^- and $\gamma_{p\ell}$, play a role in $\nu_\mu\bar{\nu}_\mu$ production. As the pressure due to nucleons rises, and the trajectory follows $\rho \sim T^{3/2}$ (see Chapter 6), the core passes fully into the e^+e^- region of dominance. Throughout most of the collapse, the diffusion of electron neutrinos from neutronization dominates energy transport, and

thermally produced neutrino pairs don't compete until quite a bit later in the collapse.

Wilson's (1977) recent central trajectories are colder than Arnett's, remaining within the region of plasmon process dominance, at least as far as the evolution has been reported. Wilson's two bounces are also shown in Figures 17 and 18. We now turn to the plasmon process.

5.7 $\gamma_{p\ell} \rightarrow \nu\bar{\nu}$

The plasmon neutrino process occurs when plasma waves, a cooperative phenomenon between the electromagnetic potential field and the electron field (and the nuclear field) damp into $\nu\bar{\nu}$ pairs. Usually they dissipate into electron-hole pairs (are absorbed by an electron in the medium and thus are Landau damped) or they dissipate into e^+e^- pairs (if the temperature is high enough). This dissipative decay couples through the electric charge, the energy is trapped by electromagnetic processes, and the diffusion of this dissipative energy takes a long time. Occasionally, with a branching ratio related to the weak coupling constant and the thermodynamic parameters of the medium the dissipation is through $\nu\bar{\nu}$ pairs, which, in collapsing iron cores, can also be trapped, but energy in this form flows from the medium much faster than by radiative or conductive transport. Iron cores whose trajectories pass to the right of the demarcation line in Figures 17 and 18 cool by this mechanism, at least until the nucleon bremsstrahlung process $N+N \rightarrow N+N+\nu+\bar{\nu}$ takes over. Of course, charged current mechanisms are also cooling the collapsing core, and throughout

most of the collapse, do so more efficiently.

The plasma waves are created by thermal fluctuations of the electric current acting cooperatively with thermal fluctuations of the electromagnetic field. Fluctuations dissipate. One mode of dissipation, via $\nu\bar{\nu}$ pairs, comes about through the relation of fluctuations in the weak current-current correlation function to dissipation: the former has the energy transfer to the medium, ω, positive, and $\nu\bar{\nu}$ pairs can be annihilated to create such a fluctuation; the latter has ω negative, and a collective plasma excitation, a plasmon, can decay into a $\nu\bar{\nu}$ pair. This provides an illustration of the famous fluctuation-dissipation theorem.

Adams, Ruderman, and Woo (1963; hereafter ARW) were the first to point out the existence of the plasmon neutrino process: they wrote the interacting electromagnetic four potential in terms of the quantized plasma waves (instead of photons), then calculated the rate at which this quantum breaks up into a virtual electron-hole pair which annihilates to create a $\nu\bar{\nu}$ pair. Their rate, when account is taken of a correction to their work given by Zaidi (1965) and of neutral current corrections (Dicus 1972), is the same as we obtain below using the more general current-current correlation function formalism. Flowers (1973) uses electromagnetic potential autocorrelations to obtain the plasma neutrino rate; his formulation follows from ours.

All of these authors obtain expressions for integrated energy loss rates. Here, we focus on the spectra of the neutrinos created

and the modifications necessary when Fermi statistics become important, as we did in the $e^+e^- \to \nu\bar{\nu}$ section.

ARW have shown that the γ_5 portion of the weak current contributes little to the plasmon neutrino rate. If the vector part of the weak current is the only important one, then the weak current-current correlation function is approximately given in terms of the electron's electromagnetic current-current correlation function (in the timelike $\omega \gtrsim k$ regime):

$$S_{J^\alpha J^\beta}(\omega k) \simeq \frac{C_{Ve}^2}{e^2} S_{J^\alpha_{em} J^\beta_{em}}(\omega k) \tag{5.17}$$

where the electromagnetic current is given by equation 2.2. In the W.S. theory, with $\sin^2\theta_W = 0.25$ exactly, $C_{V\mu}$ (which replaces C_{Ve} in 5.17) vanishes; then, the reaction rate for $\gamma_{p\ell} \to \nu_\mu \bar{\nu}_\mu$ would have to be obtained from the axial electron weak current. We do not pursue this term here.

An isotropic plasma, which, neglecting magnetic field effects, is the case for collapsing iron cores, has its electromagnetic current-current correlation function completely determined by two functions, the longitudinal and transverse dielectric permittivities. The fluctuation-dissipation theorem, a combination of A3.16 and A3.13, gives

$$S_{J^\alpha_{em} J^\beta_{em}}(k\omega) = 2f_{p\ell}(-\omega)\, \chi''_{J^\alpha_{em} J^\beta_{em}}(k,-\omega) \tag{5.18}$$

where χ'' is the absorptive response function (A3.15), the Fourier

transform in space and time of one-half of the commutator of the electromagnetic current, $[J^{\alpha}_{em}(x)\ ,\ J^{\beta}_{em}(0)]/2$. The Planck distribution, which multiplies χ'' ,

$$f_{p\ell}\ (\omega) = \frac{1}{e^{\beta\omega} - 1} \tag{5.19}$$

will turn out to be the distribution function for the plasmon.

Following Sitenko (1967) and Martin (1968), we may write the absorptive response function in terms of the complex dielectric permittivity tensor, the complex conductivity tensor, the complex electric susceptibility tensor, or the complex magnetic permittivity tensor: they are all related to each other. For isotropic plasmas, the dielectric permittivity tensor is

$$\varepsilon_{ij} = \varepsilon_{\ell}(\omega k)\ \frac{k_i k_j}{k^2} + \varepsilon_{t}(\omega k)\left(\delta_{ij} - \frac{k_i k_j}{k^2}\right)$$

where ε_{ℓ} and ε_{t} are the longitudinal and transverse dielectric constants, and the absorptive response function for the spatial current is

$$\chi''_{J^i_{em} J^j_{em}}\ (k\omega) = \frac{\omega^2}{4\pi}\left\{\frac{k_i k_j}{k^2}\ \frac{Im\ \varepsilon_{\ell}}{|\varepsilon_{\ell}|^2} + \left(\delta_{ij} - \frac{k_i k_j}{k^2}\right)\frac{(\omega^2 - k^2)^2}{|\omega^2 \varepsilon_{t} - k^2|^2}\ Im\ \varepsilon_{t}\right\} \tag{5.20}$$

The charge density-charge density dissipation is obtained from 5.20 by the application of current conservation:

$$\chi''_{\rho_{em}\rho_{em}}(k\omega) = \frac{k^i k^j}{\omega^2}\chi''_{J^i_{em}J^j_{em}}(k\omega)$$

$$= \frac{k^2}{4\pi}\frac{Im\ \varepsilon_\ell}{|\varepsilon_\ell|^2} \qquad (5.21)$$

and similarly, the remaining response functions are

$$\chi''_{\rho_{em}\ J^i_{em}} = \chi''_{J^i_{em}\ \rho_{em}} = \frac{k^j}{\omega}\chi''_{J^i_{em}J^j_{em}}$$

$$= \frac{\omega k^i}{4\pi}\frac{Im\ \varepsilon_\ell}{|\varepsilon_\ell|^2} \qquad (5.22)$$

All terms depending upon charge density fluctuations, namely 5.21 and 5.22, only involve the longitudinal dielectric permittivity. The fluctuations transverse to the direction of wave propagation, $\underset{\sim}{k}$, only involve the transverse current. When the Coulomb gauge ($\nabla\cdot\underset{\sim}{A} = 0$) is chosen for the electromagnetic potential, the vector potential couples only to the transverse current: the resulting collective mode obeys the dispersion relation of the photon, $\omega=k$, at high frequency and short wavelength. The decay of this photon-like transverse mode turns out to dominate the $\nu\bar{\nu}$ energy loss. Our results, however, which only depend upon current-current correlation functions are gauge invariant.

The longitudinal term is a charge density fluctuation: it is the self consistent scalar Coulomb field which oscillates driving the oscillations of the individual charged particles, which in turn are the source of the field.

The expressions 5.20, 5.21, and 5.22 are quite general.

Whenever the longitudinal and transverse photon propagators, $(k^2 \varepsilon_\ell (\omega,k))^{-1}$ and $(\omega^2 \varepsilon_t (\omega k)-k^2)^{-1}$, have poles, the poles dominate the behavior of the dielectric constants. The dispersion relations for longitudinal and transverse plasma waves arise from the solution to the pole position equations:

$$\text{longitudinal:} \quad \omega = \omega_\ell(k) \quad , \quad \text{where } \varepsilon_\ell(\omega_\ell(k),k) = 0 \tag{5.23}$$

$$\text{transverse:} \quad \omega = \omega_t(k) \quad , \quad \text{where } \omega_t^2 \varepsilon_t(\omega_t(k),k)-k^2 = 0 \tag{5.24}$$

Generally, the functions ω_ℓ and ω_t have both real and imaginary parts, the latter giving the negative of the damping rate ($\gamma_\ell \equiv - Im\ \omega_\ell(k)$, $\gamma_t \equiv - Im\ \omega_t(k)$). Hereafter, $\omega_\ell(k)$ denotes $Re\ \omega_\ell(k)$ and ω_t denotes $Re\ \omega_t(k)$. When damping is small ($\omega_\ell >> \gamma_\ell$), we have

$$Re\ \omega_\ell^2\ \varepsilon_\ell(\omega_\ell,k) = 0 \tag{5.25a}$$

$$\gamma_\ell = \left[\frac{Im\ (\omega^2 \varepsilon_\ell)}{\frac{\partial}{\partial \omega} Re(\omega^2 \varepsilon_\ell)} \right]_{\omega=\omega_\ell(k)} \tag{5.25b}$$

A similar set of relations define ω_t and γ_t, except the right hand side of 5.25a is k^2 instead of zero. The damping times, γ_t^{-1} and γ_ℓ^{-1}, include Landau damping (called Cerenkov absorption by Tsytovich 1961) and pair production. Tsytovich (1961) calculates the dielectric permittivities in the random phase approximation for a quantum electron plasma with a fixed positively charged background (the ionic plasma frequency is small compared with the electron plasma frequency),

and from these obtains ω_ℓ , γ_ℓ and ω_t , γ_t .

The expressions Tsytovich gives for ε_ℓ and ε_t must in general be evaluated numerically. In the e.r. , e.d. limit, when terms of order ω/μ_e and k/μ_e can be neglected, simple results are obtained (ARW and Beaudet et al. 1967):

$$\varepsilon_\ell = 1 - \left(\frac{\omega_p}{\omega}\right)^2 \left(1 + \frac{3}{5}\frac{k^2}{\omega^2}\right) \tag{5.26a}$$

$$\varepsilon_t = 1 - \left(\frac{\omega_p}{\omega}\right)^2 \left(1 + \frac{1}{5}\frac{k^2}{\omega^2}\right) \tag{5.26b}$$

from which the dispersion relations

$$\omega_\ell^2 = \frac{\omega_p^2}{2}\left(1 + \sqrt{1+12k^2/5\omega_p^2}\right) \tag{5.27a}$$

$$\omega_t^2 = \frac{\omega_p^2+k^2}{2}\left(1 + \sqrt{1+\frac{4k^2/5\omega_p^2}{(1+k^2/\omega_p^2)^2}}\right) \tag{5.27b}$$

follow. Here, the plasma frequency (for electron and positron oscillations) is given by

$$\beta\omega_p = \left(\frac{8e^2}{3\pi}\left(F_1(\eta) + F_1(-\eta)\right)\right)^{1/2} \tag{5.27c}$$

where η is the degeneracy factor of the electron. In the e.d. limit, a Sommerfeld expansion yields the approximate relation (which is adequate for our purposes)

$$\omega_p \simeq \frac{\mu_e}{18}\sqrt{1+\pi^2/3\eta^2} \tag{5.28}$$

Thus, ω_p exceeds 1 MeV when $\rho Y_e \gtrsim 4.2\times10^{10}$ g/cc , and exceeds $\beta^{-1} = kT$ when η is in excess of ~ 18 ; lines of constant η are lines of constant $\beta\omega_p$.

In the neighborhood of the plasma wave resonances $\omega = \pm\omega_\ell$(or $\pm\omega_t$) , the terms appearing in the absorptive response functions are of the classical Lorentz form with width $2\gamma_\ell$ (or $2\gamma_t$) , and these approach delta functions in the limit of infinite resonance lifetime:

$$\frac{Im\ \varepsilon_\ell}{|\varepsilon_\ell|^2} = \frac{\omega_\ell^2}{\frac{\partial}{\partial\omega}(\omega^2\varepsilon_\ell)} \cdot \frac{\gamma_\ell}{(\omega-\omega_\ell(k))^2+\gamma_\ell^2} \tag{5.29a}$$

$$\xrightarrow{\gamma_\ell \to 0} \frac{\omega_\ell^2}{\frac{\partial}{\partial\omega}(\omega^2\varepsilon_\ell)}\ \pi\ \delta(\omega-\omega_\ell) \tag{5.29b}$$

$$\frac{Im\ \varepsilon_t}{|\omega^2\varepsilon_t - k^2|^2} = \frac{1}{\omega_t^2\frac{\partial}{\partial\omega}(\omega^2\varepsilon_t)} \frac{\gamma_t}{(\omega-\omega_t)^2+\gamma_t^2} \tag{5.30a}$$

$$\xrightarrow{\gamma_t \to 0} \frac{1}{\omega_t^2\,\partial(\omega^2\varepsilon_t)/\partial\omega}\ \pi\ \delta(\omega-\omega_t) \tag{5.30b}$$

Here, we have focused only on the $\omega > 0$ part. The $\omega < 0$ part is the same except that the Lorentzian and delta function arguments are $\omega + \omega_\ell$ (or $\omega + \omega_t$).

We now put 5.29b and 5.30b into the absorptive response functions, relate these to the current-current correlation function

by 5.18 and 5.17, then use A3.20 to obtain the production kernels

$$R_p(q,q') = R_p^{(t)}(q,q') + R_p^{(\ell)}(q,q') \tag{5.31}$$

as the sum of two terms, one due to the decay of transverse plasmons, the other due to the decay of longitudinal plasmons:

$$R_p^{(j)}(q,q') = \frac{G^2 C_{Ve}^2}{4\pi e^2} f_{p\ell}(|\omega|)\omega^4(\varepsilon_j-1)^2 \phi_j \frac{2\pi}{\frac{\partial}{\partial\omega}(\omega^2\varepsilon_j)} \delta(|\omega|-\omega_j) \quad , \qquad j = \ell,t \tag{5.32}$$

Here,

$$\phi_t(\nu,\nu',c) = 2\left(1 - \frac{(\nu+\nu'c)(\nu'+\nu c)}{k^2}\right) \tag{5.33a}$$

$$\phi_\ell(\nu,\nu',c) = \frac{k^2}{\omega^2}(1+c)-1-3c+2(\nu+\nu'c)(\nu'+\nu c)/k^2 \tag{5.33b}$$

If we follow the path of ARW and quantize the plasmons, we also obtain 5.32.

The presence of the delta function in these kernels implies that for given ν and ν' , there is a unique k_j satisfying

$$\omega_j(k_j) = \nu+\nu' \quad , \qquad j = \ell,t \tag{5.34}$$

and therefore the angle between the outgoing neutrino and antineutrino (whose cosine is c) is uniquely determined:

$$c_j = (k_j^2 - \nu^2 - (\nu')^2)/2\nu\nu' \tag{5.35}$$

If k_j is not within the kinematically allowed range, $|k_m| \leq k_j \leq |\omega|$, where $k_m = \nu - \nu'$, then no decay is possible. For the transverse plasmons, only the lower bound imposes a constraint on the allowed values of ν and ν' . For longitudinal plasmons, both lower and upper bounds act to severely restrict the possible neutrino and antineutrino energies created in the decay; for example, $k_j \leq |\omega|$ implies $\nu+\nu' \leq \sqrt{8/5}\ \omega_p$. The relevant regimes in ωk_m space or equivalently $\nu\nu'$ space are shown in Figure 19. If we reinterpret k_m to be k, then this figure gives the dispersion relation curves (5.27); the transverse dispersion relation (5.27b) differs little from the often quoted $\omega^2 = \omega_p^2 + k^2$ (to within $\sim$ 5%).

The restrictions on ν and ν' are expressed by means of characteristic functions for the kinematically allowed regions:

$$\chi_t = \theta(\nu+\nu' - \omega_t(k_m)) \tag{5.36a}$$

$$\chi_\ell = \theta(\nu+\nu' - \omega_\ell(k_m))\ \theta(\sqrt{8/5}\ \omega_p - \nu - \nu') \tag{5.36b}$$

where θ is the Heaviside unit function.

The delta function makes the evaluation of production moments (3.24c) straightforward:

$$R_{pL}^{(t)}(\nu,\nu') = 2\pi^2 \left[\frac{G^2 C_{Ve}^2 \omega_p^4}{4\pi^2 e^2}\right] \cdot \frac{9}{25\nu\nu'} \frac{\chi_t\ \phi_t(\nu,\nu',c_t)}{\left(1 + \frac{1}{5}\frac{\omega_p^2}{\omega^2}\right)^3} f_{p\ell}(\nu+\nu')\ P_L(c_t) \tag{5.37a}$$

$$R_{pL}^{(\ell)}(\nu,\nu') = 2\pi^2 \left[\frac{G^2 C_{Ve}^2 \omega_p^4}{4\pi^2 e^2}\right]$$

$$\cdot \frac{5}{12\nu\nu'}\left(\frac{\omega}{\omega_p}\right)^6 \chi_\ell \, \phi_\ell(\nu,\nu',c_\ell) \, f_{p\ell}(\nu+\nu') \, P_L(c_\ell) \quad (5.37b)$$

where P_L is the Legendre polynomial of degree L. If all energies are measured in MeV, then the term in square brackets is numerically $0.7\ C_{Ve}^2\ \omega_p^4$ (s^{-1} MeV^{-1}) which sets the scale. To obtain the $\nu_\mu \bar{\nu}_\mu$ rate, C_{Ve} is replaced by $C_{V\mu}$.

In Figure 20, the L = 0 moments are plotted against the antineutrino's energy ν' for various neutrino energies ν at the conditions $T_{10} = 6.24$ and $\rho Y_e = 3.8 \times 10^{12}$ g/cc ($\omega_p = 4.5$ MeV) possibly characteristic of a first bounce. The transverse moments are zero up to some critical value at which they peak and then fall off almost exponentially; the falloff rate is steeper for lower temperatures and less steep for higher ones. The longitudinal kernels are quite spiked, centering about $\nu' = \omega_p - \nu$ which reflects the extreme constraints imposed on the allowed range of ν and ν' values. These moments are more difficult to deal with numerically than the more gently rising and falling e^+e^- moments (c.f. Figure 15). They are adequately treated using bin averaging, provided the energy bin sizes are sufficiently narrow: clearly, bins of width 5 MeV will not do (as they can in the e^+e^- case); rather 0.5 MeV bins are preferable. It is therefore difficult to deal with both plasmon and pair production at the same time.

The absorption kernels are obtained from those for production

by using 5.14.

The integral of the production moments over the antineutrino's phase space ($(\nu')^2 d\nu'/2\pi^2$) gives the rate to create a neutrino of energy ν per unit phase space. These integrals must in general be done numerically. Transverse and longitudinal spectra are given in Figure 21 for the conditions of Figure 20. The transverse rate clearly dominates over the longitudinal rate. Multiplication of these rates by $\nu^2/2\pi$ yields the number of ν_μ's created per unit time per unit energy: this quantity peaks at $\sim$ 2 MeV and has a much shallower falloff.

Since vector current dominance has been assumed, no VA interference appears, and the ν and $\bar{\nu}$ spectra are identical; the moments 5.37 are invariant under the interchange of ν and ν'.

The plasmon neutrino spectrum is of low energy relative to the pair annihilation spectrum, as can be seen in Figure 22 taken at the same temperature as in Figure 20, but at the less dense ρY_e = 1.13×10^{12} g/cc ($\omega_p \simeq 3$ MeV), and again in Figure 16 under the much hotter conditions $T_{10} = 12$, $\omega_p \simeq 4.3$ MeV. The line of demarcation between plasmon and pair dominance is drawn in Figure 18 for equal energy loss rates; the line for equal ν_μ production rates is to the left of the equal energy line due to the very different mean neutrino energies. Further, the energy dependence of the opacities ($\sim \nu^2$) implies that the ν_μ's and $\bar{\nu}_\mu$'s produced by annihilating positrons are more easily trapped than those produced by decaying plasmons.

6. THE EVOLUTION OF THE NEUTRINO DISTRIBUTION FUNCTIONS

In this chapter, we present our detailed numerical results on the behavior of neutrinos in the various stages of gravitational collapse. The first section focuses on the early evolution of the core, when it is still transparent to neutrinos, by following the trajectory of the star in ρTY_e space to the onset of trapping, which occurs at a density ρ_{trap}. We then solve the P-O equations for the evolution of the ν_e distribution function to equilibrium at a density above ρ_{trap} to elucidate the roles of the various neutrino processes involved (section two). In section three, the effects of diffusive transport on the approach to equilibrium are considered in a simple model; then dynamics is included. At a higher density than ρ_{trap}, which we call $\rho_{eq}(\nu_e)$, the neutrino distribution function is, to a good approximation, Fermi-Dirac. From this stage on, the equilibrium diffusion approximation in the core is satisfactory; this is the subject of section four. This (probably) takes us through the first hydrodynamical bounce and the large ν_e flux associated with that event. When do ν_μ's and $\bar{\nu}_\mu$'s produced by thermal processes approach an equilibrium distribution? When does the flow of energy in these ν_μ $\bar{\nu}_\mu$ pairs compete with the flow due to the neutronization ν_e's? These questions are the subject of section six, in which we also address the role of $\bar{\nu}_e$'s in the transport. At some density, $max(\rho_{eq}(\nu_e), \rho_{eq}(\nu_\mu), \rho_{eq}(\bar{\nu}_\mu), \rho_{eq}(\bar{\nu}_e))$, all of the neutrino types are in equilibrium. The core of the star then evolves in one of two directions: towards a black hole or towards a neutron star. A brief synopsis is

given of these latest stages of evolution in section seven. Finally, detailed numerical solutions are given for the P-1 equations and the flux-limited diffusion equations for Arnett's (1977) pre-bounce core and mantle structure, which we take as static; these two methods of spatial transport are tested in a configuration which bridges the diffusive flow in the core to the free streaming in the mantle.

6.1 THE TRANSPARENT PHASE

This section is based on Epstein, Norgaard, and Bond (1978), which we hereafter call ENB. ENB follow the thermodynamic evolution of the central zones of the star up to the point of neutrino trapping.

When the core of a star with mass $\gtrsim 8\ M_\odot$ passes out of silicon burning, its central temperature is $\sim 4\times10^9$K and its density is between $\sim 10^8$ g/cc (appropriate to higher mass stars) and $\sim 10^{10}$ g/cc (appropriate to lower mass stars). The evolution through core silicon burning, especially for lower mass cores (which experience a hydrodynamic core silicon flash), is not well understood (Arnett 1977a); once past it, however, the iron/nickel core evolves hydrostatically, and the mantle and core evolution are coupled; later, the core falls away from the mantle when dynamical collapse ensues.

To follow the evolution of the center of the star without doing a full hydrodynamical calculation, we assume the central density, ρ_c, varies with time according to

$$\frac{\dot{\rho}_c}{\rho_c} = \frac{\sqrt{24\pi G\rho_c}}{\chi_{eff}(\rho_c)} \qquad (6.1)$$

and parametrize the factor $\chi_{eff}(\rho_c)$, which gives the deviation of the central density's evolution timescale from the instantaneous freefall time $(24\pi G\rho_c)^{-1/2}$, by

$$\chi_{eff}(\rho_c) = \chi_0(\rho_c/\rho_0)^{\beta+1/2} \tag{6.2}$$

where χ_0 , β , and ρ_0 are three parameters which we are free to vary. Equation 6.1 is easily integrated to yield $\rho_c(t)$, which becomes infinite after $446\rho_0^{-1/2}\chi_0/(-\beta)$ seconds.

To calibrate χ_0 and β , ENB compared the solution of 6.1 with the detailed hydrodynamical calculations of core collapse of Arnett (1977), Wilson (1976), and van Riper (1978). We find $\beta = -1$ fits rather well up to $\sim 10^{12}$ g/cc. Arnett's central trajectory (see Figure 10) is fit by $\chi_0 = 137$ using his starting density $\rho_0 = 3.7\times10^9$ g/cc ; the transition from hydrostatic evolution towards freefall (but always far from it) is manifested by the behavior of χ_{eff} which drops from its starting value of 137 to 26 at 10^{11} g/cc and to 8 at 10^{12} g/cc.

In our detailed calculations, we allowed χ_0 to vary from 15 to 225, ρ_0 to vary from 10^8 to 10^{10} g/cc, and have tested $\beta = -1/2$ as well as $\beta = -1$; we further varied the other initial conditions, the starting temperature and Y_e . Typically, it takes about one second to pass from 10^9 to 10^{12} g/cc, with the last order of magnitude in density (10^{11} to 10^{12}) traversed in $\lesssim$ 10 ms.

The center of the star responds to this imposed rate of compression by heating up, radiating neutrinos and losing lepton number.

This thermodynamic reaction to the compression action and its consequences is the focus of ENB. We solve the energy equation, 3.17c, and the neutronization equation, 3.17b.

The assumption of neutrino transparency simplifies the detailed form of the neutrino source functions, which appear on the right hand side of 3.17c and 3.17b; equations similar to 5.5b, 5.5c, 5.7a, 5.7b are needed (with the Q-values included) for the reactions $e^- + p \rightarrow n + \nu_e$, $e^- + {}^A_Z \rightarrow {}^A_{(Z-1)} + \nu_e$, and $e^+ + n \rightarrow p + \bar{\nu}_e$; we take these from Epstein and Arnett (1975)(EA) which is discussed in section 5.3 of Chapter 5.

ENB also include thermal $\nu\bar{\nu}$ loss rates (sections 5.6 and 5.7) in 3.17c; these are obtained from BPS (Beaudet et al. 1967) with modifications to include neutral currents: their e^+e^- rate is multiplied by $(C_{Ve}^2+C_{Ae}^2)/2 + (C_{V\mu}^2+C_{A\mu}^2)/2$ for both $\nu_e\bar{\nu}_e$ and $\nu_\mu\bar{\nu}_\mu$ production (.73+.13 here with $\sin^2\theta_W = 0.3$); their photoneutrino rate, which is negligible compared with these other two mechanisms here, should be multiplied by the same (e^+e^-) factor; their plasmon neutrino rate is multiplied by $(C_{Ve}^2+C_{V\mu}^2)$, 1.21 plus .01 here. In these early phases, ν_e's from electron capture dominate the energy loss by typically five orders of magnitude in the ENB runs.

We also need the internal energy of matter per baryon and the matter pressure in order to solve 3.17c:

$$\varepsilon_m = \varepsilon_I + \varepsilon_e + \varepsilon_{nuc} + \varepsilon_{Coul} \tag{6.3}$$

$$p_m = p_I + p_e + p_{Coul} \tag{6.4}$$

The internal energies and pressures obtained from the independent particle model are ε_I , p_I (ideal gas equation of state (EOS) for nuclei), ε_e , p_e (ideal gas EOS for electrons and positrons) and ε_{nuc} , the nuclear binding energy per baryon. Here, nucleons are nondegenerate, and thus

$$\varepsilon_I = 3/2\ Y_I\ kT \tag{6.5a}$$

$$p_I = Y_I\ kT \tag{6.5b}$$

$$Y_I(\rho,T,Y_e) = \sum_j Y_j(\rho,T,Y_e) \tag{6.5c}$$

where Y_I is the total number of nuclear particles per baryon, with the sum in 6.5c over all nuclear species j. The electron energy is the familiar relativistic Fermi gas formula (3.71 if the subscript e replaces the subscript ν), and $p_e = \varepsilon_e \rho_B/3$. If B_j is the (positive) binding energy per nucleon of the species j, A_j its atomic number, and $g_j(T)$ its partition function, then

$$\varepsilon_{nuc} = -\sum_j B_j A_j Y_j - \sum_j \frac{\partial \ell n g_j}{\partial \beta} Y_j - (m_n - m_p) Y_e \tag{6.6}$$

Generally, the partition function term is very small and can be ignored.

The potential energy between particles gives rise to interaction corrections to the internal energy and pressure obtained from the independent particle model. In the early stages of evolution, strong nuclear forces between nuclei are unimportant; they cannot be neglected in the post bounce environment, however, and cause changes in ε_{nuc} .

The Coulomb interaction between ions (nuclei) has, as we saw in section 4.4 of Chapter 4, an effect on the elastic scattering of low energy neutrinos off nuclei. Ion-ion correlation also affects the EOS; in fact, ε_{Coul} is related to the integral of the product of the interparticle Coulomb potential and the radial pair distribution function, whose Fourier transform is, in turn, related to the static liquid structure factors (4.29). Hansen et al. (1977) fit their Monte Carlo calculations for a multicomponent plasma to the form

$$\varepsilon_{Coul} = kT \sum_j Y_j \Gamma_j^{3/2} \left(\frac{A_1}{(B_1+\Gamma_j)^{1/2}} + \frac{A_2}{(B_2+\Gamma_j)} \right) \tag{6.7a}$$

$$p_{Coul} = \frac{1}{3} \rho_B \varepsilon_{Coul} \tag{6.7b}$$

where $A_1 = -0.90$, $B_1 = 0.70$, $A_2 = 0.27$, and $B_2 = 1.32$. Here, Γ_j is defined by 4.31 for the species j. This formula gives the Debye-Huckel limit in the $\Gamma < 1$ regime and the ion-sphere result in the high Γ limit (indeed, in our numerical results we used the latter limit). Notice that A_1 is negative, and generally ε_{Coul} and p_{Coul} are also negative; at $\rho_{11} = 2$, $T_{10} = 2$, $p_I + p_{Coul}$ is actually negative for iron, but positive for helium: the plasma Coulomb interaction desires highly charged nuclei which it can keep further apart, acting oppositely to nuclear photodisintegration effects. However, throughout the ENB run regimes, both ion and Coulomb pressures are swamped by the electron pressure (less than 1%), the former due primarily to the continued presence of so many heavy nuclei: in the ENB runs, the

evolution with and without Coulomb effects is essentially the same.

The interaction of the nucleus with the plasma modifies the binding energy. A simple example of this is again the electrostatic effects which give rise to equation 6.7; in the Wigner-Seitz approximation, a modified binding energy (which follows from Baym, Bethe, and Pethick 1971, Mackie 1976)

$$B_j' = B_j + \frac{9}{10} \frac{(Z_j^{5/3})}{A_j} e^2 \left(\frac{4}{3} \pi \rho_B Y_e\right)^{4/3}$$

reproduces the ion-sphere limit of 6.7 for the electrostatic energy; however, the NSE equations which balance chemical potentials contain this modified binding energy, which results in nuclear abundances somewhat different than those of the independent particle approximation. In the ENB regime, the effect is negligible, and the central trajectories are virtually identical to those runs without this modification included. It is, however, a portent of things to come at higher density when these binding energy corrections will grow, both this Coulomb term which rises as the density rises, and the nuclear surface energy term, which is affected by strong interactions with the free nucleons in the plasma (Pethick 1978, Lattimer and Ravenhall 1978).

Figures 23 and 24, taken from ENB, present the ρT and ρY_e trajectories for $\chi_0 = 75$ and 224, a range of starting densities, and one starting temperature (4×10^9 K). The ρT histories of the central zones converge towards a common trajectory which passes through $\sim 2 \times 10^{10}$ K at $\sim 2.5 \times 10^{11}$ g/cc, independently of the compression rate

and initial density; Arnett's central trajectory (see Figure 9) and our $\chi_0 = 15$ trajectories also fall very close to this convergent one.

Why do the ρT histories converge? An electron is captured from somewhere within the Fermi sea, leaving a hole. The Fermi sea then settles, lowering slightly the Fermi level, and liberating some zero point energy; when the Q-values of the capture reactions can be neglected, and the electrons are extremely degenerate, the release is $\mu_e/6$; the other $5\mu_e/6$ is taken away by the neutrino. The liberated internal energy can be spent in heating up the electrons and ions (in the early stages of the trajectories) or in photodisintegrating nuclei; the latter is a refrigerating reaction, initially not very important, but as the temperature rises due to heating, this cooling mechanism gets larger. In addition to this energy from electron capture, there is the PdV work continually supplied by the compression. The latter dominates at high density. The convergence is due to a conspiracy between the heating and photodissociation (as measured by a heat capacity which rises with temperature) and the energy sources.

If the starting temperature is too hot (for example, 8×10^9 K, which is much hotter than we expect when coming out of silicon burning), substantial photodissociation occurs early, the above balance condition cannot be met, and one does not have convergence to a common trajectory when the starting density is 10^8 g/cc and $\chi_0 = 75$; the starting densities of 10^9 and 10^{10} g/cc do converge to the common one.

The ρY_e trajectories show no tendency to converge: if the

compression rate is rapid, little neutronization can occur and the Y_e values remain high ($Y_e \gtrsim 0.4$); a slower compression rate gives the medium time to neutronize, and relatively few electrons may be left by the time the neutrinos are trapped and the rapid neutronization phase is arrested ($Y_e \lesssim 0.15$). The Y_e curves pass quickly outside of the $Y_e = 0.44$ boundary of the EA results into regions where extrapolations are necessary, both to determine proton and heavy nucleus abundances (from NSE) and to determine electron capture rates for heavy nuclei. ENB tried many extrapolations, usually requiring the EA parameters to linearly approach constant values beyond the known regime: high, medium, and low constants (which control such things as the heavy binding energy and capture rate) were tried. Hopefully, our probe of parameter space beyond $Y_e = 0.44$ will cover the ranges found in careful treatments of the capture rates for neutron rich nuclei and the NSE mixtures in neutron rich media.

Abundances depend upon the partition functions of heavy nuclei: EA assumed only ground state partition functions in their NSE calculations, which compares with the value 172 for ^{56}Fe at 2×10^{10} K given by Fowler et al. (1978) (FEW), suggesting a large error. However, the abundances depend upon a weak power of the partition function ($Y_\alpha \sim \exp(-(2/Z_H)\ell ng)$, where Z_H is the mean heavy charge). At the above conditions, if the partition function of the typical heavy is similar to that for ^{56}Fe, the abundance differences between $g = 1$ and the more realistic $g = 172$ are less than 18% for Y_p, Y_n, Y_I, Y_α, and Y_H. At lower temperatures, the effect is even smaller.

The partition function rises rapidly with increasing temperature, and later in the collapse the abundances of heavy nuclei may be significantly higher than those obtained from the ground state partition function.

Our calculations break down when neutrino trapping occurs. The typical time for a neutrino of energy ν to diffuse from a homogeneous core of radius R_c is

$$\tau_{diff}(\nu) = \Gamma_{tr}(\nu)\ \tau_{\ell}^2 \tag{6.8a}$$

$$\tau_{\ell} = R_c/c \tag{6.8b}$$

where τ_{ℓ} is the light travel time across the core and Γ_{tr} is the transport rate (3.62); $\Gamma_{tr}\ \tau_{\ell}$ is the optical depth of the center measured from the core's surface. An estimate of the time it takes a neutrino to escape from the core is

$$\tau_{esc}(\nu) = max(\tau_{\ell}, \tau_{diff}) \tag{6.8c}$$

If $\langle\nu\rangle = \dot{q}/\dot{Y}_e$ is the mean energy at which neutrinos are produced, then a crude criterion for trapping is

$$\tau_{esc}(\langle\nu\rangle) \gtrsim min(t_{ec}, t_{dyn}) \tag{6.9a}$$

where the electron capture and dynamical times are

$$t_{ec} = \left| \frac{Y_e}{\dot{Y}_e} \right| \tag{6.9b}$$

$$t_{dyn} = \frac{\rho_c}{\dot{\rho}_c} \tag{6.9c}$$

If the neutrinos are created at a rate greater than they can diffuse away ($t_{ec} \leq \tau_{esc}$), the neutrino phase space builds up, reducing the number of states available, which lowers the neutronization rate below the free escape values ENB used. In the ENB runs, this form of trapping does not occur until after the infalling matter's velocity ($\dot{R}_c$) exceeds the neutrino diffusion velocity (R_c/τ_{esc}) and the net neutrino velocity is directed radially inward: the neutrinos are themselves collapsing, dragged along by the collapsing matter, and their phase space builds up. This dynamical trapping occurs when $\tau_{esc} > 3t_{dyn}$; even before this, enough ν_e's will occupy phase space to alter the df, and ENB chose the more conservative criterion $\tau_{esc} > t_{dyn}$. If the free proton abundance during infall is significantly higher than our values derived from EA, such as would occur in hotter core collapses, the electron capture rate can exceed the diffusion rate before dynamical trapping can occur.

In ENB, we assume a constant density core of mass 0.5 $M_\odot$ to compute R_c, and thus find when trapping occurs: the values are not very sensitive to the choice of core mass. In Figures 23 and 24, the trajectories become dashed when trapping occurs, unless Y_e falls less than 0.15 in which case we stopped the evolution. The trapping densities range from $\sim 5\times10^{10}$ to $\sim 3\times10^{11}$ g/cc, the Y_e values at trapping can be anywhere from $Y_e \sim .44$ to less than .15: the range depends upon the compression and electron capture rates. The integrated neutrino energy loss from this 1/2 $M_\odot$ core in the transparent phase ranges from $\sim 5\times10^{50}$ to $\sim 3.5\times10^{51}$ ergs. What is

the effect of these neutrinos on the overlying mantle?

This depends critically upon the dynamical behavior of the mantle. If it is falling inward at supersonic velocities, so the inertial term in the equation of motion more than balances the pressure gradient, then the neutrino luminosity $L = H_\nu \, 4\pi r^2$ at radius r would have to exceed the Eddington limit obtained by setting the inward gravitational acceleration equal to the outward neutrino acceleration (Schramm 1976):

$$L_{Edd} = 4\pi c \, Gm/\langle\kappa\rangle \tag{6.10}$$

$$\langle\kappa\rangle = \rho^{-1} \int \frac{\Gamma_{tr}(\nu)}{c} H(\nu) d\nu \; / H_\nu$$

where $\langle\kappa\rangle$ is the mean opacity, a functional of the energy flux (3.56b). This radiation would have to last for a sufficiently long time to turn infall to outflow with velocity in excess of the escape velocity calculated at radius r.

Suppose, however, the mantle is in approximately hydrostatic equilibrium: this is certainly true beyond the silicon burning shell. The neutrino momentum deposition accelerates a shell of matter outward: this does not mean the shell goes out of the hydrostatic balance between the matter pressure and the gravitational forces (except the heating due to energy deposition causes rapid volume expansion and possibly shock wave generation). If the shell expands homologously, the hydrostatic balance can be maintained if the electrons are relativistic and dominate the pressure, at least until the electrons

go nonrelativistic or some other process occurs which upsets the hydrostatic balance. The escape velocity required is that for the decoupling point, not the initial shell position; the required luminosity may then be a small fraction of the Eddington limit (perhaps 1% for a shell initially at 10^{10} g/cc).

Even in the most optimistic of circumstances, the "transparency" neutrinos do not deposit enough momentum to create a supernova event; with the upper end of the neutrino energy range and for hydrostatic mantles, ENB find one can come close.

Diffusion neutrinos from post-trapping carry off more energy from the core, but the outer portions of the core (interior to the silicon burning shell) are apparently supersonically collapsing (Arnett 1977) and thus require an Eddington luminosity for ejection.

6.2 THE APPROACH TO BETA-EQUILIBRIUM

What is the form of the ν_e distribution function after trapping, and when does it become Fermi-Dirac? This depends critically upon the free proton abundances and on the action of nonconservative scattering processes. We focus here on the density 2.54×10^{11} g/cc, a value beyond the ρ_{trap} range found in section 6.1.

Consider an infinite homogeneous medium consisting of free nucleons and electrons (and positrons and photons) which is in strong and electromagnetic equilibrium. The weak interaction, initially off, is switched on. The system produces neutrinos by the process $e^- + p \rightarrow n + \nu_e$, reabsorbs them by $\nu_e + n \rightarrow e^- + p$, and scatters them by $\nu_e + e \rightarrow \nu_e + e$ (as well as by $\nu_e + \nu_e \rightarrow \nu_e + \nu_e$ which we do not include) as

it moves through a series of nonequilibrium intermediate states to the final neutrino beta-equilibrium state characterized by the balancing of chemical potentials (3.12). The matter is always in strong and electromagnetic equilibrium throughout this change of state. The other species of neutrinos also eventually achieve equilibrium; we deal with those later. Conservative reactions ($\nu_e+N \rightarrow \nu_e+N$) play no role in the transformation, since they do not redistribute neutrinos in energy space, and there is no spatial transport in an infinite medium.

The equations describing the evolution of the nonequilibrium ν_e distribution function (df) in an infinite medium are the P-O equations of section 3.9; the system neutronizes (equation 3.17b) and heats up due to both electron capture and nonconservative scattering (equation 3.17c). We distinguish two cases: the matter plus neutrinos undergo an adiabatic transformation to beta-equilibrium (no energy transport, the more relevant case), or an isothermal transformation (the medium is in contact with a heat sink which absorbs just enough energy to keep the temperature constant). We solve these equations by the numerical methods outlined in Appendix 4. Tubbs (1978) used the Monte Carlo method to integrate the P-O equations for an isothermal transformation to beta-equilibrium in a free nucleon gas; our conclusions and his agree.

The relevant neutrino rates for this density at the temperature 2×10^{10} K and the initial Y_e of 0.4 are displayed in Figure 13. According to this graph, we expect the effect of $\nu_e e$

scattering to be small due to the large $e^- p \rightarrow n\nu_e$ production spectrum. This expectation is substantiated by the detailed numerical results shown in Figure 25, which gives the df at three times (10^{-5} , 10^{-4} , and 10^{-3} s) with and without νe → νe on. The df at 10^{-4} s shows the neutrinos slightly overproduced at high energy (relative to the final equilibrium line); these are subsequently downscattered in collisions with electrons, resulting in relatively more neutrinos in the low energy bins and relatively fewer in the high energy bins than when νe scattering is not included: this nonconservative process accelerates the approach to beta-equilibrium. Within a millisecond, the df is FD even in the lowest energy bins. At higher densities (or temperatures) the transition occurs faster; at lower densities (or temperatures) the transition is slower: these expected results are confirmed by detailed runs at various densities and temperatures.

The transformation of Y_e from its starting value of 0.4 to its beta-equilibrium value of .303, and of Y_ν from zero to 0.097 is initially rapid, slowing as equilibrium is approached, as is shown in Figure 26; the transition with and without νe scattering is almost the same. The temperature as a function of time for the adiabatic transformation is also displayed in Figure 26 with and without νe scattering: the difference is slight. The adiabatic transformation has a slightly higher Y_e (.306) at equilibrium than the isothermal one (.303).

In NSE at 2×10^{10} K, the matter consists of heavy nuclei and alphas as well as free nucleons; using the EA prescriptions with the

ENB extrapolations, we find $Y_p \sim 1.4 \times 10^{-4}$, $Y_n \sim .074$, $X_\alpha \sim .36$, $X_H \sim .57$, where X_α and X_H are the fractions of baryons locked in alphas and heavy nuclei respectively. Due to this low Y_p value, electron capture on heavies dominates the capture on protons under these conditions: $\dot{Y}_e$ is $\sim 4\ s^{-1}$ for e^-p ($\dot{Y}_e$ is $\sim 1.1 \times 10^4\ s^{-1}$ in the free nucleon gas discussed above), and $\gtrsim 60\ s^{-1}$ for e^-A, with the latter value relatively uncertain; the peak in the e^-p production spectrum for this low Y_p condition is off the scale of Figure 13. Neutrinos trickle into energy space at a low rate due to this production mechanism, are trapped by the conservative scattering reactions, and are shaped into a FD df by νe scattering. The important role played by nonconservative scattering is made evident in Figure 27 which compares the df at equal time with and without this process turned on. The equivalent FD df for the ν df at 1.2 ms, displayed in Figure 27b, shows that the conduction approximation is not a good one for these conditions.

As is evident from these two examples, the value of $Y_p(Y_e, \rho, T)$ is extremely important in determining the rate of approach to equilibrium. The low Y_p condition (the lowest cross in Figure 23) is apparently the appropriate one: the convergent trajectory of ENB passes through this point. At the middle cross, $T \simeq 2.5 \times 10^{10}$ K, and using g = 134, the ^{56}Ni partition function at this temperature according to FEW, we obtain $Y_p \sim .015$, $Y_n \sim .16$, $X_\alpha \sim .62$, and $X_H \sim .2$: electron capture on free protons likely dominates capture on heavies (it does using EA values, but see section 5.3), and

$\dot{Y}_e \sim 410\ s^{-1}$. A comparison of Figure 28a and Figure 27 shows how this intermediate Y_p accelerates the approach to beta-equilibrium. At the high cross in Figure 23, $T \simeq 3 \times 10^{10}$ K, $Y_p \sim 0.1$, and the system is similar to a gas of free nucleons; the approach to equilibrium is rapid, in millisecond time scales.

The lower the Y_p values, the more important is νe scattering in shaping the df to FD and the more necessary are differential production rates for electron capture on heavies; the trajectories indicate low Y_p values are indeed likely.

6.3 THE EFFECTS OF DIFFUSION AND DYNAMICS ON THE ν_e EVOLUTION

Neutrinos flow from the point of production. In the infinite homogeneous medium discussed in the last section, there is, of course, no net transport. Consider instead a finite homogeneous sphere, the core of section 6.1; we approximate the core itself as one spatial zone, whose transport equation, when finite-differenced in space, can be written as

$$\frac{dn(\nu)}{dt} + \frac{\theta n(\nu)}{\tau_{diff}(\nu)} = \delta^{(0)}\ [n] \qquad (6.11a)$$

where

$$n \equiv n_0\ (3/2, \nu, t)$$

is the zeroth moment of the df at the first zone's center. (The notation is n(k+1/2, ν, t) for zone k; details are given in Appendix 4.) The factor θ depends upon the value of the df at the second spatial zone's center, n(5/2,ν,t); for equal mass zones,

$$\theta = 3(1-n(5/2,\nu,t)/n(3/2,\nu,t)) \qquad (6.11b)$$

We replace the diffusion time, τ_{diff}, by the escape time, τ_{esc}, 6.8c, and thus insert an effective flux limiter in (6.11a). The source $s^{(0)}[n]$, given by 3.25b,c with only n_0 included, is also the one used in section 6.2. The energy flux at the surface of the core is

$$H(\nu) = \frac{\nu^3}{2\pi^2}\, n\, v_{diff}\, (1-n(5/2)/n) \qquad (6.12a)$$

Here, $v_{diff} = R_c/\tau_{esc}$ is the mean neutrino flow velocity. These equations assume there is a uniform fractional drain on the neutrinos in the core, with instantaneous transport from the center to the surface where they are radiated away.

In order to integrate 6.11, we must assume some value for the df in the second zone: we choose zero, so $\theta = 3$, and an upper bound is provided on transport effects; runs with $\theta = 1$ and 1/3 yield similar results to $\theta = 3$, with the effects of transport slightly less pronounced.

The diffusion time for the pure nucleon gas is shown in Figure 13; it is smaller than the millisecond or so required for equilibration, and we expect the medium to build to a steady state df, which slowly decays toward zero as lepton number and energy leak out (although it heats up due to the $\mu_e/6$ extra energy). The df in the low energy bins is not FD; for example, the 0.2-2 MeV bin has n = 0.22 at 0.1 ms, which rises to a maximum of 0.29 after a millisecond has elapsed, and then falls as lepton number decreases.

This bin is fed more by downscatter than by electron capture; both compete with the sink, transport at the speed of light. Arnett (1976) proposed a scenario in which neutrinos created at high energy, where they are trapped, downscatter to stream out the low energy window: this does occur, but is not sufficiently efficient to dominate the energy or lepton number transfer due to the small phase space available to low energy neutrinos. When no νe scattering is included, the lowest energy bin is occupied to a lesser extent but the core luminosity is only slightly smaller than when nonconservative scattering is included; many authors have come to the same conclusion (Tubbs 1978, Yueh and Buchler 1977b, Lichtenstadt 1977).

The neutrinos of high energy are in beta-equilibrium; those near the neutrino Fermi surface play the dominant role in energy transport; the number flux per unit energy is almost independent of energy, since $F \sim \nu^2 n\ R_c/\tau_d$ and the energy dependence of τ_d cancels the ν^2 , leaving n.

The more realistic NSE composition (of Figure 27) consists mostly of heavy nuclei which dominate diffusion through coherent scattering; yet the diffusion rate, which looks similar to that given in Figure 13, is almost two times larger. The low production rate suggests no equilibrium will be achieved; this is confirmed by the numerical results (Figure 28b).

The dynamical time is similar in magnitude to the diffusion and production times; at 2.54×10^{11} g/cc, it is perhaps five times the

free fall time, $\sim$ 5 ms. To know what the df looks like after trapping but before equilibrium sets in requires density evolution. We drive the density by the ENB prescription (6.1), using $\chi_0 = 75$ and $\rho_0 = 10^9$ g/cc ; we began at 5×10^{10} g/cc with $Y_e = 0.4$ and $T_{10} = 1.5$ and evolved to 4×10^{12} g/cc. Throughout most of the collapse, electron capture on heavy nuclei dominates the capture on protons due to the low Y_p values obtained from EA: Y_p does not rise beyond 10^{-3} until $\sim 10^{12}$ g/cc. Here, we include only electron capture on free protons; the neutronization is then much smaller than that evident from Figure 23, and trapping here ($\sim 7\times10^{11}$ g/cc) occurs well after trapping there (1.3×10^{11} g/cc). The df at various densities during the collapse is displayed in Figure 29: only 4% of the leptons have radiated by 5×10^{11} g/cc; trapping occurs before 7×10^{11} g/cc; by 3×10^{12} g/cc, neutrino beta-equilibrium has definitely set in. The number flux peaks at the density 4×10^{12} g/cc when it is 4×10^{57} ν_e/s; at 1.4×10^{12} it is only 6% less.

The trajectory during dynamical collapse is similar to the convergent one of ENB except in the initial phases: we start a little hotter, relax to the convergent trajectory, then follow it, passing through 2×10^{10} K at 2.6×10^{11} g/cc.

From this collapse, we find $\rho_{eq}(\nu_e) \approx 3\times10^{12}$ g/cc; if the Y_p values are higher or if electron capture on heavy nuclei is included, equilibrium would set in below this density.

6.4 THE EQUILIBRIUM DIFFUSION APPROXIMATION

Once ρ exceeds $\rho_{eq}(\nu_e)$, it is natural to use the equilibrium

diffusion approximation (EDA) to describe the transport. At prior times to this, and at densities in the outer regions of the core less than this, the df does not look much like a FD df: this suggests the conduction approximation is not a good one at these densities and temperatures, a conclusion which hinges upon the inability of nonconservative scattering to redistribute the high energy neutrinos at a sufficiently rapid pace to keep abreast of the diffusive depletion in the low energy bins. Ideally, one would couple the EDA in the inner core to an energy dependent transport scheme such as flux limited diffusion in the outer core.

To use the EDA in the interior region, it is necessary to know the neutrino diffusion constants (3.67c); generally, these must be obtained numerically. A useful limit occurs when the neutrinos are extremely degenerate: the number and energy flux follow only the neutrino chemical potential gradient

$$F_\nu = -D_0 \frac{\partial}{\partial r} \frac{\mu_\nu^3}{6\pi^2} \tag{6.13a}$$

$$H_\nu = \mu_\nu F_\nu \left[\frac{D_1}{D_0}\right] \tag{6.13b}$$

If $e^- p \rightleftarrows n\nu_e$ dominates the transport rate,

$$D_k = c^2/(3\Gamma_a'(\mu_\nu)) \tag{6.14a}$$

where Γ_a' is the modified absorption rate (3.31, 5.3, 5.4), or if νA and νN scattering dominate (4.8, 4.36),

$$D_k = c^2/(3\Gamma_{tr}(\mu_\nu)) \tag{6.14b}$$

the diffusion constants are independent of k = 0,1,2 and equal to the energy dependent diffusion constant (3.63) evaluated at the Fermi surface. If νN scattering dominates when nucleons are degenerate, 6.14b again holds. If absorption and scattering are almost equal, the situation is more complicated: the Rosseland means are of $(\Gamma_{tr,cons} + \Gamma_a')^{-1}$, and diffusion constants for different processed do not add. In the 6.14a or b limit, D_1/D_0 is one in 6.13b: it is as if each escaping neutrino carries the neutrino Fermi energy.

These simple results allow us to estimate the mean time for a neutrino to random walk its way from the core: it is the diffusion time for a neutrino at the Fermi surface

$$\langle\tau_{diff}\rangle = R^2/3D(\mu_\nu) = \tau_{diff}(\mu_\nu) \tag{6.15}$$

If Y_ν does not change in time, then μ_ν rises as the one-third power of the density, and the diffusion time from the core rises linearly with ρ . By 10^{13} g/cc, this time is ∿ 100 ms for μ_ν = 50 MeV, much longer than the dynamical time.

If we define the logarithmic gradient of the chemical potential by

$$\Phi_\mu \equiv -\frac{\partial \ell n\ \mu_\nu}{\partial \ell n\ r} \tag{6.16a}$$

then 6.13 takes on a form similar to that obtained from the

approximate diffusion treatment of section 6.3:

$$F_\nu = \Phi_\mu \frac{R_c}{\tau_{diff}(\mu_\nu)} \rho Y_\nu \qquad (6.16b)$$

$$H_\nu = \frac{4\Phi_\mu}{3} \frac{R_c}{\tau_{diff}(\mu_\nu)} \rho u_\nu \qquad (6.16c)$$

where Φ_μ is evaluated at the core surface. As the core shrinks, its surface area falls as $\rho^{-2/3}$: the lepton number flow rate ($4\pi R_c^2 F_\nu$) falls as ρ^{-1} , the core luminosity falls as $\rho^{-2/3}$. Neutrinos are therefore confined to the inner core at high density.

Further out in the core, however, neutrinos are still being created in a neutronization shell and efficiently transported from it; these ν_e's dominate the flow after the onset of strong inner core trapping.

6.5 THE HYDRODYNAMICAL BOUNCE

The neutrinos are now collapsing with the matter, exerting the pressure of a relativistic gas which just adds to that of the electrons. The nucleon thermal pressure becomes important in matter heating. The adiabatic collapse will tend to follow a $\rho \sim T^{3/2}$ trajectory: this phase is already evident in Arnett's (1977) pre-bounce trajectory, even in the ρY_e plane (see Figure 18). The degeneracy factor of the nucleons, $\eta_N \sim Y_N \rho T^{-3/2}$ remains approximately constant in this adiabatic infall if the abundances do not change too much. The nucleons may or may not be degenerate; it depends upon the earlier evolution (compare Arnett (1977) and Wilson (1977) in

Figure 9). The electron degeneracy factor, $\eta_e \sim \rho T^{-3}$, falls in this heating phase. The poorly known hot nuclear matter equation of state is needed.

At a density which depends crucially upon this EOS (van Riper 1978), the core bounces, and a shock wave propagates outward through the star, exerting a force on the infalling matter which may or may not cause ejection. The core expands and lowers its density before falling in again; the neutrino diffusion time decreases, and a neutrino diffusion wave travels through the core, probably at a lower speed than the shock wave. The interplay of the neutrinos and the shock has yet to be adequately treated (Bruenn et al. 1978). Some numerical work indicates the neutrinos at the bounce act to soften the effect of the shock, and hinder explosion (Bruenn 1975, Wilson 1977); other work suggests neutrinos and the shock may work in tandem as a one-two punch to produce a supernova (Bruenn et al. 1977).

There may be more than one bounce (Wilson 1977); with each bounce, there is a neutrino pulse superimposed upon the steady diffusion wave whose intensity is decreasing as the collapse continues; if the bounce occurs at very high density (beyond that of normal nuclear matter), trapping will be so strong that these diffusion pulses will be weak. During bounce, the center's trajectory can make wild excursions in the ρT (and ρY_e) plane; the core may then settle into a final adiabatic collapse in which core heating continues.

6.6 THE ROLE OF ν_μ, $\bar{\nu}_\mu$, and $\bar{\nu}_e$

Prior to the onset of neutronization, $\nu\bar{\nu}$ pairs of both electron and muon (and perhaps tau) types dominate the stellar luminosity. In the transparent phase, $\nu\bar{\nu}$ pairs created in either the plasmon or pair neutrino processes contribute only a small fraction to the total luminosity. When do these thermal pairs rival the neutronization neutrinos as liberators of the released gravitational energy?

If $\nu_\mu\bar{\nu}_\mu$ pairs are freely streaming, and $\dot{Q}(\nu_\mu\bar{\nu}_\mu)$ is the energy loss rate per baryon via the plasmon and pair processes, then the luminosity of the homogeneous core is

$$L_{\nu_\mu\bar{\nu}_\mu} = \dot{Q}\,(\nu_\mu\bar{\nu}_\mu)\,\frac{4}{3}\,\pi\,R_c^3\,\rho_B \tag{6.17a}$$

If the electron neutrinos are extremely degenerate, then an estimate of their luminosity is obtained using 6.16c

$$L_{\nu_e} = \Phi_\mu\,\frac{3\mu_{\nu_e}\,Y_{\nu_e}}{\tau_{diff}(\nu_e;\mu_{\nu_e})}\,(\frac{4}{3}\,\pi\,R_c^3\,\rho_B) \tag{6.17b}$$

When

$$L_{\nu_\mu\bar{\nu}_\mu} > L_{\nu_e} \tag{6.17c}$$

we may expect the radiation of $\nu_\mu\bar{\nu}_\mu$ pairs to once again become important.

To calculate 6.17b, the composition is needed to determine μ_ν : we assume a free nucleon gas with Y_e frozen at 0.2, $Y_n = 0.8$,

$Y_p = 0.2$; μ_ν is then almost equal to μ_e , Y_ν is almost one half Y_e . We also assume $\Phi_\mu = 1.0$ and take the core mass to be our canonical one half solar mass.

The regions when freely streaming $\nu_\mu \bar{\nu}_\mu$ radiation exceeds diffusive ν_e radiation are displayed in Figure 18. The core must be quite hot before we need to worry about muon neutrinos; however, these demarcation lines are crossed when the core enters into its $\rho \sim T^{3/2}$ heating stage, as we can see by extrapolating Arnett's $T\text{-}\rho Y_e$ trajectory according to this law.

A mixture in NSE under these conditions likely has fewer free protons, but almost as many free neutrons present: μ_ν will be smaller than our estimate, and the neutronization/thermal pair boundary will be lower (in temperature) in Figure 18.

Are the muon neutrinos really freely streaming? They experience the same νN and νA scattering as electron neutrinos. Are they trapped instead?

To answer this question, we solve the P-O equations: there is one equation for the ν_μ df and one for the $\bar{\nu}_\mu$ df; each type has the nonconservative scattering source 3.25c as well as the $\nu\bar{\nu}$ pair creation source 3.25d; this latter source couples the evolution of the two df's. Special attention must be paid to the numerical methods used to integrate these equations due to this coupling, the sharply spiked character of the plasmon neutrino kernels, and the five or more order of magnitude difference between the production and scattering times: these are discussed in Appendix 4.

We begin with the conditions labelled γ_{pl} in Figures 9 and 18, $\rho = 1.9\times10^{13}$ g/cc, $T = 6.24\times10^{10}$ K, $Y_e = 0.2$, $\mu_e = 81$ MeV. The $\ell = 0$ moments of the production kernels are shown in Figure 20 (which are bin averaged before they are put into the finite difference equations) and the ν_μ and $\bar{\nu}_\mu$ spectra are displayed in Figure 21. The plasmon rate ($\sim 3.13\times10^{28}$ erg cm^{-3} s^{-1}) dominates the e^+e^- rate by a factor of 3: we neglect the latter here. We include $\nu_\mu+\nu_e \rightarrow \nu_\mu+\nu_e$, $\bar{\nu}_\mu+\nu_e \rightarrow \bar{\nu}_\mu+\nu_e$ as well as $\nu_\mu+e \rightarrow \nu_\mu+e$, $\bar{\nu}_\mu+e \rightarrow \bar{\nu}_\mu+e$; the ν_e's are degenerate and in beta-equilibrium and we use the prescription of section 4.7 to evaluate the source term for this nonconservative scattering process: with a ν_e chemical potential of 72 MeV ($Y_p = 0.2$, $Y_n = 0.8$), this process dominates over $\nu_\mu e$ scattering. In order for the final equilibrium condition

$$\mu_{\nu_\mu} = \mu_{\bar{\nu}_\mu} = 0$$

to hold, we also include the annihilation $\nu_\mu\bar{\nu}_\mu \rightarrow \gamma_{pl}$.

The resulting ν_μ df at a number of timesteps is illustrated in Figure 30. At early times (0.1 ms, 1 ms), the df mainly reflects the production spectrum which is peaked near zero energy. As time passes, the $\nu_\mu\nu_e$ and $\nu_\mu e$ processes upscatter neutrinos from the low energy bins where they are produced to higher energies, thereby filling the tail of the df. By 235 ms it is an excellent approximation to assume the neutrinos are in "kinetic equilibrium" characterized by a FD df with a negative η_ν which is determined from equation 3.70 relating η_ν to the calculated Y_ν of the df. The antineutrino spectrum

looks quite similar. The two second df shown in this figure has no $\nu_\mu \nu_e$ turned on and was calculated using a different numerical method which has problems in the upper energy bins.

How does transport affect these results? The light travel time across the core is 7.4×10^{-5} s : this is the confinement time of neutrinos with energy less than 1.3 MeV. The diffusion time (with $\nu n \rightarrow \nu n$ and $\nu p \rightarrow \nu p$ included) then takes over, rising as ν^2 where ν is the neutrino energy; it is about a millisecond at 5 MeV. The bulk of the neutrinos are produced with less energy than this, and nonconservative upscattering is not efficient enough to smear out the production spectrum into an equilibrium one before the neutrinos escape. This behavior is what we find in the detailed numerical solutions (Figure 30): a very small steady state distribution results after $\sim$ 1.5 ms has elapsed.

The conditions of Figure 22 ($\rho Y_e = 1.13 \times 10^{12}$ g/cc , $T_{10} = 6.24$) fall near to Arnett's trajectory. The pair neutrinos dominate production. The average ν_μ energy is $\sim$ 35 MeV: these neutrinos will be trapped and have time to thermalize by nonconservative scattering. On the other hand, the plasmon ν_μ's are of low energy and will almost freely stream. The ν_e transport exceeds this radiation here.

The extrapolation of Arnett's trajectory passes through our $\nu_e / \nu_\mu \bar{\nu}_\mu$ demarcation line at the point labelled e^+e^- in Figures 9 and 18: $T_{10} = 12$, $\rho Y_e = 4 \times 10^{12}$ g/cc. The plasmon spectrum exceeds the pair spectrum only at low energies (Figure16); its integrated loss rate is much smaller: we neglect it here. Again, the $\nu_\mu \nu_e$ scattering

rate dominates the $\nu_\mu e$ rate (Figure 31). In Figure 32, three stages of the ν_μ evolution are shown: by one millisecond, the ν_μ df is approximately in kinetic equilibrium with $\eta_\nu = -2.8$, and it remains a FD df as continued production drives η_ν towards zero. Notice that the 0.75 second histogram has overshot the final $\eta_\nu = 0$ df: with our numerical methods, $\nu_\mu \bar{\nu}_\mu \rightarrow e^+e^-$ has failed to arrest the growth in the neutrino number since it is numerically tiny compared to the scattering rates.

The transport time due to neutrino nucleon scattering (Figure 31) is extremely rapid; the corresponding diffusion times are quite long, especially at the (high) mean production energy. The pair annihilation neutrinos are trapped for a sufficiently long time for $\nu_\mu \nu_e$, $\nu_\mu e$, $\bar{\nu}_\mu \nu_e$, and $\bar{\nu}_\mu e$ scattering to shape the production spectrum into a FD spectrum, a result confirmed by the numerical runs (the histograms are very similar to those in Figure 32).

The conduction approximation is therefore applicable to pair-produced neutrinos at least by the point of crossover into the $\nu_\mu \bar{\nu}_\mu$ region above the demarcation line in Figure 18, and probably well before (by Figure 22's conditions). We expect the same will hold true for plasmon-produced neutrinos by the time the demarcation line on the plasmon dominated side in Figure 18 has been crossed since the densities are so high there that even low energy neutrinos will be effectively trapped, and higher temperatures give more upscattering; no runs have been performed to check this yet.

Even though the chemical potentials are negative, the flow is

still down these, as well as temperature, gradients: the constitutive equations 3.67a,b,c still hold for the number and energy flux. The diffusion coefficients are those appropriate to Maxwell-Boltzmann df's; if the energy dependent diffusion coefficient has a power law dependence on ν ,

$$D(\nu) \sim \nu^{-\alpha} \tag{6.18a}$$

with $\alpha = 2$ for nondegenerate nucleons, 3 for degenerate nucleons (and low energy neutrinos), then

$$D_k = \frac{(k+2-\alpha)!}{(k+2)!} D(T) \quad , \quad k = 0,1,2 \tag{6.18b}$$

These constitutive equations then enter 3.58:

$$\frac{\partial}{\partial t} (Y(\nu_\mu)+Y(\bar{\nu}_\mu)) + 4\pi \frac{\partial}{\partial b} r^2 (F_\nu(\nu_\mu)+F_\nu(\bar{\nu}_\mu))$$

$$= 2(\dot{Y}_{\nu_\mu})(\gamma_{p\ell} \to \nu_\mu\bar{\nu}_\mu + e^+e^- \to \nu_\mu\bar{\nu}_\mu) \tag{6.18c}$$

$$\frac{\partial}{\partial t} (u_\nu(\nu_\mu)+u_\nu(\bar{\nu}_\mu)) + \frac{1}{3} (u_\nu(\nu_\mu)+u_\nu(\bar{\nu}_\mu)) \frac{\partial}{\partial t} \left(\frac{1}{\rho_B}\right)$$

$$+ 4\pi \frac{\partial}{\partial b} r^2 (H_\nu(\nu_\mu)+H_\nu(\bar{\nu}_\mu)) = \dot{Q}_{\nu_\mu\bar{\nu}_\mu} \tag{6.18d}$$

where Y_ν and u_ν are given by 3.70 and 3.71 respectively, and $\dot{Y}_{\nu_\mu}$ and $\dot{Q}$ are the free streaming number and energy production rates per baryon for these thermal processes (A2.41 and A2.43 for $e^+e^- \to \nu\bar{\nu}$). The constraint

$$\eta_{\nu_\mu} = \eta_{\bar{\nu}_\mu} \tag{6.18e}$$

is imposed upon these equations.

In fact, energies and currents of the electron neutrinos should be added into 6.18d, and 6.18c is augmented by the $\dot{Y}_{\nu_e}$ equation or else the temperature would be overdetermined.

The production described by the right hand side of 6.18c and d causes η_ν to build towards zero. If we continued describing evolution by these equations, we would overshoot zero: there is no shutoff mechanism on the production side at equilibrium. As η_ν nears zero, the Maxwell-Boltzmann diffusion constants 6.18b no longer hold. Once it is zero, we cannot use 6.18; rather, we should use the EDA, 3.67b with $\eta_\nu = 0$ plugged into 3.58a and the production side set to zero: production balances absorption. For example, when $\alpha = 2$, we obtain

$$\frac{\partial T}{\partial t} = \left[\frac{\eta_2}{12\eta_4}\right] \frac{1}{T^3} \frac{1}{r^2} \frac{\partial}{\partial r} r^2 \, D(T) \, T^3 \frac{\partial T}{\partial r} \qquad (6.19)$$

from the gray energy equation; the constant coefficient in square brackets $(5/(7\pi^2))$ is instead $\eta_1/6\eta_3$ if the gray muon neutrino number transport equation is used, where

$$\eta_k = \sum_{n=1}^{\infty} \frac{(-1)^{n+1}}{n^k}$$

The temperature is again overdetermined by these differing equations. The solution to this dilemma is to ignore the muon number equation, and use in the energy transport equation the constitutive equation for the full H_ν summed over all neutrino types; we still need the electron

lepton number conservation equation 3.59c to determine μ_{ν_e} .

Muon neutrinos are not freely streaming and the demarcation line of Figure 18 does not really reflect the boundary between ν_e and $\nu_\mu\bar{\nu}_\mu$ dominance of the energy flow. The ν_μ plus $\bar{\nu}_\mu$ flux satisfies

$$H_\nu(\nu_\mu+\bar{\nu}_\mu) = -D(T)\,\frac{T^3}{6(\hbar c)^3}\,\frac{\partial T}{\partial r} \tag{6.20}$$

which leads to a core luminosity of

$$L_{\nu_\mu\bar{\nu}_\mu} = \Phi_T\,\frac{1}{\tau_{diff}(\nu_\mu;T)}\,\frac{T^4}{6(\hbar c)^3\rho_B}\,(\tfrac{4}{3}\,\pi\,R_c^3\rho_B) \tag{6.21a}$$

$$\Phi_T \equiv -\,\frac{\partial \ell n\ T}{\partial \ell n\ r} \tag{6.21b}$$

The ratio of the power in $\nu_\mu\bar{\nu}_\mu$ to the power in ν_e (6.17b) is then

$$\frac{L_{\nu_\mu\bar{\nu}_\mu}}{L_{\nu_e}} = \frac{\Phi_T}{\Phi_\mu}\,\frac{\tau_{diff}(\nu_e;\mu_{\nu_e})}{\tau_{diff}(\nu_\mu;T)}\,\frac{\pi^2}{3\eta_{\nu_e}^4} \tag{6.21c}$$

$$\sim\ \pi^2/3\eta_{\nu_e}^2 \tag{6.21d}$$

If we neglect the opacity due to absorption which affects ν_e and not ν_μ , the ratio of diffusion times $\sim \eta_{\nu_e}^2$ for nondegenerate nucleons; equation 6.21d follows if we also assume Φ_T and Φ_μ are equal. This relation predicts the muon neutrino flow will exceed the ν_e flow only after the matter has heated up enough (or lost enough ν_e's) for η_{ν_e} to fall below 1.81; at this stage, however, the ν_e's are only semidegenerate, and the temperature gradient term in the ν_e flux has

to be included.

We conclude that the diffusive flow of ν_e's dominates that of ν_μ and $\bar{\nu}_\mu$ till the very latest collapse phases, when the core is very hot. Two effects modify 6.21d and soften this conclusion. With electron number frozen and a $\rho \sim T^3$ inner structure, Φ_T and Φ_μ would indeed be equal; since $\rho \sim T^{3/2}$, the temperature gradient is steeper than the chemical potential gradient ($\Phi_T \sim 2\Phi_\mu$, raising the boundary to ~ 2.57). The absorption rate, $\Gamma'_a(\mu_\nu)$, exceeds $\Gamma_{tr}(\nu n;\mu_\nu)$ when $Y_p > 0.13$ if protons and neutrons are nondegenerate and we have a pure nucleon gas. Since we cannot just sum on diffusion coefficients for various processes to obtain the total diffusion coefficient, we would have to do detailed numerical integrations to find this additional enhancement factor: just summing the absorption and scattering diffusion times gives an additional enhancement of 1.6 at $Y_p = 0.2$, $Y_n = 0.8$; for lower Y_p values, this factor is close to one.

Wilson et al. (1975), using a rather crude form of the source function for ν_μ and $\bar{\nu}_\mu$, find the energy loss in muon neutrinos and antineutrinos actually exceeds the loss in electron neutrinos when their luminosities are integrated over the entire core collapse time: ν_e's dominate the luminosity first, then as ν_e falls, the ν_μ luminosity rises.

The creation of muon pairs is suppressed by their high mass. Muon production through ν_μ absorption on electrons is suppressed by the degeneracy of the final state ν_e's. When the temperature is in

excess of 20 MeV, muon capture on nucleons begins to play a role in maintaining the ν_μ df's equilibrium.

If tau neutrinos couple in the same manner as muon neutrinos, they too will be in equilibrium at high density, with zero chemical potential, and their transport will be by diffusion.

Of possible observational interest are the electron antineutrinos, since these may be seen in Lande's detectors if a nearby core collapse occurs (section 2.1). In the neutronization dominated phase, there are few of them: not only are the thermal production processes slow, but the final electron neutrino states are inhibited by their degeneracy; this makes the $\bar{\nu}_e$ evolution the most difficult to follow numerically. This phase space blocking implies the $\bar{\nu}_e$'s will be created preferentially with low energy, and therefore escape even more easily than muon neutrinos. Further, there are too few positrons around for $e^+ n \rightarrow \bar{\nu}_e p$ to be a copious producer until the core enters its adiabatic heating phase and η_{ν_e} drops significantly. The equilibrium chemical potential for $\bar{\nu}_e$'s is the negative of the electron neutrino chemical potential. The df is a Maxwell-Boltzmann; the $\bar{\nu}_e$ number goes as $\exp(-\eta_{\nu_e})$, yet the mean energy is 3T. At a temperature of 10 MeV, we may expect most of these neutrinos to be trapped. Even then, the larger opacity and the remaining number of neutronization ν_e's make it the least effective of all the energy transporters. How large the flux is depends upon the density-temperature profiles at late stages.

6.7 EVOLUTION TO THE FINAL STATE

There are two paths the collapsing core may take: one is towards a black hole, the other to a neutron star.

If the core undergoes complete collapse to a black hole on a dynamical time which is short compared with the diffusion time (the likely case), few neutrinos escape. The core is adiabatically heating, creating exotic states of matter with nucleons perhaps breaking down into their component parts and strange particles being produced by weak processes. All species of neutrinos are in equilibrium, tied to the matter, and collapse with it beyond the horizon: they provide no signature of the final phases of the event.

If the hot neutron star core is less massive, it can cool to a final cold neutron star state. After the bouncing of the core has ceased, it may still be dynamical, subject to ringing (Hansen 1966). However, it primarily cools to rid itself of the released gravitational energy from collapse and loses lepton number by radiating its residual neutronization ν_e's. The equilibrium df's are kept up by the thermal processes. The lower opacity likely results in $\nu_\mu \bar{\nu}_\mu$ domination of the energy transport in the earliest cooling phases, with ν_e , $\bar{\nu}_e$ domination in later phases due to their higher production rates (when the neutrinos have gone out of equilibrium). The chemical potential of the ν_e's at nuclear matter density (if $Y_e = Y_p = 0.1$) is $\sim$ 155 MeV which yields a diffusion time or order six seconds for a 1.4 $M_\odot$ hot neutron star. It takes this long for the neutronization ν_e's to finally leave. While this loss

is going on, other processes than $e^- p \rightarrow n\nu_e$ keep the phase space filled (modified URCA process, pion-condensate-mediated electron capture).

When all of the neutronization neutrinos have radiated away so Y_e is $\sim$ 0.04 to 0.05, its cold neutron star value (Baym, Bethe, and Pethick 1971), and the thermally produced neutrinos no longer fill phase space up to $\mu_\nu = 0$, this final state of gravitational core collapse becomes the initial state for the usual treatments of neutron star cooling, such as those of Tsuruta (1974) and Tsuruta et al. (1972). (See also Brown 1977.) Within an hour or so, the temperature has dropped below an MeV. The cooling rate in the final approach to a cold neutron star remnant depends upon whether there is superfluidity of one or both of the neutron and proton fluids, whether a pion condensate forms, and what the magnetic field strength is.

6.8 SPATIAL TRANSPORT

So far, the effects of diffusion from the core have only been treated in a one zone model. In this section, the results of the numerical solutions to the full nonlinear partial differential equations of transport are presented.

The P-1 equations (section 3.8), with the Eddington factor (3.49a) determined by the elliptic distribution equation (3.45), are integrated by the techniques of section A4.4 in Appendix 4; similar methods are used to solve the flux limited diffusion (FLD) equations (section 3.10, with the flux limiter given by 3.64). We build the

neutrino distribution function from zero within an assumed static structure.

The ν_e source functions included are those of electron capture on free protons, neutrino absorption on free neutrons, conservative scattering by nucleons and nuclei, and nonconservative neutrino-electron scattering, with the $\ell = 0$ and 1 moments of the scattering kernel included. Eighteen energy groups are used; these give a much more detailed picture of the ν df than in previously published works. The treatment of νe scattering given here is a major improvement over the prescriptions used in the FLD codes of Arnett (1977), Wilson (1976), and Bruenn (1975).

Our numerical methods have the great advantage of stability in the neighborhood of equilibrium (compare with Yueh and Buchler 1977b, Arnett 1977, Wilson 1976): equilibrium diffusion can be accurately treated at the same time as free streaming.

The outer boundary condition used in these calculations was the standard Marshak BC, $n_1 = n_0/2$; this BC leads to problems, as we shall see.

We must assume a structure for the collapsing core and mantle. The only pre-bounce configuration published in sufficient detail to be useful is that of Arnett (1977), which we used to obtain the $\rho T Y_e$ structure. His extrapolations of the EA fitting formulae give nuclei of mass 300 in the inner core; we use the ENB extrapolations (unfortunately, well beyond their conceivable range of validity) to get a slightly different composition profile than Arnett's, with nuclei of maximum mass 62. The composition profiles used here and in Arnett (1977) are

characterized by relatively low free proton abundances.

The code has the capability of temperature and Y_e evolution; however, these changes were not allowed in these calculations due to the unknown behavior of the composition functions, in particular of Y_p (ρ, T, Y_e).

The three regions mentioned in Chapter 1 are reasonably well defined in this core.

The inner core, ranging in density from a central value of 1.5×10^{13} g/cc to $\sim 5 \times 10^{12}$ g/cc is characterized by high neutron abundances ($Y_n \sim .54$ in the center to $\sim .4$ on the boundary), most of the protons locked in alphas ($X_\alpha \sim .3$), many locked in heavy nuclei ($X_H \sim .14$ to $\sim .3$), and only a few free ($Y_p \sim .011$ to $\sim 10^{-3}$). The central temperature is 8 MeV, falling to 4 MeV at the boundary. The inner core is highly neutronized, with $Y_e \sim .15$ to .2.

The core-mantle, with density ranging from $\sim 2 \times 10^{11}$ to 6×10^{8} g/cc consists primarily of iron peak nuclei ($X_H \sim .7$), with the remaining nucleons in alphas, apart from a few percent of free neutrons, and a few parts per million of free protons. The maximum temperature is about an MeV, and Y_e's range from $\sim .4$ to near .5.

In between the inner core and the core-mantle lies a transition region, the neutronization shell, where most of the action occurs. It is not sharply defined, but ranges in density from $\sim 5 \times 10^{12}$ to $\sim 2 \times 10^{11}$ g/cc. Within these zones, the iron into alpha phase transition occurs and the bulk of the neutronization occurs: heavy nuclei are the most abundant by mass in the outer zones, whereas the interior is

almost equal parts heavy, alpha, and free neutron; Y_e drops from $\sim .36$ to $\sim .23$ at the neutronization shell/inner core boundary. The free proton abundances range from $\sim 6 \times 10^{-6}$ to $\sim 3 \times 10^{-4}$. By not including electron capture on heavies, we do not adequately represent the dominant role this neutronization shell plays in neutrino production.

Figure 33 compares the calculated neutrino df for four zones: the central zone, a zone near the inner core/neutronization shell boundary, one near the neutronization shell/core-mantle boundary, and one characteristic of the core-mantle. Figure 34 displays the electron neutrino luminosity profile at various times.

The central zone reaches equilibrium in sixty microseconds (see Figure 33); the rest of the inner core attains it somewhat later, but within a few milliseconds the EDA holds . The neutrino chemical potentials range from 30 to 40 MeV, and the neutrinos are only semidegenerate ($\eta \sim 5$); the mean neutrino energy is 38 MeV at the center, 24 MeV on the boundary; the neutrino abundance per baryon is $\sim .02$ over the core. All of these numbers would be considerably higher if the classical picture of an inner core of free nucleons holds.

The P-1 and FLD methods agree in the inner core. A manifestation of this is the common luminosity profile within the first one quarter of a solar mass (Figure 34), which is attained in less than a half a millisecond.

The mean free path of the neutrinos in the 10-12 MeV bin (group five) is 0.76 km in the center and 0.77 km at the boundary of the inner core (which has a lower density, but more heavy nuclei for coherent

scattering to compensate); the center is $\sim$ 32 mean free paths from the boundary. The Eddington factors are all one third, and the flux limiter is one. The ratio of the first to zeroth moment, n_1/n_0, for this energy group is 3.5×10^{-5} at 1.4×10^{13} g/cc, and is an order of magnitude higher near the edge of the inner core.

From Figure 33, it is evident that the neutrino df's in the neutronization shell are not FD at 3.6 ms; they are essentially the same at steady state. Transport from interior shells rather than neutrino creation and annihilation within the zone dominates the flow. The luminosity peak (at $\sim 10^{12}$ g/cc and 1/2 $M_\odot$) moves outward at early times as the diffusion wave from inner core neutrino production propagates outward. Differences between FLD and P-1 begin to appear: at 2×10^{11} g/cc, the Eddington factors are 0.53 in group one, .343 in group five; the flux limiters are 0.25 in one and 1.0001 in five; the mean neutrino energy is 10.5 MeV for FLD and 9.7 MeV for P-1.

The behavior of the P-1 and FLD solutions becomes radically different as we enter the core-mantle and the outer boundary is neared.

The FLD luminosity approaches a constant value in the outer zones. Free streaming is operative, and the power into a zone equals the power out. The neutrinos obey $H(\nu) = J(\nu)c$; at the outer boundary, they find the Marshak BC must be obeyed, and there is a small downturn in luminosity there (Figure 34).

The P-1 solution is much more sensitive to the choice of BC: as the neutrino wave nears the surface, it experiences the BC there and finds it cannot satisfy it except with a luminosity precipitously

falling near the surface. The number of neutrinos builds up, the luminosity peak becomes broader, and at 3.7 ms, a bulge begins in the luminosity at $\sim 4 \times 10^{10}$ g/cc. This bulge builds as time progresses, rising toward the surface rather than approaching a steady state constant value. Although this is the solution to the problem posed, it is not physically realistic.

The free streaming nature of the neutrinos near the outer boundary suggests a BC of form H = Jc rather than H = Jc/2 is more appropriate. Clearly, more numerical experiments with different BC's are necessary in order for the P-1 and FLD methods in the core-mantle to be meaningfully compared.

The small effect of the outer BC on the FLD solution suggests we can still extract information from this solution. The mean neutrino energy at steady state is 9 MeV at 4×10^{10} g/cc, and 7.3 MeV at 1.5×10^{9} g/cc; for the latter condition, all of the flux limiters differ from unity, most notably in group one, where $\varphi = 150$; the mean free path is 600 km for group 5 at this low density, and neutrinos are effectively decoupled from matter.

Is this neutrino flow likely to create an explosion? The ratio of the outward acceleration due to neutrinos to the inward gravitational acceleration is just the ratio of the neutrino luminosity to the Eddington limit (6.10). At steady state this is 0.018 for the central zone, it peaks between 2 and 4×10^{12} g/cc at .042, falls to .007 at 2×10^{11}, to .005 at 4×10^{10}, and to .002 at 1.5×10^{9} g/cc. The possibility for explosion by neutrino momentum deposition alone is bleak

in this particular configuration.

The inclusion of electron capture on heavy nuclei will increase the luminosity from the neutronization shell, and probably shift the peak closer to the core-mantle region. This will improve the chances for explosion, but will the increased luminosity be sufficient? The results of Arnett and Wilson suggest it is not.

The solution to the neutrino transport portion of the supernova problem within the context of the modern theory of neutrino interactions will rest upon a better treatment of electron capture on neutron-rich nuclei and on a resolution to the equation of state dilemma.

APPENDIX 1

THE DERIVATION OF THE P-N METHOD

A1.1 THE P-N APPROXIMATION: DERIVATION

We begin with the BTE 3.15

$$\mathcal{D}_s[n] + \mathcal{D}_v[n] = \mathcal{S}[n]$$

where

$$\mathcal{S} = \mathcal{S}_\beta + \mathcal{S}_{sc} + \mathcal{S}_{th} + \mathcal{S}_{\nu\nu}$$

and $\mathcal{S}_\beta$, $\mathcal{S}_{sc}$, and $\mathcal{S}_{th}$ are given by 3.5, 3.4 and 3.6 respectively; the self scattering term, $\mathcal{S}_{\nu\nu}$, applicable to $\nu+\nu \rightarrow \nu+\nu$ is:

$$\mathcal{S}_{\nu\nu}[n] = -\frac{1}{(2!)^2}\int \frac{d^3q_2}{(2\pi)^3}\,\frac{d^3q_3}{(2\pi)^3}\,\frac{d^3q_4}{(2\pi)^3}\,(2\pi)^4\,\delta^{(4)}\,(q+q_2-q_3-q_4)$$

$$|\langle \nu_3\nu_4|T|\nu_1\nu_2\rangle|^2 \Big\{ n(q)n(q_2)(1-n(q_3))(1-n(q_4))$$

$$- n(q_3)n(q_4)(1-n(q_2))(1-n(q))\Big\} \qquad \text{(A1.1)}$$

We adopt the notation

$$\langle f,g\rangle \equiv \frac{1}{2}\int_{-1}^{1} d\mu\; f(\mu)g(\mu) \qquad \text{(A1.2)}$$

to denote the inner product over angles of the two functions f and g. The ℓ^{th} moments of the df and source function are then

$$n_\ell = \langle P_\ell, n\rangle \qquad \text{(A1.3a)}$$

$$\mathcal{S}^{(\ell)} = \langle P_\ell,\, n\rangle \qquad \text{(A1.3b)}$$

Using the two Legendre polynomial identities

$$(2\ell+1)\mu\, P_\ell = (\ell+1)P_{\ell+1} + \ell P_{\ell-1} \qquad \text{(A1.4a)}$$

$$(1-\mu^2)\frac{dP_\ell}{d\mu} = \frac{\ell(\ell+1)}{2\ell+1}(P_{\ell-1} - P_{\ell+1}) \qquad \text{(A1.4b)}$$

it is easy to show that, for $\ell \geq 1$,

$$\left\langle P_\ell, \mathcal{D}_s[n] \right\rangle = \frac{\partial n_\ell}{\partial t} + \frac{\ell+1}{2\ell+1}\left[4\pi r^2 \rho \frac{\partial}{\partial b} n_{\ell+1} + \frac{(\ell+2)}{r} n_{\ell+1}\right] + \frac{\ell}{2\ell+1}\left[4\pi r^2 \rho \frac{\partial}{\partial b} n_{\ell-1} - \frac{(\ell-1)}{r} n_{\ell-1}\right] \qquad \text{(A1.5)}$$

If $\ell=0$, the last term on the right hand side vanishes, and A1.5 also holds, even though n_{-1} is not defined; we take n_{-1} , n_{-2} , ... to be zero. Again using a combination of A1.4a and A1.4b, for $\ell \geq 2$,

$$\left\langle P_\ell, \mathcal{D}_v[n] \right\rangle = \left(\frac{3v}{r} + \frac{\dot{\rho}}{\rho}\right)\left\{\frac{(\ell+1)(\ell+2)}{(2\ell+1)(2\ell+3)}\left[\nu \frac{\partial}{\partial \nu} n_{\ell+2} + (\ell+3) n_{\ell+2}\right] + \frac{\ell(\ell-1)}{(2\ell-1)(2\ell+1)}\left[\nu \frac{\partial}{\partial \nu} n_{\ell-2} - (\ell-2) n_{\ell-2}\right] + \frac{1}{(2\ell-1)(2\ell+3)} \cdot \left[(2\ell(\ell+1)-1)\nu \frac{\partial}{\partial \nu} n_\ell + \ell(\ell+1) n_\ell\right]\right\} - \frac{v}{r}\nu \frac{\partial}{\partial \nu} n_\ell \qquad \text{(A1.6)}$$

which is also valid for $\ell=0$ and $\ell=1$. The transport side of the moment equations is given by A1.5 and A1.6, the terms in square brackets with subscripts s and v respectively in 3.23a, 3.24a, 3.25a.

The moments of the source s_β are

$$s_\beta^{(\ell)} = \left\langle P_\ell, s_\beta \right\rangle = -n_\ell (\Gamma_a + \Gamma_p) \quad , \ell \geq 1 \qquad \text{(A1.7a)}$$

$$s_\beta^{(0)} = \left\langle 1, s_\beta \right\rangle = -n_0 (\Gamma_a + \Gamma_p) + \Gamma_p \quad , \ell = 0 \qquad \text{(A1.7b)}$$

The scattering kernel is, in the local rest frame of matter, a

function of ν,ν' and $\gamma=\hat{q}\cdot\hat{q}'$. The moments of the scattering kernel, $R(\nu,\nu',\gamma)$, are

$$R_\ell(\nu,\nu') = \left\langle P_\ell(\gamma),\ R(\nu,\nu',\gamma)\right\rangle \ . \tag{A1.8}$$

Now γ can be expressed in terms of $\mu = \hat{q}\cdot\hat{e}_r = \cos\theta$, $\mu' = \hat{q}'\cdot\hat{e}_r$ $= \cos\theta'$ and an azimuthal angle ϕ by

$$\gamma = \mu\mu' + \sqrt{(1-\mu^2)}\sqrt{1-(\mu')^2}\cos\phi \ . \tag{A1.9}$$

The integration over $\tilde{q}'$ in δ_{sc} includes an integration over the differential solid angle $d\Omega_{\tilde{q}'} = d\mu' d\phi$. We apply the addition theorem for spherical harmonics

$$P_\ell(\gamma) = \frac{4\pi}{2\ell+1}\sum_{m=-\ell}^{\ell} Y_{\ell m}(\theta,\phi)\, Y^*_{\ell m}(\theta',0) \tag{A1.10}$$

and immediately perform the ϕ-integration

$$\frac{1}{2}\int_{-1}^{1} P_\ell(\gamma)d\phi = 2\pi P_\ell(\mu')P_\ell(\mu) \tag{A1.11}$$

in δ_{sc} to obtain:

$$\begin{aligned}\delta_{sc}^{(\ell)} = \left\langle P_\ell,\delta_{sc}\right\rangle = -\Gamma_s n_\ell + \int_{\nu'}\sum_{\ell'=0}^{\infty}(2\ell'+1)R_{\ell'}(\nu',\nu)\left\langle P_\ell,P_{\ell'}\right\rangle \\ \cdot\left\langle P_{\ell'},n(\nu')\right\rangle + \int_{\nu'}\sum_{\ell'}(2\ell'+1)[R_{\ell'}(\nu,\nu')-R_{\ell'}(\nu',\nu)] \\ \cdot\ \left\langle P_\ell,P_{\ell'},n(\nu)\right\rangle\left\langle P_{\ell'},n(\nu')\right\rangle\end{aligned} \tag{A1.12}$$

In order to evaluate $\left\langle P_\ell,P_{\ell'},\ n(\nu)\right\rangle$, we express the product $P_\ell P_{\ell'}$ in terms of Clebsch-Gordon coefficients:

$$P_\ell(\mu)P_{\ell'}(\mu) = \sum_{L=|\ell-\ell'|}^{\ell+\ell'} \langle \ell\ell'00|L0\rangle^2 \, P_L(\mu) \qquad \text{(A1.13)}$$

to get the result in a suitable form:

$$\delta_{sc}^{(\ell)} = -n_\ell(\nu)\Gamma_s(\nu) + \int_{\nu'} R_\ell(\nu',\nu)n_\ell(\nu') + \int_{\nu'} \sum_{\ell'=0}^{\infty} \sum_{L=|\ell-\ell'|}^{\ell+\ell'} \langle \ell\ell'00|L0\rangle^2$$
$$\cdot(2\ell'+1)n_L(\nu)n_{\ell'}(\nu') \; [R_{\ell'}(\nu,\nu')-R_{\ell'}(\nu',\nu)] \qquad \text{(A1.14)}$$

In the specific cases $\ell=0$ and $\ell=1$, the Clebsch-Gordon coefficients are

$$\langle 0\ell'00|L0\rangle^2 = \delta_{\ell'L} \qquad \text{(A1.15a)}$$

$$\langle 1\ell'00|L0\rangle^2 = \frac{\ell'+1}{2\ell'+1} \; \delta_{L,\ell'+1} + \frac{\ell'}{2\ell'+1} \; \delta_{L,\ell'-1} \qquad \text{(A1.15b)}$$

which, when put into A1.14, give $\delta_{sc}^{(0)}$ and $\delta_{sc}^{(1)}$ in equations 3.23c and 3.24c.

The moments of δ_{th} are taken in the same manner as those of δ_{sc} , following steps A1.8 through A1.14, with the result

$$\delta_{th}^{(\ell)} = \langle P_\ell, \delta_{th}\rangle = (\delta_{\ell 0}-n_\ell(\nu)) \; \Gamma_{th}(\nu) - \int_{\nu'} R_{p\ell}(\nu,\nu')\bar{n}_\ell(\nu')$$
$$+ \int_{\nu'} \sum_{\ell'=0}^{\infty} \sum_{L=|\ell-\ell'|}^{\ell+\ell'} \langle \ell\ell'00|L0\rangle^2(2\ell'+1)$$
$$\cdot \; n_L(\nu)\bar{n}_{\ell'}(\nu') \; [R_{p\ell'}(\nu,\nu')-R_{a\ell'}(\nu,\nu')] \qquad \text{(A1.16)}$$

In particular, using A1.15 we obtain 3.23d and 3.25d.

A1.2 NEUTRINO-NEUTRINO SCATTERING

The reaction $\nu_e+\nu_e \to \nu_e+\nu_e$ may be important as a thermalizer of the ν_e df. Beginning with the effective Lagrangian for the $(\bar{\nu}_e\nu_e)(\bar{\nu}_e\nu_e)$ coupling, 2.22, it is straightforward to calculate the

amplitude for the reaction:

$$\langle \nu_3\nu_4 | T | \nu_1\nu_2 \rangle = \frac{-G}{2\sqrt{2}} \frac{\alpha_e^2}{\sqrt{16\,\nu_1\nu_2\nu_3\nu_4}} \left[\bar{u}_3\gamma^\mu(1-\gamma_5)u_1\bar{u}_4\gamma_\mu(1-\gamma_5)u_2\right.$$

$$\left. - \bar{u}_4\gamma^\mu(1-\gamma_5)u_1\bar{u}_3\gamma_\mu(1-\gamma_5)u_2\right]$$

$$= \frac{-G}{\sqrt{2}} \frac{\alpha_e^2}{\sqrt{16\,\nu_1\nu_2\nu_3\nu_4}} \left[\bar{u}_3\gamma^\mu(1-\gamma_5)u_1\bar{u}_4\,\gamma_\mu(1-\gamma_5)u_2\right] \qquad \text{(A1.17)}$$

The incoming neutrinos are labelled 1 and 2 with energies, momenta, and Dirac spinors ν_1, ν_2, $\underset{\sim}{q}_1$, $\underset{\sim}{q}_2$, u_1, and u_2 respectively; the outgoing neutrinos are labelled 3 and 4. The second line follows from the first by a Fierz transformation. This amplitude is the same as that for $\nu_e + e \to \nu_e + e$ with C_{Ve} and C_{Ae} replaced by α_e^2 . (See Appendix 2, equation A2.16a,b.) The matrix-element-squared is

$$\left|\langle \nu_3\nu_4 | T | \nu_1\nu_2 \rangle\right|^2 = \frac{8G^2\alpha_e^2}{\nu_1\nu_2\nu_3\nu_4} (q_1\cdot q_2)(q_3\cdot q_4) \qquad \text{(A1.18)}$$

The cross section for this reaction can be easily obtained using Lenard's theorem:

$$\int \frac{d^3q_3}{(2\pi)^3\nu_3} \frac{d^3q_4}{(2\pi)^2\nu_4} (2\pi)^4\, \delta^{(4)}\,(k-q_3-q_4)\; q_3^\alpha\, q_4^\beta$$

$$= \frac{1}{24\pi} (2k^\alpha k^\beta + k^2 g^{\alpha\beta})\,\theta(k^2)\,\theta(k^0) \qquad \text{(A1.19)}$$

where q_3, q_4 are null 4-vectors, and $\theta(x)$ is the Heaviside unit function (1 if $x > 0$, 0 if $x < 0$). The result is the invariant

$$\sigma(\nu_e + \nu_e \to \nu_e + \nu_e) = \frac{G^2}{\pi}\,\alpha_e^2\, s \qquad \text{(A1.20)}$$

where s is the square of the center of mass energy,

$$s = (q_1+q_2)^2 = 2(q_1 \cdot q_2) \qquad \text{(A1.21)}$$

In this calculation, the final phase space has been divided by a factor of 2! to account for indistinguishability of the final state particles; no additional factor of 1/2! is included in the initial state for the cross section, but is included in the rate calculation (see below).

The squared amplitude is obtained for other neutrino scattering reactions by the substitutions in A1.18:

$$\nu_e+\bar{\nu}_e \to \nu_e+\bar{\nu}_e \quad : \quad q_2 \to -q_4 \ , \ q_4 \to -q_2 \qquad \text{(A1.22a)}$$

$$\nu_e+\nu_\mu \to \nu_e+\nu_\mu \quad : \quad \alpha_e^2 \to \alpha_e\alpha_\mu \qquad \text{(A1.22b)}$$

$$\nu_e+\bar{\nu}_\mu \to \nu_e+\bar{\nu}_\mu \quad : \quad \alpha_e^2 \to \alpha_e\alpha_\mu \ , \ q_2 \to -q_4 \ , \ q_4 \to -q_2 \qquad \text{(A1.22c)}$$

$$\nu_e+\bar{\nu}_e \to \nu_\mu+\bar{\nu}_\mu \quad : \quad \alpha_e^2 \to \alpha_e\alpha_\mu \ , \ q_3 \to -q_3 \ , \ q_2 \to -q_2 \qquad \text{(A1.22d)}$$

(and $\nu_\mu+\bar{\nu}_\mu \to \nu_e+\bar{\nu}_e$)

No factors of 2! are required in the calculation of these cross sections, which are given in Table 2.2. Our cross sections for the reactions $\nu_e\nu_\mu \to \nu_e\nu_\mu$, $\nu_e\bar{\nu}_\mu \to \nu_e\bar{\nu}_\mu$ differ from those inferred from Flowers and Sutherland (1976) by a factor of four; our $\nu_e\nu_e \to \nu_e\nu_e$ and $\nu_e\bar{\nu}_e \to \nu_e\bar{\nu}_e$ cross sections agree with theirs.

It is very difficult to deal with $\delta_{\nu\nu}$ in the P-N method for arbitrary N. It is possible to evaluate $\delta_{\nu\nu}$ if we keep only the ℓ=0 and ℓ=1 moments, but the result is very complicated. Here, we

assume the ν df's are dominated by the $\ell=0$ terms; when the neutrinos have built up a high enough concentration that $\nu+\nu \to \nu+\nu$ becomes important, this assumption will be valid. In A1.1 we distinguish two terms, $\mathcal{S}_{\nu\nu}^{IN}$ and $\mathcal{S}_{\nu\nu}^{OUT}$, corresponding to scattering into and out of the beam; the former is proportional to $1-n(q)$, the latter to $n(q)$:

$$\mathcal{S} = \mathcal{S}_{\nu\nu}^{IN} + \mathcal{S}_{\nu\nu}^{OUT}$$

We follow the subsequent derivation for $\mathcal{S}^{OUT}$; the derivation for $\mathcal{S}^{IN}$ is similar. Hereafter, we identify ν_1, $\underset{\sim}{q}_1$ with ν, $\underset{\sim}{q}$. We integrate over $\underset{\sim}{q}_4$ in A1.1 to get rid of the momentum-conserving delta function:

$$\mathcal{S}^{OUT} = -n_0(1) \int \frac{d^3q_2}{(2\pi)^3} \frac{d^3q_3}{(2\pi)^3} n_0(2)(1-n_0(3))(1-n_0(4))$$

$$\cdot 2\pi\ \delta(\nu_4-\varepsilon_4)\ 2G^2 \frac{\nu_1\nu_2}{\nu_3\nu_4} (1-\hat{q}_1\cdot\hat{q}_2)^2$$

where

$$n_0(i) = n_0(\nu_i) \qquad i = 1,\ldots,4$$

$$\nu_4 = \nu_1+\nu_2-\nu_3$$

$$\varepsilon_4 = ||\underset{\sim}{q}_1+\underset{\sim}{q}_2-\underset{\sim}{q}_3|| = (k^2-2k\nu_3 \cos\theta_3+\nu_3^2)^{1/2}$$

$$k^2 = \nu_1^2+\nu_2^2 + 2\nu_1\nu_2 \cos\theta_2$$

We transform the $\cos\theta_3$ integration into one over ε_4, which we

use to get rid of the remaining delta function, then transform the $\cos\theta_2$ integration into one over k:

$$\mathcal{S}^{OUT} = -n_0(1)\int_0^\infty d\nu_2 \int_0^\infty d\nu_3\, n_0(2)(1-n_0(3))(1-n_0(4))$$
$$\cdot \frac{G^2}{16\pi^3\nu_1^2}\int \chi(k)dk\ ((\nu_1+\nu_2)^2-k^2)$$

where the characteristic function is

$$\chi(k) = \chi_{(\max(|\nu_1-\nu_2|,|\nu_1+\nu_2-2\nu_3|),\ \nu_1+\nu_2)}(k)$$
$$= (1 \text{ if k is in the indicated range, 0 otherwise}).\text{(A1.23)}$$

If we define the dimensionless polynomial

$$g(\varepsilon) = \frac{1}{\nu_1^5}\left[\frac{8}{15}(\nu_1+\nu_2)^5-(\nu_1+\nu_2)^4\varepsilon + \frac{2}{3}(\nu_1+\nu_2)^3\varepsilon^2 - \frac{1}{5}\varepsilon^5\right] \qquad \text{(A1.24)}$$

then

$$\mathcal{S}_{\nu\nu} = \int_0^\infty d\nu_2 \int_0^\infty d\nu_3 \Big\{\chi_{(0,\nu_1)}(\nu_2)[\chi_{(\nu_2,\nu_1)}(\nu_3)g(\nu_1-\nu_2) + \chi_{(0,\nu_2)}(\nu_3)$$
$$\cdot g(\nu_1+\nu_2-2\nu_3) + \chi_{(\nu_1,\nu_1+\nu_2)}(\nu_3)g(2\nu_3-\nu_1-\nu_2)\Big\} + \chi_{(\nu_1,0)}(\nu_2)$$
$$\cdot [\chi_{(\nu_1,\nu_2)}(\nu_3)g(\nu_2-\nu_1) + \chi_{(0,\nu_1)}(\nu_3)g(\nu_1+\nu_2-2\nu_3) + \chi_{(\nu_2,\nu_1+\nu_2)}(\nu_3)$$
$$\cdot g(2\nu_3-\nu_1-\nu_2)]\Big\}\frac{G^2}{16\pi^3}\ \nu_1^3\ \Big\{-n_0(\nu_1)n_0(\nu_2)(1-n_0(\nu_3))(1-n_0(\nu_1+\nu_2-\nu_3))$$
$$+ n_0(\nu_3)n_0(\nu_1+\nu_2-\nu_3)(1-n_0(\nu_1))(1-n_0(\nu_2))\Big\} \qquad \text{(A1.25)}$$

The approximation, then, is to let

$$\mathcal{S}^{(0)}_{\nu\nu} = \mathcal{S}_{\nu\nu} \qquad \text{(A1.26a)}$$

$$\mathcal{S}^{(\ell)}_{\nu\nu} = 0 \quad , \quad \ell \geq 1 \quad . \qquad \text{(A1.26b)}$$

In $\mathcal{S}_{sc}$, there is one neutrino energy integration to perform once the ν df is known, and there are no constraints on the range of integration; in $\mathcal{S}_{\nu\nu}$, there are two neutrino energy integrations which must be done, and there are restrictions imposed on their ranges. Both become summations after a group averaging over energy bins has been performed; we do not further discuss this here, as it more rightly belongs in the numerical methods section, Appendix 4.

APPENDIX 2
INDEPENDENT PARTICLE PROCESSES

In this rather technical appendix, we compute in the first section the current-current correlation function for a free electron gas, and in the second section apply the result to nuclear matter in both the nondegenerate and extremely degenerate limits, in particular deriving moments of the zero temperature νN scattering kernels. We return to νe scattering in section three, where moments of the kernels for this process are obtained. In section four, production and absorption kernels for $e^+e^- \to \nu\bar{\nu}$ are given, along with integrated production rates.

A2.1 $\nu+e \to \nu+e$

The kernel for neutrino electron scattering is given in terms of correlation functions by equation A3.10 in Appendix 3, with the total current replaced by that of the electron A3.4. The current-current correlation function for the electron field, when electrons and positrons are independent quasiparticles, can be separated into four parts:

$$S_{J_e^\alpha J_e^\beta}(k\omega) = S_{\alpha\beta}^{e^-e^-} + S_{\alpha\beta}^{e^+e^+} + S_{\alpha\beta}^{e^+e^-} + \tilde{S}_{\alpha\beta}^{e^+e^-} \qquad \text{(A2.1)}$$

The first term is used in $\nu+e^- \to \nu+e^-$, the second in $\nu+e^+ \to \nu+e^+$, the third in $e^++e^- \to \nu+\bar{\nu}$, and the fourth in $\nu+\bar{\nu} \to e^++e^-$. The (e^-e^-) part of the correlation function is given (for ν_e scattering) by

$$S^{ee}_{\alpha\beta}(k\omega) = \sum_{pp'} f_e(p)(1-f_e(p'))(2\pi)^4\,\delta^{(4)}(p+k-p')\,\frac{1}{E\,E'}$$

$$\cdot\Big\{(C_{Ve}^2+C_{Ae}^2)(p^\alpha p^{\beta\prime}+p^\beta p^{\alpha\prime}-p\cdot p' g^{\alpha\beta}) + 2C_{Ve}C_{Ae}\,i\varepsilon^{\alpha\beta}(p',p)$$

$$+ m_e^2(C_{Ve}^2-C_{Ae}^2)g^{\alpha\beta}\Big\} \qquad \text{(A2.2)}$$

where the summation over momentum means an integration

$$\sum_p \equiv \int \frac{d^3p}{(2\pi)^3} \qquad \text{(A2.3)}$$

To derive the expression, we note that for a noninteracting gas of electrons, the spatial Fourier transform of that part of the weak current which does not involve positrons is

$$\tilde{J}^\mu_e(\underset{\sim}{k},t) = \sum_{p\sigma\sigma'} a^\dagger_{p-k,\sigma}(t)a_{p\sigma'}(t)\,\frac{\bar{u}(p-k,\sigma)}{\sqrt{2E_{p-k}}}\,\gamma^\mu(C_{Ve}-C_{Ae}\gamma_5)\frac{u(p\sigma')}{\sqrt{2E_p}} \qquad \text{(A2.4)}$$

where $a_{p\sigma'}(t)$ annihilates an electron of momentum $\underset{\sim}{p}$ and spin σ' at time t; $u(p\sigma')$ is a Dirac spinor normalized as in equation 2.28. The energy of the electron is E_p .

In order to evaluate $S^{ee}_{\alpha\beta}$, we need the thermal average

$$\langle a_j^\dagger a_k a_\ell^\dagger a_m\rangle = f_j f_\ell\,\delta_{kj}\,\delta_{\ell m}(1-\delta_{j\ell}) + f_j(1-f_\ell)\delta_{jm}\delta_{k\ell}(1-\delta_{j\ell})$$

$$+ f_j\delta_{j\ell}\delta_{kj}\delta_{\ell m} \qquad \text{(A2.5)}$$

where

$$f_j = \langle a_j^\dagger a_j\rangle = (e^{\beta(E_j-\eta_e)}+1)^{-1} \qquad \text{(A2.6)}$$

is the mean occupation number of orbital j , a single particle state;

the j means $p_j\sigma_j$, and $\delta_{j\ell}$ means a delta function in momentum and spin. We then obtain

$$\left\langle \tilde{J}^{\mu}(kt)\tilde{J}^{\nu}(-kt')\right\rangle = \sum_{j\ell} \frac{f_j(1-f_\ell)}{2E_j 2E_\ell}\; e^{i(E_j-E_\ell)(t-t')}\delta_{p_\ell,p_j+k}$$

$$\cdot\; \bar{u}_j\gamma^{\mu}(C_{Ve}-C_{Ae}\gamma_5)u_\ell \bar{u}_\ell\gamma^{\nu}(C_{Ve}-C_{Ae}\gamma_5)u_j \qquad \text{(A2.7)}$$

$$+ \text{ (time independent terms which are zero when } \underset{\sim}{k}=0)$$

The time independent k=0 parts include $\left\langle \tilde{J}^{\mu}(kt)\right\rangle\left\langle \tilde{J}^{\nu}(-kt')\right\rangle$, and a term like the time dependent one, but with a $\delta_{j\ell}$ inserted. These terms when we Fourier transform in t-t' , give a $\delta^{(4)}(k)$ contribution; no 4-momentum is transferred to the medium.

The equilibrium distribution function f_j is independent of spin σ_j , and the spin sums can be performed in A2.7, turning it into a trace similar to 2.42a,

$$S^{ee}_{\alpha\beta} = \sum_{pp'} f_e(p)(1-f_e(p'))\;\frac{1}{4E\,E'}\;(2\pi)\delta(E_p+\omega-E_{p'})\delta_{p+k,p'}$$

$$\cdot\; \mathrm{Tr}(\not{p}+m)\gamma^{\alpha}(C_{Ve}-C_{Ae}\gamma_5)(\not{p}'+m)\gamma^{\beta}(C_{Ve}-C_{Ae}\gamma_5) \qquad \text{(A2.8)}$$

When the traces are evaluated, equation A2.2 is obtained.

One of the virtues of the method of correlation functions is that the $f_e(1-f_e')$ Fermi function term arises naturally as opposed to being imposed as in the exercise of Fermi's Golden Rule, equation 3.2.

If we change the sign of C_A in A2.2, and the df's to those of the positron, we obtain the (e^+e^+) part of the correlation function.

If we replace C_{Ve} and C_{Ae} by one, set $m_e=0$, and replace f_e by n_ν, the neutrino df, we obtain the $(\nu\nu)$ correlation function. The ensemble in which the expectation value A2.6 is taken is then a nonequilibrium one, which is reflected in the nonequilibrium nature of n_ν. If we set $C_{Ae}= -1$ instead, the $(\bar{\nu}\bar{\nu})$ correlation function results.

A2.2 $\nu+N \rightarrow \nu+N$

If we replace C_{Ve}, C_{Ae} by C_{VN}, C_{AN}, with N = n,p, and m_e by the nucleon mass, m_N, we obtain the current-current correlation function for independent nucleons. In the low energy limit, when the nucleon velocities are small compared with the velocity of light, $p^\alpha \sim m_N \delta^{\alpha 0}$, and the only surviving components of the correlation functions are (compare with A3.26, A3.27)

$$S_{00}^{NN} = C_{VN}^2 \, n_N \, S_{NN}^D \tag{A2.9a}$$

$$S_{ij}^{NN} = C_{AN}^2 \, n_N \, S_{NN}^D \, \delta_{ij} \tag{A2.9b}$$

where the dynamic liquid structure factor for independent nucleons is

$$S_{NN}^D(\underset{\sim}{k}\omega) = \frac{2}{n_N} \sum_{pp'} f_N(p)(1-f_N(p'))2\pi\delta(E_p-E_{p'}+\omega) \cdot (2\pi)^3\delta^{(3)}(\underset{\sim}{p}-\underset{\sim}{p}'+\underset{\sim}{k}) \tag{A2.10}$$

That this formula holds is not contingent upon the noninteraction hypothesis; it is derivable within the framework of Hartree-Fock theory. Correlations among nucleons are included if they can be described by a single particle Hartree-Fock potential, or, for that matter, by any other single particle potential; this is the independent-

particle approximation (deShalit and Feshbach 1974) used in zero temperature nuclear matter theory, which can be extended to finite temperature (Fetter and Walecka 1971). In infinite nuclear matter, the Hartree-Fock states are plane waves labelled by momentum and spin, with energy

$$E_{p\sigma} = \frac{p^2}{2m} + U(p) \tag{A2.11}$$

where U(p) is the Fourier transform of the self-consistent potential. The nucleon is dressed by its interaction with other nucleons, ceasing to be a bare particle, becoming a quasiparticle; it is these which scatter the neutrinos. The analysis leading to A2.9, A2.10 follows the same path.

For noninteracting, nonrelativistic (n.r.) nucleons, A2.10 can be evaluated exactly:

$$n_N \, S^D_{NN}(k\omega) = \frac{m^2 T}{\pi k} \frac{1}{1-e^{-\beta\omega}} \left\{ \ell n(1+e^{\beta(\mu-\varepsilon)}) - \ell n(1+e^{\beta(\mu-\varepsilon-\omega)}) \right\} \tag{A2.12a}$$

where T is the temperature in energy units, m is the nucleon mass, μ is the nucleon's chemical potential, and

$$\varepsilon = \frac{m}{2k^2} (\omega - k^2/2m)^2$$

In the nondegenerate limit (n.d.), the result is a Gaussian in ω,

$$S^D_{NN}(k\omega) \xrightarrow[n.d.]{} \left(\frac{2\pi m}{T} \right)^{1/2} \frac{e^{-\beta\varepsilon}}{k} \tag{A2.12b}$$

with mean $k^2/2m$ and standard deviation

$$\sigma = \sqrt{\frac{T}{m}} \quad k = \frac{kv_{rms}}{\sqrt{3}}$$

where v_{rms} is the root mean square velocity of the particles. The integral of A2.10c over ω , the static liquid structure factor, is one. To form moments of the scattering kernel obtained using A2.10c is very difficult, since we must do a k-integration, and there is both a k^{-2} and a k^{+2} term in the exponential. The conservative approximation assumes A2.10c is reasonably well approximated by a delta function at ω=0. This will be so if both the mean and the variance are small compared with the incident neutrino energy, i.e., if ν is small compared with the nucleon mass and v_{rms} is small compared with the speed of light. If all of the target particles were at rest, the liquid structure factor would be $2\pi\ \delta(\omega - k^2/2m)$: the dispersion in ω space is due to the thermal motion of the nucleons. Neutrinos can be downscattered and upscattered in energy over a peak of width $\sim \nu v_{rms}$; when one integrates over final neutrino energy, the downscattering and upscattering almost balance, and the net effect is for the neutrino to deposit $\sim \nu^2/m$ in the medium. Tubbs (1978) has noted that when this small energy loss is multiplied by the scattering rate, the result is about the same as that obtained when the higher mean energy loss in neutrino-electron scattering is multiplied by its smaller scattering rate. However, the νe process can downscatter high energy neutrinos to low energies in one step; the νn process must go through all intermediate energies in many small steps, and as the energy lowers, the scattering rate lowers as its square. Production processes fill

low energies at low rates, high energies at high rates. The speed of approach to a Fermi Dirac df is determined by the rate at which high energy neutrinos can be funnelled into the unfilled phase space at low energies; νe scattering is much more effective at this than νN scattering. Everything said here about νN scattering in the nondegenerate limit applies equally to νA scattering, except that the nucleon mass is replaced by the much greater nuclear mass, and the conservative approximation is correspondingly better.

At zero temperature, in the extremely degenerate (e.d.) limit, the dynamic structure factor reduces to

$$S^{D}_{NN}(k\omega) \xrightarrow[e.d.]{} \frac{3\pi m^2}{kp_F^3}\ \theta(\omega)\ [\omega\ \chi_{(0,\mu-\omega)}(\varepsilon) + (\mu-\varepsilon)\ \chi_{(\mu-\omega,\mu)}(\varepsilon)] \quad \text{(A2.12c)}$$

where p_F is the Fermi momentum, χ is the characteristic function for the indicated range, and $\theta(\omega)$ is the Heaviside unit function of ω, expressing the fact that the zero temperature medium can transfer no energy to the neutrino. When $\omega \gtrsim kv_F + k^2/2m$, where v_F is the Fermi velocity, the structure factor, which is plotted in Figure 6, vanishes; this region of ω-k space is not accessible kinematically when only particle-hole pair creation is considered.

Moments of the zero temperature scattering kernel can be given analytically. The qualitative form of these functions differ when in different regions of ω-k_m space, where $k_m = \nu+\nu'$ is the maximum possible momentum transferred to the neutrino, corresponding to backward scattering. The appropriate domains in this space reflect the two regions of the structure function, and are displayed in

Figure 7; indeed, when we reinterpret k_m to be just k, the structure function is linear in ω interior to the line $\omega = kv_F - k^2/2m$, and is quadratic exterior to it. Particle-hole pair creation is not kinematically allowed in the region to the left of the $\omega = kv_F + k^2/2m$ line. The four regions in ω-k_m space are defined by

$$\begin{aligned} \text{Region I} &: \mu \leq \omega \ , \ q_0 \leq k_m \\ \text{Region II} &: \omega \leq \mu \ , \ q_0 \leq k_m \leq q_1 \\ \text{Region III} &: \omega \leq \mu \ , \ q_1 \leq k_m \leq 2p_F - q_1 \\ \text{Region IV} &: \omega \leq \mu \ , \ 2p_F - q_1 \leq k_m \end{aligned} \tag{A2.13a}$$

where

$$q_0 = p_F \ (\sqrt{1+\omega/\mu} \ -1)$$

$$q_1 = p_F \ (1- \sqrt{1-\omega/\mu} \ )$$

The highly oblique ν, ν' axes are also displayed in this figure. Large regions of $\nu\nu'$ space are inaccessible to νN scattering at zero temperature: given ν, there is both a minimum value ν' must exceed in order to satisfy the kinematical constraint, and a maximum value which it cannot exceed, namely ν . When the temperature is finite, all regions of this space become accessible.

The ℓ=0 moment of the scattering kernel is explicitly

$$\begin{aligned} R_0(\nu \to \nu') &= F(q_0, k_m) \qquad \text{Region I and II} \\ &= F(q_0, q_1) + G(q_1, k_m) \qquad \text{Region III} \end{aligned} \tag{A2.13b}$$

$$= F(q_0,q_1) + G(q_1,2p_F-q_1) + F(2p_F-q_1,k_m) \quad \text{Region IV}$$

where

$$G(s,t) = \frac{G^2m^2}{\pi 2\nu\nu'}\left[(C_{VN}^2+3C_{AN}^2+(C_{VN}^2-C_{AN}^2)\frac{1+x^2}{2x})\omega(t-s)-(C_{VN}^2-C_{AN}^2)\frac{\omega}{6\nu\nu'}(t^3-s^3)\right]$$

$$F(s,t) = \frac{G^2m^2}{\pi 2\nu\nu'}\left[(C_{VN}^2+3C_{AN}^2+(C_{VN}^2-C_{AN}^2)\frac{1+x^2}{2x})\left\{(\mu+\frac{\omega}{2})(t-s)+\frac{t^3-s^3}{6m}\right.\right.$$

$$\left.\left.+\frac{m\omega}{2st}(t-s)\right\}-(C_{VN}^2-C_{AN}^2)\frac{\omega}{2\nu\nu'}\left\{(\mu+\frac{\omega}{2})\frac{(t^3-s^3)}{3}+\frac{t^5-s^5}{10m}+\frac{m\omega}{2}(t-s)\right\}\right]$$

Typical $\nu n \to \nu n$ moments for various incident neutrino energies are plotted as a function of the outgoing neutrino energy in Figure 8. The density is 5×10^{13} g/cc, the free neutron to baryon ratio is 0.9; the Fermi momentum is then 183 MeV and the Fermi velocity is 0.2 (which is also the velocity chosen for Figure 7). If neutrino beta-equilibrium holds (equation 3.12), then $Y_{\nu_e} = 0.03$, and the neutrino Fermi energy is 74 MeV; these neutrinos dump $\sim$20% of their energy in each collision, in contrast with the conservative case.

To obtain the scattering rate, these expressions must be integrated over the final neutrino energy. When the initial neutrino energy is small compared with the nucleon Fermi momentum, this is particularly easy. The liquid structure factor is approximated by a curve rising linearly in ω and truncated at $\omega = kv_F$. From Figure 6, we can see that this is a good approximation as long as $k \ll 2p_F$, and therefore $\nu+\nu' \ll 2p_F$. Then, we integrate over ν' along a constant ν line between the $\omega = kv_F$ line and the $\omega = 0$ line (see Figure 7), with

the result

$$\Gamma_s(\nu) = n_N \frac{G^2}{\pi} \nu^2 \frac{\nu}{p_F} (C_{VN}^2 + 3C_{AN}^2 - (C_{VN}^2 - C_{AN}^2)(\frac{1-v_F}{5}))/(1+v_F)^3,$$

$$\nu << p_F \qquad \text{(A2.13c)}$$

which is quite similar to the conservative approximation value 4.35 except for the ν/p_F suppression factor.

Nucleon interaction effects may be crudely taken into account by assuming A2.11 is described by

$$E_{p\sigma} = \frac{p^2}{2\tilde{m}_N^*} + \text{constant} \qquad \text{(A2.14)}$$

where $\tilde{m}_N^*$ is a mean approximate effective mass, which depends upon temperature, density and Y_N. It also depends upon momentum; however, for symmetric nuclear matter ($Y_n = Y_p$) at zero temperature and at normal nuclear density ($\rho = 2.82 \times 10^{14}$ g/cc, $p_F/\hbar = 1.36$ fm^{-1} = 268 MeV/c), $\tilde{m}_N^* = 0.7\ m_N$ over an energy range from 10 to 70 MeV, a value determined empirically from the confrontation of optical model predictions with experiment (Jeukenne et al. 1976). At any other density, and for Y_n and Y_p not equal, one must resort to theoretical predictions of $\tilde{m}_N^*$; these are not available over a wide density and composition range. At low densities, it is one. The temperature dependent effective mass would replace m in equation A2.12 for the structure factor, and a zero temperature effective mass would replace m in A2.12c for the zero temperature structure factor, and in A2.13b for the scattering kernel. The mass does not appear in the low energy approximation to the scattering lifetime, A2.13c, however it should be multiplied by

$(\tilde{m}_N^*/m_N^*)^2$, where m_N^* is the effective mass in the neighbourhood of the Fermi surface, defined by equation 4.42. These two effective masses are apparently not equal: the Fermi surface value, m_N^* , is slightly higher than the mean value, $\tilde{m}_N^*$, perhaps $\sim m_N$ instead of $\sim 0.7 m_N$ at normal nuclear density (Jeukenne et al. 1975 and references therein).

A2.3 NEUTRINO-ELECTRON SCATTERING KERNELS

In order to evaluate the kernels, given by A3.10 when A2.3 is substituted, we need

$$\varepsilon_{\alpha\beta}(q',q)\varepsilon^{\alpha\beta}(p',p) = 2(q'\cdot p\ q\cdot p' - q'\cdot p'\ q\cdot p) \qquad \text{(A2.15)}$$

to obtain

$$R(q\to q') = (C_{Ve}+C_{Ae})^2\,\gamma + (C_{Ve}-C_{Ae})^2\,\bar{\gamma} + (C_{Ve}^2-C_{Ae}^2)\,\gamma_M \qquad \text{(A2.16a)}$$

where

$$\gamma(q\to q') = 2G^2 \sum_{p_1 p_2} \frac{(p_1\cdot q)(p_2\cdot q')}{\nu\nu' E_1 E_2} (2\pi)^4 \delta^{(4)}(p_1+q-p_2-q') f_{p_1}(1-f_{p_2}) \qquad \text{(A2.16b)}$$

$$\bar{\gamma}(q\to q') = \gamma(-q'\to -q) \qquad \text{(A2.16c)}$$

$$\gamma_M = 2G^2 \sum_{p_1 p_2} \frac{m_e^2 (q\cdot q')}{\nu\nu' E_1 E_2} (2\pi)^4 \delta^{(4)}(p_1+q-p_2-q')\, f_{p_1}(1-f_{p_2}) \qquad \text{(A2.16d)}$$

We assume electrons are extremely relativistic; then γ_M can be neglected relative to γ and $\bar{\gamma}$. Integrals of γ_M over q' are less than 1% of the equivalent integral of γ and $\bar{\gamma}$ (Tubbs and Schramm 1975).

Using energy-momentum conservation to relate $p'\cdot q' = p\cdot q$, and integrating over the momentum p_2 , we obtain

$$\gamma = 2G^2 \sum_{p_1} f(E_1)(1-f(E_1+\omega))2\pi\ \delta(E_1+\omega-E_2)\ \frac{\nu E_1}{\nu' E_2}\ (1-\hat{p}_1\cdot\hat{q})^2$$

where $\omega = \nu-\nu'$. We next integrate over the electron solid angle to get rid of the delta function of energy. To do so, we let $\mu = \hat{q}\cdot\hat{k} = \cos\theta$, $\mu' = \cos\theta' = \hat{p}_1\cdot\hat{k}$: then

$$\hat{p}_1\cdot\hat{q} = \cos\theta' \cos\theta + \sin\theta' \sin\theta \cos\phi'$$

The integral over ϕ' is straightforward. The μ' integration becomes an integration over $E_2 = |\underset{\sim}{p}_1+\underset{\sim}{k}|$, with the result

$$\gamma = \frac{G^2}{\pi}\frac{\nu}{\nu' k}\int_0^\infty dE\ f(E)\ (1-f(E+\omega))\ E^2 Q(\mu_0',\mu)\ \chi(E) \qquad \text{(A2.17)}$$

where χ is the characteristic function for the set $[k-\omega/2,\infty)$: it is zero unless E is within that range. We have let

$$\mu_0' = \frac{\omega}{k} - \frac{(k^2-\omega^2)}{2Ek} \qquad \text{(A2.18)}$$

$$Q(\mu',\mu) = (1-\mu'\mu)^2 + \frac{1}{2}(1-(\mu')^2)(1-\mu^2)$$

The next step is to expand Q in ν, ν', k, and E:

$$E^2 Q(k,E,\nu,\nu') = \nu^2 \frac{(k^2-\omega^2)^2}{4k^4} \sum_{n=0}^{2}\sum_{m=0}^{2}\left(\frac{E}{\nu}\right)^n P_{nm}(x)\ \left(\frac{k}{\nu}\right)^{2m} \qquad \text{(A2.19)}$$

The P_{nm} are polynominals in $x = \nu'/\nu$:

$$P_{20}(x) = \frac{3}{2}(1+x)^2$$
$$P_{21} = -\frac{1}{2}$$
$$P_{22} = P_{12} = 0$$
$$P_{10} = \frac{3}{2}(1+x)^2(1-x)$$
$$P_{11} = \frac{1}{2}(1+3x)$$

$$P_{00} = \frac{3}{8}(1-x^2)^2$$
$$P_{01} = \frac{1}{4}(1-3x^2)$$
$$P_{02} = \frac{3}{8}$$

This is as far as we take the kernel γ which is used in the BTE; notice that the relation A2.15 can be used to get $\bar{\gamma}$ from A2.17 and A2.19.

Moments of the scattering kernel are defined by equation 3.24b. The integration over $c = \hat{q}\cdot\hat{q}'$ transforms to an integration over k, which is constrained by

$$|\omega| \leq k \leq min\ (\nu+\nu' ,\ 2E+\omega) \qquad \text{(A2.20)}$$

and results in the further condition on E : $E \geq -\omega$. The ℓ^{th} moment of γ is

$$\gamma_\ell(\nu\to\nu') = \frac{2G^2}{3\pi}\frac{\nu^3}{(\nu')^2}\int_{max(0,-\omega)}^{\infty} dE\ f(E)(1-f(E+\omega))\phi_\ell(E,\nu,\nu') \qquad \text{(A2.21)}$$

where

$$\phi_\ell(E,\nu,\nu') = \int_{|\omega|}^{min(2E+\omega,\nu+\nu')} \frac{dk}{\nu}\ \frac{3E^2}{4\nu^2}\ Q\ P_\ell\left(1-\frac{k^2-\omega^2}{2\nu\nu'}\right)$$
$$= \phi_{\ell<}\ \theta(\nu'-E) + \phi_{\ell>}\ \theta(E-\nu') \qquad \text{(A2.22)}$$

where θ is the Heaviside unit function, $\phi_{\ell<}$ has the upper limit of k integration $2E+\omega$, $\phi_{\ell>}$ has it $\nu+\nu'$. These functions can be reduced to a more usable form after much tedious algebra. Rather miraculously, many cancellations occur; for example, the functions ϕ are polynomials in E. We find

$$\phi_{0>} = x^3\left[2\varepsilon^2+(4-3x)\varepsilon + \frac{6x^2}{5} - 3x+2\right] \quad , \text{ for } E \geqslant \nu' \tag{A2.23a}$$

$$\phi_{0<} = \varepsilon^3\left[\frac{\varepsilon^2}{5} + \varepsilon + 2\right] \quad , \text{ for } E<\nu' \tag{A2.23b}$$

$$\phi_{1>} = \frac{(1+x^2)}{2x}\,\phi_{0>} - \frac{1}{2x}\cdot x^3\left[\varepsilon^2\left(2+2x-\frac{8}{5}x^2\right) + \varepsilon\left(4+x-\frac{22}{5}x^2+\frac{9}{5}x^3\right)\right.$$
$$\left. - \frac{18}{35}x^4 + \frac{9}{5}x^3 - \frac{8}{5}x^2 - x+2\right] \tag{A2.23c}$$

$$\phi_{1<} = \frac{(1+x^2)}{2x}\,\phi_{0<} - \frac{1}{2x}\cdot \varepsilon^3\left[\frac{24}{35}\varepsilon^4 + \frac{6}{5}\varepsilon^3(3-x) + \frac{1}{5}\varepsilon^2(37-26x+x^2)\right.$$
$$\left. + \varepsilon y(7-x) + 2y^2\right] \tag{A2.23d}$$

$$\phi_{2>} = \frac{3}{2x}(1+x^2)\,\phi_{1>} - \frac{(3+10x^2+3x^4)}{8x^2}\,\phi_{0>} + \frac{3}{8x^2}\cdot x^3\left[\varepsilon^2\left(\frac{2}{7}x^4 - \frac{4}{5}x^3 +4x+2\right)\right.$$
$$+ \varepsilon\left(-\frac{9}{35}x^5 + \frac{32}{35}x^4 - \frac{2}{5}x^3 - \frac{12}{5}x^2 +5x+4\right) + \frac{2x^6}{35} - \frac{9}{35}x^5$$
$$\left. + \frac{2}{7}x^4 + \frac{2}{5}x^3 - \frac{6}{5}x^2 +x+2\right] \tag{A2.23e}$$

$$\phi_{2<} = \frac{3}{2x}(1+x^2)\phi_{1<} - \frac{(3+10x^2+3x^4)}{8x^2}\,\phi_{0<} + \frac{3}{8x^2}\cdot \varepsilon^3\left[\frac{16}{7}\varepsilon^6 + \frac{48}{7}\varepsilon^5(2-x)\right.$$
$$+ 16\varepsilon^4\left(\frac{15}{7} - \frac{78}{35}x + \frac{3}{7}x^2\right) + \frac{4}{5}\varepsilon^3\, y(57-36x+3x^2)$$
$$\left. + \frac{\varepsilon^2 y^2}{5}(169-50x+x^2) + \varepsilon y^3(13-x) + 2y^4\right] \tag{A2.23f}$$

where we have let

$$\varepsilon = E/\nu$$

$$y = 1-x$$

$$x = \nu'/\nu$$

We also obtain

$$\bar{\gamma}_\ell(\nu\to\nu') = \frac{2G^2}{3\pi}\,\frac{\nu^3}{(\nu')^2}\int_{max(0,-\omega)}^{\infty} dE\; f(E)(1-f(E+\omega))\;\bar{\phi}_\ell(E,\nu,\nu') \tag{A2.24}$$

where $\bar{\phi}_\ell$ also splits into $\nu'<E$ and $\nu'>E$ parts:

$$\bar{\phi}_{0>} = x^3 \left[2\varepsilon^2 - \varepsilon x + \frac{x^2}{5}\right] \quad , \text{ for } E > \nu' \tag{A2.25a}$$

$$\bar{\phi}_{0<} = \varepsilon^3 \left[\frac{1}{5}\varepsilon^2 - x\varepsilon + 2x^2\right] \quad , \text{ for } E < \nu' \tag{A2.25b}$$

$$\bar{\phi}_{1>} = \frac{(1+x^2)}{2x}\bar{\phi}_{0>} - \frac{1}{2x}\cdot x^3\left[\varepsilon^2(2+2x-\frac{8}{5}x^2) + \varepsilon(-x-\frac{14}{5}x^2+\frac{7}{5}x^3) - \frac{11}{35}x^4 + \frac{4}{5}x^3 + \frac{1}{5}x^2\right] \tag{A2.25c}$$

$$\bar{\phi}_{1<} = \frac{(1+x^2)}{2x}\bar{\phi}_{0<} - \frac{1}{2x}\cdot \varepsilon^3\left[\frac{24}{35}\varepsilon^4 + \frac{6}{5}\varepsilon^3(1-3x) + \frac{1}{5}\varepsilon^2(1-26x+37x^2) + \varepsilon yx(7x-1) + 2y^2x^2\right] \tag{A2.25d}$$

$$\bar{\phi}_{2>} = \frac{3(1+x^2)}{2x}\bar{\phi}_{1>} - \frac{(3+10x^2+3x^4)}{8x^2}\bar{\phi}_{0>} + \frac{3}{8x^2}\cdot x^3\left[\varepsilon^2(\frac{2}{7}x^4 - \frac{4}{5}x^3+4x+2) + \frac{\varepsilon}{35}(-11x^5+44x^4-42x^3-196x^2-35x) + \frac{x^2}{35}(3x^4-16x^3+30x^2+56x+7)\right] \tag{A2.25e}$$

$$\bar{\phi}_{2<} = \frac{3(1+x^2)}{2x}\bar{\phi}_{1<} - \frac{(3+10x^2+3x^4)}{8x^2}\bar{\phi}_{0<} + \frac{3}{8x^2}\varepsilon^3\left[\frac{16}{7}\varepsilon^6 + \frac{48}{7}\varepsilon^5(1-2x) + \frac{16}{35}\varepsilon^4(15-78x+75x^2) + \frac{4}{5}\varepsilon^3 y(3-36x+57x^2) + \frac{\varepsilon^2 y^2}{5}(1-50x+169x^2) + \varepsilon y^3(13x-1) + 2y^4x^2\right] \tag{A2.25f}$$

The functions ϕ_ℓ are continuous but not continuously differentiable at $\varepsilon=x$ $(E=\nu')$.

Yueh and Buchler (1977b) have derived similar expressions for the $\ell=0$ and $\ell=1$ moments; our results agree with theirs except for $\bar{\phi}_0$: ours satisfies continuity at $\varepsilon=x$; theirs does not.

The functions $\phi_{0>}$, $\phi_{0<}$, $\bar{\phi}_{0<}$ are monotone increasing in E

and positive for $\nu' < \nu$; $\bar{\phi}_{0>}$ is positive and is monotone increasing in its range $E > \nu'$. Each of the functions, when extended to all ε , provide upper bounds on ϕ_0 , $\bar{\phi}_0$; in particular, when $\phi_{0>}$ is used as a bound on ϕ_0 , $\bar{\phi}_{0>}$ as a bound on $\bar{\phi}_0$, we obtain a usable expression for the kernels:

$$\gamma(\nu\to\nu') \lesssim \frac{2G^2}{3\pi} \frac{\nu' T}{(1-e^{-\beta\omega})} \left[2\left(\frac{T}{\nu}\right)^2 \Delta F_2 + \frac{T}{\nu} (4-3x)\ \Delta F_1 + \left(\frac{6x^2}{5} - 3x + 2\right) \Delta F_0 \right], \quad \nu' \lesssim \nu \tag{A2.26a}$$

$$\bar{\gamma}(\nu\to\nu') \lesssim \frac{2}{3} \frac{G^2}{\pi} \frac{\nu' T}{(1-e^{-\beta\omega})} \left[2\left(\frac{T}{\nu}\right)^2 \Delta F_2 - \frac{T}{\nu} x\ \Delta F_1 + \frac{x^2}{5} \Delta F_0 \right], \quad \nu' \lesssim \nu \tag{A2.26b}$$

where T is the temperature in energy units, and

$$\Delta F_k = F_k(\eta_e) - F_k(\eta_e - \beta\omega) \tag{A2.26c}$$

is the difference of Fermi functions defined in equation 3.68. This is a good approximation when $\nu' << \mu_e$. We can, for example, make a Sommerfeld expansion of the Fermi function, then integrate over ν' , retaining only the lowest order terms in η_e and ν/μ_e to get

$$\Gamma_s(\nu) = \frac{G^2}{10\pi}\ n_e\ \frac{\nu^3}{\mu_e}\ \left[(C_{Ve}+C_{Ae})^2 + (C_{Ve}-C_{Ae})^2\right] , \quad \nu << \mu_e \tag{A2.27a}$$

which agrees with the extreme degenerate low energy limit for the scattering lifetime given by Tubbs and Schramm (1975). Similarly, by using Lenard's theorem we obtain

$$\Gamma_s(\nu) = \frac{2}{3}\ \frac{G^2}{\pi}\ \nu\ \rho_B\ u_e\ \left[(C_{Ve}+C_{Ae})^2 + \frac{1}{3}\ (C_{Ve}-C_{Ae})^2\right] \tag{A2.27b}$$

which holds in the extreme degenerate case, with $\nu >> \mu_e$, and also

in the nondegenerate case for all neutrino energies. Here, u_e is the electron energy per baryon.

Generally, we must evaluate the kernels by numerically integrating over the electron energies; we adopt a Gauss-Laguerre integration procedure for this task. Due to the nature of the overlap of the Fermi functions in equation A2.21 for small ω (the integration is sharply peaked near the Fermi surface), numerical integrations are facilitated by the use of the property

$$f(E)(1-f(E+\omega)) = \frac{f(E) - f(E+\omega)}{1-e^{-\beta\omega}} \qquad \text{(A2.28)}$$

We also make use of equation (3.6) to calculate the $\nu' \gtrless \nu$ kernel given the $\nu \lessgtr \nu'$ kernel. Further, to obtain scattering rates, $\Gamma_s(\nu)$, we must numerically integrate over ν'. The limiting cases are only of limited utility, but serve as a useful check of the numerical integrations.

A2.4 PRODUCTION AND ABSORPTION KERNELS: $e^+e^- \to \nu\bar{\nu}$

In the independent quasiparticle approximation, $S^{ee}_{\alpha\beta}$ vanishes for timelike k : the reaction $e \to e\nu\bar{\nu}$ cannot proceed. If dynamical correlations are included, with the electron gas modified by collision with themselves, with nuclei, or with photons, then this part of the correlation function develops a nonzero timelike k part, and the emission of $\nu\bar{\nu}$ pairs can proceed, as in the processes $\gamma_{p\ell} \to \nu\bar{\nu}$, $e + \gamma_{p\ell} \to e+\nu+\bar{\nu}$, $e+e \to e+e+\nu+\bar{\nu}$, and $e+{}^A_Z \to e+{}^A_Z+\nu+\bar{\nu}$. Of these, the plasma neutrino process is the most important in supernova cores. In nuclear matter, the process $N+N \to N+N+\nu+\bar{\nu}$

dominates among the thermal mechanisms.

Still, within the independent quasiparticle approximation, there is a thermal emission process which can proceed, namely the pair annihilation process: $S^{e^+e^-}_{\alpha\beta}$ is nonzero for $\omega \gtrsim k$; indeed, it is zero for $\omega<k$. The modifications required of A2.2 are:

$$S^{e^+e^-}_{\alpha\beta} : \quad 1-f\,(p') \to \bar{f}(p') \;;\; p' \to -p' \quad \text{in the delta function} \tag{A2.29}$$

$$\tilde{S}^{e^+e^-}_{\alpha\beta} : \quad f(p) \to 1 - \bar{f}(p) \quad ; \quad p \to -p \quad \text{in the delta function} \tag{A2.30}$$

Here, $\bar{f}$ is the df of the positron. The $\nu\bar{\nu}$ production kernel in the extreme relativistic limit is then

$$R_p(q,q') = (C_{Ve}+C_{Ae})^2\, \gamma_p\,(q,q') + (C_{Ve}-C_{Ae})^2\, \bar{\gamma}_p\,(q,q') \tag{A2.31}$$

$$\gamma_p(q,q') = 2G^2 \sum_{p_1 p_2} f(p_1)\, \bar{f}(p_2)\, \frac{(p_1\cdot q)(p_2\cdot q')}{\nu\,\nu' E_1 E_2} \cdot (2\pi)^4 \delta^{(4)}\,(p_1+p_2+k) \tag{A2.32}$$

$$\bar{\gamma}_p(q,q') = \gamma_p(q',q) \tag{A2.33}$$

where $k = -(q+q')$.

The subsequent derivation is very similar to that undertaken for the scattering reaction. There is one important difference:

$$\mu_0' = \frac{(-\omega)}{k} - \frac{(\omega^2-k^2)}{2Ek}$$

is of opposite sign to A2.18. The characteristic function χ in A2.17 then becomes $\chi_{((|\omega|-k)/2,(|\omega|+k)/2)}(E)$: the integration over E is no longer semi-infinite. The expression for E^2Q is the same as A2.19,

but the polynomials are slightly different:

$$P_{nm}(e^+e^- \to \nu\bar{\nu}\ ;\ x) = (-1)^n\ P_{nm}(\nu e \to \nu e\ ;\ -x)$$

Again we take moments as in equation A3.24c.

The constraint on k is, instead of A2.20, now

$$max\ (|\nu-\nu'|\ ,\ |2E+\omega|) \leqslant k \leqslant |\omega|$$

which then imposes the condition on E: $0 \leqslant E \leqslant |\omega|$. Finally, we get

$$\gamma_{p\ \ell}(\nu,\nu') = \frac{2G^2}{3\pi}\frac{\nu^3}{(\nu')^2}\int_0^{|\omega|} f(E)\bar{f}(|\omega|-E)\ dE\ \phi_{p\ell}(E,\nu,\nu') \qquad \text{(A2.34)}$$

plus the equivalent relation for $\bar{\gamma}_{p\ell}$ in terms of $\bar{\phi}_{p\ell}$, where

$$\phi_{p\ell} = \phi_{L\ell}\,\chi_{(0,\nu')}(E) + \phi_{M\ell}\,\chi_{(\nu',\nu)}(E) + \phi_{H\ell}\,\chi_{(\nu,|\omega|)}(E), \text{ for } \nu'<\nu \qquad \text{(A2.35)}$$

and similarly for $\bar{\phi}_{p\ell}$. The three ranges for E arise from which value holds for the lower range of k-integration: $|\omega|-2E$ for L, $\nu-\nu'$ for M, and $2E+\omega$ for H. It can be shown that

$$\phi_{L\ell}\left(\frac{E}{\nu}\ ;\ \frac{\nu'}{\nu}\right) = -\phi_{\ell<}\left(-\frac{E}{\nu}\ ;\ -\frac{\nu'}{\nu}\right) \quad ,\ \nu' < \nu \qquad \text{(A2.36)}$$

$$\phi_{M\ell}\left(\frac{E}{\nu}\ ;\ \frac{\nu'}{\nu}\right) = -\phi_{\ell>}\left(-\frac{E}{\nu}\ ;\ -\frac{\nu'}{\nu}\right) \quad ,\ \nu' < \nu \qquad \text{(A2.37)}$$

which relates the e^+e^- functions to those for neutrino-electron scattering. The same relations are true for the barred functions, $\bar{\phi}_{L\ell}$ etc., with the same limitation, $\nu' < \nu$. After much algebra, we can show

$$\phi_{H0}(x,\varepsilon) = \phi_{0<}(-x,-\varepsilon) + F_0 \tag{A2.38a}$$

$$F_0 = \varepsilon^2 2z\ (1-x+x^2) - \varepsilon\ z^2(1-2x+3x^2) + \frac{1}{5}\ z^3(1-3x+6x^2)$$

$$\bar{\phi}_{H0}(x,\varepsilon) = \bar{\phi}_{0<}(-x,-\varepsilon) + F_0 + G_0 \tag{A2.38b}$$

$$G_0 = -2\varepsilon y z^3 + y z^4$$

$$\phi_{H1}(x,\varepsilon) = \phi_{1<}(-x,-\varepsilon) + \frac{1}{2x}\ (F_1 - (1+x^2)F_0) \tag{A2.38c}$$

$$F_1 = -\frac{1}{5}\ \varepsilon^2\ z^3\ (8x^2-14x+8) + \frac{1}{5}\ \varepsilon z^4\ (9x^2-14x+7) - \frac{z^5}{35}\ (18x^2-27x+11)$$

$$\bar{\phi}_{H1}(x,\varepsilon) = \bar{\phi}_{1<}(-x,-\varepsilon) + \frac{1}{2x}\ (F_1 - G_0\ \frac{z^2}{5} - (1+x^2)(F_0+G_0)) \tag{A2.38d}$$

$$\phi_{H2}(x,\varepsilon) = \phi_{2<}(-x,-\varepsilon) + \frac{1}{8x^2}\ (3F_2 - 6(1+x^2)F_1 + (3+2x^2+3x^4)F_0) \tag{A2.38e}$$

$$F_2 = z^5\ \frac{\varepsilon^2}{35}\ (10x^2-22x+10) - \varepsilon\ \frac{z^6}{35}\ (9x^2-22x+11) + \frac{z^7}{35}\ (2x^2-5x+3)$$

$$\bar{\phi}_{H2}(x,\varepsilon) = \bar{\phi}_{2<}(-x,-\varepsilon) + \frac{1}{8x^2}\ (3(F_2+G_0\ \frac{z^4}{35}) - 6(1+x^2)(F_1 - G_0\ \frac{z^2}{5}) + (3+2x^2+3x^4)(F_0+G_0)) \tag{A2.38f}$$

where

$$z = 1+x$$

and ε, x, y are as above. These formulae hold only for $\nu'<\nu$, i.e., $x<1$. To obtain $\nu>\nu'$, we use the symmetry

$$\bar{\gamma}_{p\ell}(\nu',\nu) = \gamma_{p\ell}(\nu,\nu') \tag{A2.39}$$

Again, it is necessary to numerically integrate over the electron

energy; because the range of integration is finite, we use Gauss-Legendre integration. To obtain $\Gamma_p(e^+e^- \rightarrow \nu\bar{\nu}\ ;\ \nu)$, we need to do a further numerical integration. Once we have obtained the production kernels, we need only apply equation 3.9 to get the absorption kernels.

When the neutrinos are nondegenerate, a number of quantities can be obtained by the use of Lenard's formula, A1.19, on A2.31. Thus, the lifetime of a positron of energy $\bar{E}$ to annihilate on some plasma electron to produce a $\nu_e\ \bar{\nu}_e$ pair is

$$\frac{1}{\tau_{e^+}(\bar{E})} = \rho_B \frac{2G^2}{9\pi} (C_{Ve}^2 + C_{Ae}^2)\ u_e\ \bar{E}$$

$$= 9.55\ u_e\ \bar{E}\ \rho_{11}\ s^{-1} \qquad \text{(A2.40)}$$

where the electron energy per baryon, u_e, is in MeV (it is $0.75\mu_e Y_e$ for an extremely degenerate gas). As usual, the Weinberg model is adopted, with $\sin^2\theta_W = 0.3$. The rate to produce $\nu_\mu\ \bar{\nu}_\mu$ pairs is then $\sim$ 18% of the rate to produce $\nu_e\ \bar{\nu}_e$ pairs. The rate per baryon to produce $\nu_e\ \bar{\nu}_e$ pairs, when A2.40 is integrated over the positron distribution, is

$$(-\dot{Y}_{e^+})(e^+e^- \rightarrow \nu_e\bar{\nu}_e) \equiv \frac{n_e n_{e^+}}{\rho_B} \langle\sigma v\rangle\ (e^+e^- \rightarrow \nu_e\bar{\nu}_e)$$

$$= \frac{1}{\tau_{e^+}(u_{e^+})} \qquad \text{(A2.41)}$$

where u_{e^+} is the average positron energy per baryon, which, for a degenerate electron gas, is

$$u_{e^+} = 3TY_{e^+} \tag{A2.42a}$$

$$Y_{e^+} = \frac{2T^3}{\rho_B \pi^2 (\hbar c)^3} \; e^{-\eta_e} = 4.38\text{x}10^{-4} \; \frac{T^3}{\rho_{11}} \; e^{-\eta_e} \tag{A2.42b}$$

where T is the energy in MeV. The number of positrons in the medium, and therefore the rate of pair annihilation is a sensitive function of the electron degeneracy parameter η_e .

The energy loss per baryon is

$$\dot{Q}\ (e^+e^- \rightarrow \nu_e \bar{\nu}_e) \equiv \frac{1}{\rho_B} n_e \; n_{e^+} \left\langle (E+\bar{E})\ \sigma v \right\rangle$$

$$= \frac{T}{\tau_{e^+}(u_{e^+})} \cdot \left(\frac{F_4}{F_3} (\eta_e) + \frac{F_4}{F_3} (-\eta_e) \right) \tag{A2.43}$$

For degenerate electrons, these Fermi integrals can be evaluated, yielding the mean energy which the $\nu_e \; \bar{\nu}_e$ pair carries off, namely $4\mu_e/5 + 4T$: it is electrons near the Fermi surface which annihilate, giving the neutrinos a considerable fraction of the Fermi energy.

APPENDIX 3

CORRELATION FUNCTIONS

The use of correlation functions to describe the scattering of a probe from a medium is well known. When the energy transfer to the medium is small compared with the energy of the probe, a static (equal time) correlation function suffices. This is a valid approximation for X-ray scattering by solids, liquids, and gases if the atomic states remain unchanged, and an expression in terms of the static liquid structure factor (SLSF) was first given by Zernike and Prins (1927). If the energy transfers cease to be negligible, the dynamic liquid structure factor (DLSF) is the appropriate generalization of the SLSF; van Hove (1954a, 1954b) introduced these functions and used them in the analysis of slow neutron scattering from ferromagnetic crystals. Both of these factors are related to Fourier transforms of the autocorrelation of the density of scattering sites, $\rho(\underset{\sim}{x})$, namely to $\langle\rho(\underset{\sim}{x},t)\rho(\underset{\sim}{x}=0)\rangle$ and $\langle\rho(\underset{\sim}{x})\rho(\underset{\sim}{x}=0)\rangle$ for the DLSF and the SLSF respectively. The expectation values are taken in the thermodynamic ensemble of the medium. From the SLSF, we obtain the radial or pair distribution function, which together with the interparticle potential allows the determination of the equation of state (Goodstein 1975). That it, and its dynamic counterpart, carry so much information suggests, and it is the case, that it is quite difficult to calculate.

The autocorrelations of the electromagnetic 4-currents are related to the complex dielectric constants. At low frequency, the

Coulomb screening of charges is described; at high frequency, plasma oscillations are described. These correlation functions have been used by Martin (1968) to give a general treatment of energy loss by a fast charged particle through a medium. Martin further points out that the space-space part of the electromagnetic currents can be used to treat Cerenkov radiation by moving particles.

The charge density autocorrelation is also used in the theory of inelastic electron scattering by a nucleus: the nucleus is the medium, a zero temperature system of fermions (Fetter and Walecka 1971).

When neutrinos scatter from a medium, weak current-current correlation functions provide an appropriate framework within which to work; the emission and absorption of neutrino-antineutrino pairs then follows automatically.

A3.1 DERIVATION OF THE SCATTERING KERNEL

Suppose a neutrino of momentum $q^\mu = (\nu, \underset{\sim}{q})$ scatters once from a medium initially in the state i with energy E_i, thereby going to a final neutrino momentum $q^{\mu'} = (\nu', \underset{\sim}{q}')$. We wish to obtain the scattering rate for the inclusive reaction $\nu+i \rightarrow \nu+X$, where X is anything; we are not interested in the final state of the matter. The transition rate for this process is given by Fermi's Golden Rule, and first order perturbation theory is valid:

$$\text{Rate } (\nu(q)+i \rightarrow \nu(q')+X) = \sum_f 2\pi\delta(\nu+E_i-\nu'-E_f).$$

$$\cdot \left\langle \nu(q);i \left| \int d^3x \, \frac{G}{\sqrt{2}} : \ell_\mu(\underset{\sim}{x}) J^\mu(x) : \right| f;\nu'(q') \right\rangle .$$

$$\cdot \left\langle \nu'(q');f \left| \int d^3\underset{\sim}{y} \, \frac{G}{\sqrt{2}} : \ell_\nu(\underset{\sim}{y}) J^\nu(\underset{\sim}{y}) : \right| i;\nu(q) \right\rangle \qquad \text{(A3.1)}$$

where the sum is over all possible final states of the medium after scattering. The neutrino current is

$$\ell_\mu(x) = \bar{\nu}_\ell(x) \, \gamma_\mu(1-\gamma_5)\nu_\ell(x) \qquad \text{(A3.2)}$$

and there is one for each type of neutrino, ℓ=e,μ,τ. . . , and the matter current is

$$J^\mu(x) = J^\mu_e + J^\mu_{had,NC} \qquad \text{(A3.3)}$$

where $J^\mu_{had,NC}$ is given by equation 2.33, and for our purposes the nonrelativistic limit 2.36 suffices, and

$$J^\mu_e = \bar{e} \, \gamma^\mu(C_{V\ell} - C_{A\ell}\gamma_5)e \qquad \text{(A3.4)}$$

where ℓ is again e, μ, or τ depending upon which type of neutrino we are interested in. Both ℓ_μ and J^μ are self adjoint.

The trick is now to turn the energy conserving delta function into a time integral. If we assume the neutrinos and the matter from which they scatter are uncorrelated, then the neutrino part of the matrix element can be evaluated and separated from the matter part:

$$\text{Rate } (\nu(q)+i \to \nu(q')+X) = \frac{G^2}{8\nu\nu'} \bar{u}(q)\gamma_\mu(1-\gamma_5)u(q')\bar{u}(q')\gamma_\nu(1-\gamma_5)u(q)$$

$$\cdot \int d^3x\, d^3y\, dt . e^{+i\omega t} . e^{-i\underset{\sim}{k}\cdot(\underset{\sim}{x}-\underset{\sim}{y})}$$

$$\cdot \sum_f \langle i|e^{iHt}:J^\mu(\underset{\sim}{x}):e^{-iHt}|f\rangle\langle f|:J^\nu(\underset{\sim}{y}):|i\rangle \quad \text{(A3.5)}$$

In this expression, we have let $k^\mu = (\omega,\underset{\sim}{k}) = (\nu-\nu',\underset{\sim}{q}-\underset{\sim}{q}')$ denote the 4-momentum transfer to the medium. The dots : : indicate normal ordering of whatever is between them, and it is implicit in what follows. The Hamiltonian H is the full matter Hamiltonian, including strong and electromagnetic forces, but not weak forces; it also includes the particle rest masses. We let $J^\mu(xt)$ denote the current in the Heisenberg representation, that is, evolved according to e^{-iHt}. The summation over f can now be performed: it gives the identity. The neutrino spinor terms can be turned into a trace with the result given by equation 2.42. Thus, A3.5 becomes

$$\text{Rate } (\nu(q)+i \to \nu(q')+X) = \frac{G^2}{\nu\nu'} (q_\mu q'_\nu + q_\nu q'_\mu - q'\cdot q\, g_{\nu\mu} + i\varepsilon_{\mu\nu}(q,q')).$$

$$\cdot \int d^3x\, d^3y\, dt\, e^{i\omega t}\, e^{-i\,\underset{\sim}{k}\cdot(\underset{\sim}{x}-\underset{\sim}{y})}$$

$$\cdot \quad \langle i|J^\mu(\underset{\sim}{x}t)J^\nu(\underset{\sim}{y},0)|i\rangle \quad \text{(A3.6)}$$

We adopt the notation for Fourier transforms

$$\tilde{J}^\mu(k,t) \equiv \int d^3x\, e^{-i\,\underset{\sim}{k}\cdot\underset{\sim}{x}}\, J^\mu(\underset{\sim}{x},t) \quad \text{(A3.7a)}$$

$$J^\mu(\underset{\sim}{k},\omega) \equiv \int dt\, e^{i\omega t}\, \tilde{J}^\mu(\underset{\sim}{k},t) \quad \text{(A3.7b)}$$

The matter is described by a statistical ensemble; each of the possible initial states has some probability, some weight, in this ensemble which is characterized by a density matrix ρ ; for a zero temperature system, ρ is microcanonical, consisting of one state only, the ground state. Matter in stars is in local thermodynamic equilibrium characterized by a local grand canonical ensemble with a density matrix

$$\rho = \exp(\beta(\Omega + \sum_j \mu_j N_j - H)) \tag{A3.8}$$

where Ω is the thermodynamic potential, μ_j is the chemical potential of species j and N_j is its number operator. The trace of an operator A with respect to ρ is its ensemble average

$$\langle A \rangle = \mathrm{Tr}\rho A \tag{A3.9}$$

If we thermally average the rate expression A.36 over states i, we finally obtain

$$R(q \to q') = \frac{G^2}{\nu\nu'} (q_\mu q_\nu' + q_\nu q_\mu' - q' \cdot q \, g_{\mu\nu} + i\varepsilon_{\mu\nu}(q,q')) \cdot \frac{1}{V} \langle J^\mu(\underset{\sim}{k},\omega) \, \tilde{J}^\nu(-\underset{\sim}{k},0) \rangle \tag{A3.10}$$

As it stands, this formula includes all scattering processes except neutrino-neutrino scattering. Only in the case where positrons are involved do we have to worry about the normal ordering implicit in the current-current correlation function (CCCF), $V^{-1}\langle J^\mu(\underset{\sim}{k}\omega)\tilde{J}^\nu(-k,0)\rangle$:

here, V is the box normalizing volume. For translationally invariant media, this CCCF is $\left\langle J^{\mu}(k,\omega)J^{\nu}(\underset{\sim}{x}=0,t=0)\right\rangle$. (When one is dealing with individual nuclei, this relation does not hold; it does hold in stellar situations.) The CCCF is manifestly a tensor in translationally invariant media; it is a tensor under Lorentz transformations in arbitrary media.

Can the neutrinos be statistically independent of the matter in which they are created and in which they propagate if indeed they are confined, downscattered in energy, and reabsorbed? The mean free paths do indeed become short as the density rises, but even at nuclear matter densities, 50 MeV neutrinos still have mean free paths measured in meters. Matter is in LTE. We may envision the star divided into cells; each cell is in thermodynamic equilibrium described by a grand canonical ensemble; the parameters temperature, chemical potential, and volume vary from cell to cell. Through each cell, whose size is characterized by mean baryon number, not volume, which therefore shrinks with increasing density, the neutrinos pass almost unperturbed. It is only because there are so many cells and so many neutrinos that the phenomena of trapping occurs. Neutrinos are indeed statistically independent. Dependences on the cell, labelled by the position vector at its center, and on time, have been suppressed in the previous and the following equations.

A3.2 THE RESPONSE FUNCTION

We now turn to some general relations among correlation functions, using Martin's notation with a few minor changes. Suppose

A and B are two arbitrary operators, not necessarily self adjoint. Define the AB correlation function:

$$S_{AB}(t-t') = \langle A(t)B(t') \rangle \quad . \tag{A3.11}$$

That S_{AB} is a function only of $t-t'$ is an assumption, called the stationary property. In fact, since the ensemble is slowly evolving in time on the dynamical or neutronization timescale as the core collapses, this property does not hold. However, this function approaches the uncorrelated value $\langle A(t) \rangle \langle B(t') \rangle$ for time differences of order the electromagnetic or strong relaxation time, which is tiny compared with the collapse time. The Fourier transform in $t-t'$ of S_{AB} satisfies

$$S^{*}_{AB}(\omega) = S_{B}\dagger_{A}\dagger(\omega) \tag{A3.12}$$

$$S_{BA}(\omega) = e^{\beta(\omega-\Delta\mu)} \; S_{AB}(-\omega) \tag{A3.13}$$

where

$$\Delta\mu \equiv \sum_{j} \mu_{j} \Delta n_{j} \tag{A3.14a}$$

$$[N_{j},A] = \Delta n_{j} A \tag{A3.14b}$$

and in the latter imposed relation, the Δn_{j} are assumed to be integers, a relation which is true for currents. The absorptive response function

$$\chi''_{AB}(t-t') = \frac{1}{2} \left\langle [A(t),B(t')] \right\rangle \tag{A3.15}$$

is related to the AB correlation function by

$$\chi''_{AB}(\omega) = \frac{1}{2} S_{AB}(\omega)(1-e^{-\beta(\omega+\Delta\mu)}) \tag{A3.16}$$

from which follows the fluctuation dissipation theorem, with S_{AB} or at least its symmetric part giving the fluctuations, and χ''_{AB} describing the dissipation.

If $B^{\dagger} = A$, then, from A3.12, the AB correlation function is real. This is true, for example, if $A = \rho(\underset{\sim}{k})$, $B = \rho^{\dagger}(+\underset{\sim}{k}) = \rho(-\underset{\sim}{k})$, where $\rho(k)$ is the Fourier transform of a density.

We define another important correlation function, the time ordered product

$$\chi^{T}_{AB}(t-t') = \left\langle TA(t)B(t') \right\rangle \tag{A3.17}$$

The Lehmann representation for this function is simply

$$\chi^{T}_{AB}(\omega) = \int_{-\infty}^{\infty} \frac{d\omega'}{2\pi i} \left[\frac{S_{AB}(\omega')}{\omega-\omega'+i\varepsilon} - \frac{S_{BA}(\omega')}{\omega+\omega'-i\varepsilon} \right] \tag{A3.18}$$

where ε is a positive infinitessimal. Then in the important special case of real correlation functions,

$$S_{AA}{}^{\dagger}(\omega) = \frac{1}{1+e^{-\beta(\omega+\Delta\mu)}} \; Im\left[-i\ \chi^{T}_{AA}{}^{\dagger}(\omega)\right] . \tag{A3.19}$$

where Im denotes the imaginary part.

If the time-ordered product can be developed into a diagrammatic expansion, then $S_{AA}{}^{\dagger}$ would follow; this is a standard procedure at zero temperature; it is more difficult to execute at finite temperature, but, formally at least, the procedures have been worked out (Fetter and Walecka 1971).

A3.3 THERMAL $\nu\bar{\nu}$ PRODUCTION KERNELS

For the scattering kernel, A3.10, there is a constraint on k^{α} ; it is a spacelike vector ($k^2<0$). When we enter into the timelike domain, what, if anything, does A3.10 represent? If $\omega<0$, then production is described, and if $\omega>0$, then absorption is represented. Thus

$$R_p(q,q') = \text{A3.10} \quad , \quad \text{with } k^{\mu} = -(q+q')^{\mu} \tag{A3.20}$$

$$R_a(q,q') = \text{A3.10} \quad , \quad \text{with } k^{\mu} = (q+q')^{\mu} \tag{A3.21}$$

The regions in ω-k space are indicated in Figure 3. When we calculate moments of these kernels, we are integrating over a range of k values for fixed ω ; for scattering, the range is from $|\omega|$ to $\nu+\nu'$, and for production and absorption it is from $|\nu-\nu'|$ to $|\omega|$.

A3.4 STRUCTURE FUNCTIONS

The current-current correlation function is a tensor of rank two; two 4-vectors are specified: the momentum transfer k^{α} , and the mean 4-velocity of the medium $(U^{\alpha}) = (1,0,0,0)$. We may expand $S_{J^{\alpha}J^{\beta}}(k)$ in terms of 6 tensors of rank two built from k and U:

$$S_{J^\alpha J^\beta}(k) \equiv \frac{1}{V}\left\langle J^\alpha(\underset{\sim}{k},\omega)\tilde{J}^\beta(-\underset{\sim}{k},0)\right\rangle \tag{A3.22}$$

$$= \mathcal{R}_1 U^\alpha U^\beta + \mathcal{R}_2(U^\alpha U^\beta - g^{\alpha\beta}) + i\,\varepsilon^{\alpha\beta}(U,k)\mathcal{R}_3 + \mathcal{R}_4\, k^\alpha k^\beta + \frac{\mathcal{R}_5}{2}(k^\alpha U^\beta + k^\beta U^\alpha)$$

$$+ \mathcal{R}_6\,\frac{1}{2}(k^\alpha U^\beta - k^\beta U^\alpha) \tag{A3.23}$$

Each of the $\mathcal{R}_i$ is a function of k and U. They are scalars under Lorentz transformations, therefore the $\mathcal{R}_i$ are functions only of the combinations k^2 , $k\cdot U$, and the thermodynamic variables of the medium. If we define $\omega = k\cdot U$, then

$$\mathcal{R}_i = \mathcal{R}_i(\omega, k^2, \mu_j, T) \tag{A3.24}$$

Time reversal invariance implies $\mathcal{R}_6$ vanishes. The scattering of neutrinos by the medium, or the production and absorption of $\nu\bar{\nu}$ pairs, gives information only on the scalars $\mathcal{R}_1$, $\mathcal{R}_2$, and $\mathcal{R}_3$:

ν scattering: $R(q\to q') = G^2\,[\mathcal{R}_1(1+c)+3\mathcal{R}_2(1-\frac{1}{3}c)+2(\nu+\nu')\mathcal{R}_3(1-c)]$ (A3.25a)

$\bar{\nu}$ scattering: $\bar{R}(q\to q') = G^2\,[\mathcal{R}_1(1+c)+3\mathcal{R}_2(1-\frac{1}{3}c)-2(\nu+\nu')\mathcal{R}_3(1-c)]$ (A3.25b)

$\nu\bar{\nu}$ production: $R_p(q,q') = G^2[\mathcal{R}_1(1+c)+3\mathcal{R}_2(1-\frac{1}{3}c)-2(\nu-\nu')\mathcal{R}_3(1-c)]$ (A3.25c)

$\nu\bar{\nu}$ absorption: $R_a(q,q') = G^2[\mathcal{R}_1(1+c)+3\mathcal{R}_2(1-\frac{1}{3}c)+2(\nu-\nu')\mathcal{R}_3(1-c)]$ (A3.25d)

The $\mathcal{R}_3$ term arises from V-A interference; through it, neutrinos and antineutrinos have different scattering kernels; through it, the ν energy spectrum produced in thermal $\nu\bar{\nu}$ production differs from the

$\bar{\nu}$ energy spectrum. There is an energy scale associated with $\mathcal{W}_3$. For nucleon processes, the energy scale is set by the nucleon mass, m_N. If we are interested only in processes satisfying $\nu,\nu' << m_N$, then this term can be neglected. Further, $\mathcal{W}_4$, $\mathcal{W}_5$ and $\mathcal{W}_6$ can also be neglected in this limit; then, for nuclear processes

$$\mathcal{W}_1(\omega,k^2) \simeq S_{J^\circ J^\circ}(k) \tag{A3.26}$$

$$\mathcal{W}_2(\omega,k^2) \simeq S_{\underset{\sim}{J}\cdot\underset{\sim}{J}}(k)/3 \tag{A3.27}$$

in the low energy limit. Notice the similarity between A3.25a, A3.25b with the $\mathcal{W}_3$ term neglected and the angular dependences in equation 4.1.

If the ensemble is microcanonical, appropriate for a set of energy levels of a nucleus with the same spin J_i and energy E_i,

$$\rho_i = \frac{1}{2J_i+1} \sum_M |iM\rangle\langle iM| \tag{A3.28}$$

then

$$S_{J^\circ J^\circ} = \mathcal{W}_1 = \sum_f 2\pi\delta(\omega+E_i-E_f) \left\langle (C_{V0}+C_{V1}\ t_3) e^{i\ \underset{\sim}{k}\cdot\underset{\sim}{r}} \right\rangle_{fi}^2 \tag{A3.29}$$

$$\longrightarrow 2\pi\delta(\omega)\ (C_{V0}A + C_{V1}\ \frac{Z-N}{2})^2 \quad \text{as } k\to 0$$

$$S_{\underset{\sim}{J}\cdot\underset{\sim}{J}} = 3\mathcal{W}_2 = \sum_f 2\pi\delta(\omega+E_i-E_f)\ \left\langle (C_{A0}+C_{A1}\ t_3)\underset{\sim}{\sigma}\ e^{i\ \underset{\sim}{k}\cdot\underset{\sim}{r}} \right\rangle_{fi}^2 \tag{A3.30}$$

These particular CCCF, A3.29 and A3.30, are sometimes called strength

functions in nuclear physics. Knowledge of them gives all the information necessary to calculate both elastic and inelastic neutrino scattering.

At very high energies, in the same ensemble, the function $\mathcal{R}_3$ ceases to be negligible; $\mathcal{R}_1$, $\mathcal{R}_2$, and $\mathcal{R}_3$ are then related to the neutrino structure functions defined to treat deep inelastic neutrino experiments (Ellis and Jaffe 1973). At Fermilab energies, the neutrino wavelength is very short, a few millifermis, and the CCCF's tell of the quark content of the nucleon; the parton model is applicable. Even at Cern PS neutrino energies, the wavelength is measured in tenths of fermis; the internal structure of the nucleon is still that which is measured. At LAMPF energies, the neutrino sees the nucleon as a unit, an "elementary" particle, but the nucleus in which it is housed is composite. At reactor neutrino energies, the nucleus itself is seen as a unit with some total weak charge; the scattering is coherent. Passing to even larger wavelengths, we have neutrinos Bragg scattering off crystals. The structure functions $\mathcal{R}_1$, $\mathcal{R}_2$, and $\mathcal{R}_3$ contain all this information.

A3.5 CHARGED CURRENT CORRELATION FUNCTIONS

The electron capture reaction, and its inverse, neutrino absorption, must be treated differently since the leptonic current involves electrons. If we use the Lagrangian 2.34, and follow through an analysis similar to the one which led to A3.10, we obtain the production rate for ν_e's by electron capture (and by e^+ emission) in the form

$$\Gamma_p(q) = G^2\cos^2\theta_c \frac{1}{V}\langle(\bar{\psi}_e \not{J}_{had,CC})(-\underset{\sim}{q},-\nu)\not{q}(\not{J}^{\dagger}_{had,CC}\psi_e)(\underset{\sim}{q},t=0)\rangle \qquad (A3.31)$$

Here, $\underset{\sim}{q}$ is the momentum of the neutrino, ν is its energy, ψ_e is the electron field, $J_{had,CC}$ is the hadronic current, 2.35 or 2.37, and

$$(\bar{\psi}_e \not{J}_{had,CC})(-\underset{\sim}{q},-\nu) \equiv \int d^3\underset{\sim}{x}\, dt\, e^{i\,\underset{\sim}{q}\cdot\underset{\sim}{x}_e - i\nu t}\bar{\psi}_e(xt) J^{\mu}_{had,CC}(xt)\gamma_{\mu} \qquad (A3.32)$$

Generally, the electrons are correlated with the nucleons by Coulomb interactions, both by static screening and by the modification of free waves to Coulomb wave functions: the latter effect is included in the Coulomb factor $F(Z,E_e)$ in 2.46. In the high energy limit, these correlations cease to be important; this is especially true for electron captures on low Z nuclei; then, we obtain

$$\Gamma_p(q) = \int \frac{d^3p}{(2\pi)^3} f_e(\underset{\sim}{p}) \frac{G^2\cos^2\theta_c}{E_e\nu}$$

$$\cdot (p_\alpha q_\beta + q_\alpha p_\beta - q\cdot p\, g_{\alpha\beta} + i\,\varepsilon_{\alpha\beta}(q,p)) S_{J^\alpha J^\beta\dagger}(k) \qquad (A3.33)$$

If we neglect possible nuclear polarizations due to magnetic fields, a very small effect even for strong fields, we can again make an expansion of the form A3.23, and neglect terms of order ν/m_N, to obtain:

$$\Gamma_p(q) = \int \frac{d^3p}{(2\pi)^3} f_e(p)\, G^2\cos^2\theta_c \cdot$$

$$\cdot [S_{J_0 J_0^\dagger}(k,\omega)(1+c) + S_{\underset{\sim}{J}\cdot\underset{\sim}{J}^\dagger}(k,\omega)(1-\tfrac{1}{3}c)] \qquad (A3.34)$$

where $c = \hat{q}\cdot\hat{p}_e$, and $k = (\omega,\underset{\sim}{k}) = p-q$. The absorption rate is similarly (where now $k = q-p$)

$$\Gamma_a(q) = \int \frac{d^3p}{(2\pi)^3} (1-f_e(p))\, G^2\cos^2\theta_c$$

$$\cdot[S_{J_0^\dagger J_0}(\underset{\sim}{k},\omega)(1+c) + S_{\underset{\sim}{J}^\dagger\cdot\underset{\sim}{J}}(k,\omega)(1-\tfrac{1}{3}c)] \qquad \text{(A3.35)}$$

If we were to use an ensemble of the form A3.28 appropriate to a stationary nucleus, then the Coulomb correlations could be put in by inserting the Coulomb factor $F(Z,E_e)$ into the formulae for Γ_p and Γ_a , A3.34 and A3.35. In this case, $S_{J_0^\dagger J_0}$ and $S_{J^\dagger\cdot J}$ are proportional to the beta strength functions defined in, for example, Itoh et al. (1977).

A3.6 DETAILED BALANCE RELATIONS

The formula A3.13 can be used to derive in a general manner the detailed balance relations among scattering, production, and absorption coefficients. Since the weak neutral matter current commutes with the number operators for all the species of particles in the medium, $\Delta\mu = 0$,

$$S_{J^\alpha J^\beta}(-k) = e^{-\beta\omega}\, S_{J^\beta J^\alpha}(k) \qquad \text{(A3.36)}$$

$$\mathcal{R}_i(-k) = \varepsilon_i\, e^{-\beta\omega}\, \mathcal{R}_i(k) \quad , \quad \varepsilon_i = 1 \text{ if } i=1,2, \; -1 \text{ if } i=3 \qquad \text{(A3.37)}$$

and we obtain the relations 3.6 and 3.9 of Chapter 3.

The charged hadronic current satisfies the commutation relations

$$[N_n \ , \ J_{had,CC}] = -J_{had,CC} \qquad \text{(A3.38a)}$$

$$[N_p \ , \ J_{had,CC}] = J_{had,CC} \qquad \text{(A3.38b)}$$

and the electron field satifies

$$[N_e \ , \ \psi_e] = - \psi_e \qquad \text{(A3.38c)}$$

where N_n and N_p are the neutron and proton operator, and N_e is the number of electrons minus the number of positrons. These relations imply $\Delta\mu = \mu_p + \mu_e - \mu_n$ for the operator $\bar{\psi}_e \not{J}_{had,CC}$ which arises in A3.31 ; if we combine A3.31 and the similar expression that one gets for Γ_a , we get 3.11, which is the detailed balance relation between production and absorption. Notice that the neutron and proton number operators are for the total number of nucleons, bound and free, and so then are μ_n and μ_p ; by the nuclear statistical equilibrium assumption, these reduce to the chemical potentials of the free neutrons and protons.

APPENDIX 4 NUMERICAL METHODS

In this appendix, we detail some of the numerical techniques used to solve the differential equations set up in Chapter 3.

A4.1 METHODS OF INTEGRATION AND INVERSION

To obtain the electron-positron equation of state, we need the degeneracy factor, η , given ρ, T, Y_e . For $\eta > 7$, we use the first Sommerfeld correction to evaluate the Fermi integrals (3.68); for η in the range $-5 < \eta < 7$, we use Gauss-Laguerre integration to evaluate F_k and a Newton-Raphson method to invert it.

We use the Epstein and Arnett (1975) fitting formulae to obtain the nuclear part of the equation of state, except for the free nuclear gas (which is trivial).

We invert the matter energy per baryon, $\varepsilon_m(\rho,T,Y_e)$, which is directly determined by the integration of 3.17c, to obtain the temperature, $T(\varepsilon_m,\rho,Y_e)$,by a Newton-Raphson method.

The equations describing the transparent phase are solved by the fourth order Runge-Kutta technique.

The energy integrations necessary to evaluate moments of the νe scattering kernels and of the $e^+e^- \rightarrow \nu\bar{\nu}$ production kernels are evaluated using Gauss-Laguerre and Gauss-Legendre numerical integrations respectively.

A4.2 ENERGY BIN AVERAGING

The P-O equation (6.11a) expresses the time evolution of the neutrino distribution function, $n(\nu,t)$, which is a function of time

and neutrino energy; in order to numerically integrate these equations, both variables must be discretized. We assume the df is approximately a step function in energy space,

$$n(\nu,t) = \sum_j n(j,t)\ \chi_{[\nu_j,\nu_{j+1})}(\nu) \tag{A4.1}$$

which assumes the constant value n(j,t) in the j-th energy group, $[\nu_j,\nu_{j+1})$, (whose characteristic function is χ).

We multiply the P-O equation by ν^2 , insert A4.1, then integrate over group j; when, for example, $e^- p \rightleftarrows n\ \nu_e$ and $\nu_e e \to \nu_e e$ are included, we obtain (with $\theta = 0$ in 6.11a)

$$\frac{dn(j,t)}{dt} = -\Gamma_a'(j)n(j,t) + \Gamma_p(j) - \left(\sum_{j'}(1-n(j',t))R(j \to j')\right)n(j,t) \tag{A4.2}$$
$$+ \left(\sum_{j'} n(j',t)\ \frac{(\Delta\nu^3)_{j'}}{(\Delta\nu^3)_j}\ R(j' \to j)\right)\ (1-n(j,t))$$

Here, the bin average of the production rate is

$$\Gamma_p(j) \equiv \frac{3}{(\Delta\nu^3)_j}\int_{\nu_j}^{\nu_{j+1}} \nu^2 d\nu\ \Gamma_p(\nu) \tag{A4.3a}$$

where

$$(\Delta\nu^3)_j \equiv \nu_{j+1}^3 - \nu_j^3 \tag{A4.3b}$$

The bin average of the scattering rate is defined in a similar manner:

$$R(j \to j') \equiv \frac{3}{(\Delta\nu^3)_j} \int_{\nu_j}^{\nu_{j+1}} \nu^2 d\nu \int_{\nu_{j'}}^{\nu_{j'+1}} (\nu')^2 d\nu' \; R_0(\nu \to \nu') \qquad \text{(A4.3c)}$$

This way of averaging was used to ensure no neutrino number is lost in neutrino-electron collisions. We evaluate the integrals A4.3a and c numerically, using a simple two point trapezoidal rule. This was tested by comparison with Simpson rule evaluations; further, the scattering rate, which is the sum over j' of A4.3c, agrees in the low and high energy limits with analytic formulae (A2.27). The bin average of the thermal production kernels are also defined by A4.3c; integrated energy loss rates calculated by this method agree with the BPS rates, provided the energy bin size is not too big.

We store the matrix R(j,j') in a grid in the variables η and T; to include ℓ = 0, 1, and 2 moments of the scattering kernel for the wide range of η and T values necessary in the spatial runs takes us to the limit of the storage capacity of CDC 7600 small core memory. When we do a table lookup, a three point linear bivariate interpolation is performed.

When the neutrino-neutrino scattering source function A1.25 is put through the prescription given to obtain A4.2, problems arise for the reasons mentioned in Appendix 1.

Most authors finite difference 6.11a in energy space: the energy ν would be taken at a discrete number of points and the source functions would be evaluated at those points. Although the group averaging technique is more elegant, the approximations necessary to

evaluate the integrals may not make it more accurate than finite differencing; it is certainly no less accurate; accuracy comes from the inclusion of more energy groups. Eighteen were used in ν_e evolution (see Figure 29); twenty-five were used in $\nu_\mu \bar{\nu}_\mu$ runs, spaced as in Figures 30 and 32.

A4.3 THE HOMOGENEOUS CODE

The $\dot{Y}_e$, $\dot{\varepsilon}_m$, and $\dot{n}(j,t)$ equations (one for each j) form a system of coupled nonlinear ordinary differential equations (ODE's).

There are many standard methods for solving ODE's which we have tried: fourth order Runge-Kutta, Milne's predictor-corrector method, and a number of iteration schemes. These methods conserve lepton number exactly, and all work as long as the timestep size does not get too large.

The size of the step is determined by the energy bin in which the largest changes in the df occur. At the beginning of the runs, these are determined by the production or absorption times. Neutrino rates typically go as the square of the energy: the characteristic evolution times for the highest (125-150 MeV) bin is ten thousand times shorter than the lowest bin's evolution time (.2-2 MeV): we clearly must increase the timestep size to well beyond the characteristic high energy time in order to do significant evolution. A small deviation from equilibrium (say, in the direction of production) amplifies, for in the next step, an overbalancing absorption occurs. The oscillations grow, then begin to downscatter into lower energy bins, wreaking havoc there.

This timestep size problem becomes especially acute when the production time is many orders of magnitude greater than the absorption or scattering times, when Y_p values are low or a thermal $\nu\bar{\nu}$ production mechanism is operating.

We rewrite the source function, the right hand side of A4.2, in the form

$$\frac{dn(j,t)}{dt} = -a_j\, n(j,t) + p_j \tag{A4.4}$$

where p_j is the effective production rate in energy group j (including scattering into the beam),

$$p_j = \Gamma_p(j) + \sum_{j'} R(j' \to j)\, \frac{(\Delta\nu^3)_{j'}}{(\Delta\nu^3)_j}\, n(j') \tag{A4.5a}$$

and

$$a_j = p_j + \Gamma_a(j) + \sum_{j'} R(j \to j')(1-n(j')) \tag{A4.5b}$$

is the effective modified absorption rate; both are functionals of the matter energy, Y_e , and the distribution function.

If a and p are practically time independent between time t and t + δt, A4.4 can be integrated exactly to yield a first prediction for the df:

$$n^{(0)}(j,t+\delta t) = \frac{p_j^{(0)}}{a_j^{(0)}} + \exp\,(-a_j^{(0)}\delta t)\left[n(j,t) - \frac{p_j^{(0)}}{a_j^{(0)}}\right] \tag{A4.6}$$

However, lepton number is evolving, with predicted value at t+δt

$$Y_e^{(0)}(t+\delta t) = Y_e(t) + \delta t \sum_j \frac{(\Delta\nu^3)_j}{6\pi^2} \left(-a_j^{(0)} n(j,t) + p_j^{(0)}\right) \qquad \text{(A4.7)}$$

A similar prediction holds for $\varepsilon_m^{(0)}$ and therefore the temperature $T^{(0)}$.

The first prediction, A4.6, will overshoot (if, for example, Y_e is decreasing) or undershoot the exact solution due to time dependence of the effective production and absorption coefficients. We make a second prediction by first using $n^{(0)}$, $Y_e^{(0)}$, $T^{(0)}$ to obtain $p^{(1)}$, $a^{(1)}$, and from these obtain $n^{(1)}$, $Y_e^{(1)}$, and $T^{(1)}$. This second prediction tends to act in the opposite direction: $n^{(1)}$ tends to undershoot if $n^{(0)}$ overshoots.

From these two predictions, we form a corrector:

$$n(j,t+\delta t) \equiv n^c(j,t+\delta t) = q\, n^{(0)} + (1-q) n^{(1)} \qquad \text{(A4.8)}$$

$$Y_e(t+\delta t) = q\, Y_e^{(0)} + (1-q)\, Y_e^{(1)} \qquad \text{(A4.9)}$$

where q is a parameter we are free to vary. We choose q to conserve lepton number.

The functionals a and p depend upon changes in the thermodynamic variables, which, once the extremely rapid phase of neutronization occurs, change slowly (see Figure 26). They also depend upon the distribution function, but only in an integral (summation) sense, and are not very sensitive to changes in any one group's value.

We peg the timestep size to changes in p and a; we must still

choose it short in the rapid evolution phases, but can let it grow near equilibrium which the df approaches smoothly; the numerical solutions do not deviate from equilibrium once it is attained.

A similar technique is used to solve the P-0 equations for $\nu_\mu \bar{\nu}_\mu$ pairs: there, we have required $Y_{\nu_\mu} = Y_{\bar{\nu}_\mu}$ as the q constraint condition. Comparisons with a forward differencing iterative method show similar results (Figure 30). As we mentioned in section 6.6, the df tends to overshoot the $\mu = 0$ equilibrium.

A4.4 THE SPATIAL CODE

The spatial code is similar to the homogeneous code multiplied by the number of spatial zones, except that nearest neighbor zones are coupled.

We finite difference the P-1 equations (section 3.8) in space, following the techniques and notation of Falk and Arnett (1977). We split the range of the baryon number coordinate, b, into zones labelled by an integer k which runs from zero to some maximum k_m. The thermodynamic variables (temperature, density, energy, pressure, Y_e, and other compositions) and the even moments of the df are defined at the zone centers, labelled by $k + 1/2$. Odd moments of the df and the dynamical variables (radius, velocity, total baryon number interior to zone k) are defined on zone boundaries.

If a quantity such as the density ρ is defined at the zone centers, its value on the zone boundaries is approximated by

$$\langle\rho\rangle(k) = \frac{(\rho(k+1/2)\Delta m(k+1/2) + \rho(k-1/2)\Delta m(k-1/2))}{2\Delta m(k)} \qquad \text{(A4.10)}$$

where $\Delta m(k+1/2) = M(k+1) - M(k)$ is the difference in baryon number between the (k+1)-st zone and the k-th zone: it is the baryon number enclosed within zone k. Here, we adopt the symbol of mass for baryon number given in units of Avagadro's number. The mass difference

$$\Delta m(k) \equiv (\Delta m(k+1/2) + \Delta m(k-1/2))/2 \tag{A4.11}$$

is defined in such a way that $\langle 1 \rangle_k = 1$.

Values defined on the zone boundaries such as the radius R are approximated at the zone centers by

$$\langle R \rangle (k+1/2) \quad \frac{(\Delta m(k+1)R(k+1) + \Delta m(k)R(k))}{2\Delta m(k+1/2)} \tag{A4.12}$$

The P-1 equations (3.25 and 3.26) with the dynamics neglected become

$$\frac{\partial n(k+1/2)}{\partial t} + \frac{c\rho(k+1/2)}{\Delta m(k+1/2)} (A(k+1)j(k+1) - A(k)j(k))$$

$$= -a(k+1/2)n(k+1/2) + p(k+1/2) \tag{A4.13}$$

$$\frac{\partial j(k)}{\partial t} + \frac{cA(k)\langle \rho \rangle (k)}{3\Delta m(k)} [n(k+1/2)(2/3 + f(k+1/2))$$

$$- n(k-1/2)(2/3 + f(k-1/2))] + \frac{3c}{R(k)} \langle (f-1/3)n \rangle (k)$$

$$= -\Upsilon(k)j(k) + \mu(k) \tag{A4.14}$$

where n and j are the $\ell = 0$ and $\ell = 1$ moments of the df respectively, f is the Eddington factor (3.49a), and A is the area ($4\pi R^2$) . The

effective modified absorption coefficient, a, consists of those terms in 3.25b,c which multiply $n(\nu)$; the effective production coefficient, p , consists of those terms which do not; we include the $\ell = 1$ terms which arise from nonconservative scattering in p, but not the $\ell = 2$ terms, as they enter into a. In a similar manner, the effective transport coefficient, Υ , consists of the terms multiplying j in 3.26b,c ; the rest of the terms make up μ , the effective momentum production coefficient, which arises from scattering into the beam. In all of these coefficients, the appropriate averages, A4.10 and A4.12, must be included where necessary.

In our first treatment of these equations, we finite differenced A4.14 in time, took the j on the right hand side (RHS) at the later time (backward differenced), inserted this equation into A4.13, with the n on the RHS at the earlier time (forward differenced). The result is a system of linear equations of form

$$A(k+1/2)n(k+3/2,t+\delta t) + B(k+1/2)n(k+1/2,t+\delta t) + C(k+1/2)n(k-1/2,t+\delta t) = \mathcal{D}(k+1/2) \qquad (A4.15)$$

which can be written as a matrix equation: the matrix is then tridiagonal and can be inverted to yield the df at time $t+\delta t$ in terms of the coefficients A, B, C, and $\mathcal{D}$ which depend upon the df at time t. Actually, our technique included many iterations; the coefficients then depended upon the df and the thermodynamic parameters at prior iterations.

Another method is to take n on the RHS of A4.13 at forward times: the equations are twice backward differenced, but lepton number is no longer conserved.

We adopted a method similar to that used in the homogeneous code: A4.14 is integrated over a time interval, yielding $j(k,t+\tau)$ in terms of an (unknown) integral over n, which we evaluate by assuming a linear variation in $n(k+1/2,t)$ between its values at t and $t+\delta t$. The flux, j, is inserted into A4.13, and the resulting expression is integrated over time. A tridiagonal equation, A4.15, results with A, B, C, D complicated functions of past time values and exponentials of $a\delta t$ and $\gamma\delta t$.

Special attention must be given to boundary conditions; for example, $C = 0$ for the inner zone $k = 1$, $A = 0$ for the outer zone $k = k_m$. The Marshak BC (3.51) expresses $j(k_m)$ as a linear combination of $j(k_m-1)$ and $n(k_m-1/2)$.

In practice, we do not solve A4.15, but rather A4.15 multiplied by $(\Delta\nu^4)_j/8\pi^2$, which yields the energy density.

The flux limited diffusion equations are simpler: A4.14 has $f = 1/3$, and no $\partial j/\partial t$ and μ terms; a flux limiter now divides γ . Again A4.15 is obtained, with different coefficients than in the P-1 method.

The neutronization and energy equations are solved by forward differencing. At each timestep, the effective absorption, production, and transport coefficients must be obtained, and exponentials taken of these.

This code has been tested on a simple problem: a delta function source at the center of a homogeneous sphere; the BC are Marshak; the code reproduces accurately the long time behavior, which can be obtained analytically. Further, the code reproduces the homogeneous code results when all transport is shut off.

REFERENCES

Abers, E.S. and Lee, B.W. 1973, Physics Reports 9, 1.

Adams, J.B., Ruderman, M.A., and Woo, C.H. 1963, Phys. Rev. 124, 1383.

Adler, S.L., et al. 1975, Phys. Rev. D11, 3309.

Arnett, W.D. 1966, Canadian J. Phys. 44, 2553.

————. 1967, Canadian J. Phys. 45, 1621.

————. 1972a, Ap.J. 176, 681.

————. 1972b, Ap.J. 176, 699.

————. 1974a, Ap.J. 193, 169.

————. 1974b, Ap.J. 194, 373.

————. 1974c, Late Stages of Stellar Evolution, ed. Taylor (IAU), p.1.

————. 1976, Chicago Workshop on Weak Interactions and Gravitational Collapse.

————. 1977, Ap.J. 218, 815.

————. 1977a, Ap.J. Suppl. 35, 145.

Avignone, F.T., III 1970, Phys. Rev. D2, 2609.

Baade, W. and Zwicky, F. 1934, Phys. Rev. 45, 138.

Bahcall, J.N. 1964, Phys. Rev. B136, 1547.

————. 1977, Ap.J.Lett. 216, L115.

Bahcall, J.N. and Frautschi, S.C. 1964, Phys. Rev. B136, 1547.

Bahcall, J.N. and Wolf, R.A. 1965, Phys. Rev. B140, 1452.

Bahcall, J.N. Trieman, S.B., and Zee, A. 1974, Phys. Lett. 52B, 275.

Bahcall, J.N. and Davis, R., Jr. 1976, Science 191, 264.

Bahcall, J.N. and Ulrich, R.K. 1976, Ap.J. 170, 593.

Baier, V.N. and Khriplovich, J.B. 1964, Soviet Astron.-AJ 7, 599.

Baird, P.E.G., et al. 1977, Phys. Rev. Lett. 39, 798.

Barish, B.C., et al. 1975 (CITF collaboration). 1975, Phys. Rev. Lett. 34, 538.

Barish, B.C. 1978, Physics Reports (to be published).

Barish, S.J., et al. 1974, Phys. Rev. Lett. 36, 448.

Barkat, Z. 1975, Ann. Rev. Astr. Ap. 13, 45.

Barnes, C.A., et al. 1978, Phys. Rev. Lett. 40, 840.

Baym G., Bethe, H.A., and Pethick, C.J. 1971, Nucl. Phys. A175, 225.

Beaudet, G., Petrosian, V. and Salpeter, E.E. 1967, Ap.J. 181, 393.

Benvenuti, A., et al. (HPWF collaboration). 1974, Phys. Rev. Lett. 32, 800.

Bernabeu, J. 1975, Cern preprint TH. 2073.

Bjorken, J.D. and Drell, S.D. 1964, Relativistic Quantum Mechanics (New York: McGraw-Hill).

Blietschau, J., et al. (Gargamelle collaboration). 1976, Nucl. Phys. B114, 189.

———————————————————————————. 1977, Nucl. Phys. B118, 218.

Bludman, S. 1958, Nuovo Cimento 9, 443.

Bludman, S.A. and van Riper, K.A. 1977, preprint UPR-0077T.

Brown, G.E. 1977, Comments Astrophys. 7, 67.

Bruenn 1975, Ann. NY Acad. Sci. 262, 80.

Bruenn, S.W., Arnett, W.D., and Schramm, D.N. 1977, Ap. J., 213, 213.

Bruenn, S.W., Buchler, J.R., and Yueh, W.R. 1978, Ap.J. Lett. 221, L83.

Brush, S.G., Sahlin, H.L., and Teller, E. 1966, J. Chem. Phys. 45, 2102.

Burbidge, E.M., Burbidge, G., Fowler, W.A., and Hoyle, F. 1957, Rev. Mod. Phys. 29, 547.

Cameron, A.G.W. 1958, Mem. Soc. Roy. Sci. Liège, 5th Ser. 3, 163.

Castor, J.I. 1972, Ap. J. 178, 779.

Cazzola P., De Zotti, G., Saggion, A. 1971, Phys. Rev. D3, 1722.

Chechetkin, V.M., Imshenik, V.S., Ivanova, L.N., and Nadezhin, D.K. 1976, preprint.

Chevalier, R. 1976, Ap. J. 207, 872.

Clark, D.H. and Stephenson, F.R. 1977, The Historical Supernovae (Oxford: Pergamon Press).

Clayton, D.D. 1968, Principles of Stellar Evolution and Nucleosynthesis (New York: McGraw-Hill).

Cline, D. et al. (HPW collaboration). 1976a, Phys. Rev. Lett. 37, 252.

———————————————— . 1976b, Phys. Rev. Lett. 37, 648.

Cline, D. and Fry, W.F. 1977, Ann. Rev. Nucl. Sci. 27, 209.

Colgate, S.A. and White, R.H. 1966, Ap. J. 143, 626.

Colgate, S.A. and McKee, C. 1969, Ap. J. 157, 623.

Comella, J.W., et al. 1969, Nature 221, 453.

Cowsik, R. and McLelland, J.M. 1972, Phys. Rev. Lett. 29, 669.

Crawford, J.P., Hansen, C.J., and Mahanthappa 1976, Ap. J. 206, 208.

de Boer, W.P.H. and van Weert, Ch.G. 1976, Physica 85A, 566.

de Shalit, A. and Feshbach, H. 1974, Theoretical Nuclear Physics Volume 1: Nuclear Structure (New York: Wiley).

Dicus, D.A. 1972, Phys. Rev. D6, 941.

Dicus, D.A., Kolb, E., Schramm, D., and Tubbs, D. 1976, Ap. J. 210, 481.

Donnelly, T.W., et al. 1974, Phys. Lett. 49B, 8.

Donnelly, T.W., Dubach, J., and Haxton, W.C. 1975, Nucl. Phys. A251, 353.

Dumand 1976, Proceedings of the Summer Workshop (FNAL).

Efremenko, V. 1976, Proc. Neutrino Conference (Aachen), p. 663.

Ehlers, J. 1971, General Relativity and Cosmology, ed. Sachs (New York: Academic Press).

Ellis, J. and Jaffe, R. L. 1973, SLAC-PUB-1353.

Engelbrecht, C., Fowler, W. A., and Woosley, S. E. 1978, Orange Aid Preprint 520.

Epstein, R. I. and Arnett, W. D. 1975, Ap. J. 201, 202.

Epstein, R. I., Norgaard, H., and Bond, J. R. 1978, submitted for publication, Nordita preprint 78/12.

Faissner, H., et al. 1976, Proc. Neutrino Conference (Aachen).

Falk, S. W. and Arnett, W. D. 1977, Ap. J. 33, 515.

Festa, G. C. and Ruderman, M. A. 1969, Phys. Rev. 180, 1227.

Fetter, A. L. and Walecka, J. D. 1971, Quantum Theory of Many Particle Systems (New York: McGraw-Hill).

Finzi, A. and Wolf, R. A. 1967, Ap. J. 150, 115.

Flowers, E. 1973, Ap. J. 180, 911.

Flowers, E. and Itoh, N. 1974, Ap. J. 206, 218.

Flowers, E. G., Sutherland, P. G., and Bond, J. R. 1975, Phys. Rev. D 12, 315.

Flowers, E. G. and Sutherland, P. G. 1976, Ap. J. 208, L19.

Fowler, W. A. 1978, private communication.

Fowler, W. A. and Hoyle, F. 1964, Ap. J. Suppl. 9, 201.

Fowler, W. A., Fuller, G., and Newman, M. J. 1977, Summer Workshop on Supernovae (U.C. Santa Cruz).

Fowler, W. A. and Fuller, G. 1978, private communication.

Fowler, W. A., Engelbrecht, C., and Woosley, S. E. 1978, OAP-520.

Frati, W., et al. 1975, Ann. NY Acad. Sci. 262, 219.

Fraley, G. 1968, Ap. Space Sci. 2, 96.

Freedman, D. Z. 1974, Phys. Rev. D 9, 1389.

Freedman, D. Z., Schramm, D. N., and Tubbs, D. L. 1977, Ann. Rev. Nucl. Sci. 27, 167.

Gandelman, G. M. and Pinaev, V. S. 1960, Soviet Phys. JETP 10, 764.

Gell-Mann, M. and Glashow, S. 1961, Ann. Phys. (N.Y.) 15, 437.

Gold, T. 1968, Nature 218, 731.

Goodstein, D. L. 1975, States of Matter (New Jersey: Prentice Hall).

Green, L. C. 1977, Sky and Telescope 54, 11.

Gurr, H. S., Reines, F., and Sobel, H. W. 1974, Phys. Rev. Lett. 33, 179.

_____. 1976, Phys. Rev. Lett. 34, 315.

Hansen, C. J. 1966, PhD thesis (Yale University).

Hansen, J. P. 1973, Phys. Rev. A 8, 3096.

Hansen, J. P. and Pollock, E. L. 1973, Phys. Rev. A 8, 3110.

Hansen, J. P., Torrie, G. M., and Vieillifosse, P. 1977, Phys. Rev. A 16, 2153.

Hasert, F. J., et al. (Gargamelle collaboration). 1973, Phys. Lett. 46B, 138.

_____. 1973a, Phys. Lett. 46B, 121.

_____. 1975, Phys. Lett. 59B, 485.

Higgs, P. W. 1964, Phys. Rev. Lett. 12, 132.

Hung, P. Q. and Sakurai, J. J. 1977a, UCLA preprint, UCLA/77/TEP/13.

_____. 1977b, Phys. Lett. 72B, 208.

Ikeuchi, S., et al. 1971, Prog. Theor. Phys. 46, 1713.

Imshenik, V. S. and Nadezhin, D. K. 1971, IAM preprint No. 18 (Moscow).

_____. 1973, Soviet Phys. JETP 36, 821.

Itoh, N. 1975, Prog. Theor. Phys. 54, 1580.

Itoh, N., Kohyama, Y., and Fujii, A. 1977, Nuc. Phys. A 827, 501.

Ivanova, L. N., Imshenik, V. S., and Nadezhin, D. K. 1967, preprint, subsequently published in Sci. Inf. Astr. Council USSR Acad. Sci. 13 (1969).

Jeukenne, J. P., Lejeune, A., and Mahaux, C. 1976, Physics Reports 25C, 83.

Kadanoff, L. P. and Baym, G. 1962, Quantum Statistical Mechanics (New York: W. A. Benjamin).

Kiguchi, M. 1977, Prog. Theor. Phys. 58, 1766.

Kirshner, R. P., Oke, J. B., Penston, M., and Scarle, L. 1973, Ap. J. 185, 303.

Kirshner, R. P. and Kwan, J. 1975, Ap. J. 197, 415.

Konopinski, E. J. 1966, The Theory of Beta Radioactivity (Oxford).

Kuchowicz, B. 1972, The Cosmic ν, Polish Nuclear Energy Information Center publication NEIC-RR-47.

Lamb, D. Q. and Pethick, C. J. 1976, Ap. J. Lett. 209, L77.

Lande, K., et al. 1974, Nature 251, 485.

Lasher, G. 1975, Ap. J. 201, 194.

Lattimer, J. M. and Ravenhall, D. G. 1977, University of Illinois preprint.

Le Blanc, J. and Wilson, J.R. 1970, Ap. J. 161, 541.

Lee, B. W. and Weinberg, S. 1977, Phys. Rev. Lett. 39, 165.

Lee, W., et al. (CIR collaboration). 1976, Phys. Rev. Lett. 37, 186.

Lewis, L. L., et al. 1977, Phys. Rev. Lett. 39, 795.

Lichtenstadt, I., et al. 1977, preprint.

Lindquist, R. W. 1966, Ann. Phys. (N.Y.) 37, 487.

Lowry, M. M., et al. 1978, see Barnes et al. 1978.

Mackie, F. D. 1976, Ph.D. thesis (University of Illinois).

Margolis, S. H., Schramm, D. N., and Silberberg, R. 1978, Ap. J. 221, 990.

Martin, P. C. 1968, Many Body Physics, eds. DeWitt, C. and Balian, R. (New York: Gordon and Breach), p. 37.

Mazurek, T. J. 1975, Ap. and Space Sci. 35, 117.

_____. 1976, Ap. J. Lett. 207, L87.

_____. 1977, Summer Workshop on Supernovae (U.C. Santa Cruz).

Mazurek, T. J., Truran, J. W., and Cameron, A.G.W. 1974, Ap. and Space Sci. 27, 261.

Maxwell, O., Brown, G. E., Campbell, D. K., Dashen, R. F., and Manassah, J. T. 1977, Ap. J. 216, 77.

Meier, D., et al. 1976, Ap. J. 204, 869.

Migdal, A. B. 1978, Rev. Mod. Phys. 50, 107.

Osborn, R. K. and Yip, S. 1966, The Foundations of Neutron Transport Theory (New York: Gordon and Breach).

Perl, M. L., et al. 1977, Phys. Lett. 70B, 487.

Pethick, C. J. 1978, private communication.

Pollock, E. L. and Hansen, J. P. 1973, Phys. Rev. A8, 3110.

Pomraning, G. C. 1973, Radiation Hydrodynamics (Oxford: Pergamon Press).

Pontecorvo, B. 1963, Sov. Phys. Uspekhi 6, 1.

_____. 1967, Zh. Eksp. Teor. Fiz. 53, 1717.

Rakavy, G. and Shaviv, G. 1967, Ap. J. 148, 803.

Reines, F. 1977, Dumond Workshop (Fermilab).

Reines, F., et al. 1971, Phys. Rev. D 4, 80.

Roos, M. 1974, Nucl. Phys. B 77, 420.

Sakashita, S. and Nishida, M. 1964, Prog. Theor. Phys. 31, 727.

Sakurai, J. J. 1976, UCLA preprint, UCLA/76/TEP/21.

Salam, A. 1968, Elementary Particle Physics, ed. Svortholm, N. (Stockholm: Almquist and Wiksell), p. 367.

Sato, K. 1975, Prog. Theor. Phys. 54, 1325.

Sawyer, R. F. 1975, Phys. Rev. D11, 2740.

Schramm, D. N. 1976, Nukleonika 21, 727.

Schwartz, R. A. 1967, Ann. Phys. 43, 42.

Sitenko, A. G. 1967, Electromagnetic Fluctuations in Plasma (New York: Academic Press).

Sobel, H. W. 1976, Proc. Neutrino Conference (Aachen), p. 678

Takahashi, K. 1971, Prog. Theor. Phys. 45, 1466.

Takahashi, K. and Yamada, M. 1969, Prog. Theor. Phys. 44, 663.

Tammann, G. 1974, Supernovae and Supernovae Remnants, ed. Cosmovici, C. B. (Boston: Reidel), Part IV.

Trippe, T. G., et al. 1976, Review of Particle Properties, Rev. Mod. Phys. Suppl. 48, S1.

Tsuruta, S. 1974, Cooling of Dense Stars, in Physics of Dense Matter (Boston: Reidel).

Tsuruta, S., Canuto, V., Lodenquai, J., and Ruderman, M. 1972, Ap. J. 176, 739.

Tsytovich, V. N. 1961, Soviet Phys. JETP 13, 1249.

Tubbs, D. L. 1978, Ap. J. Suppl., in press.

Tubbs, D. L., and Schramm, D. N. 1975, Ap. J. 201, 467.

van Hove, L. 1954a, Phys. Rev. 95, 249.

_____. 1954b, Phys. Rev. 95, 1374.

van Riper, K. A. 1977, Enrico Fermi Institute Preprint No. 77-42.

Weaver, T. A., Zimmerman, G. B., and Woosley, S. E. 1977, Livermore preprint UCRL-80460.

Weinberg, S. 1962, Phys. Rev. 128, 1457.

_____. 1967, Phys. Rev. Lett. 19, 1264.

_____. 1972, Phys. Rev. D 5, 1412.

Weinberg, S. 1976, Phys. Rev. Lett. 36, 294.

Wilson, J. R. 1971, Ap. J. 163, 209.

_____. 1974, Phys. Rev. Lett. 32, 849.

_____. 1976, Livermore preprint.

_____. 1977, Summer Workshop on Supernovae (U.C. Santa Cruz).

Wilson, J. R., et al. 1975, Ann. NY Acad. Sci. 262, 54.

Yang, C. N. and Mills, R. 1954, Phys. Rev. 96, 191.

Yueh, W. R. and Buchler, J. R. 1976, Ap. and Space Sci. 41, 221.

_____. 1977a, Ap. J. Lett. 211, L121.

_____. 1977b, Ap. J. 217, 565.

Zaidi, M. H. 1965, Nuovo Cimento 40A, 502.

Zel'dovich, Ya. B. 1967, Sov. Phys. JETP Lett. 6, 316.

Zel'dovich, Ya. B. and Novikov, I. D. 1971, Relativistic Astrophysics, Vol. 1 (Chicago: University of Chicago).

Zernike, F. and Prins, J. 1927, Z. Physik 41, 184.

TABLE 1

The coefficients needed to specify the neutral current interaction, and their values in the Weinberg-Salam theory. (Section 2.2)

TABLE 1

COEFFICIENTS		W.S. VALUES†
α_e		1
α_μ	$(=\alpha_e)$	1
C_{Ve}	$(=\alpha_e c_{Ve}+1)$	$1/2 + 2x$
C_{Ae}	$(=\alpha_e c_{Ae}+1)$	$1/2$
$C_{V\mu}$	$(=\alpha_\mu c_{Ve})$	$-1/2 + 2x$
$C_{A\mu}$	$(=\alpha_\mu c_{Ae})$	$-1/2$
C_{Vn}		$-1/2$
C_{An}		$-g_A/2$
C_{Vp}		$1/2 - 2x$
C_{Ap}		$g_A/2$
C_{V0}	$(=\alpha_e c_{V0})$	$- x$
C_{V1}	$(=\alpha_e c_{V1})$	$1 - 2x$
C_{A0}	$(=\alpha_e c_{A0} g_{A0})$	0
C_{A1}	$(=\alpha_e c_{A1} g_A)$	g_A

† $x = \sin^2 \theta_W$, $g_A \simeq 1.25$

TABLE 2

Cross sections for many of the processes important in gravitational collapse. (Sections 2.5, 2.6, 2.8, A1.2)

TABLE 2

COUPLING	PROCESS	CROSS SECTION*
$(\bar{\nu}\nu)(\bar{N}N)$	$\nu_\ell + A_i \to \nu_\ell + A_i$ $(\ell = e,\mu)$ $\bar{\nu}_\ell + A_i \to \bar{\nu}_\ell + A_i$	$\sigma = \frac{G^2}{\pi}\left[\left(C_{Vn}N_i + C_{Vp}Z_i\right)^2 + \left\langle (C_{A0} + C_{A1}t_3)\underset{\sim}{\sigma}\right\rangle_{ii}^2\right]\nu^2$
	$\nu_\ell + A_i \to \nu_\ell + A_f$ $\bar{\nu}_\ell + A_i \to \bar{\nu}_\ell + A_f$	$\sigma = \frac{G^2}{\pi}\left(\nu - Q_{if}\right)^2 \left\langle (C_{A0} + C_{A1}t_3)\underset{\sim}{\sigma}\right\rangle_{fi}^2$, $Q_{if} = M_f - M_i$
	$\nu_\ell + N \to \nu_\ell + N$ $\bar{\nu}_\ell + N \to \bar{\nu}_\ell + N$	$\sigma = \frac{G^2}{\pi}\nu^2\left(C_{VN}^2 + 3C_{AN}^2\right)$, $N = n,p$
	$A_i \to A_f + \nu_\ell + \bar{\nu}_\ell$	$\Gamma_{fi} = \frac{G^2}{60\pi^3} Q_{fi}^5 \left\langle (C_{A0} + C_{A1}t_3)\underset{\sim}{\sigma}\right\rangle_{fi}^2$, $Q_{fi} = M_i - M_f$
$(\bar{\nu}\nu)(\bar{e}e)$	$\nu_\ell + e^- \to \nu_\ell + e^-$ $(\ell = e,\mu)$ $\bar{\nu}_\ell + e^+ \to \bar{\nu}_\ell + e^+$	$\sigma = \frac{G^2}{\pi} s \frac{1}{4}\left[\left(C_{V\ell} + C_{A\ell}\right)^2 + \frac{1}{3}\left(C_{V\ell} - C_{A\ell}\right)^2\right]$, $\sqrt{s} >> m_e$
	$\bar{\nu}_\ell + e^- \to \bar{\nu}_\ell + e^-$ $\nu_\ell + e^+ \to \nu_\ell + e^+$	$\sigma = \frac{G^2}{\pi} s \frac{1}{4}\left[\left(C_{V\ell} - C_{A\ell}\right)^2 + \frac{1}{3}\left(C_{V\ell} + C_{A\ell}\right)^2\right]$, $\sqrt{s} >> m_e$
	$e^+ + e^- \to \nu_\ell + \bar{\nu}_\ell$ $(\ell = e,\mu)$	$\sigma = \frac{G^2}{3\pi} s \frac{1}{4}\left(C_{V\ell}^2 + C_{A\ell}^2\right)$, $\sqrt{s} >> m_e$
	$\nu_\ell + \bar{\nu}_\ell \to e^+ + e^-$	$\sigma = \frac{G^2}{3\pi} s \left(C_{V\ell}^2 + C_{A\ell}^2\right)$, $\sqrt{s} >> m_e$

TABLE 2 (continued)

COUPLING	PROCESS	CROSS SECTION*
$(\bar{\nu}\nu)(\bar{\nu}\nu)$	$\nu_e+\nu_e \rightarrow \nu_e+\nu_e$	$\sigma = \frac{G^2}{\pi}\alpha_e^2 s$
	$\nu_e+\bar{\nu}_e \rightarrow \nu_e+\bar{\nu}_e$	$\sigma = 2\frac{G^2}{3\pi}\alpha_e^2 s$
	$\nu_\mu+\nu_e \rightarrow \nu_\mu+\nu_e$	$\sigma = 2\frac{G^2}{\pi}\alpha_e\alpha_\mu s$
	$\bar{\nu}_\mu+\nu_e \rightarrow \bar{\nu}_\mu+\nu_e$	$\sigma = 2\frac{G^2}{3\pi}\alpha_e\alpha_\mu s$
	$\left\{\begin{array}{l}\nu_e+\bar{\nu}_e \rightarrow \nu_\mu+\bar{\nu}_\mu \\ \nu_\mu+\bar{\nu}_\mu \rightarrow \nu_e+\bar{\nu}_e\end{array}\right\}$	$\sigma = 2\frac{G^2}{3\pi}\alpha_e\alpha_\mu s$

* $\frac{G^2}{\pi} = 1.63\times10^{-44}(\text{MeV})^{-2}\ \text{cm}^2$; $\sqrt{s}$ = center of mass energy ; $(\bar{\nu}\nu)(\bar{N}N)$ cross sections are lab frame

FIGURE 1

The experimental situation in neutral current interactions is exemplified by the errors in $\sin^2 \theta_W$ if the experiments are analyzed within the framework of the Weinberg-Salam model. The experimental values in inclusive deep inelastic neutrino scattering have sharpened somewhat since this figure, taken from Cline and Fry (1977), was made. "Reproduced, with permission, from Annual Review of Nuclear Science, Volume 27. © 1977 by Annual Reviews Inc." (Section 2.2)

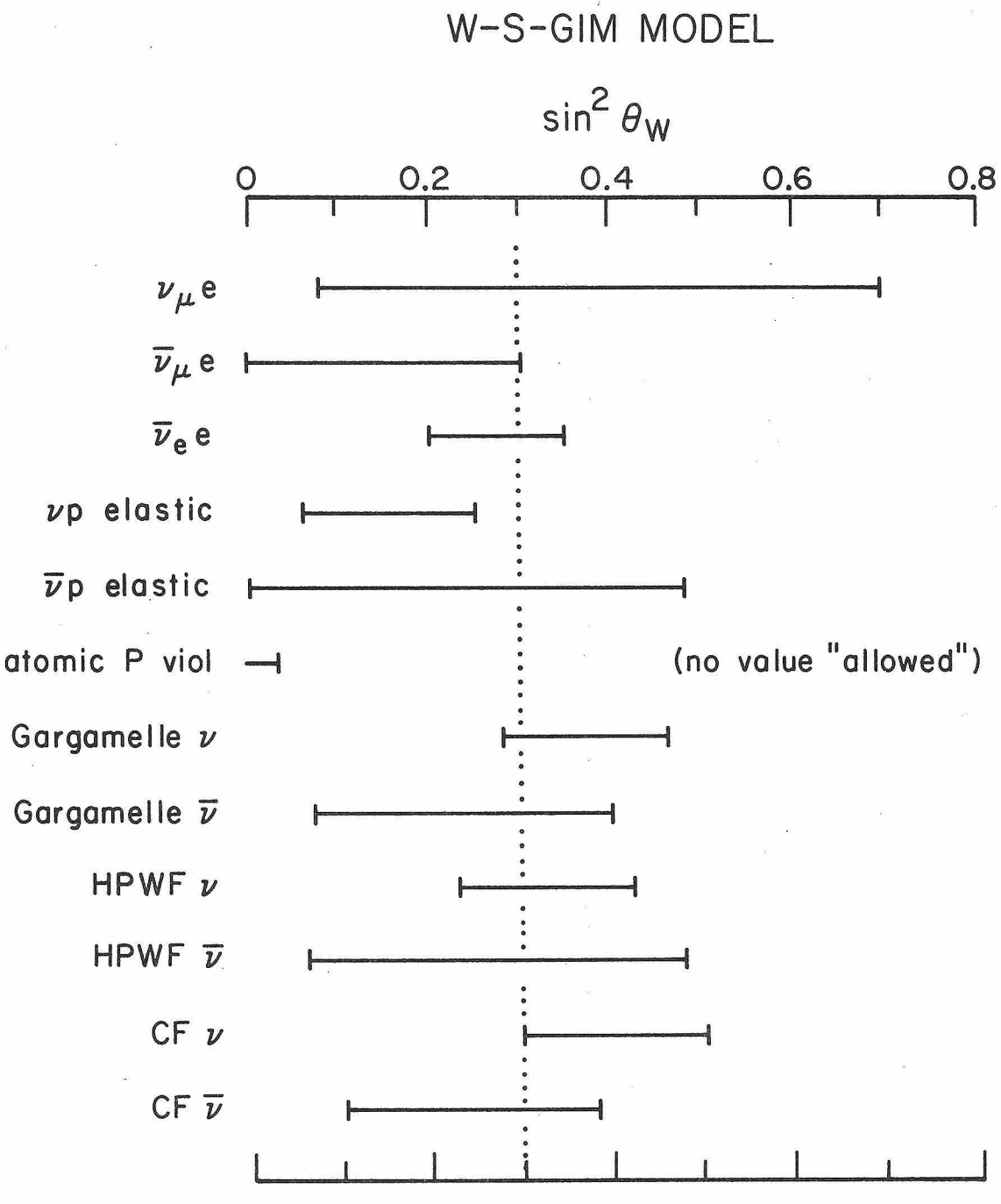
W-S-GIM MODEL
sin² θW
0
0.2
0.4
0.6
0.8
νμ e
ν̄μ e
ν̄e e
νp elastic
ν̄p elastic
atomic P viol
(no value "allowed")
Gargamelle ν
Gargamelle ν̄
HPWF ν
HPWF ν̄
CF ν
CF ν̄

Fig. 1

FIGURE 2

The ratio of the $\ell = 2$ and 3 moments of the df to the $\ell = 0$ moment is given as a function of the ratio of the first to zeroth moment for an elliptic distribution (equation 3.44). The function α , defined by equation 3.45b, is also plotted. This function is used to obtain the Eddington factor (3.49a) in the P-1 method. (Section 3.7)

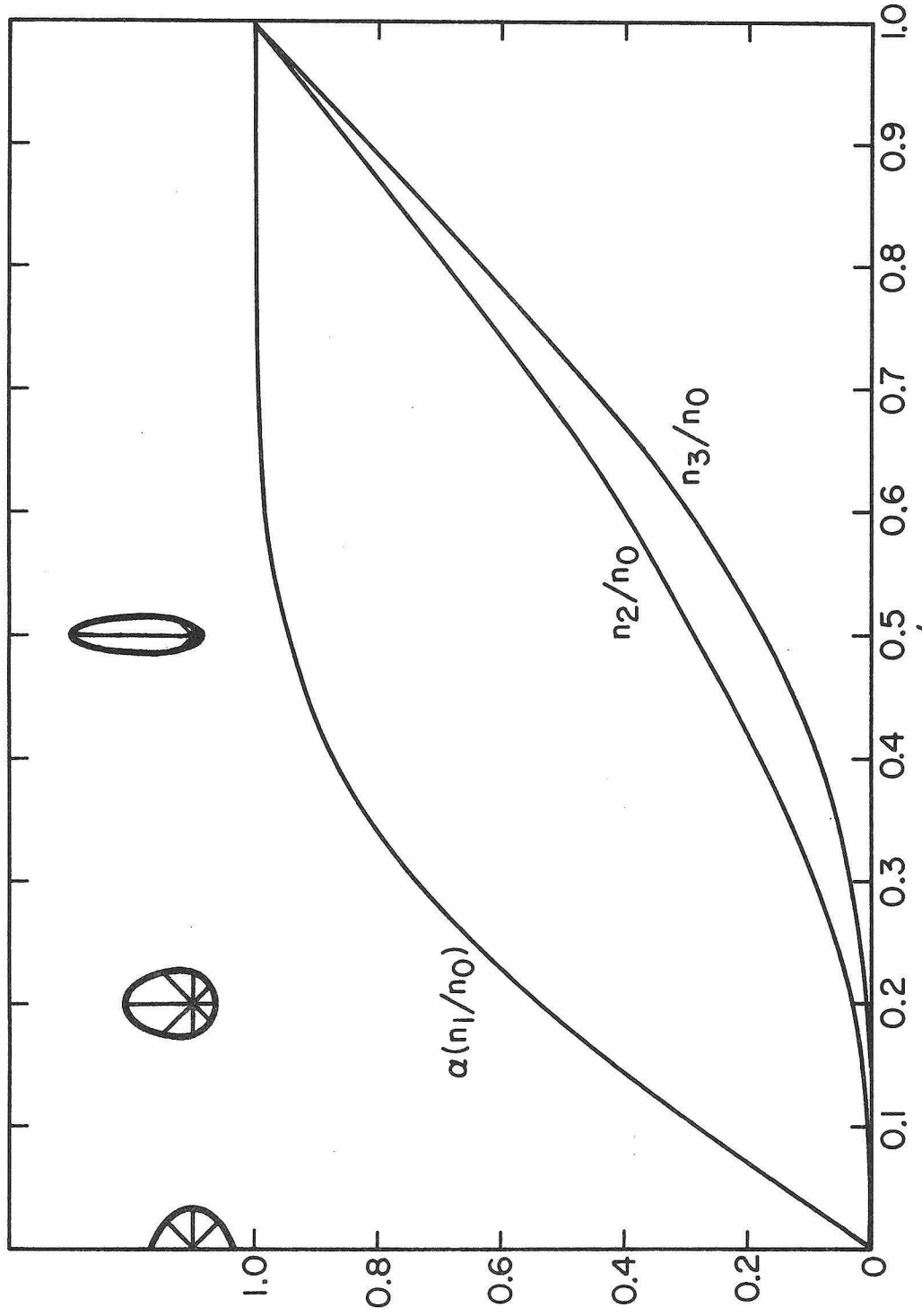
0
0.2
0.4
0.6
0.8
1.0
0.1
0.2
0.3
0.4
0.5
0.6
0.7
0.8
0.9
1.0
n_1/n_0
n_2/n_0
n_3/n_0
$\alpha(n_1/n_0)$

Fig. 2

FIGURE 3

An illustration of the processes which the current-current correlation function describes in various domains of ω-k space. Moments of the scattering kernel, which are functions of the incoming neutrino energy, ν, and the outgoing neutrino energy, ν', are obtained by integrations with respect to k over the dashed line. Similar k-integrations must be performed to obtain moments of the production and absorption kernels, but in the timelike negative and positive cones respectively.(Sections A3.3 and 5.5)

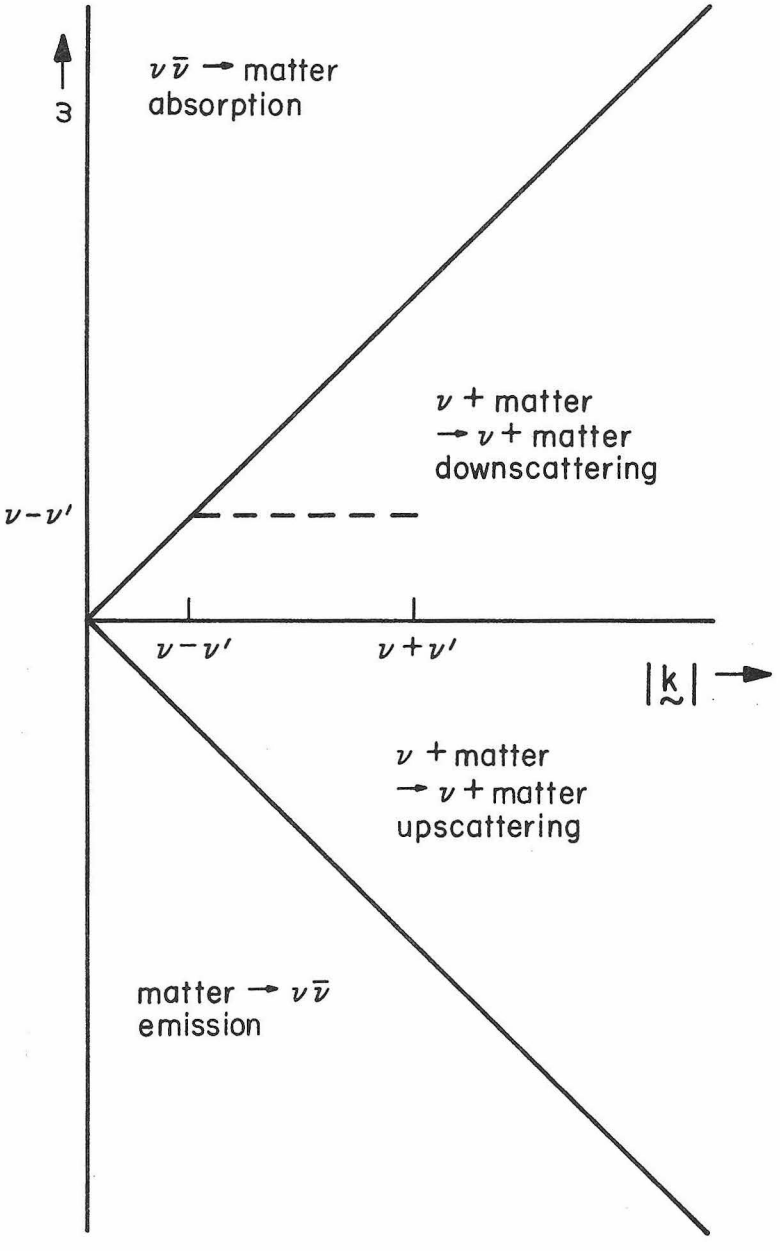
3
$\nu\bar{\nu}$ → matter
absorption
ν + matter
→ ν + matter
downscattering
$\nu-\nu'$
$\nu-\nu'$
$\nu+\nu'$
$|\underset{\sim}{k}|$ →
ν + matter
→ ν + matter
upscattering
matter → $\nu\bar{\nu}$
emission

Fig. 3

FIGURE 4

The static liquid structure factor vs. ka for a $\Gamma = 10$ Coulomb plasma (Hansen 1973) (solid line). The dashed line is the Debye-Huckel static liquid structure factor. (Section 4.4)

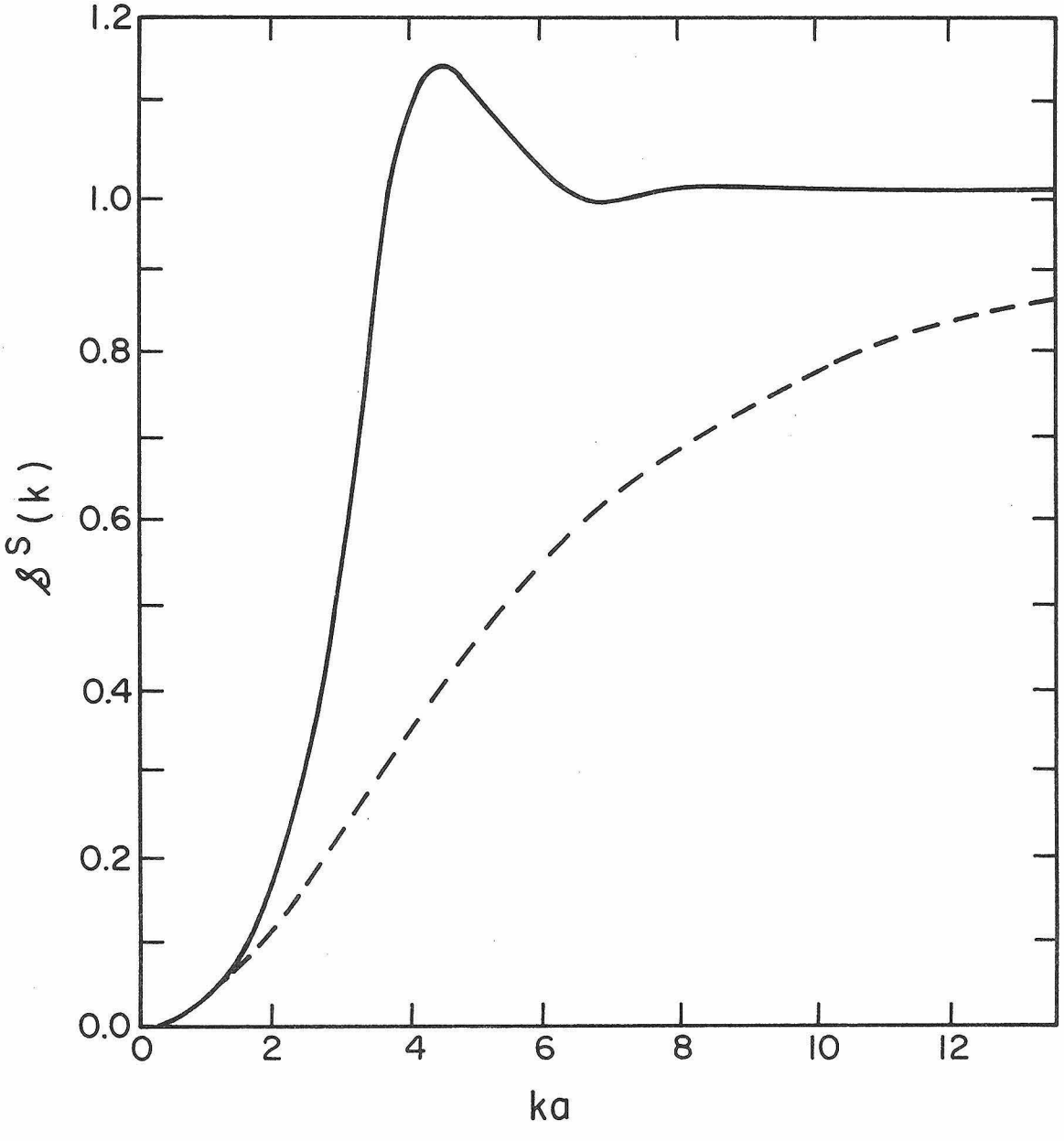

Fig. 4

FIGURE 5

The ratio of the transport rate with finite nuclear size corrections (labelled FNS) and ion-ion correlation effects (labelled IIC) to the transport rate with none of these corrections, for an iron-nickel plasma with $\Gamma = 10$; the FNS curve is independent of Γ. (Sections 4.3 and 4.4)

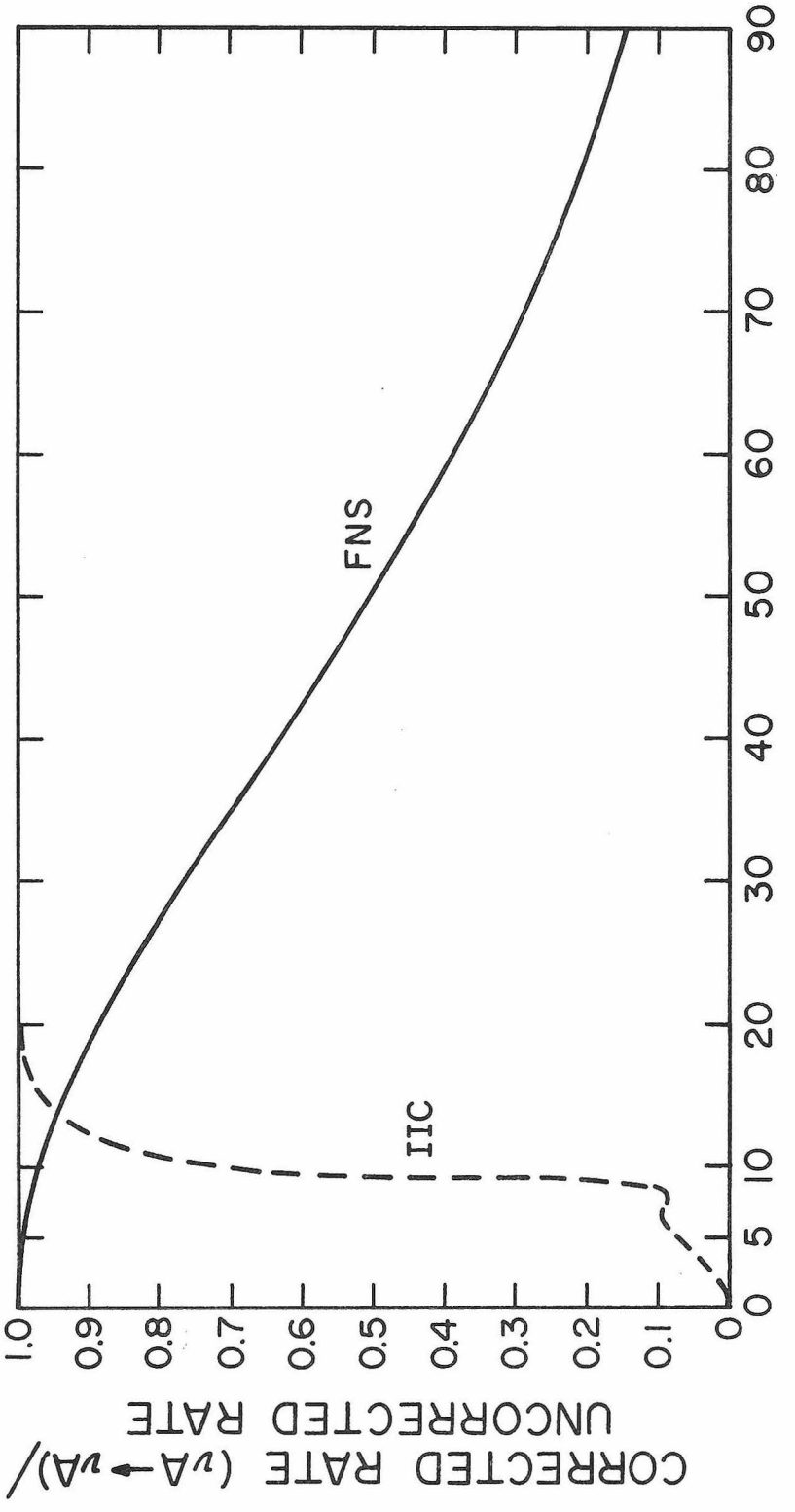
CORRECTED RATE ($\nu_A \rightarrow \nu_A$)/
UNCORRECTED RATE
1.0
0.9
0.8
0.7
0.6
0.5
0.4
0.3
0.2
0.1
0
0 5 10 20 30 40 50 60 70 80 90
ν (MeV)
FNS
IIC

Fig. 5

FIGURE 6

The zero temperature dynamic liquid structure factor of nuclear matter in the independent quasiparticle approximation as a function of ω for fixed k; for illustration purposes we have chosen $k = 0.2\ p_F$. (Section 4.5 and A2.2)

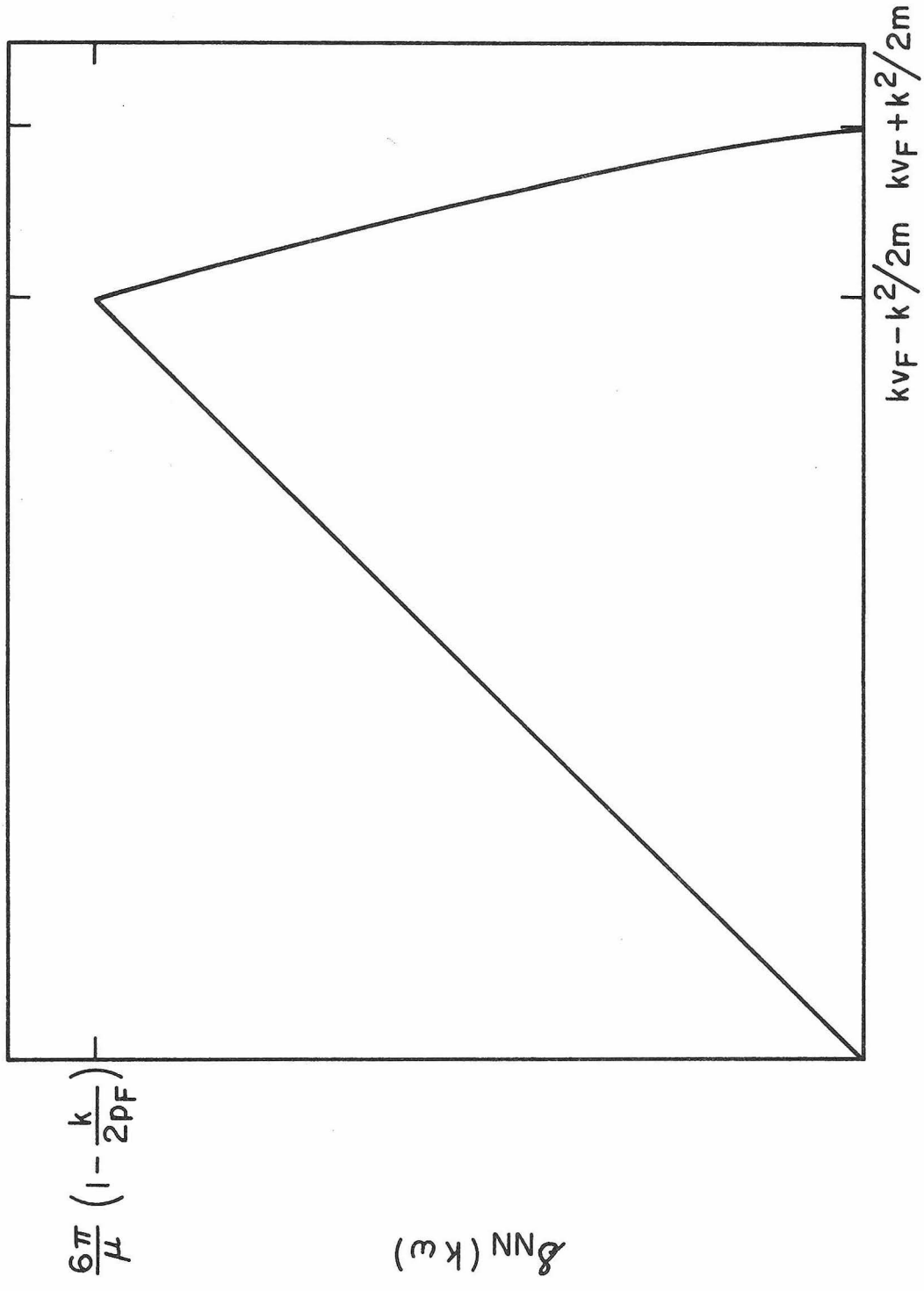
$\frac{6\pi}{\mu}\left(1-\frac{k}{2p_F}\right)$
$\rho_{NN}(k\omega)$
$kv_F-k^2/2m$
$kv_F+k^2/2m$
ω

Fig. 6

FIGURE 7

The appropriate regions for νN scattering at zero temperature in the $\omega = \nu - \nu'$ against $k_m = \nu + \nu'$ plane. The regions I to IV are defined by A2.13. The ν, ν' axes are also shown. The region $\omega < 0$, and the region between the ω axis and the line $\omega = k^2/2m + kv_F$ are not kinematically allowed. (Section 4.5 and A2.2)

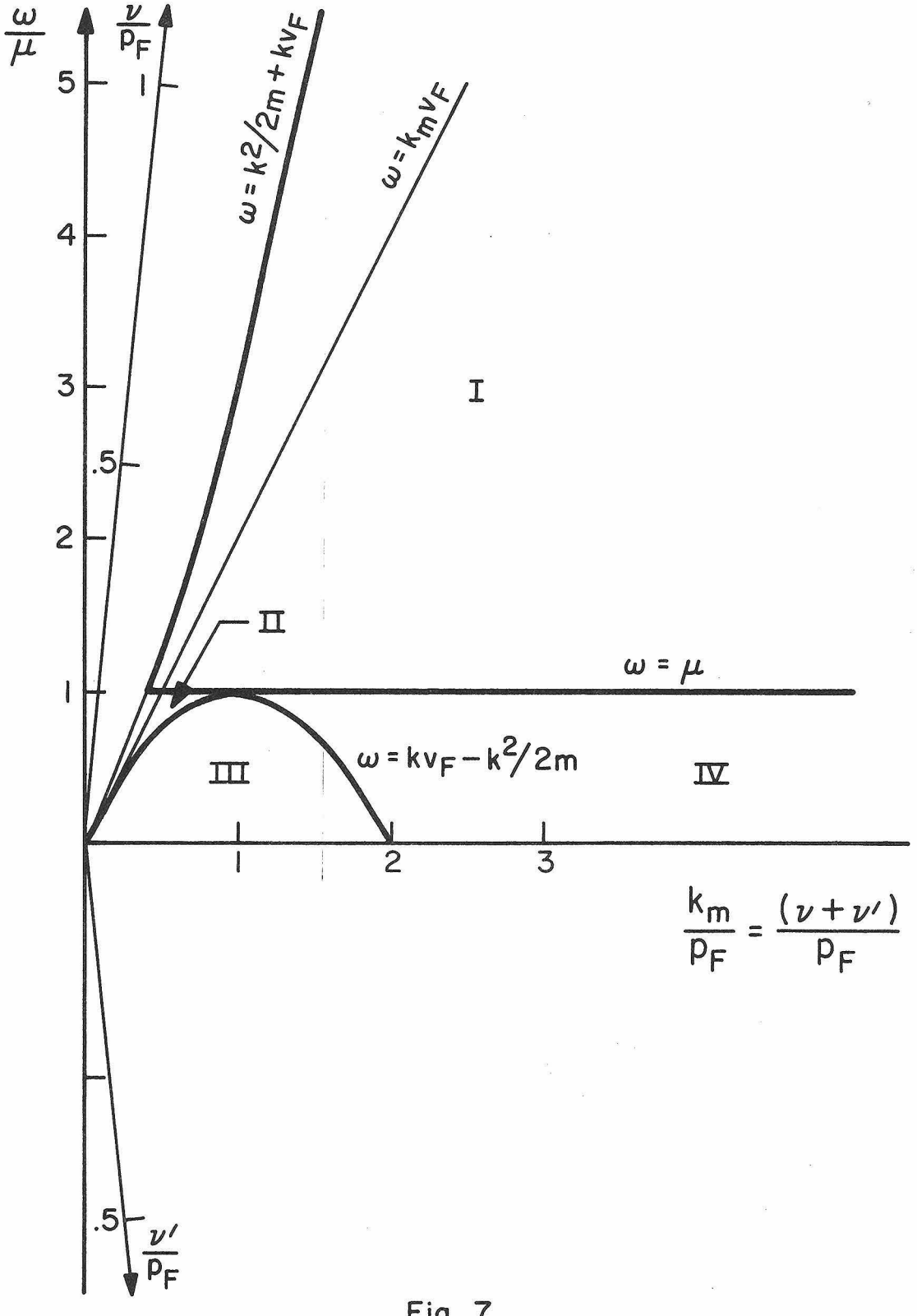
ω/μ
ν/p_F
5
1
4
3
.5
2
1
ω = k²/2m + kv_F
ω = k_m v_F
I
II
ω = μ
III
ω = kv_F − k²/2m
IV
1
2
3
k_m/p_F = (ν + ν′)/p_F
.5
ν′/p_F

Fig. 7

FIGURE 8

The differential scattering rate for neutrinos by neutrons in a zero temperature degenerate gas at $\rho = 5 \times 10^{13}$ g/cc, $Y_n = 0.9$ is plotted against final neutrino energy, ν', for 3 incident neutrino energies, 10, 50, and 100 MeV. The neutron Fermi energy is 17.9 MeV, and the Fermi momentum is 183.3 MeV.(Section 4.5 and A2.2)

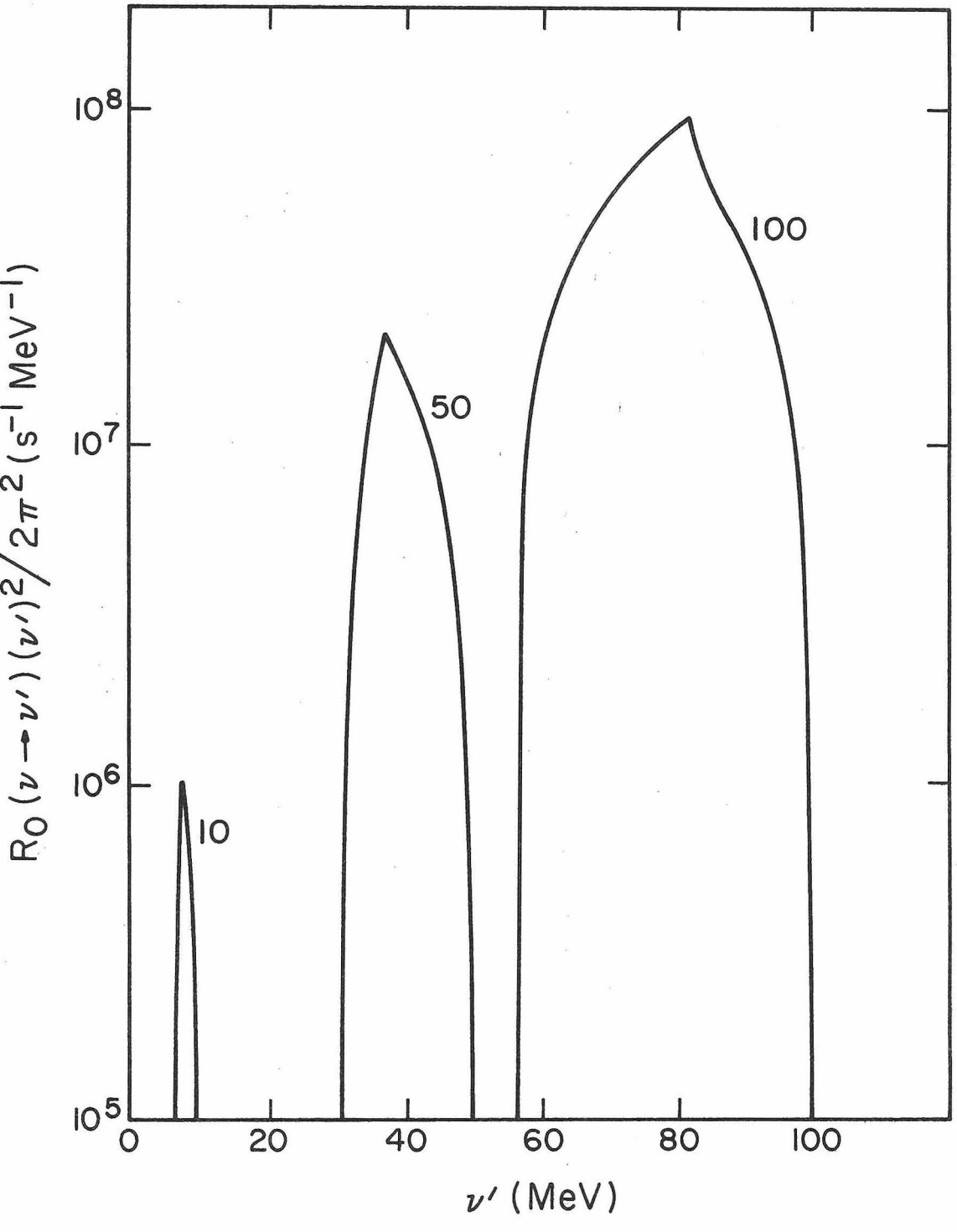
10^8
10^7
10^6
10^5
$R_0(\nu \to \nu')(\nu')^2/2\pi^2$ (s^{-1} MeV^{-1})
10
50
100
0
20
40
60
80
100
ν' (MeV)

Fig. 8

FIGURE 9

The density-temperature region of interest. The dashed line is the typical evolution of the central zone of a collapsing star in a hydrodynamic code (Arnett 1977). The points W1 and W2 are Wilson's (1977) two recorded hydrodynamic bounces. The nuclear degeneracy lines are η_B = 0, 5, and 10 (if Y_n = 1, these are η_n lines). The arrow denotes normal nuclear density, 2.8×10^{14} g/cc. The points labelled ep, $\gamma_{p\ell}$, e^+e^- are the conditions under which we focus on the evolution of ν_e's with source electron capture on free protons and the evolution of ν_μ's and $\bar{\nu}_\mu$'s with source $\gamma_{p\ell} \rightarrow \nu\bar{\nu}$ and $e^+e^- \rightarrow \nu\bar{\nu}$ respectively (Chapter 6). (Sections 4.5, 6.1, 6.2, 6.5, 6.6)

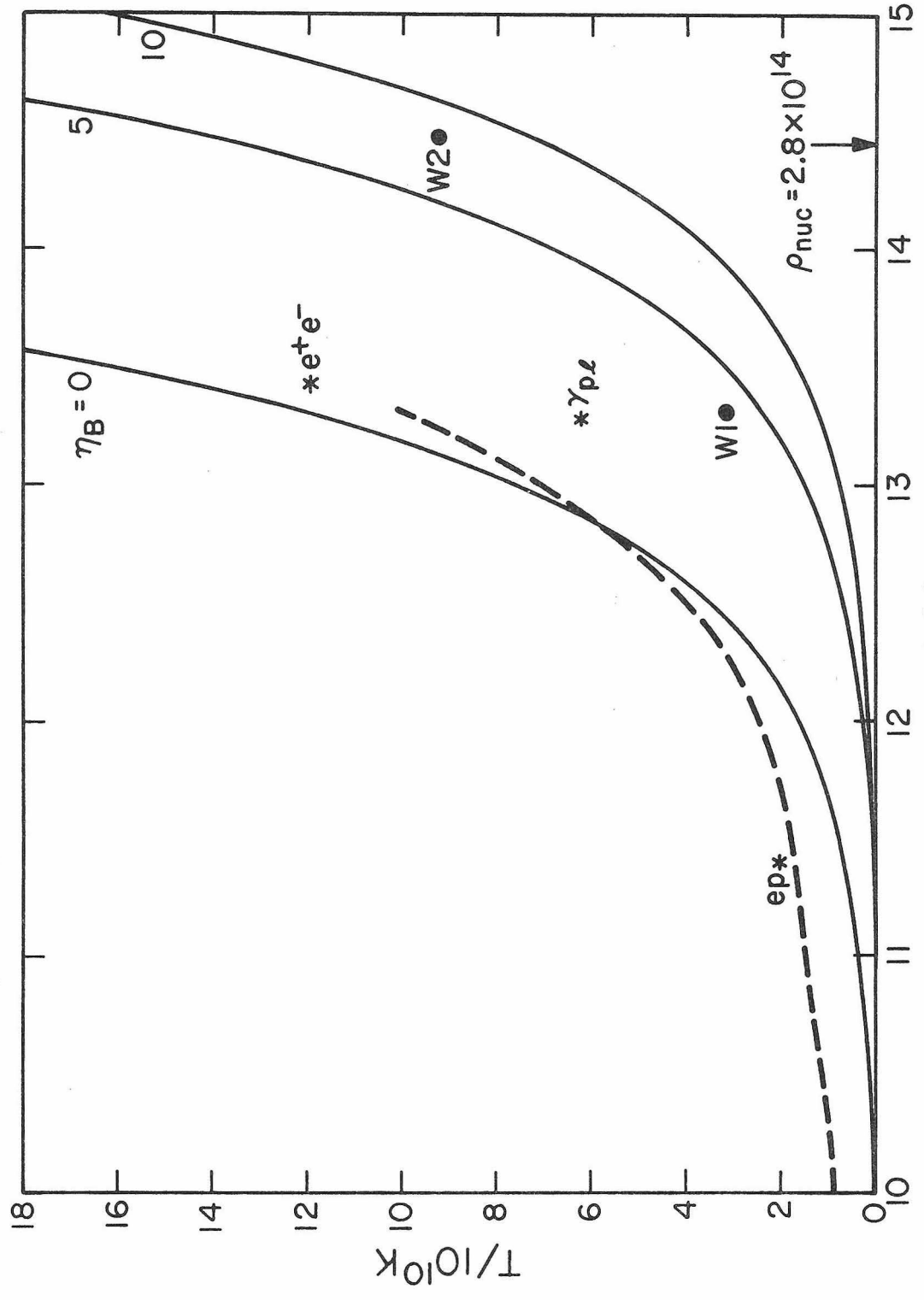
$\eta_B = 0$
5
10
$*e^+e^-$
$*\gamma_{p\ell}$
ep*
W1
W2
$\rho_{nuc} = 2.8 \times 10^{14}$
$T/10^{10}K$
LOGρ
0
2
4
6
8
10
12
14
16
18
10
11
12
13
14
15

Fig. 9

FIGURE 10

For three incident neutrino energies, ν = 10 MeV, 25 MeV and 50 MeV, the ℓ = 0 moment of the $\nu_e e \rightarrow \nu_e e$ scattering kernel is plotted against the outgoing neutrino energy. The temperature is 2×10^{10} K, the electron degeneracy parameter is 14, and $\rho_{11} Y_e = 1$. The electron chemical potential is indicated by the arrow. Upward pointing arrows under the curves denote the incident energies.(Section 4.6)

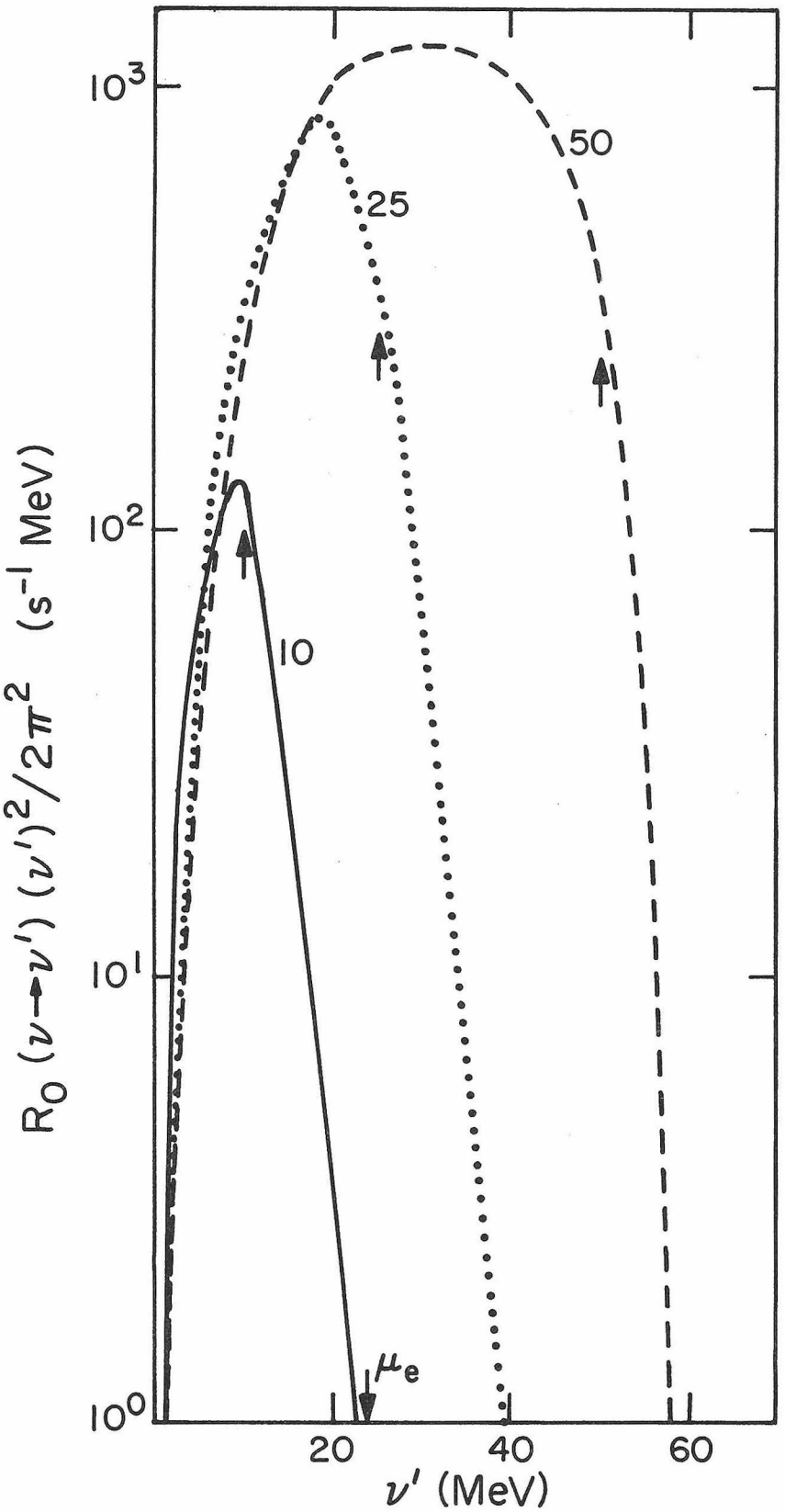
10^3
10^2
10^1
10^0
$R_0(\nu \to \nu')(\nu')^2/2\pi^2$ $(s^{-1}$ MeV)
50
25
10
μ_e
20
40
60
ν' (MeV)

FIGURE 10

FIGURE 11

The $\ell = 0$ moments of the $\nu_e e \to \nu_e e$ kernels at incident energy 25 MeV are given for two different temperatures, 2×10^{10} K and 3×10^{10} K, with the same chemical potential which is shown by a downward pointing arrow. Considerably more upscattering ($\nu' > \nu$) is allowed by the higher temperature kernel. (Section 4.6)

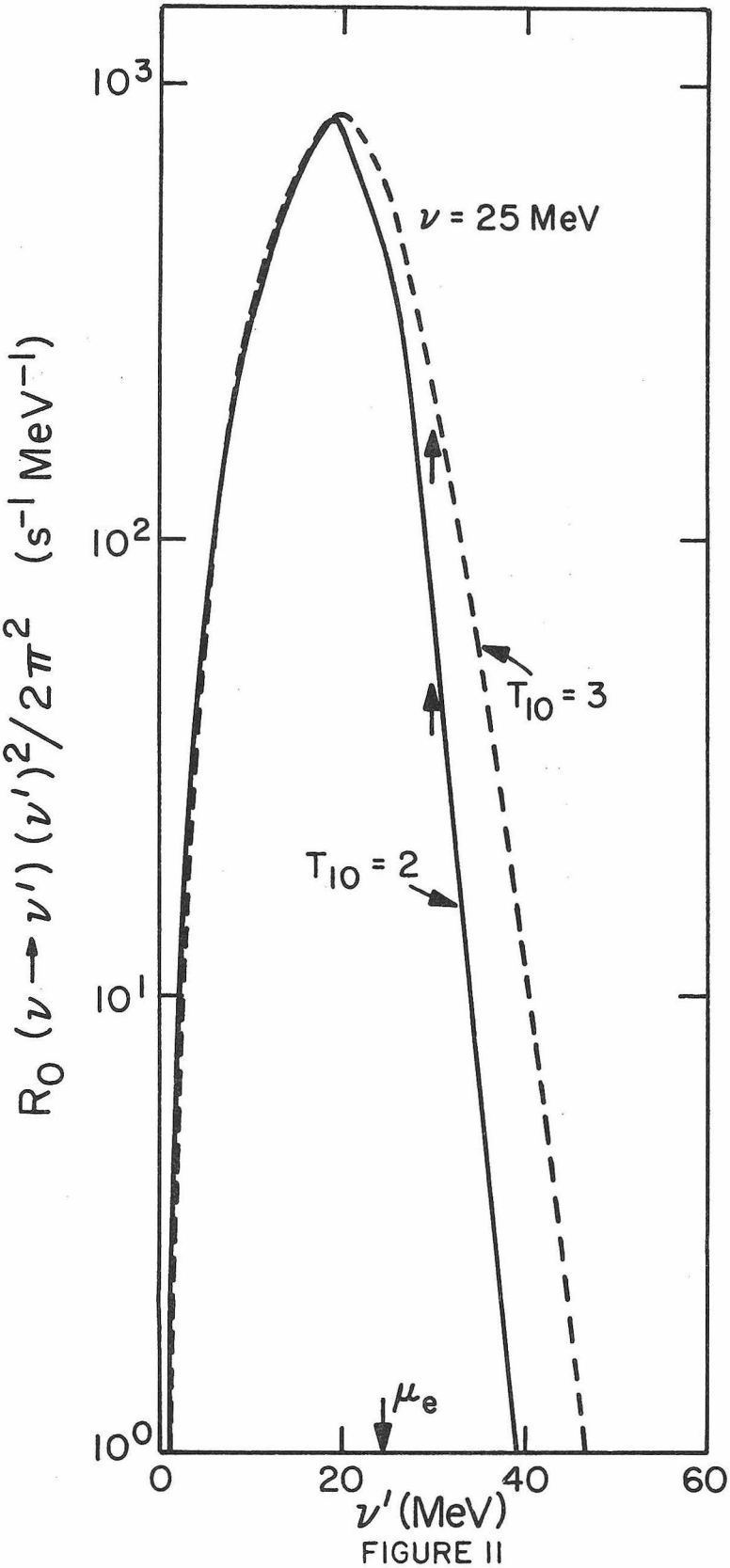
10^3
10^2
10^1
10^0
$R_0(\nu \rightarrow \nu')(\nu')^2/2\pi^2$ $(s^{-1}\,MeV^{-1})$
ν = 25 MeV
T_{10} = 3
T_{10} = 2
μ_e
0
20
40
60
ν' (MeV)

FIGURE 11

FIGURE 12

The first three moments, ℓ = 0, 1, 2, of the $\nu_e e \rightarrow \nu_e e$ scattering kernel at $\rho_{11} Y_e = 1$, $T_{10} = 2$ for an incident neutrino energy of 25 MeV.(Section 4.6)

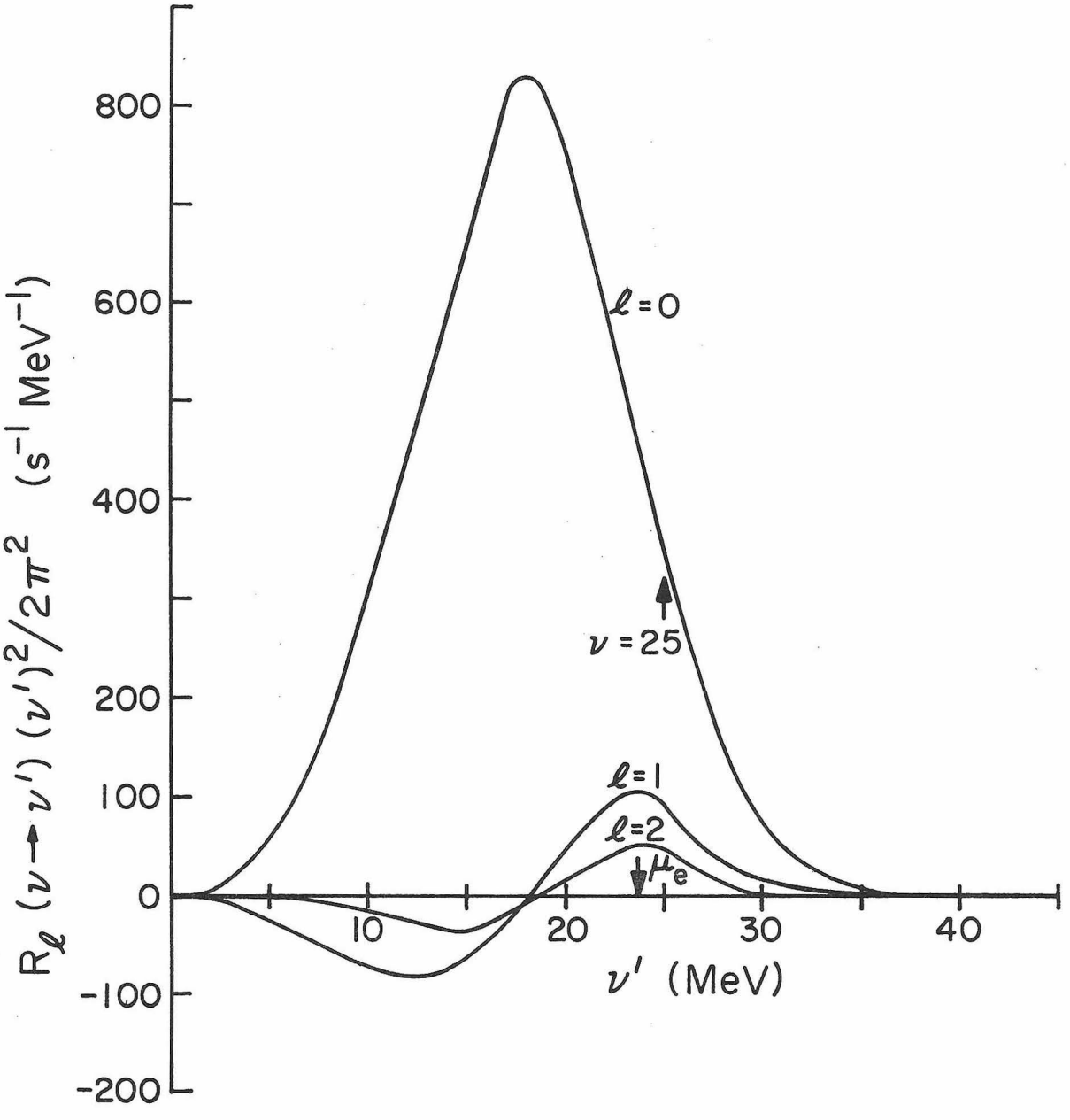
800
600
400
200
100
0
-100
-200
10
20
30
40
$R_\ell(\nu \to \nu')(\nu')^2/2\pi^2$ $(s^{-1}\,MeV^{-1})$
ν' (MeV)
$\ell=0$
$\nu=25$
$\ell=1$
$\ell=2$
μ_e

FIGURE 12

FIGURE 13

Graph of the transport rate against energy at $\rho = 2.54 \times 10^{11}$ g/cc, $T = 2 \times 10^{10}$ K, $Y_e = 0.4$, $Y_n = 0.6$, $Y_p = 0.4$. It is the scattering rate which is plotted for the electrons. At this temperature and density, we would actually have a mixed composition, consisting of alphas, neutrons, and protons, and some heavy nuclei. In order for $\nu\alpha \rightarrow \nu\alpha$ to dominate $\nu n \rightarrow \nu n$, it is necessary that the mass fraction in alphas be 6 times greater than the mass fraction in neutrons; in order for $\nu + A \rightarrow \nu + A$ to dominate, the mass fraction in heavies ($A \sim 56$) would have to be $\sim 44\%$ of that in free neutrons. Those curves would look very similar to the νn curve ($\sim \nu^2$). Also displayed are the production ($e^- p \rightarrow n\nu_e$) and absorption ($\nu_e n \rightarrow e^- p$) rates, as well as their sum, Γ'_a. The total transport rate Γ_{tr} is the sum over all the individual rates. The inverse diffusion time for neutrinos to escape a one-half solar mass core at this density (radius = 98 km) is τ_{diff}^{-1} : R/c is the light travel time across the core. (Sections 4.6, 5.1, 6.2, and 6.3)

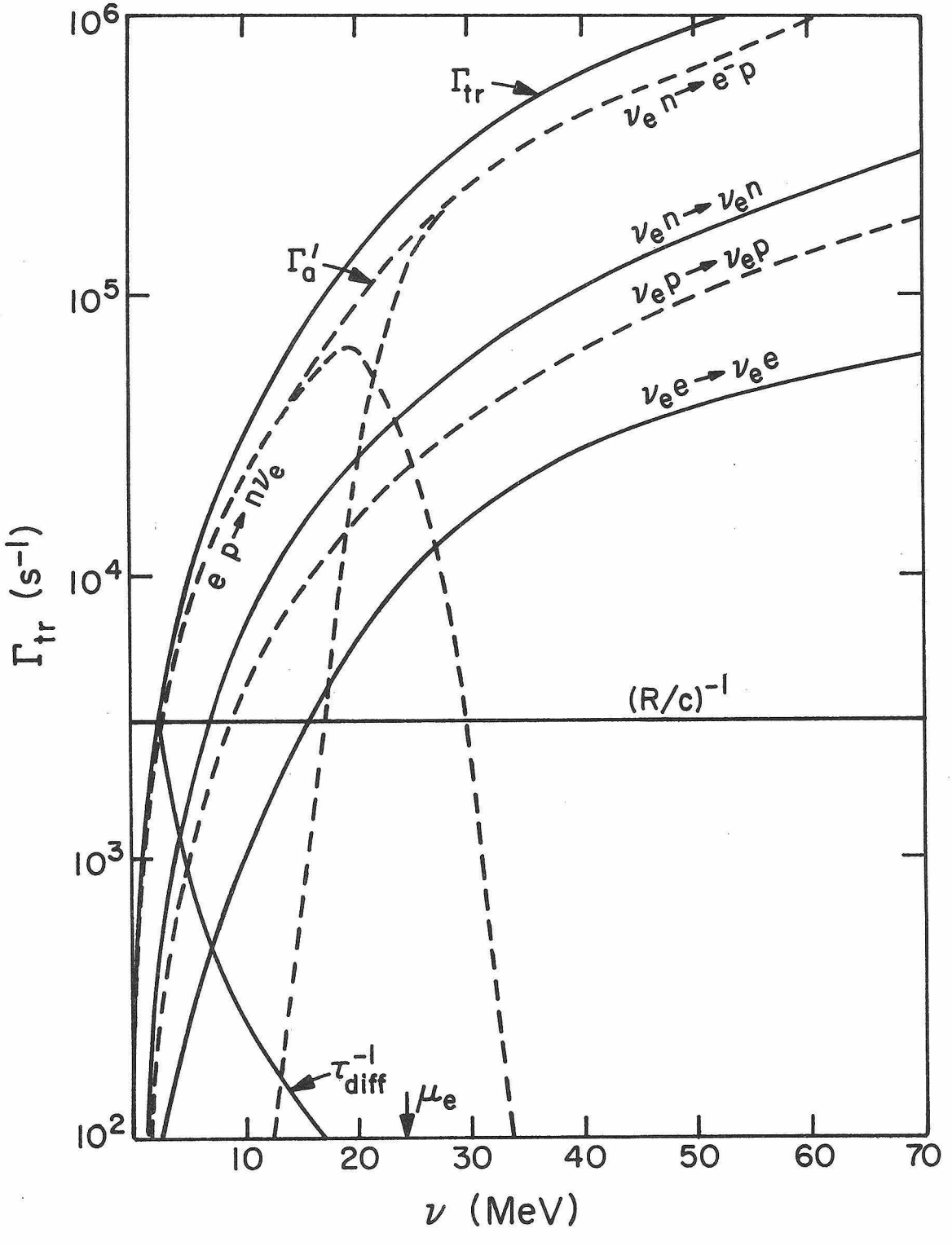
10^6
10^5
10^4
10^3
10^2
Γ_{tr} (s^{-1})
Γ_{tr}
Γ_a'
$\nu_e n \rightarrow e^- p$
$\nu_e n \rightarrow \nu_e n$
$\nu_e p \rightarrow \nu_e p$
$\nu_e e \rightarrow \nu_e e$
$e^- p \rightarrow n\nu_e$
$(R/c)^{-1}$
τ_{diff}^{-1}
μ_e
10
20
30
40
50
60
70
ν (MeV)

FIGURE 13

FIGURE 14

A comparison of the $\nu_e e \rightarrow \nu_e e$ scattering rate with the neutrino nucleus transport rate at typical mantle conditions: $\rho = 10^{10}$ g/cc, $T_{10} = 1$, $Y_e = 0.46$, $\eta_e = 10$; the mantle is assumed to be composed only of A = 56 nuclei. (Section 4.6)

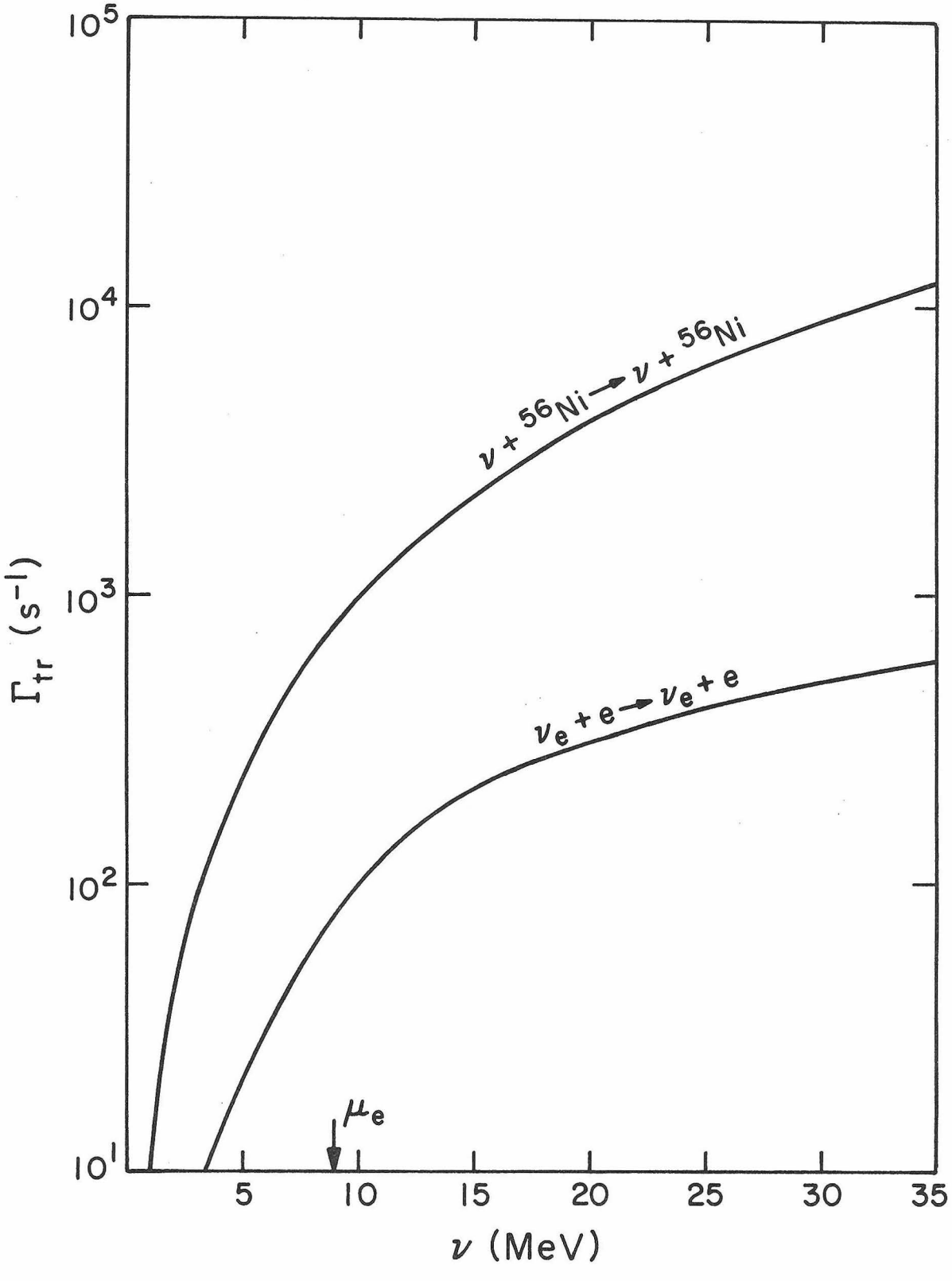
10^5
10^4
10^3
10^2
10^1
Γ_{tr} (s^{-1})
$\nu + {}^{56}Ni \rightarrow \nu + {}^{56}Ni$
$\nu_e + e \rightarrow \nu_e + e$
μ_e
5
10
15
20
25
30
35
ν (MeV)

FIGURE 14

FIGURE 15

The $\ell = 0$ moments of the production kernels for $e^+e^- \rightarrow \nu_\mu \bar{\nu}_\mu$ are plotted against the $\bar{\nu}_\mu$'s energy ν' for 4 values of the ν_μ's energy, 9, 40, 80, and 120 MeV. The conditions are $T = 1.2 \times 10^{11}$ K (= 10.34 MeV), $\eta_e = 7.5$, $\rho Y_e = 4.05 \times 10^{12}$.

(Sections 5.6 and 6.6)

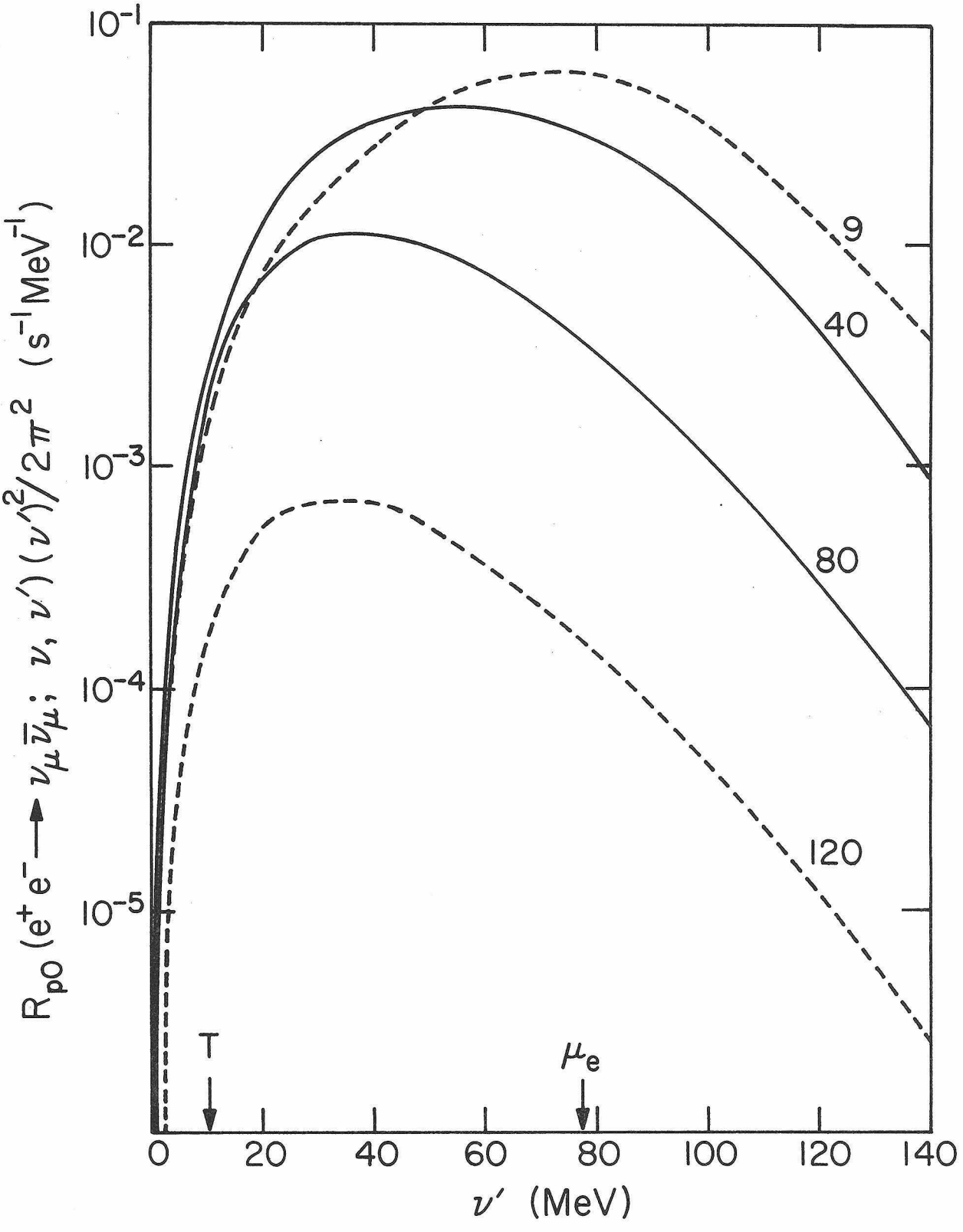
10^{-1}
10^{-2}
10^{-3}
10^{-4}
10^{-5}
$R_{p0}(e^+e^- \rightarrow \nu_\mu \bar{\nu}_\mu;\ \nu, \nu')(\nu')^2/2\pi^2$ ($s^{-1}MeV^{-1}$)
9
40
80
120
T
μ_e
0
20
40
60
80
100
120
140
ν' (MeV)

FIGURE 15

FIGURE 16

The $\nu_\mu(\bar{\nu}_\mu)$ production rates for $e^+e^- \rightarrow \nu_\mu\bar{\nu}_\mu$ are plotted against neutrino (antineutrino) energy for the conditions of Figure 15. A comparison with the total plasmon neutrino process production rate is also given (2.4×10^{29} erg cm^{-3} s^{-1} are radiated by $\gamma_{p\ell} \rightarrow \nu_\mu\bar{\nu}_\mu$, compared with 4.3×10^{32} erg cm^{-3} s^{-1}, for $e^+e^- \rightarrow \nu_\mu\bar{\nu}_\mu$). (Sections 5.6, 5.7, and 6.6)

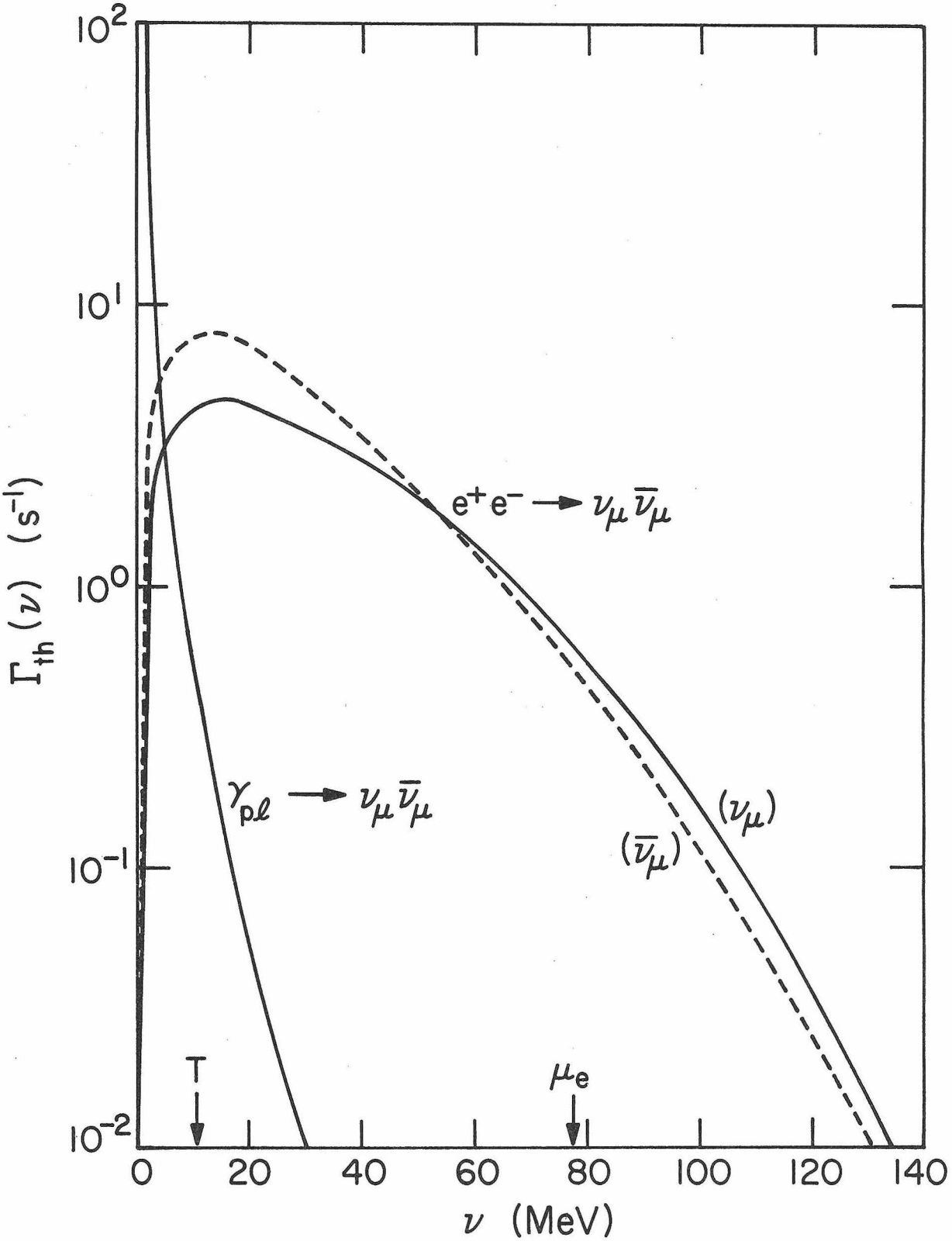
10^2
10^1
10^0
10^{-1}
10^{-2}
$\Gamma_{th}(\nu)$ (s^{-1})
$e^+e^- \rightarrow \nu_\mu \bar{\nu}_\mu$
$\gamma_{p\ell} \rightarrow \nu_\mu \bar{\nu}_\mu$
(ν_μ)
$(\bar{\nu}_\mu)$
T
μ_e
0
20
40
60
80
100
120
140
ν (MeV)

FIGURE 16

FIGURE 17

A graph in the temperature $-\rho Y_e$ plane displaying the region in which $e^+e^- \rightarrow \nu_e\bar{\nu}_e$ dominates the energy loss (to the left of the speckled line), and the region in which $\gamma_{pl} \rightarrow \nu_e\bar{\nu}_e$ dominates the energy loss (to the right) among the thermal $\nu\bar{\nu}$ emission mechanisms. Arnett's (1977) trajectory (dashed line) and the position of Wilson's (1977) first two hydrodynamical bounces (W1 and W2) are also shown. The constant η lines (0, 5, 10, 20, 40) are also displayed; these are also lines of constant $\beta\omega_p$ with values 0.1, 0.296, 0.566, 1.118, and 2.229 respectively, where ω_p is the plasma frequency. (Sections 5.6, 5.7)

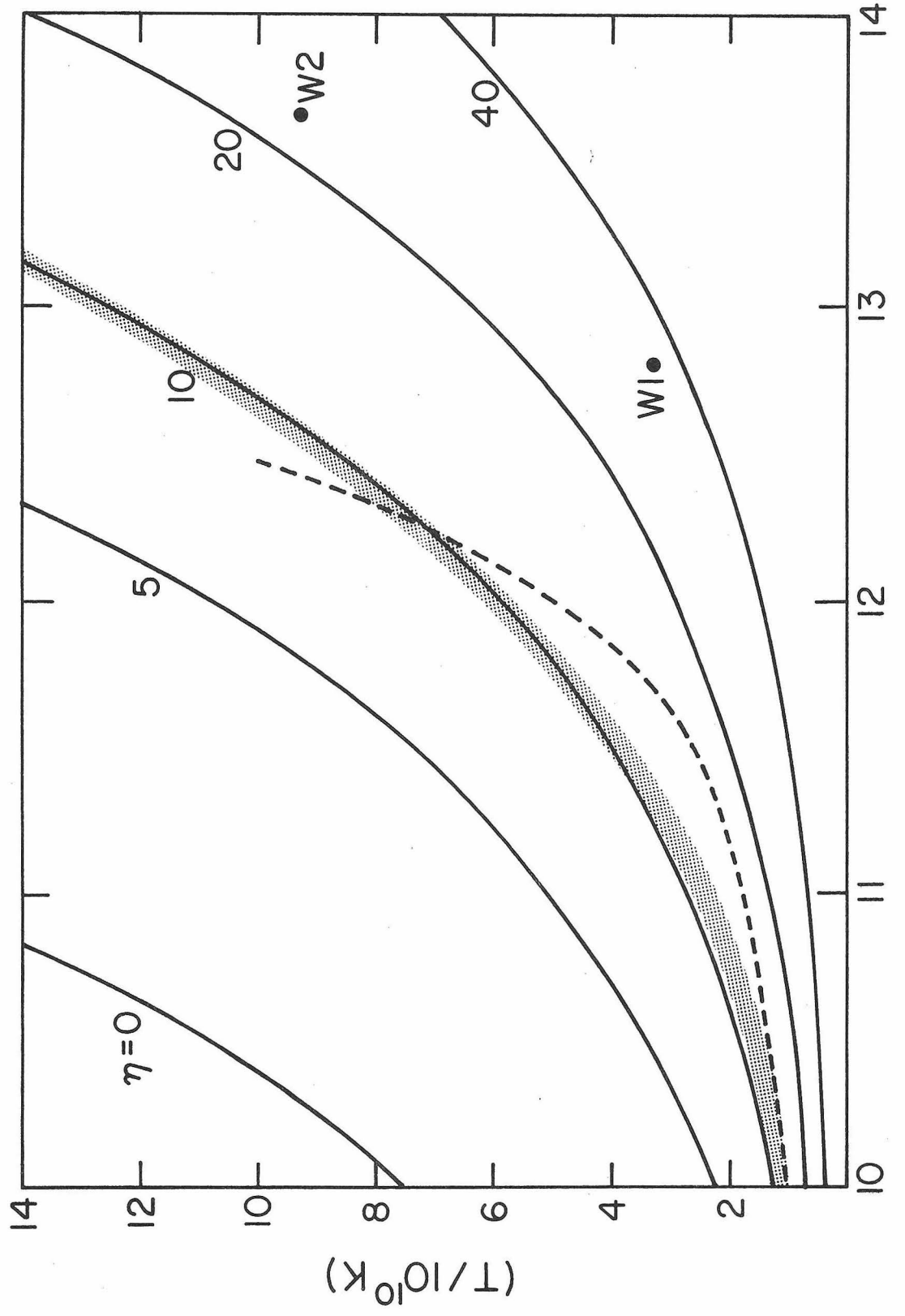

FIGURE 17

FIGURE 18

This graph is similar to Figure 17, but the demarcation is between $e^+e^- \rightarrow \nu_\mu \bar{\nu}_\mu$ and $\gamma_{p\ell} \rightarrow \nu_\mu \bar{\nu}_\mu$ (the former dominates the energy loss to the left of the speckled line, the latter to the right). We evolve the ν_e df under the conditions labelled ep in sections 6.2 and 6.3. We evolve the ν_μ and $\bar{\nu}_\mu$ df's under the conditions labelled e^+e^- and $\gamma_{p\ell}$ in section 6.6. The dashed line is Arnett's (1977) trajectory, and the thin solid line is a $\rho Y_e \sim T^{3/2}$ trajectory which passes through the point labelled by an open circle. The points W1 and W2 are Wilson's (1977) bounce conditions. In the shaded region, the freely streaming energy loss rate for thermal $\nu\bar{\nu}$ emission processes exceeds the diffusion rate of degenerate electron neutrinos from a 1/2 $M_\odot$ homogeneous core whose free proton and neutron abundances are frozen at 0.2 and 0.8 respectively. (Sections 5.6, 5.7, and 6.6)

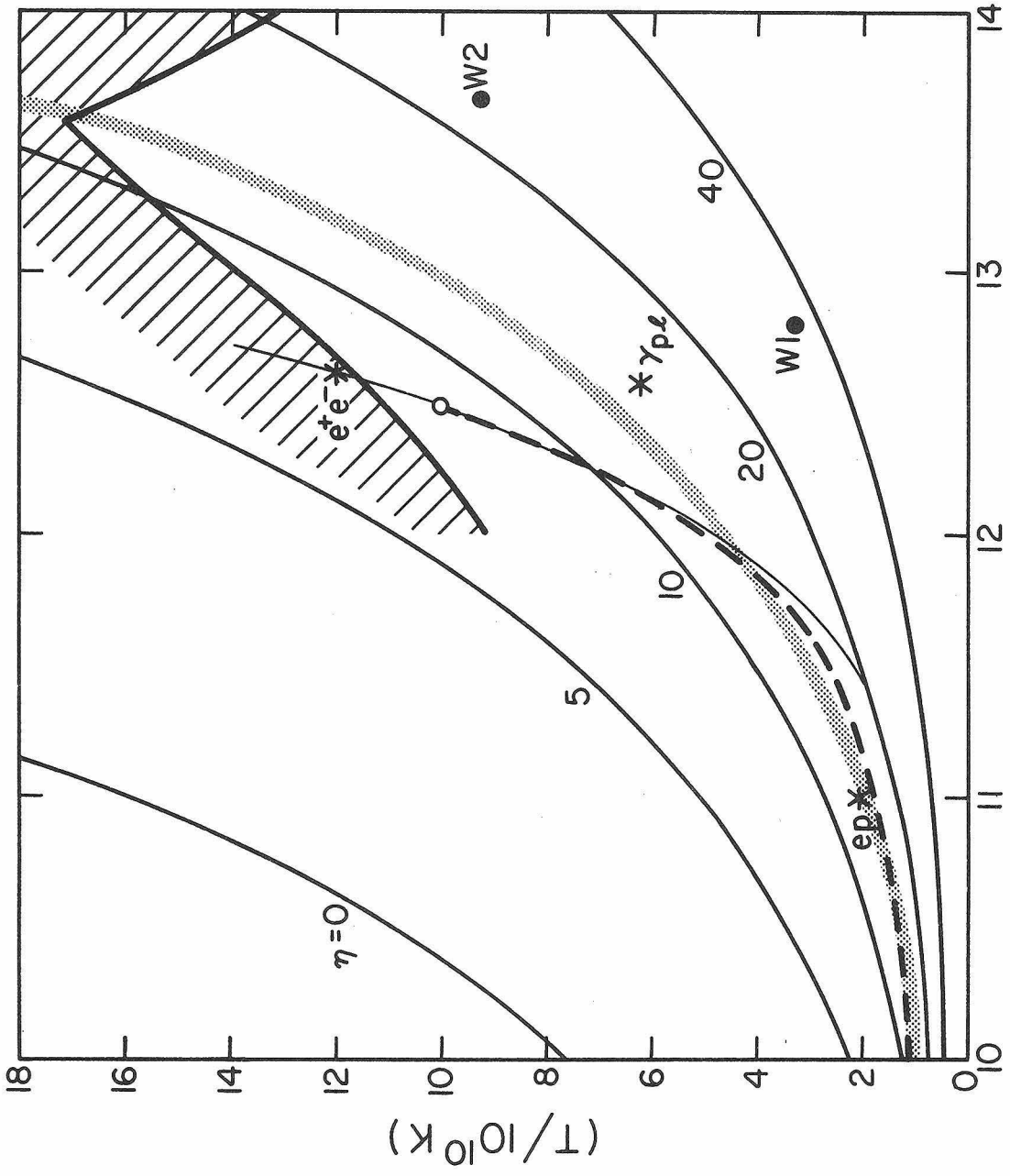

Fig. 18

FIGURE 19

The dispersion relations for longitudinal ($\omega_\ell(k)$) and transverse ($\omega_t(k)$) plasmons in ωk space. When $k = k_m = \nu - \nu'$, these curves give the boundary between the region in $\nu\nu'$ space where neutrinos and antineutrinos can be produced. Transverse plasmons create neutrinos of energy ν and antineutrinos of energy ν' in the cross hatched region. Longitudinal plasmons create $\nu\bar{\nu}$'s only in the shaded region. (Section 5.7)

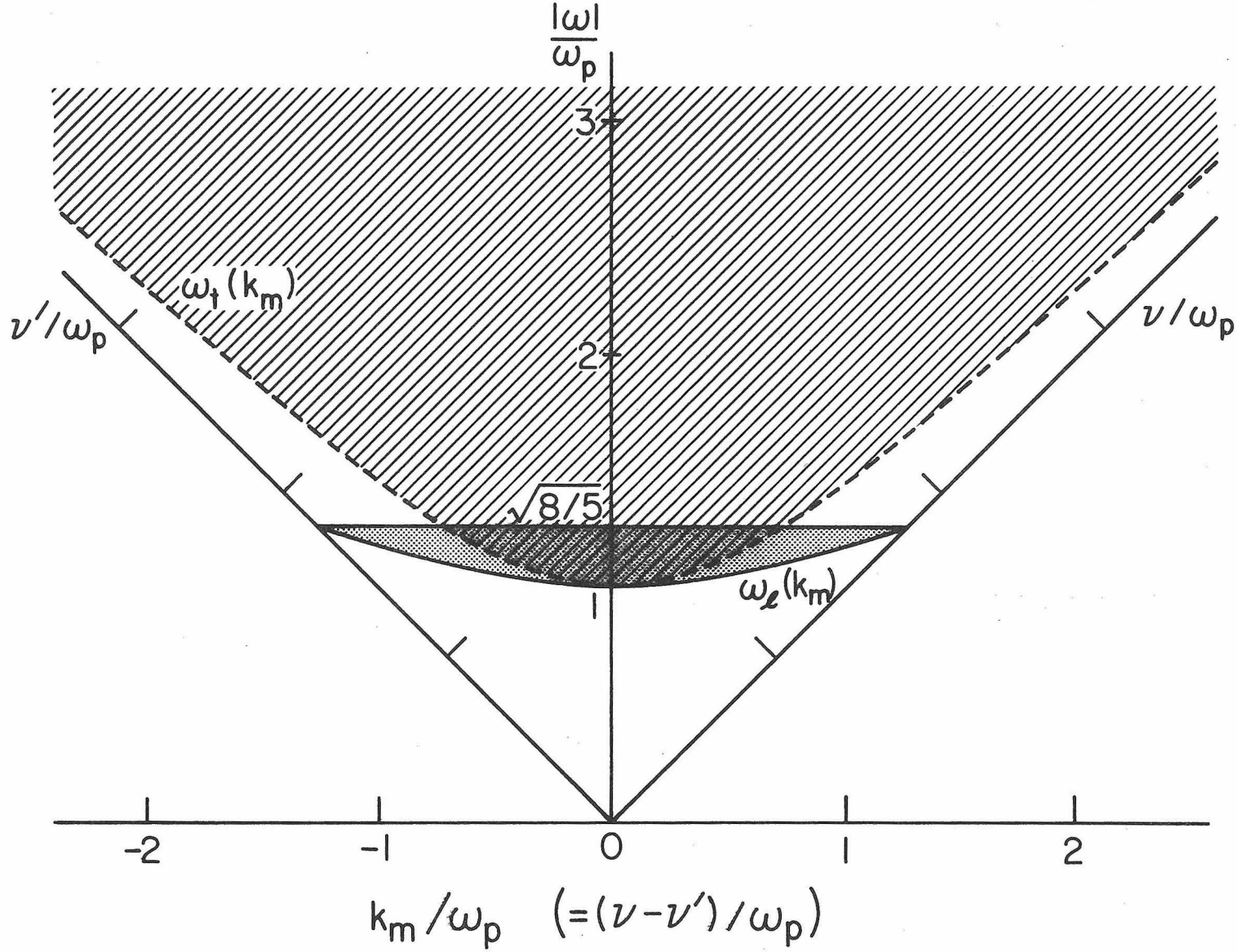

FIGURE 19

FIGURE 20

The ℓ = 0 moments of the transverse (tr) and longitudinal (long) plasmon neutrino process production kernels for various ν_μ energies (1.5, 4.0, and 8.0 MeV) against $\bar{\nu}_\mu$ energy. The temperature is 6.24×10^{10} K , η_e = 15, and ρY_e = 3.8×10^{12} g/cc. (Section 5.7)

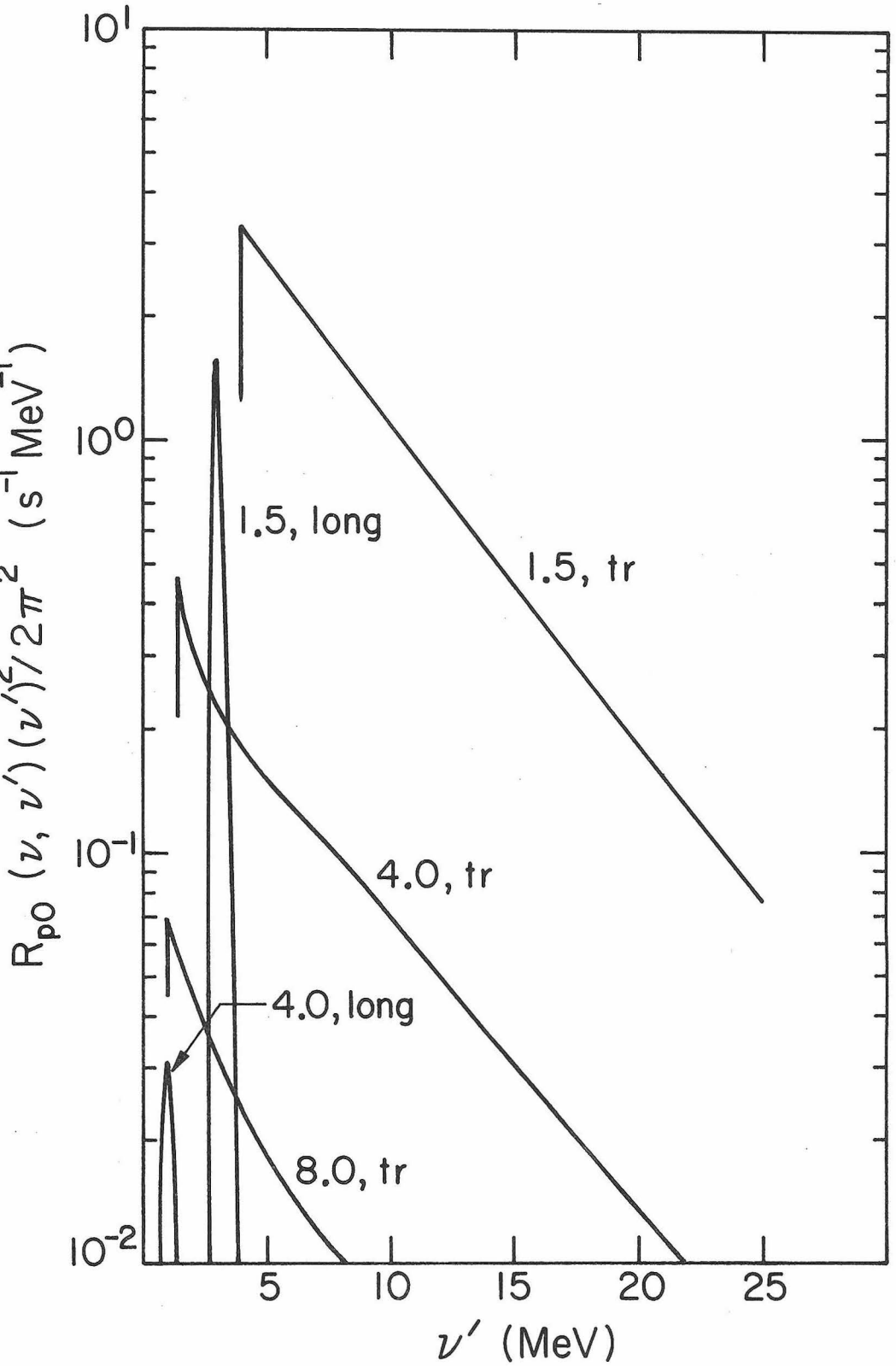
10^1
10^0
10^{-1}
10^{-2}
$R_{p0}(\nu, \nu')(\nu')^2/2\pi^2$ $(s^{-1}MeV^{-1})$
1.5, long
1.5, tr
4.0, tr
4.0, long
8.0, tr
5
10
15
20
25
ν' (MeV)

FIGURE 20

FIGURE 21

A comparison of the transverse and longitudinal plasmon neutrino process spectra for the conditions given in Figure 20. (Sections 5.7 and 6.6)

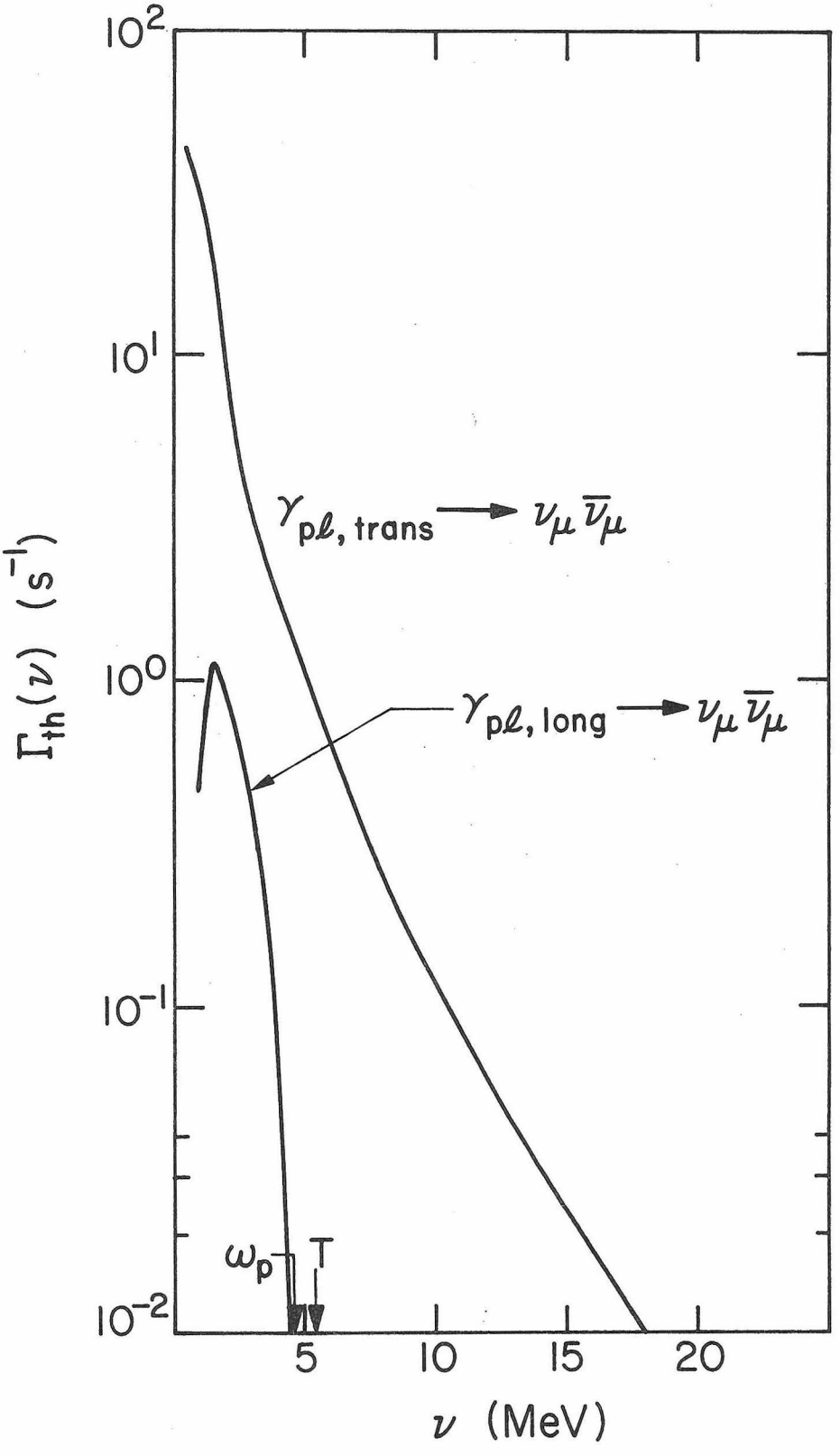
10^2
10^1
10^0
10^{-1}
10^{-2}
$\Gamma_{th}(\nu)$ (s^{-1})
$\gamma_{p\ell,\,trans} \rightarrow \nu_\mu \bar{\nu}_\mu$
$\gamma_{p\ell,\,long} \rightarrow \nu_\mu \bar{\nu}_\mu$
ω_p
T
5
10
15
20
ν (MeV)

FIGURE 21

FIGURE 22

A comparison of the plasmon (longitudinal plus transverse) neutrino process ν_μ production rate compared with the pair ν_μ production rate at $\eta = 10$, $T_{10} = 6.24$, $\mu_e = 53.8$ MeV, and $\rho Y_e = 1.13 \times 10^{12}$ g/cc. Choosing a definite $Y_e = 0.25$, so $\rho = 4.52 \times 10^{12}$, and for illustration purposes, $Y_n = 0.8$, $Y_p = 0.2$ (therefore neglecting the α's present), the diffusion time for a 1/2 $M_\odot$ core at this density is also plotted. The energy radiated in plasmon neutrinos is 3.5×10^{27} and in pair neutrinos is 3.2×10^{29} erg cm^{-3} s^{-1} . The energy radiated due to the decay of longitudinal plasmons alone is 2.5×10^{25} erg cm^{-3} s^{-1} ; the spectrum for this process is also shown. (Sections 5.7 and 6.6)

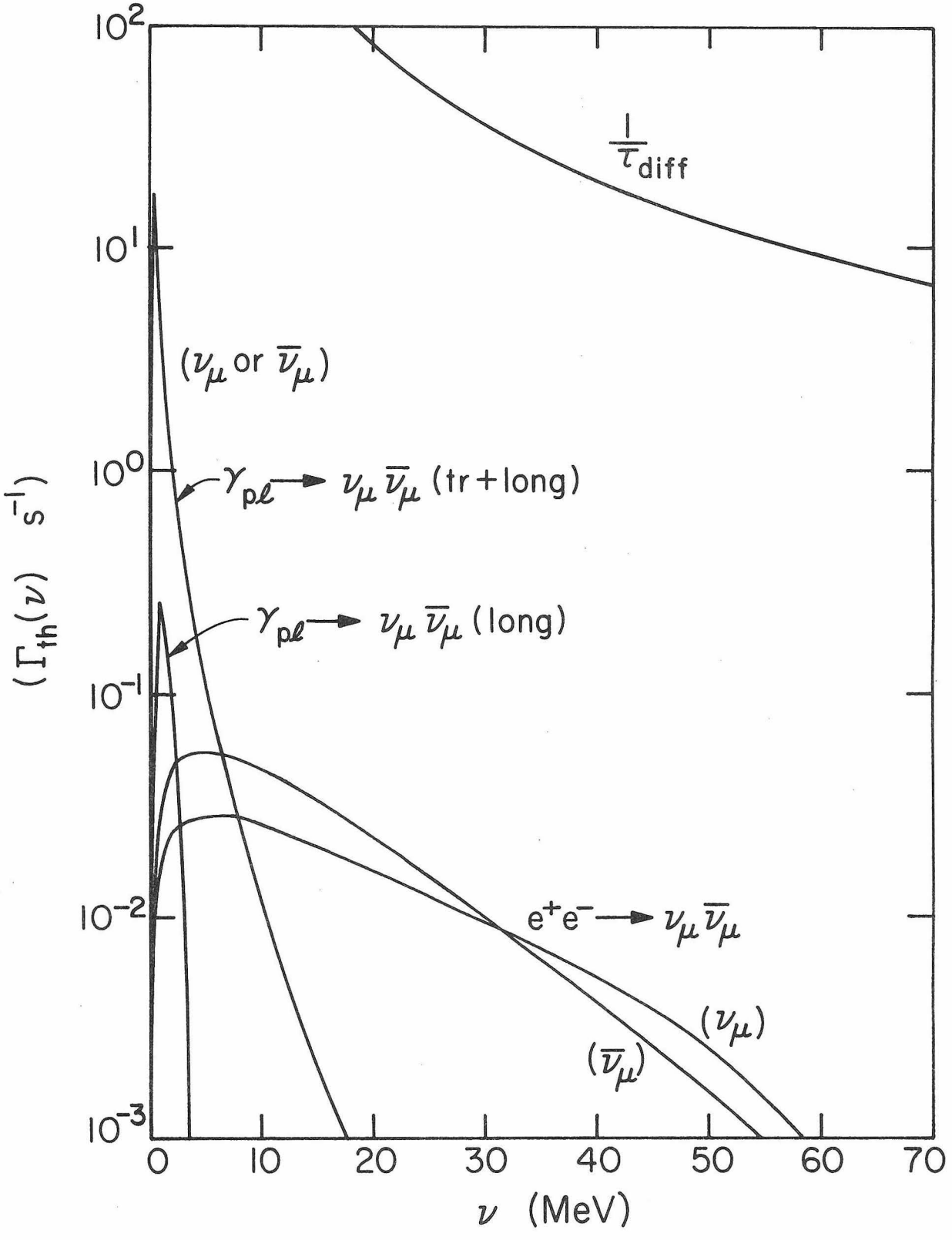
10^2
10^1
10^0
10^{-1}
10^{-2}
10^{-3}
$(\Gamma_{th}(\nu)\ s^{-1})$
$\frac{1}{\tau_{diff}}$
$(\nu_\mu \text{ or } \bar{\nu}_\mu)$
$\gamma_{p\ell} \rightarrow \nu_\mu \bar{\nu}_\mu$ (tr + long)
$\gamma_{p\ell} \rightarrow \nu_\mu \bar{\nu}_\mu$ (long)
$e^+e^- \rightarrow \nu_\mu \bar{\nu}_\mu$
(ν_μ)
$(\bar{\nu}_\mu)$
0
10
20
30
40
50
60
70
ν (MeV)

FIGURE 22

FIGURE 23

The ρT and ρY_e trajectories of ENB for the starting densities of 10^8, 10^9, and 10^{10} g/cc, the starting temperature of 4×10^9 K, the initial Y_e of 0.5, for $\chi_0 = 75$. The lines become dashed after trapping has occurred (see section 6.1 for discussion). The squares and triangles indicate the ENB estimate of when a core of mass 0.7 and 0.3 $M_\odot$ respectively would become dynamically decoupled from the regions above it. The three crosses indicate the thermodynamic conditions under which the approach to beta-equilibrium is calculated in section 6.2.

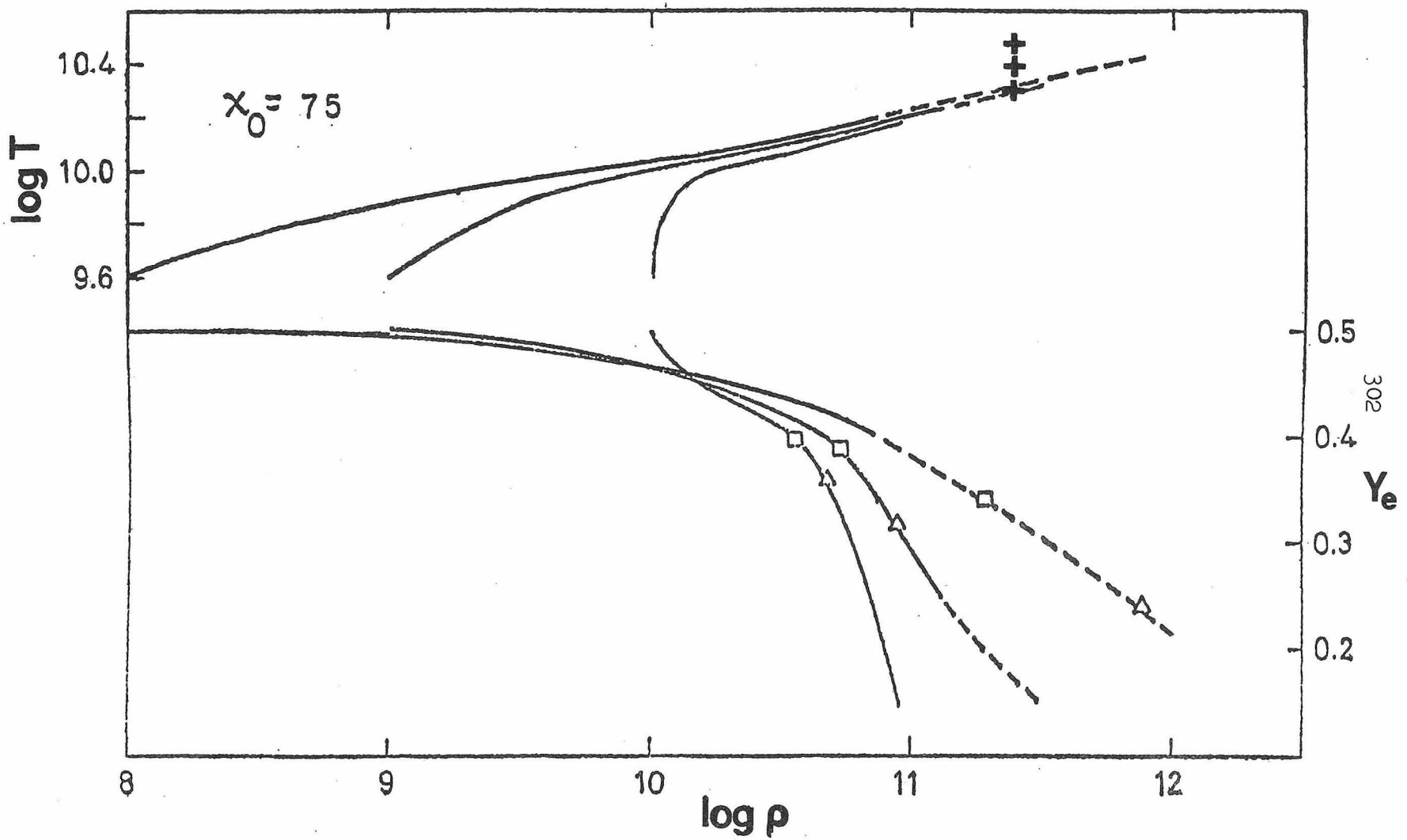

Fig. 2 3

FIGURE 24

The same as Figure 23 except that $\chi_0 = 224$.

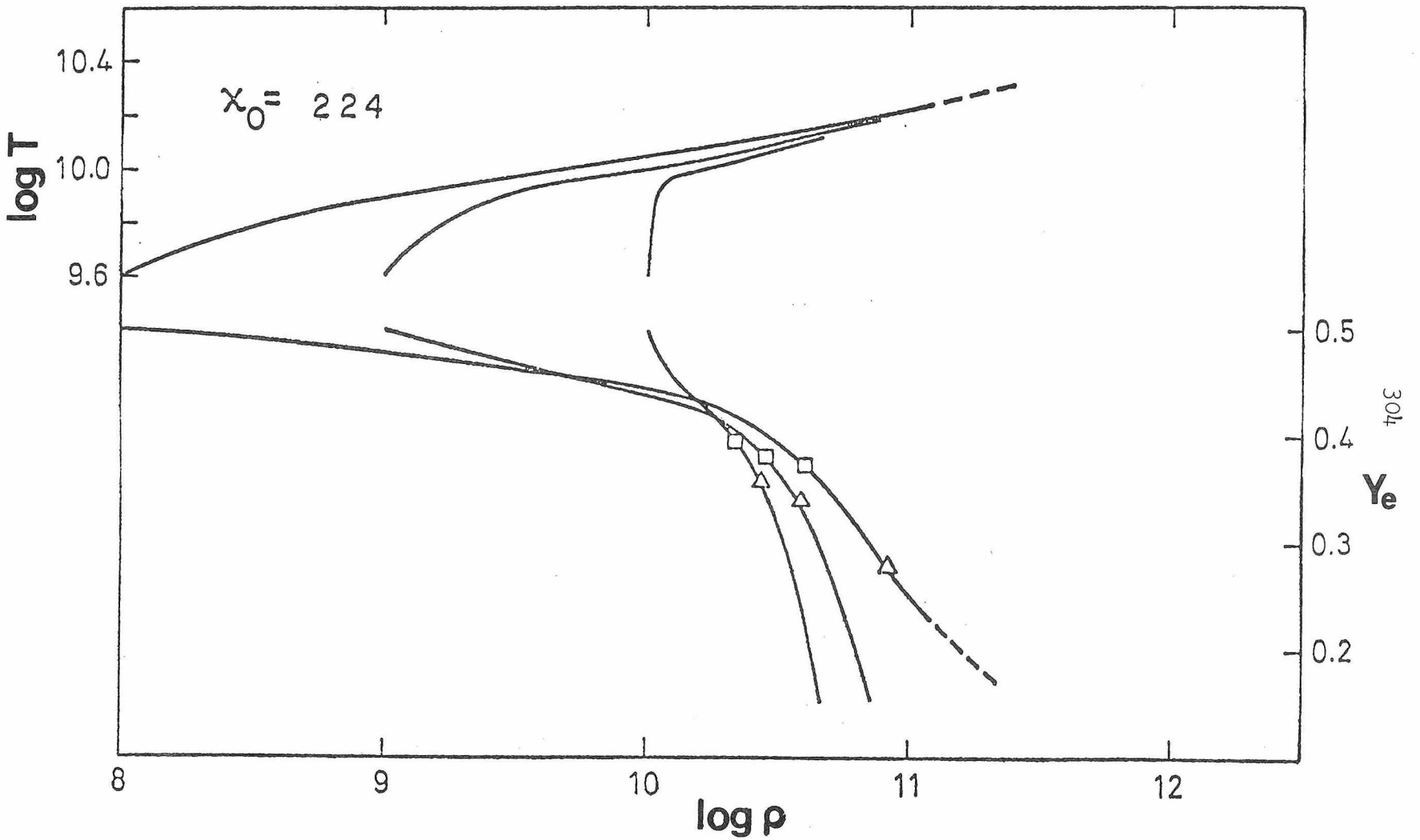

Fig. 24

FIGURE 25

The evolution of the ν_e df in a gas of free nucleons plus electrons at the density 2.54×10^{11} g/cc; the initial temperature and Y_e are 2×10^{10} K and 0.4 respectively. The three times indicated are 10^{-5} , 10^{-4} , and 10^{-3} s. The graph (b) has ν_ee scattering turned on; (a) does not. The equilibrium FD df is also shown, and its chemical potential, μ_ν , is indicated. (Section 6.2)

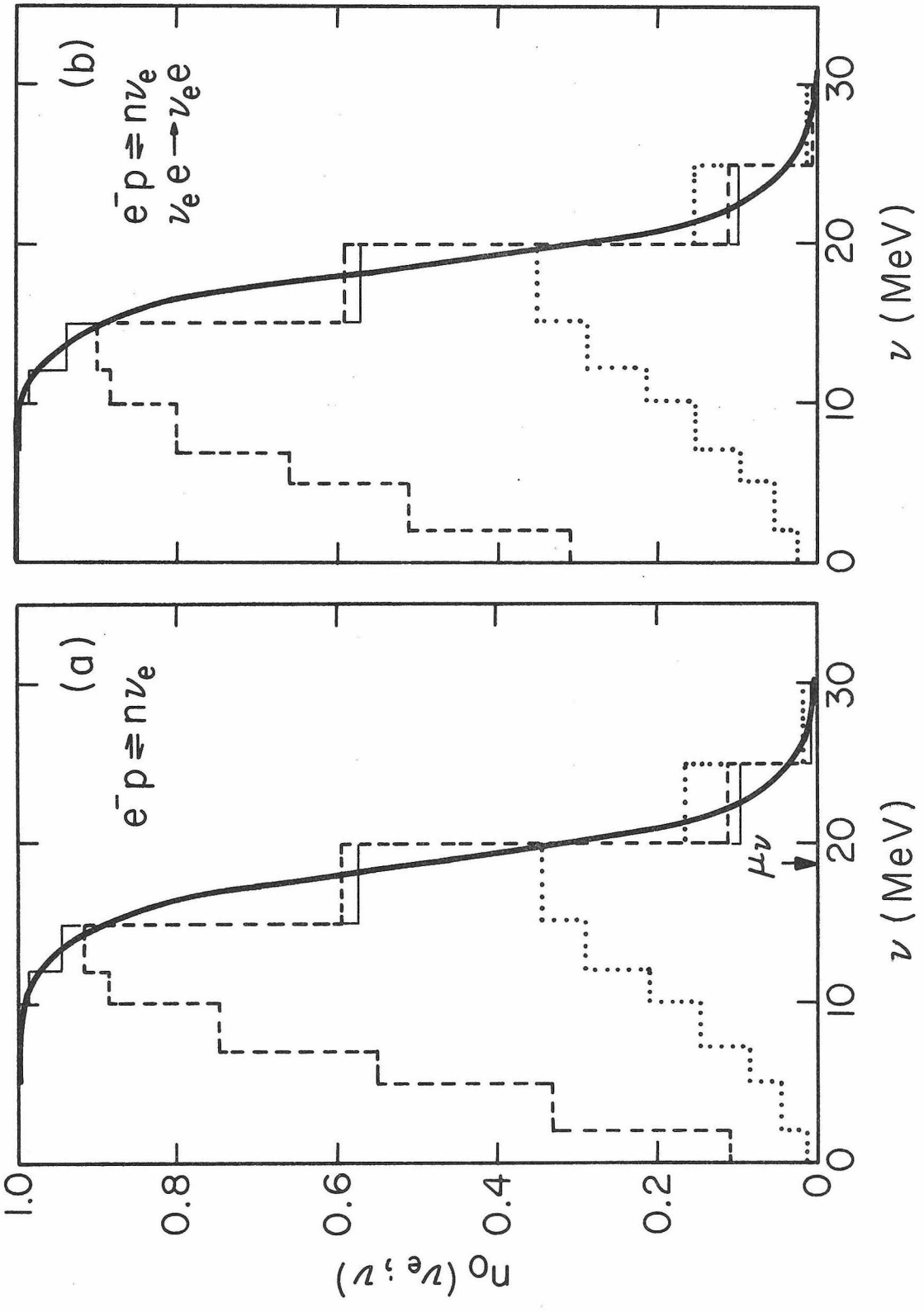

Fig. 25

FIGURE 26

The time dependence of Y_e , Y_ν , and T during the transformation to beta-equilibrium for the conditions of Figure 25. (Section 6.2)

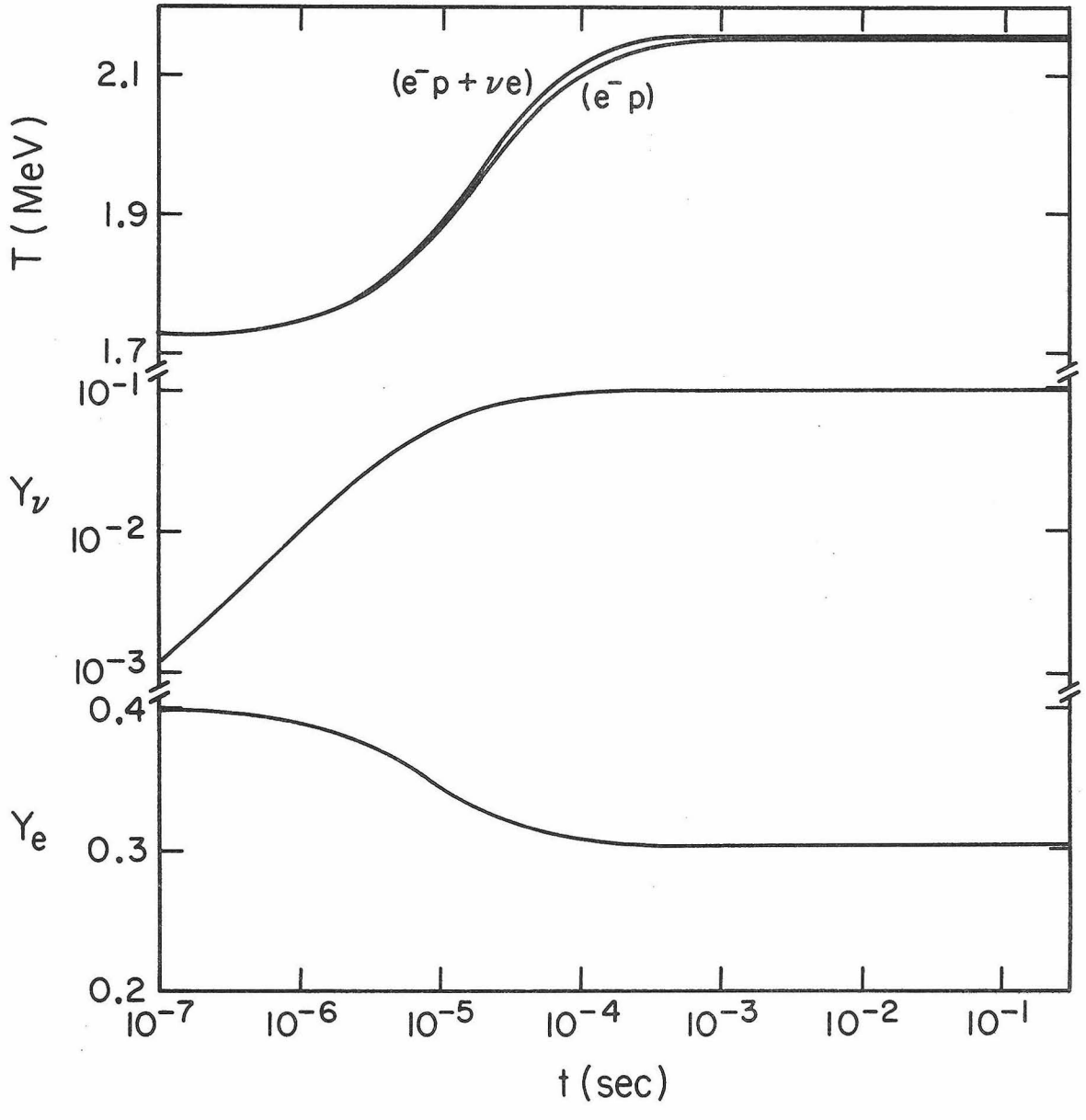
T (MeV)
2.1
1.9
1.7
$(e^- p + \nu e)$
$(e^- p)$
Y_ν
10^{-1}
10^{-2}
10^{-3}
Y_e
0.4
0.3
0.2
10^{-7}
10^{-6}
10^{-5}
10^{-4}
10^{-3}
10^{-2}
10^{-1}
t (sec)

Fig. 26

FIGURE 27

Figure (a) shows the approach to equilibrium with $e^- p \leftrightarrows n\nu_e$ only included, under the condition $T = 2\times10^{10}$ K, $\rho = 2.54\times10^{11}$ g/cc, $Y_e = 0.4$. The starting Y_p and Y_n are 1.43×10^{-4} and .0744, the final values are $.89\times10^{-4}$, .0750; the final Y_e = .3873, Y_ν = .0127. The times are .1094 ms (dot), 1.27 ms (dash), 12.4 ms (solid). Even after 1.9 s, equilibrium is still not attained in the lowest energy bins.

Figure (b) is the same as figure (a), but with $\nu_e + e \rightarrow \nu_e + e$ also turned on. The times are 0.1004 ms (dot), 1.17 ms (dash), and 14.6 ms (solid). The light dashed continuous line is the equivalent equilibrium Fermi-Dirac df at the time 1.17 ms ($\eta_\nu = 1.5$): the conduction approximation does not work here. By 60 ms, equilibrium is reached; the chemical potential, μ_ν , is also shown. (Section 6.2)

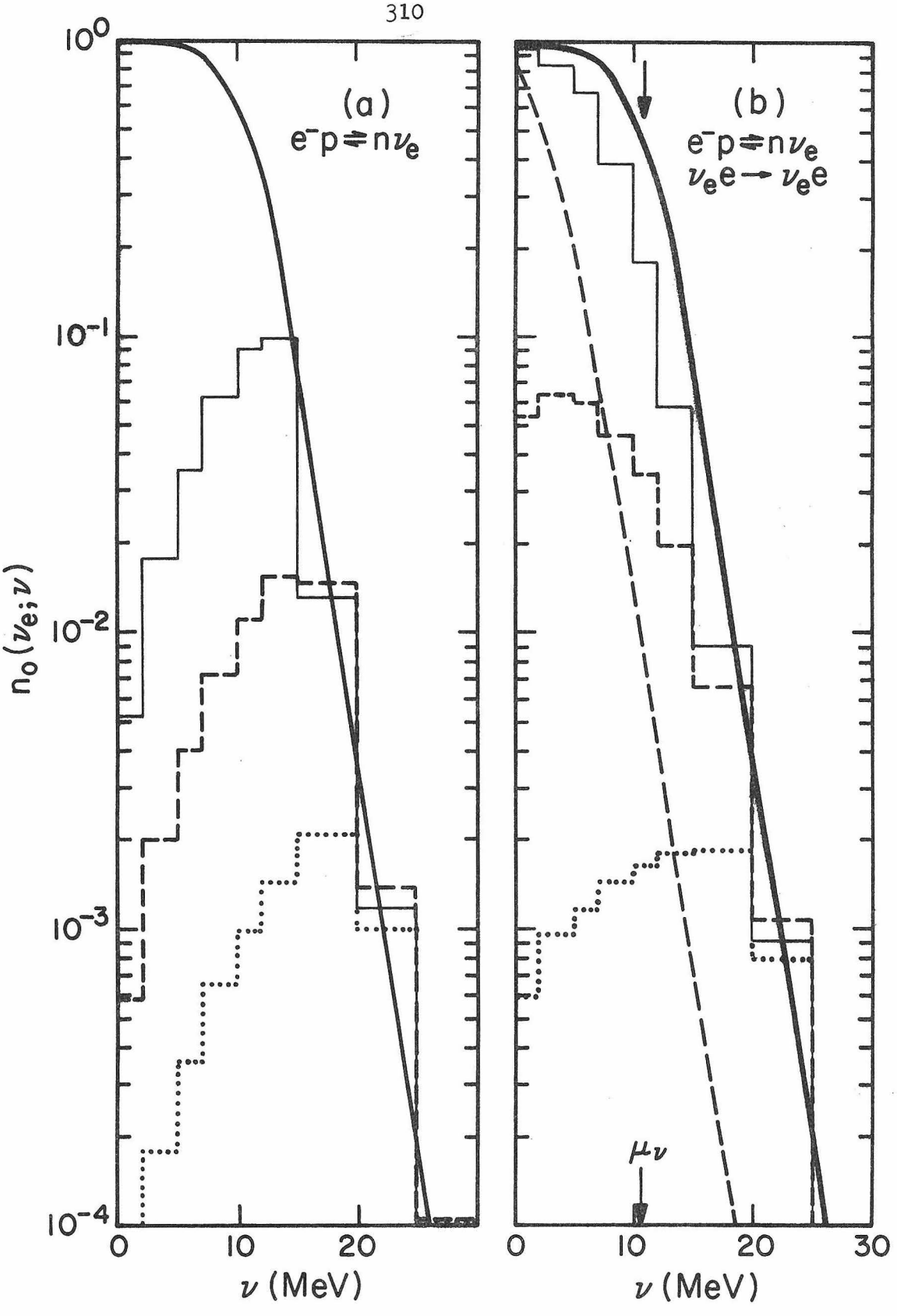
(a)
e⁻p⇌nνe
(b)
e⁻p⇌nνe
νee→νee
μν
n0(νe;ν)
ν (MeV)
ν (MeV)
10⁰
10⁻¹
10⁻²
10⁻³
10⁻⁴
0
10
20
0
10
20
30

Fig. 27

FIGURE 28

The curve (a) shows the approach to equilibrium under the hotter initial temperature 2.5×10^{10} K at the same density and Y_e as in Figure 27. The times are .1 ms (dotted line), .7647 ms (dashed line), and 19.9 ms (solid line); the continuous curve gives the equilibrium df, with $Y_e = 0.3609$, $Y_\nu = .039$. The starting Y_p and Y_n are .015 and .16, the final ones are .005863 and .1791 respectively. (Section 6.2)

The curve (b) shows the effect of diffusive transport from a homogeneous sphere of mass 0.5 $M_\odot$ and radius 98 km on the approach to equilibrium for the conditions of Figure 27. The matter heats up: the temperature at 60 ms is 2.476×10^{10} K (which incidentally causes the proton abundance to increase to 7.9×10^{-4} rather than decrease with neutronization). The medium has lost .128 leptons per baryon to diffusion at this stage, has a Y_e of .2707, which is still depleting, and a Y_ν of 1.69×10^{-3}, which is also depleting; the continuous curve is the equilibrium curve if the neutrinos were in beta-equilibrium at 60 ms and the solid histogram is the calculated df at this time. The df at 10 ms is similar to this one. The df at .1081 ms (dot) and 1.004 ms (dash) is also shown. The light solid curve is the energy flux of neutrinos from the homogeneous sphere; the axis is to the right. (Section 6.3)

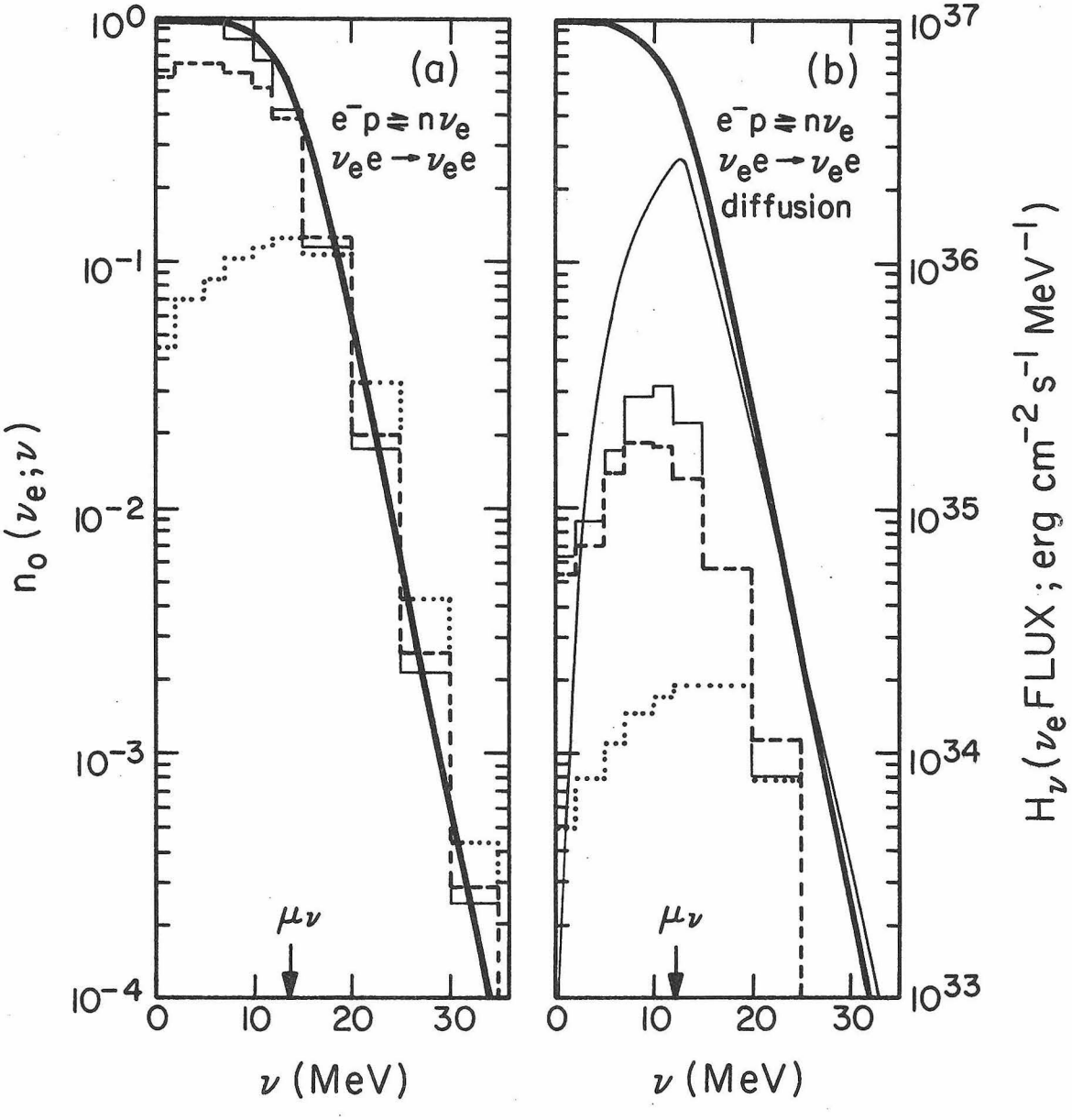
(a)
$e^- p \rightleftharpoons n\nu_e$
$\nu_e e \rightarrow \nu_e e$
μ_ν
$n_0(\nu_e;\nu)$
ν (MeV)
(b)
$e^- p \rightleftharpoons n\nu_e$
$\nu_e e \rightarrow \nu_e e$
diffusion
μ_ν
ν (MeV)
$H_\nu(\nu_e$ FLUX ; erg cm^{-2} s^{-1} MeV^{-1})

Fig. 28

FIGURE 29

This graph shows the effect of dynamics as well as diffusion on the approach to equilibrium, when $e^- p \rightleftarrows n\nu_e$ and $\nu_e e \rightarrow \nu_e e$ are included. The df's are given at the following densities, temperatures, Y_e's and Y_p's: 7×10^{10} g/cc, 1.36 MeV, 0.3998, 2.34×10^{-5} (dot-dash); 10^{11} , 1.45, 0.3994, 3.7×10^{-5} (dot); 3×10^{11} , 1.79, 0.3948, 1.43×10^{-4} (dashed), and at this stage only 3.9×10^{-3} leptons per baryon have been lost, the remaining 1.3×10^{-3} leptons are trapped ν_e's ; 8.3×10^{11} , 2.35 , .3668, 6.3×10^{-4} (solid), a point at which we would say trapping has occurred; if electron captures on heavy nuclei (which dominates throughout most of this collapse) were included, the trapping density would be earlier; 4.1×10^{12}, 4.42, 0.26, 4.7×10^{-3} , $Y_\nu = .0326$, and here we certainly have a Fermi-Dirac df except for the very small depression in the 0.2 - 2 MeV bin, as is evidenced by the continuous curve which is a FD df with $\eta_\nu = 7.4$. (Section 6.3)

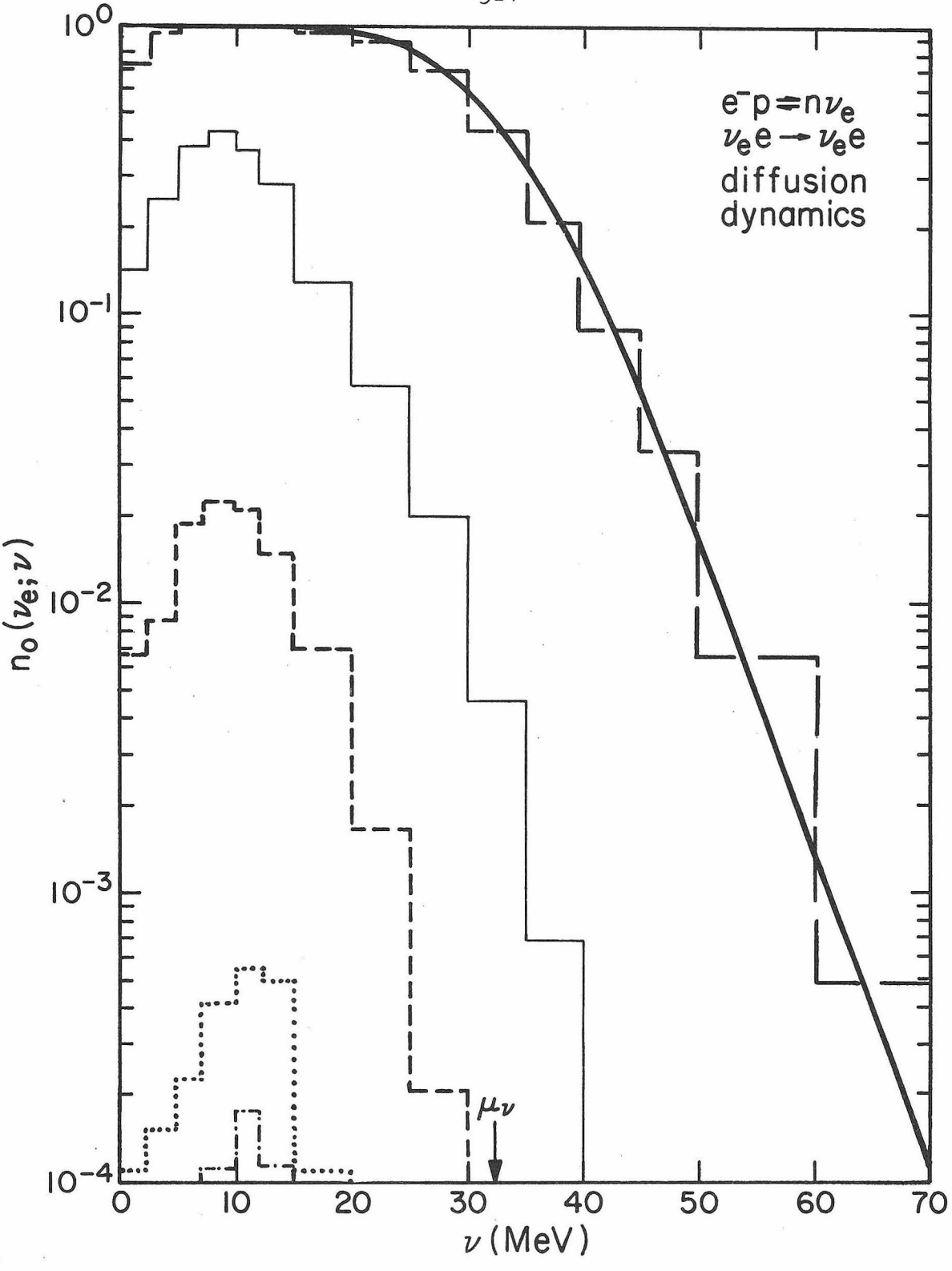
10^0
10^{-1}
10^{-2}
10^{-3}
10^{-4}
$n_0(\nu_e;\nu)$
$e^-p \rightleftharpoons n\nu_e$
$\nu_e e \rightarrow \nu_e e$
diffusion
dynamics
μ_ν
0
10
20
30
40
50
60
70
ν (MeV)

Fig. 29

FIGURE 30

The ν_μ df evolution for the conditions $\rho = 1.9 \times 10^{13}$ g/cc, $Y_e = 0.2$, $T = 6.24 \times 10^{10}$ K, $\eta_e = 15$, $\mu_e = 80.7$ MeV, $\eta_{\nu_e} = 13.37$, $\mu_{\nu_e} = 71.9$ MeV (for a free nucleon gas with $Y_n = 0.8$, $Y_p = 0.2$). The processes included are $\gamma_{p\ell} \rightarrow \nu_\nu \bar{\nu}_\mu$, $\nu_\mu \bar{\nu}_\mu \rightarrow \gamma_{p\ell}$, $\nu_\mu e \rightarrow \nu_\mu e$, and $\nu_\mu \nu_e \rightarrow \nu_\mu \nu_e$ (which dominates $\nu_\mu e$ with this neutrino chemical potential). The times are .102 ms, .96 ms, 20 ms, 105 ms ($Y_\nu = Y_{\bar{\nu}} = 4.41 \times 10^{-6}$) , 235 ms ($Y_\nu = 9.74 \times 10^{-6}$). Only 41% of the neutrinos are within $\nu \lesssim 12.5$ MeV once thermalization is attained. The equivalent neutrino chemical potentials are obtained from the Y_ν computed for the curve. When diffusion is turned on, almost all of the neutrinos escape, and a steady state distribution results after 1.5 ms (the dotted histogram). The $\bar{\nu}_\mu$ evolution is quite similar. (Section 6.6)

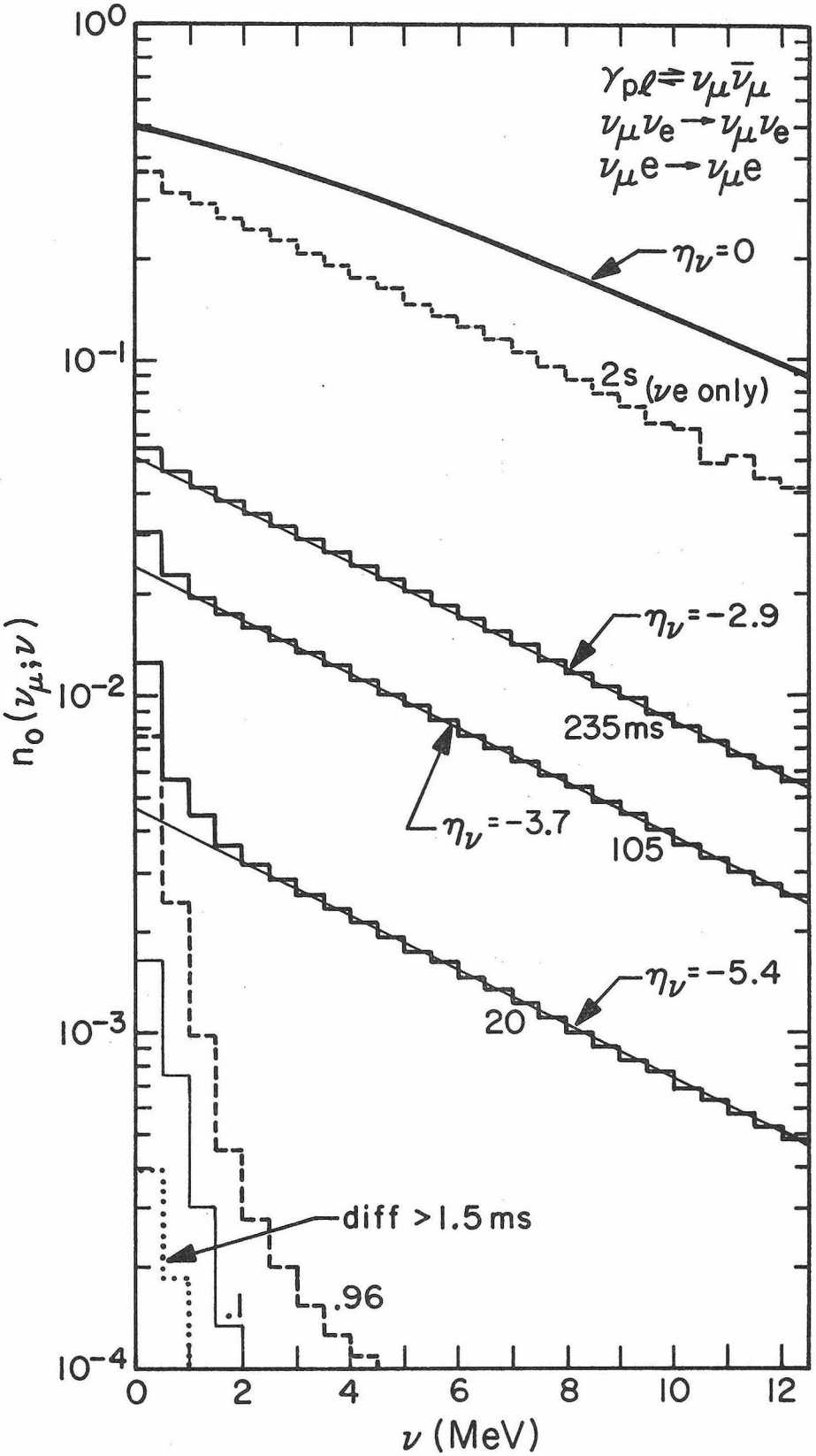
$\gamma_{p\ell} \rightleftharpoons \nu_\mu\bar{\nu}_\mu$
$\nu_\mu\nu_e \rightarrow \nu_\mu\nu_e$
$\nu_\mu e \rightarrow \nu_\mu e$
$\eta_\nu = 0$
2s (νe only)
$\eta_\nu = -2.9$
235ms
$\eta_\nu = -3.7$
105
$\eta_\nu = -5.4$
20
diff >1.5 ms
.96
.1
$n_0(\nu_\mu;\nu)$
10^0
10^{-1}
10^{-2}
10^{-3}
10^{-4}
0
2
4
6
8
10
12
ν (MeV)

Fig. 30

FIGURE 31

This graph presents a comparison of the scattering of muon neutrinos by electron neutrinos and electrons under the conditions $T_{10} = 12$, $\mu_e = 77.6$ MeV, $\eta_e = 7.5$, $\mu_\nu = 58.3$, $\eta_\nu = 5.64$ at $\rho = 2.7 \times 10^{13}$ g/cc, $Y_e = 0.15$; to get μ_ν, a pure nucleon gas in beta-equilibrium was assumed. Transport times for $\nu n \rightarrow \nu n$ ($Y_n = .85$) and $\nu p \rightarrow \nu p$ ($Y_p = 0.15$) are also shown, along with the very steeply falling diffusion rate, τ_{diff}^{-1}, from a 1/2 $M_\odot$ core at this density; τ_ℓ is the light crossing time of the core. The conditions of this figure are the same as those of Figure 16, where the thermal production process spectra are shown. (Section 6.6)

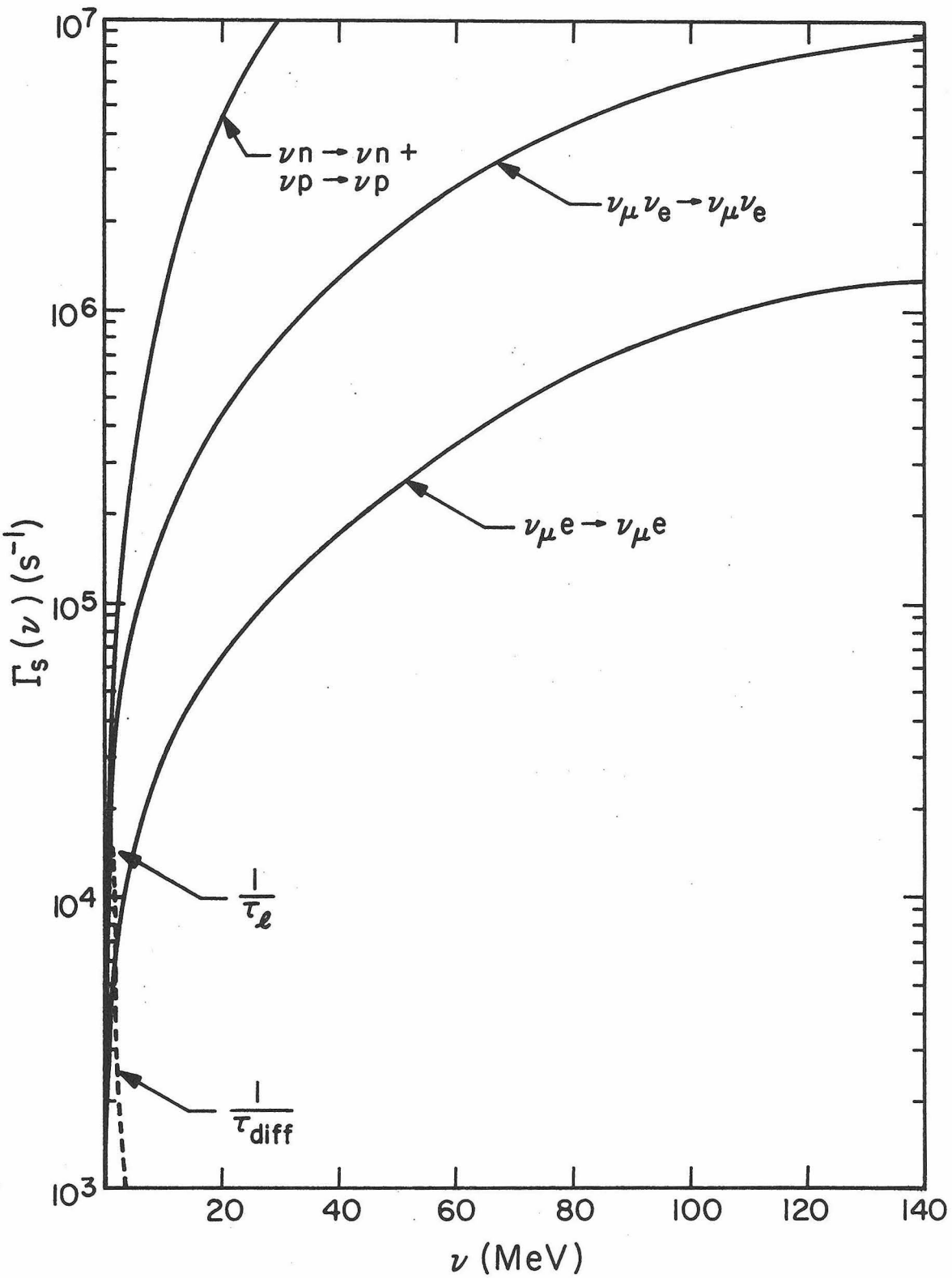
10^7
10^6
10^5
10^4
10^3
$\Gamma_s(\nu)\,(s^{-1})$
$\nu n \rightarrow \nu n +$
$\nu p \rightarrow \nu p$
$\nu_\mu \nu_e \rightarrow \nu_\mu \nu_e$
$\nu_\mu e \rightarrow \nu_\mu e$
$\frac{1}{\tau_\ell}$
$\frac{1}{\tau_{diff}}$
20
40
60
80
100
120
140
ν (MeV)

Fig. 31

FIGURE 32

The evolution of the ν_μ df under the thermodynamic conditions given in Figure 31, when the pair annihilation process is the $\nu_\mu\bar{\nu}_\mu$ producer, and $\nu_\mu\nu_e$ and $\nu_\mu e$ scattering (as well as the similar $\bar{\nu}_\mu$ processes) are included. The equivalent neutrino degeneracy parameter, η_ν, and the corresponding equilibrium FD df are shown, along with the calculated ν_μ histograms at the three times indicated; the values of Y_ν are $1.45\text{x}10^{-5}$, $5.4\text{x}10^{-5}$, and $.924\text{x}10^{-3}$. (Section 6.6)

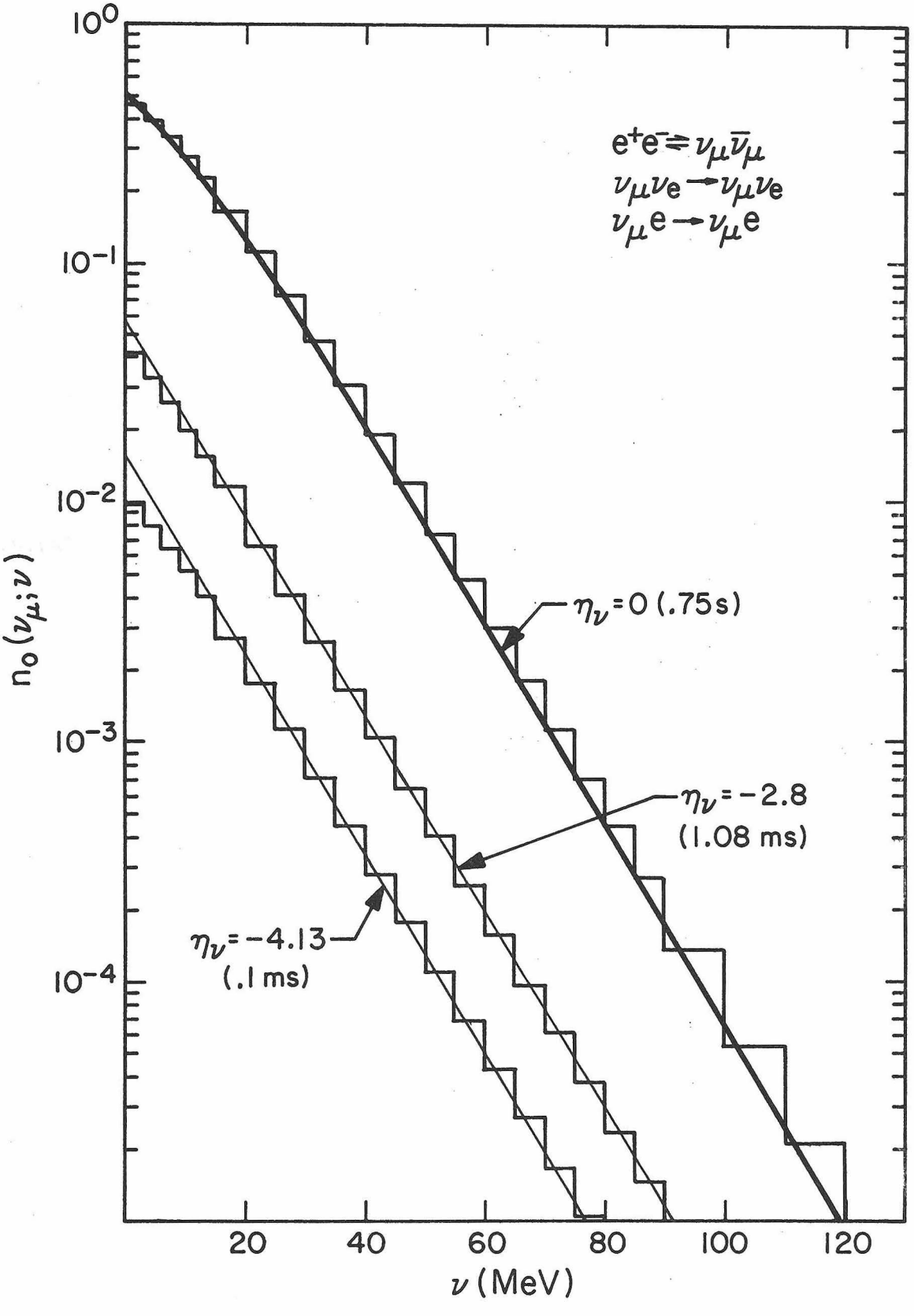
10^0
10^{-1}
10^{-2}
10^{-3}
10^{-4}
$n_0(\nu_\mu;\nu)$
$e^+e^- \rightleftharpoons \nu_\mu\bar{\nu}_\mu$
$\nu_\mu\nu_e \rightarrow \nu_\mu\nu_e$
$\nu_\mu e \rightarrow \nu_\mu e$
$\eta_\nu = 0$ (.75s)
$\eta_\nu = -2.8$
(1.08 ms)
$\eta_\nu = -4.13$
(.1 ms)
20
40
60
80
100
120
ν (MeV)

Fig. 32

FIGURE 33

The $\ell = 0$ moment of the ν_e distribution function as calculated by the P-1 method at 3.677 ms (solid histograms) and by the FLD method (dotted histograms) at 3.605 ms for various zones in the core: K = 1, $\rho = 1.52 \times 10^{13}$ g/cc, T = 7.74 MeV, $Y_e = 0.17$, $Y_p = .01127$, $Y_n = .539$, $\eta_\nu = 4.75$; K = 10, 2.25×10^{12}, 2.81, .298, 8.35×10^{-5}, .0999, 8.309; K = 13, 2.14×10^{11}, 1.52, .39, 5.44×10^{-6}, .0411, 7.154; K = 15, 3.98×10^{10}, 1.153, 0.426, 2.4×10^{-6}, .0249, .8097. The continuous solid curves are the FD df's if the zone is in beta-equilibrium. The central zone P-1 and FLD histograms are indistinguishable. (Section 6.8)

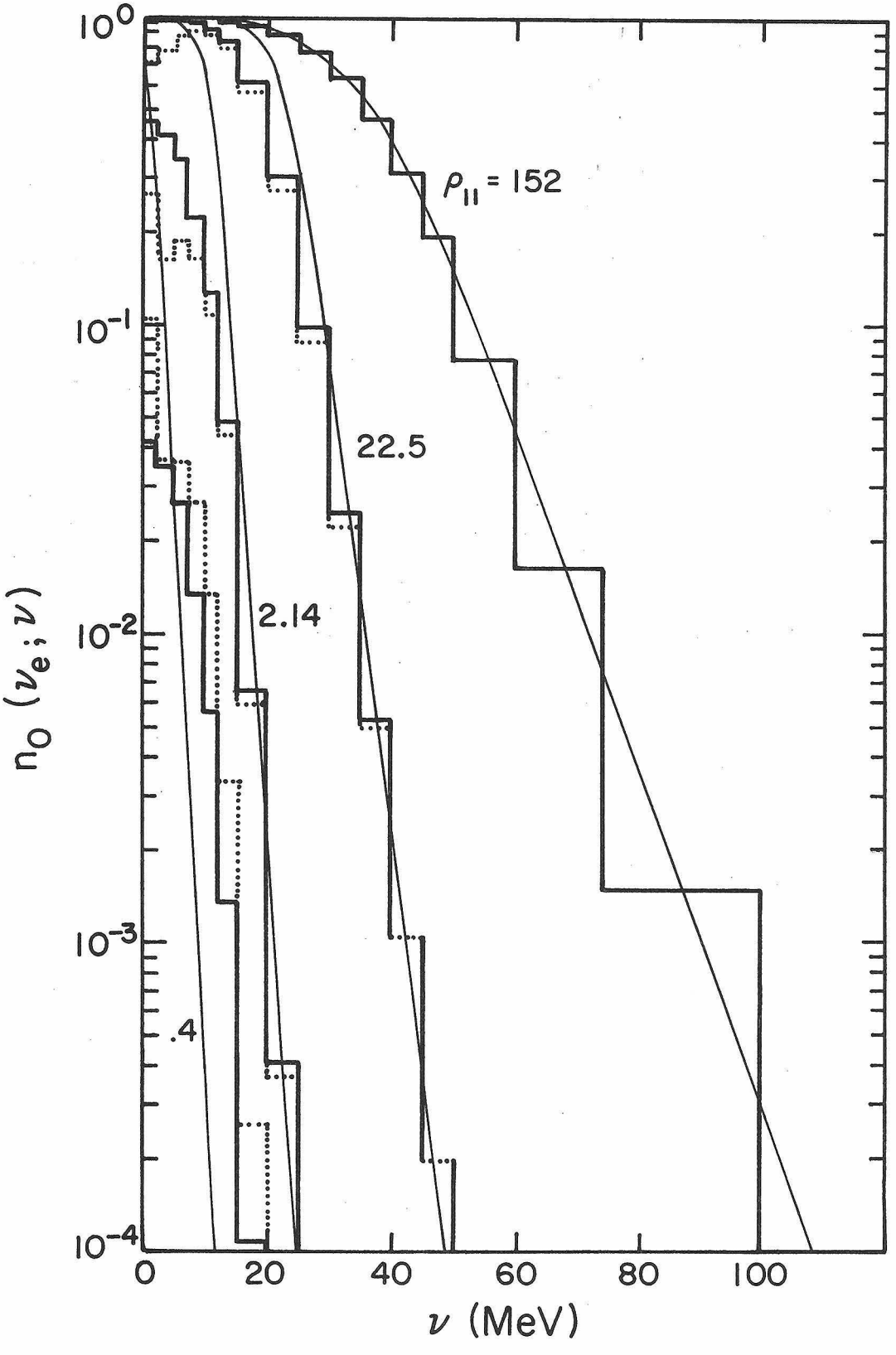
10^0
10^{-1}
10^{-2}
10^{-3}
10^{-4}
$n_0(\nu_e;\nu)$
$\rho_{11} = 152$
22.5
2.14
.4
0
20
40
60
80
100
ν (MeV)

Figure 33

FIGURE 34

The electron neutrino luminosity is plotted against the radial coordinate of mass enclosed within radius r, m_r, for various times. The solid curves are the P-1 luminosity profiles, the dotted and dashed are the FLD profiles. The positions of various densities (in g/cc) within the core are shown by arrows. The light travel time across the core is 1.3 ms. The glitch at 1/4 $M_\odot$ is a composition effect. (Section 6.8)

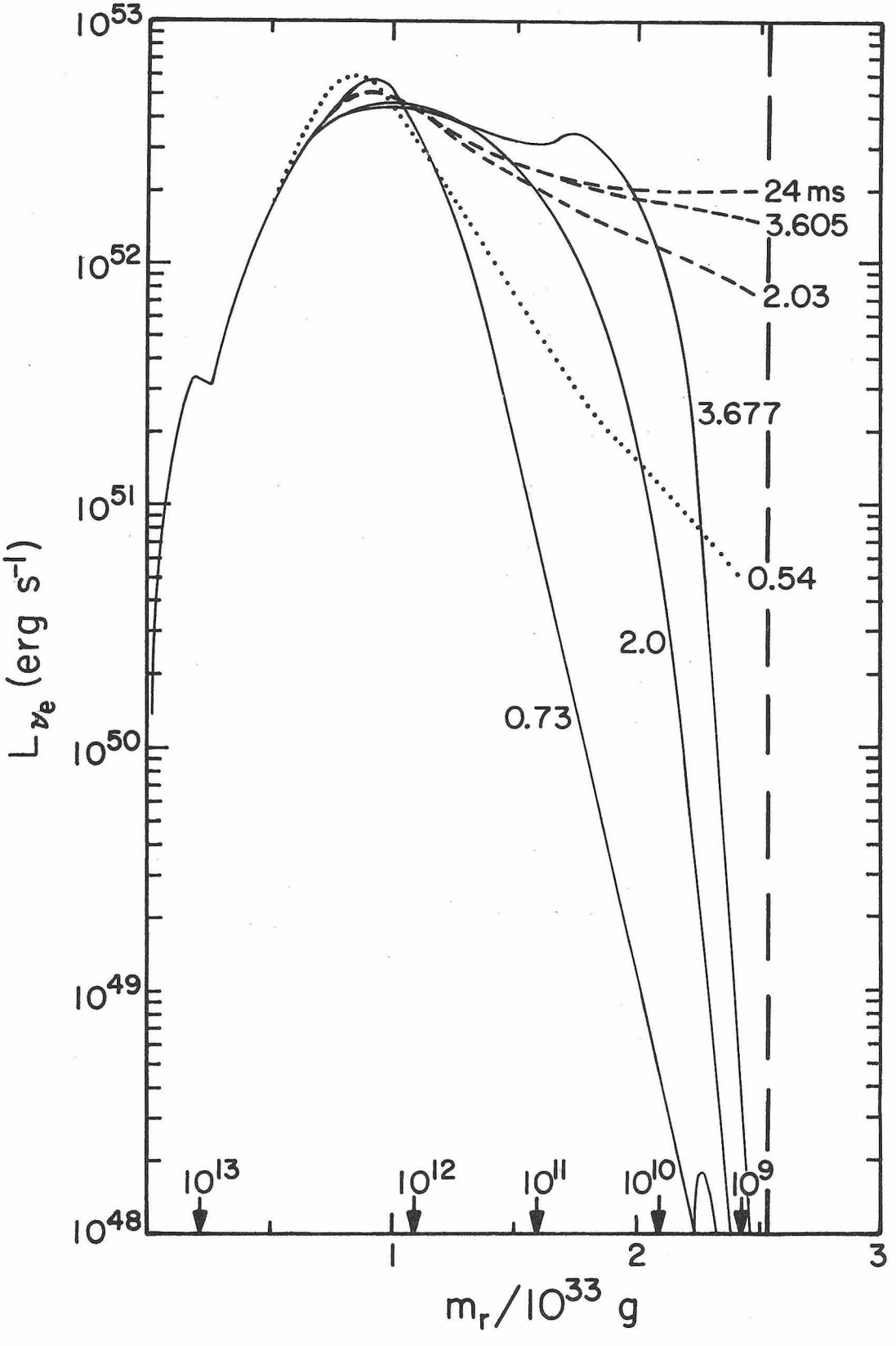
10^{53}
10^{52}
10^{51}
10^{50}
10^{49}
10^{48}
L_{ν_e} (erg s^{-1})
24 ms
3.605
2.03
3.677
0.54
2.0
0.73
10^{13}
10^{12}
10^{11}
10^{10}
10^{9}
1
2
3
$m_r/10^{33}$ g

Figure 34